University of Niš
Faculty of Electronic Engineering

Aneta Prijić

Design and optimization of electrical contacts and thermal cutoffs

PhD Dissertation
-updated version-

Niš, Serbia, 2015.

This PhD Dissertation is realized under the projects "Investigation and development of technology for electrical contacts manufacturing" and "Development of technology for thermal cutoffs manufacturing", financed by the Ministry of Science of the Republic of Serbia.

Contents

II Thermal cutoffs

Abstract

This Dissertation is focused on the design and optimization of the two types of metal based switching devices: rivet electrical contacts and S–type thermal cutoffs.

Theoretical basis of the electrical contacts design is employed for the adequate contact material selection, determination of the proper set of contact geometry and dimensions, and estimation of the minimum contact force value. Contacts of the solid and clad type, with rounded head are considered within two supporting structures. Obtained results of 3–D simulation of mechanical, electrical and thermal characteristics of the selected contacts in a steady state regime are presented. Simulations are carried out in the coupled physical domains by the direct solving method. Special emphasis is put on the dependencies of the operating temperature and maximum equivalent stress in the contacts under various working conditions. On the basis of the obtained results, optimization of the rivet electrical contacts is realized by the appropriate selection of the contact material, determination of the geometry and dimensions of contacts and definition of the rated current value. The optimization was conducted by functional, economic, ecological and reliability issues. Feasibility of contacts implementation into the specific switching devices with predefined rated currents and number of switching cycles before the failure are outlined. Analyzed dependencies and optimization results are described in details.

Theoretical basis of design and optimization procedures of thermal cutoffs are summarized. Parameters of functionality, quality and reliability are specially considered, since they are crucial for the appropriate choice of geometry, dimensions and materials of cutoffs constitutive elements.

Thermodynamic and microstructure characterization of the low melting alloys for thermal cutoffs purposes are elaborated. A new method for evaluation of the liquidus surfaces of the ternary systems is proposed. It is based on the standard 3–D surface modeling principles, and is applicable for any ternary system whose phase diagrams of binary subsystems and a few appropriate experimental points are known. The liquidus temperature can be determined from this 3–D surface by geometrical rules for any arbitrary composition of the ternary system. Moreover, the range of compositions of ternary alloys that have desired liquidus temperature can be easily extracted. Microstructure characteristics of the two eutectic low–melting alloys are also presented. Investigation was performed by SEM and EDS techniques, and the obtained results are discussed from the aspects of thermal cutoff technology development.

The results of 3–D electrical and thermal simulation of thermal cutoffs with two cutoff temperatures for the rated current of 12 A and rated voltage of 250 V (S–95 and S–138 type) are analyzed. The functionality and quality parameters of thermal cutoffs are determined by the simulation. Optimization of thermal cutoffs geometry and dimensions is proposed considering functional, economic and technological aspects.

The results of electro–thermal characteristics investigation of S–138 thermal cutoff

industrial prototypes by the thermovision imaging are presented. Thermal boundary conditions for the simulation, which are crucial for the successful optimization of the cutoffs, are set according to the obtained results. On the basis of the temperature distributions in the cutoffs under different working conditions, the temperature rise due to the self–heating is registered, the cutoff temperature is determined, and the response time of the cutoffs is evaluated. Thermal characteristics of the housing and conductive elements of the cutoffs are also analyzed.

As a result of the performed design and optimization procedures of thermal cutoffs, a technology line for their industrial production is presented. Complete process flow diagram for the S–type cutoffs is proposed. It includes preparation and assembling of the constitutive elements and quality and reliability testing procedures.

Introduction

Despite the extensive development of semiconductor devices dedicated to the electrical circuits control, switching devices made of metals and their alloys still have a broad, often irreplaceable role. Their basic elements are electrical contacts, which switch on and off electrical current in the circuit by mechanical action. Therefore, the electrical contacts have numerous applications in the devices as relays, electrical switches, thermostats, and motor starters. In everyday life, they can be found in the home electrical installation switches, home appliances, automotive ignition coils, as well as in most office equipment and industrial facilities. Electrical contacts characteristics are of importance for the standard power engineering, electronics and telecommunications and from the reliability point of view especially for the automotive and aviation industry. During their lifetime, electrical contacts are subjected to different loading and environmental conditions. They are used for electrical switching in the range from several μV and μA to thousands of V and A. Some of the contacts are activated rarely, while others have to sustain up to 10^9 switching cycles in a relatively short time interval. The switching itself is often performed in a chemically aggressive ambient [1].

Since electrical contacts perform their action inside various switching devices they have diverse geometries (rivet, cross, rectangle, disc, button) and dimensions. Electrical contacts are, based on the construction, classified as a solid and a clad. The solid contacts are entirely made of an electrically highly conductive material (mostly precious metals or their alloys), while the clad contacts are mainly made of copper, with one or both contacting surfaces plated with a thin layer of an appropriate contact material.

The basic parameters of contact switching capabilities are: electrical and thermal conductivities, hardness and elasticity limit, chemical reactivity, and resistance to wear, electro-migration and erosion due to the arcing. Besides these characteristics, which are determined by the contact material properties, it is important to consider contacts from the geometry and tribology aspects characterized by the shape and dimensions of contacts, the contact force, and the supporting structure properties [2]. Therefore, the main steps in the design and optimization of electrical contacts are selection of the contact materials, acceptance of the appropriate geometry and dimensions of contacts, and determination of the minimal contact force value.

To achieve a proper functionality of electrical contacts during the projected lifetime, they should have high conductivity, mechanical strength, and resistance to the electrical and chemical degradation effects. Prediction of the characteristics and reliable operation time of contacts subjected to the various working conditions is complex task, since there is no precise information about all parameters that may affect their operation. Analytical models of contact characteristics under the specific working conditions, as well as the appropriate statistical approximations give insight into some aspects of their reliability [3–5]. Numerical simulation of mechanical, electrical and thermal characteristics provides more efficient design and optimization procedures of electrical contacts. In

that manner, consideration of all available exploitation data in electrical and mechanical domains is required [6–8].

Analysis of the electro–thermal heating effects in the electrical contacts and switching devices by Finite Element Analysis (FEA) can be found in the literature [6–13]. Considerations are mainly related to a selected group of devices of specified geometry and applied materials [10], [11]. Analysis domains are mainly 2–D, while supporting structures are introduced by the specific boundary conditions [12]. Mechanical behaviour of the contacts is considered independently [13], or as a separate step in a sequentially coupled analysis [8].

Significant indicators of functionality, quality and reliability of electrical contacts are values of their operating temperatures at rated currents and maximum equivalent stress under defined contact force. Namely, electrical contacts are characterized by values of the allowed temperature rise above the ambient temperature for the given contacting ambient, and knowledge of the operating temperature is relevant to set the maximum current values that contacts can be loaded. On the other hand, simultaneous action of the contact force and electro–thermally induced stress in specific contact areas cause equivalent stress which, due to the large number of switching cycles, leads to the fatigue, and even to the contact failure. Therefore, the maximum number of switching cycles that still provides reliable contact operation represents important issue in the definition of contact quality and reliability.

One specific group of the metal based switching devices are thermal cutoffs whose main feature is non–resetting. Thermal cutoffs (also konown as thermal fuses or thermal links) are devices intended for the protection of various electrical systems from the overheating and/or possible burning. They detect excessive temperature rise in the system, caused by the over–rated values of the current or by disturbed environmental thermal operating conditions, and irreversibly break electrical circuit. Their advantages in the electrical circuits protection are small dimensions, fast response, electrical insulation of the active parts, and a low price. Thanks to these, thermal cutoffs have a broad implementation areas, such are electric motors and transformers, home appliances, office equipment, lightning devices, and other electronic systems. The increase of operation and handling security levels of devices, demands adjustment of thermal cutoffs to different applications. In addition to the requirements in terms of the higher rated current and wider range of functioning temperature, there are demands toward smaller dimensions, easier installation, and even use as a current fuse [14]. The only disadvantage of thermal cutoffs in home applications is that their replacement requires intervention by the service person.

Functioning of the thermal cutoffs is based on the low temperature alloys property to melt at a specific (low) temperature. Conductive parts of the cutoff are soldered by this kind of alloy and connections between them are broken when melting temperature (cutoff temperature) is reached. Thermal cutoffs are classified by design, rated functioning temperature, and rated current and voltage values [15–17]. Design of thermal cutoffs depends on the cutoff principle (with a fusing material or with a spring), the shape and dimensions of the leads (radial, axial or strip), and the housing type (ceramic, plastic or metal). Rated functioning temperature is determined by the melting temperature of the soldering alloy and it is in the range from 70 °C to 240 °C. The rated current and voltage represent set of AC and DC values that define operating conditions of the thermal cutoffs.

The low melting alloys have melting temperature bellow 250 °C. In most cases they are multi–component, with tin, lead or silver as a basic component and one or more low

melting elements as bismuth, indium, antimony or gallium as additive for fine tuning of the melting point. They are used as a soldering material in devices that do not operate at high temperatures, and their thermodynamic and microstructure characterization is important for development of the lead–free soldering techniques [18–20].

Phase diagrams of multi–component alloys have essential role in the determination of alloys with predefined characteristics, specification of their manufacturing processes, and forecast of their behaviour during the exploitation. They enable visual representation of the state of the material as a function of the composition, temperature, and pressure. Experimental assessment of multi–component phase diagrams represents time consuming, expensive, and difficult process. Therefore, phase diagram modeling has an important contribution. Phase diagrams of ternary alloys at constant pressure are 3–dimensional, but their representation is in most cases two–dimensional. Namely, liquidus and solidus surfaces are presented by the projections of isothermal and cotectic lines inside the triangle on whose sides are chemical compositions of binary subsystems. Calculation of thermodynamic parameters of multicomponent alloys and generation of their phase diagrams is the main interest of so–called CALPHAD (CALculation of PHAse Diagrams) group during the last four decades [21].

CALPHAD method for the determination of phase equilibrium in multicomponent systems is based on the minimization of the total free Gibbs energy. Dependence of the Giggs energy on the temperature, pressure and each phase concentration is described by the appropriate mathematical models. Parameters of these models are determined by the specific software, on the basis of thermodynamic databases. In this way, phase diagrams of systems are created by utilizing the phase diagrams of the lower level subsystems. However, thermodynamic databases, as well as specialized software for 3–D diagrams generation, are commercial and not public available.

The parameters of functionality, quality and reliability of thermal cutoffs include thermal, electrical and mechanical domains. Rated functioning temperature and holding temperature are basic parameters of thermal cutoffs of the specific construction at rated current and ambient temperature. These parameters are crucial for the appropriate implementation of the thermal cutoffs. The quality and reliability of thermal cutoffs are determined by the operating temperature rise due to the electro–thermal effects and response time. The operating temperature rise is defined by the properties of the conducting elements and thermal characteristics of the cutoff housing. The response time is specified in the laboratory testing conditions and is mainly dependent on the thermal properties of the cutoff structural elements. The values of these parameters are primarily considered in design and optimization procedures of the thermal cutoffs, assuring adequate selection of material, geometry and dimensions of their structural elements. For this purpose, an appropriate finite element analysis of the cutoffs is employed.

Experimental monitoring of temperature distribution in the vicinity and inside the thermal cutoffs under various electrical and thermal operating conditions enables determination of their parameters. Thermovision camera has an important role in the imaging of the temperature distributions in the field of medicine, meteorology, power and thermal engineering, tribology and material science [22–24]. In the electronic engineering, thermovision imaging is used for the analysis of thermal distributions in the variety of the passive and active devices and systems [25, 26]. In that manner, it can be used for thermal cutoff design and optimization purposes. Although thermovision imaging is primarily focused on functional testing and rarely to quantitative determination of ther-

mal parameters [27], its advantage is in the contactless, non–destructive temperature measurement of the investigated device and its parts. In the case of thermal cutoffs, the use of specialized temperature chambers is avoided and functioning of the thermal cutoffs in the near real operating conditions is enabled.

This Dissertation has two major parts, based on the investigated switching device. In the first part, results of the design and optimization of the rivet electrical contacts are presented. The solid and clad bimetallic contacts within two supporting structures are considered. Based on the theoretical concepts, presented in Chapter 1, contact materials are selected, geometry and dimensions of the contacts are defined, and minimal contact force value is determined. 3–D simulation of selected contacts is performed to obtain their mechanical, electrical and thermal characteristics under steady state conditions, and results are presented in Chapter 2. Direct, coupled–field simulation procedures are employed, with special emphasis on the dependences of operating temperature and maximum equivalent stress on the exploitation conditions. On the basis of the obtained results, optimization of the rivet electrical contacts is performed, in a view of the selected contact materials, geometrical and dimensional design parameters, and defined rated currents. Functional, economical, ecological and reliability aspects are considered. Moreover, applicability of the selected contact type within predefined switching device, with specified rated current and number of reliable switching cycles are outlined. Analysed dependencies and optimization results are presented in details in Chapter 3.

The second part of the Dissertation is devoted to the design and optimization of S–type thermal cutoffs. In Chapter 4 are discussed theoretical assumptions of these procedures. Special attention is given to the functionality, quality and reliability as the basis for an appropriate choice of the geometry, dimensions and materials of thermal cutoffs structural elements.

In Chapter 5, results of thermo–dynamic and microstructure characterization of low–melting alloys for thermal cutoff purposes are presented. A new method for estimation of liquidus surface of ternary alloys is described in details. The method is based on the known phase diagrams of binary subsystems and minimal set of experimental data, with a software for surface modeling as a numerical tool. Generated 3–D phase diagrams enable extraction of the liquidus temperature for specified composition of the ternary system, as well as determination of the alloy composition that has desired melting temperature value. Also, results of microstructure analysis (by SEM and EDS techniques) of two eutectic alloys important for the application in thermal cutoffs are given. This enables specification of their processing parameters and forecast of mechanical characteristics of soldering joints realized from these alloys.

Chapter 6 is dedicated to the results of 3–D electrical and thermal simulation of thermal cutoffs with two cutoff temperatures, rated current of 12 A and rated voltage of 250 V (S–95 and S–138 types). Based on simulation results, optimization of geometry and dimensions of thermal cutoffs is suggested in a view of functional, economic, technological and quality aspects.

The results of thermovision investigation of electro–thermal characteristics of S–138 cutoff realized in the form of an industrial prototype are given in Chapter 7. Based on the temperature distribution in the cutoff under different operating conditions, temperature rise due to the self–heating is determined, cutoff temperature is specified, and response time is estimated. Thermal characteristics of the housing and conductive parts of the cutoffs are also investigated. Obtained results are used for determination of the boundary thermal conditions necessary for efficient optimization of the cutoffs through numerical

simulation of their electrical and thermal characteristics.

The most important results of the investigation are summarized in the Conclusion. As a result of the design and optimization procedures, complete production line of cutoffs is proposed. The flowchart of technological sequences for production of S type cutoffs is presented, with specified steps for the preparation and assembling of the constitutive parts, as well as the procedures for quality and reliability testing.

Part I

Electrical contacts

Chapter 1

Fundamentals of electrical contacts design and optimization

The role of electrical contacts is to enable or disable (switch) flow of electrical current in the circuit, with as less as possible signal distortion. Design and optimization of electrical contacts should provide their efficient and reliable operation during the projected lifetime. These demands are fulfilled by contacts with high electrical and thermal conductivity, high resistance to the wear and arc discharge, and chemical stability. Characteristics of contacts are determined by the contact material properties, their geometry and dimensions, and by the contact force value [28].

Poorly designed contacts, besides unsatisfying functionality, may over time partially lose their switching capabilities. Degradation of contact properties has origin in the different electrical, mechanical and chemical processes introduced by the operating conditions (rated current, temperature, mounting position, chemically aggressive environment).

Taking into account all parameters that determine functionality and reliability of electrical contacts, main steps in their design and optimization are selection of contact materials, definition of the geometry and dimensions, and determination of the minimum contact force value.

1.1 Functionality, quality and reliability parameters of electrical contacts

Current flow through the contact, due to its electrical resistance, cause so–called Joule's heat dissipation. This is the reason why *electrical resistance of the contact* represents basic parameter of its functionality and need to be as low as possible. Resistance of the electrical contact consists of the bulk resistance and contacting resistance. *Bulk resistance* has constant value, determined by the electrical conductivity of the contact material and geometry and dimensions of the contact. It can be reduced by selection of a highly conductive contact material. *Contacting resistance* has variable value dependent on the interface of the contacting surfaces. This resistivity can be reduced by higher values of the contact force [29].

During the contact operation, it is necessary to obtain removal of the dissipated heat from the contacting area. Therefore, *thermal conductivity* has to be considered as a parameter in the design of electrical contacts. It is determined by the thermal

conductivity of the contact material, mechanism of the heat removal and area of the surface from which the heat is removed. Better thermal characteristics of contacts are obtained by the implementation of contact materials with the high thermal conductivity and selection of the contact shape that provides considerable free surfaces.

Electrical contacts are often exposed to the high electrical currents, frequent and numerous switching cycles, and chemically aggressive environment. As a result of these operating conditions, contact characteristics degrade during time and eventually they may fail. Determination of the contact reliability is a complex problem due to the lack of precise information about all parameters that may influence their characteristics under various operating conditions.

1.1.1 Degradation of electrical contacts

Basic physical and chemical phenomena that occur in contacts and represent sources of degradation effects are operating temperature rise, arc discharge, chemical reactivity and material fatigue. Degradation effects limit long–term and reliable operation of designed electrical contacts and can be considered from the electrical and mechanical aspects. The effects of electrical nature are:

- increase of the contact resistance (due to the numerous thermal phenomena and chemical reactivity);
- impedance mismatch of the two contacting parts;
- electromagnetic interference,

while mechanical nature have:

- wear (material transfer due to sticking or evaporation and erosion caused by arc discharge and corrosion);
- welding (due to the high electrical current density and arc discharge);
- modified contact shape (cracks, plastic deformation).

The amount of contact characteristics degradation during the one switching cycle basically depends on the contact material and contact geometry and dimensions. It also depends on the rated current value, duration of the arc discharge, contacting gap and medium inside it, contacting speed, stress induced during contacting, and contact bouncing [30]. Many of the effects are result of the several phenomena, which are often mutually related, and for minimization of the negative consequences balance between design parameters is needed.

1.1.1.1 Operating temperature rise

Operating temperature of contacts has a significant impact on their mechanical and electrical characteristics. Rise of the operating temperature during the current flow defines maximum current value that contact of the specified geometry and material can sustain for defined time period without degradation of characteristics. This value represents *rated current value* as one of the basic contact design parameters. If contact force has low value during the contact closing (switching–on), sliding and/or bouncing

occurs and through contact passes current of the value much higher than the rated one. This is *inrush current* and it implies significant local operating temperature rise followed by the material transfer and contact evaporation [28].

The value of the operating temperature includes three components: ambient temperature, temperature rise due to the contacting resistance, and temperature rise due to the bulk resistance. Temperature rise due to the contacting resistance can not be strictly specified since it depends on the contact shape, hardness, electrical and thermal conductivity of the contact materials, value of the contact force, thickness of the oxide layer on the contacting surfaces, as well as contact sliding. Temperature rise ΔT, due to the bulk resistance, is proportional to the square of the current flowing through the contact I, and in the simple form it can be expressed as [31]:

$$\Delta T = \frac{I^2 L^2}{\sigma k A^2}, \tag{1.1}$$

where L is the length of the conducting path through the contact, A is cross section of the contact, σ is electrical conductivity, and k is thermal conductivity of the contact material. This expression assumes several simplifications related to the contact structure and underlying physical processes: contacting parts have the same length and cross–sections; thermal energy is generated at a constant rate within the contacts body, while the contact resistance is negligible; there is no heat removal by convection or radiation and it is transferred through the contact body toward its fixed ends and absorbed there; maximum temperature exists at the contacting surfaces. A large number of assumptions dictates usage of this expression with the aim to compare the different materials rather than for any quantitative forecast. Relation (1.1) confirms statement that materials with higher conductivities (electrical and thermal) provide better contact operation. Besides, these materials allow thinner and narrower cross–sections and therefore less contact dimensions which is important from the economic aspects of the contacts mass production [32].

The complex mutual relation exists among contact design variables, its material characteristics and key performance parameters. This dynamic interaction is presented by the operating temperature rise in Fig. 1.1 which shows the influence of certain variable on the other. When increase of the first variable produces or allows increase of the second one, there is a "plus" sign by the arrowhead, while the sign "minus" indicates that increase of the first variable produces or allows decrease of the second one. Temperature rise leads to the increase of the contact bulk resistance due to the increase of the contact material electrical resistivity. At the same time, thermal expansion and stress relaxation in the contact material with time modifies the contact force and indirectly increases contacting resistance. In mechanical sense, thermal expansion induces additional stress at the contact and supporting structure interface. Temperature rise also leads to increased corrosion of the contacting surfaces, and therefore an increase of the contacting resistance. All of these effects are interrelated and depend on several factors such as the shape of contacts, type of the contact material, and environmental conditions.

In practice, allowable temperature rise values for defined contact materials and environment are prescribed by specific standards [34]. Contacts design procedure should provide acceptable increase of the contact resistance and consequently temperature rise within the limits defined by standards for the rated current value.

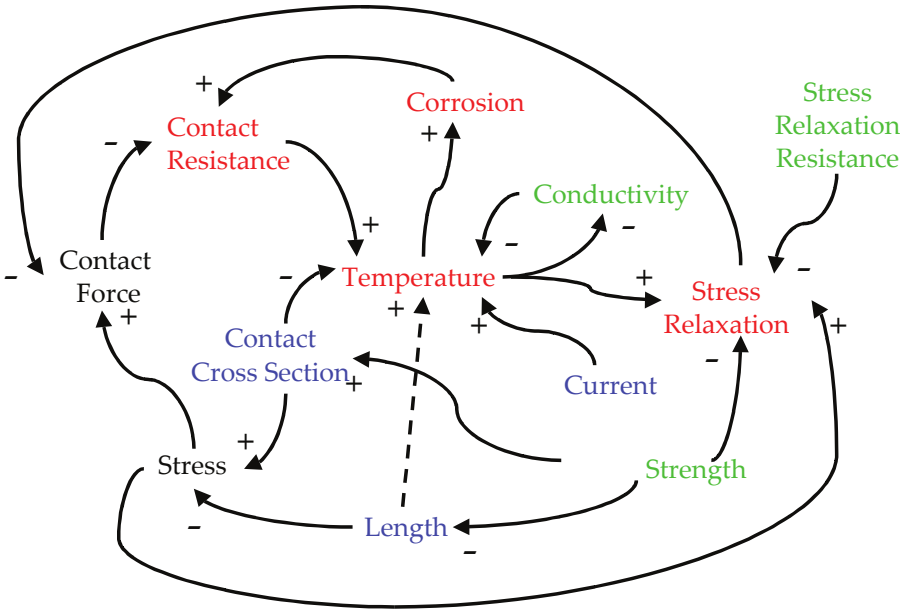

Figure 1.1: Dynamic interaction among contact design parameters (blue), material characteristics (green), and key performance parameters (negative influence – red) [33].

1.1.1.2 Arc discharge

Arc discharge is a process in which electrical current flows through the gap between two charged surfaces. It can occur during the contact closing before two contacting surfaces touch each other, or during the opening at the moment of the contact surfaces separation. Electrical arc occurs when potential difference between contacting surfaces exceeds value of the *minimum arc voltage* and available current in the circuit exceeds *minimum arc current*. These quantities depend on each other and also on the contacting surfaces materials, the gap and the medium between the contact elements [30].

Arc discharge in the contacts is a negative phenomenon due to several reasons. Primarily, it causes transfer of the material from positively to negatively charged contacting surface in contacts in DC circuits. The heat generated during discharge can cause melting of the contacting surfaces, which can be welded if the gap between them is narrow. If the opening force is sufficient to break the welded joint, contacting surfaces will separate but they will be ruptured. When the opening force is insufficient, contacting surfaces will be permanently welded [35]. The energy released by the arc discharge helps contact material vaporization, as well as creation of oxides and corrosion layers at the contact surfaces, thus increasing the contacting resistance. Another negative effect is generation of electromagnetic interference, which in the form of noise can significantly affect the operation of electronic devices.

Contact bouncing during closing leads to multiple arc discharge. In order to reduce damage of the contacts, it is necessary to reduce the number and height of the bounce by choosing the appropriate supporting structure [36]. Control of the damage during the opening can be achieved by minimization of the arc discharge duration through rapid increase of the gap between the contacting surfaces. However, rapid increase of the contacting gap increase bouncing and it is necessary to find a compromise between these two effects. Appropriate selection of the contact materials (resistant to arcing erosion and wear) can also minimize undesirable effects of the arcing [37].

1.1.1.3 Chemical reactivity

Nonconductive layers may be formed at the contact areas exposed to the chemically aggressive environment, leading to the degradation of the conducting layer and rise of the contact resistance. This phenomenon is known as the *corrosion*. The most common chemical corrosion activators are oxygen (formation of oxide), various sulphuric, chlorine and silicate compounds, as well as organic materials. Some metals are susceptible to self–limiting or so–called *passive corrosion*. Once formed oxide or sulphide layer does not grow any further, but protects underlying base material from the influence of the atmosphere. In *active corrosion* base material continuously corrode and the corrosion product spreads out from its origin. Contacts suffer from three types of corrosion: creep, pore and fretting corrosion [30, 38–40].

Clad or pre–plated contacts can be subjected to *creep corrosion* if they have bare edges exposed to the atmosphere. This type of corrosion is schematically presented in Fig. 1.2, where corrosion from the bare edges spreads over the surface and consequently increase contact resistance. Creep corrosion can be avoided or decreased by plating of the contacts after blanking or by introducing underplating layer of non-corrosive material.

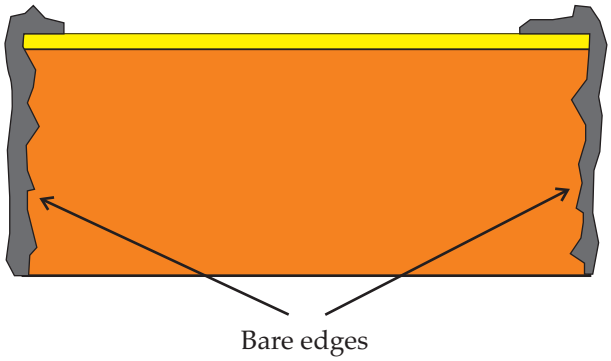

Figure 1.2: Creep corrosion due to the bare edges [39].

Contact platings often contain imperfections such as pores or cracks. If the base material is exposed to a corrosive environment through these micro holes, *pore corrosion* may occur [41]. Base material corrosion can be localized inside the pores and invisible at the surface, but also can spread out. Pore corrosion with severely corroded base material is presented in Fig. 1.3. Pore corrosion can be minimized by using thicker plating layers or an inter–layer.

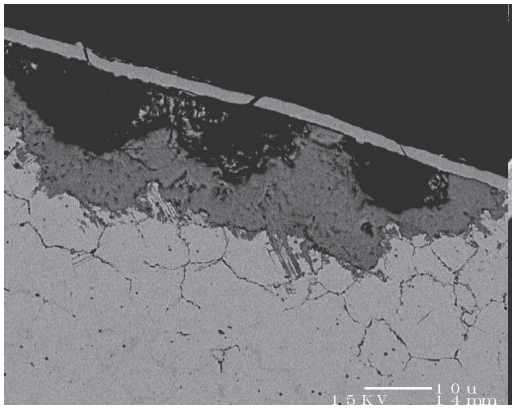

Figure 1.3: Base material corrosion due to pores/cracks in the plating layer [39].

Plated contacts where contact point oscillates on a microscopic scale may have disrupted contacting layer due to the *fretting corrosion* [38,42]. Numerous contacting cycles with nonfixed contact point form thicker oxide layer as presented in Fig. 1.4. Fretting corrosion can be eliminated by sufficiently high value of the contact force to stabilize contacting point or by lubrification of the contacting surfaces to inhibit oxidation and reduce wear [43,44].

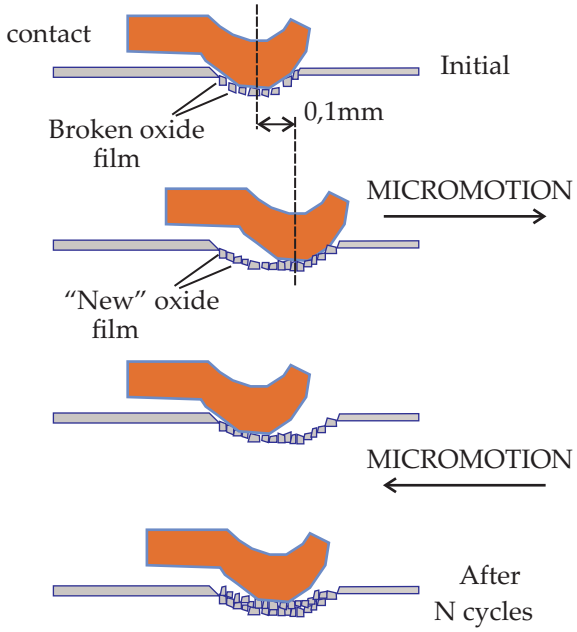

Figure 1.4: Fretting corrosion [38].

1.1.1.4 Fatigue

Impact energy released by the contact closing causes stress in materials and fatigue. When numerous switching cycles are applied, cracks may occur in the contacting material. The increased number and size of cracks over time leads to the degradation of contacting surfaces and eventually to the failure [30]. Failures due to the fatigue are sudden and responsible for almost 90 % of fractures in metals. This kind of failure occurs at the lower stress levels then during continuous static load of the contact materials.

Fatigue tests are presented by so–called S–N diagrams which give dependence of the maximum stress (S) on the number of load cycles before failure due to the fatigue (N). S–N diagrams for copper and silver (two most common contact materials) are presented in Fig. 1.5. From S–N diagrams, *fatigue strength* (stress value that will cause failure for the defined load cycles number) and *fatigue life–time* (number of load cycles before the failure for the specific stress value) can be determined [45]. During contact design these two parameters enable determination of the contact force value for the expected lifetime or estimation of the reliable contact operation time under the given equivalent load stress.

The fatigue strength is related to the material yield strength and depends on its microstructure characteristics (grain size, ductility), surface treatment and the possibility of corrosion. Environmental stress parameters (temperature, frequency and mean value of the contact force) also affect fatigue. Resistance of the specific device to the failure due

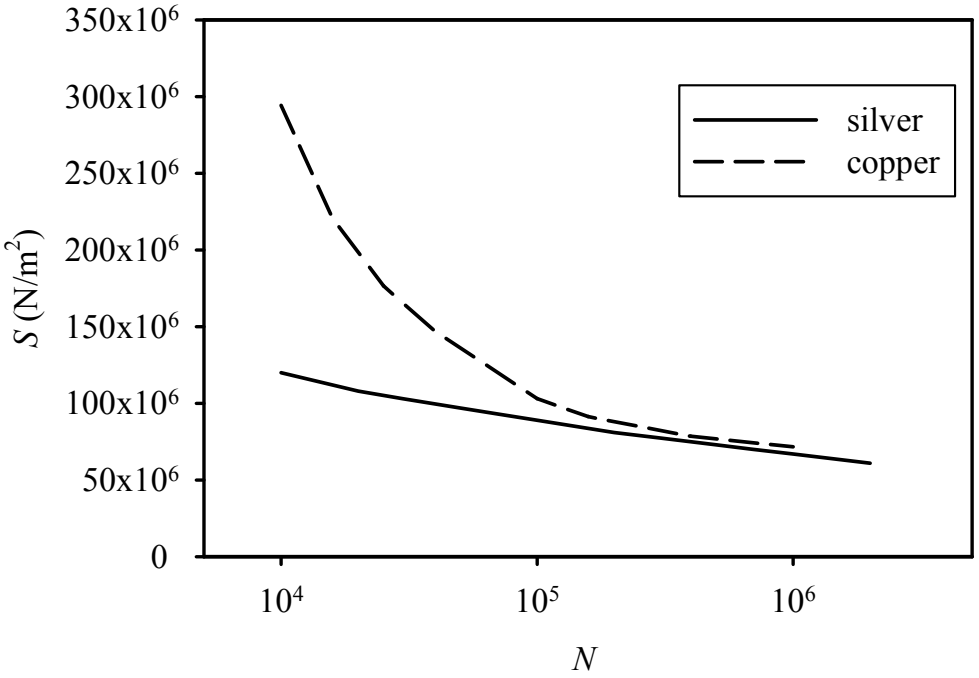

Figure 1.5: S–N diagrams for silver and copper [46], [47].

to fatigue can be increased by improved design, modified manufacturing procedures, use of materials with higher strength limit, and by surface strengthening [48].

1.2 Design tolerances

During the design of contacts, three types of tolerances are important: material tolerances, manufacturing tolerances and system tolerances. Moreover, tolerances may be superpositioned giving so–called stack tolerances [49].

Material tolerances are associated to the raw material and usually are specified by the producer. Material parameters as elastic modulus, yield strength, tensile strength, elongation, conductivity, formability have values within certain range or meet a set of minimum values. In numerical analysis during the design of contacts, average values of material parameters are used. Also, variations in size of the strip material that contacts are made of (length, width, thickness) affect their characteristics.

Manufacturing tolerances are specified by technical drawings. These tolerances provide partial control over the final product shape after diverse manufacturing steps. Namely, batch production may result in parts which differ from their prototypes. The difference originates from various rolling, stamping and forming procedures of the contact materials [49]. The residual stress after rolling and slitting of the strip, and after stamping procedure differs from contact to contact depending on the contact material, its thermal treatment and processing procedures. This results in different contacts performance under the load. Since designers usually assume optimal dimensions and material properties, tolerances provide that none of the contact characteristics considerably differs from its optimal value [50].

System tolerances are imposed by the assembly manufacturer. These usually include tolerances of dimensions and positions of the assembled parts, as well as tolerances

in respect to electrical specifications of parts. Imposed system tolerances have impact on tolerances of constitutive parts in a view of proper material selection and forming processes.

Overall, if material, manufacturing and system tolerances are met, the device will operate within specified limits. However, there is still a possibility that the mutual interaction of individual tolerances lead to improper functioning of contacts. It is described by *stack tolerances* and for good performance of contacts tight dimension tolerances are necessary.

1.3 Selection of contact materials

The goal of contact materials development is to obtain reliable and effective contacting with minimal costs and without any ecological issues. Improvement of mechanical and electrical material properties are governed by better performance in specific applications. For low power contacts the most important characteristic is contacting resistance, while for high power contacting crucial is resistance to welding and arc discharge. Contacts which are most of the time in a closed state need to have stable value of the contact resistance during the lifetime [51].

In order to maintain good electrical contact performance, contact surfaces are often plated with a thin layer of another material. The basic material is usually copper, while selected plating material must have high conductivity and hardness, to be resistant to corrosion and temperature rise, and to easily adheres to the copper. The plating minimizes formation of the corrosion layer on the contact surfaces, increases resistance to wear and material transfer due to arc discharge, and reduces friction in sliding contacts. Various highly conductive or noble metals and their alloys, as well as sintered compounds are used as plating material. The most common materials are silver, gold, tin, nickel, copper, platinum, wolfram, and nowadays, beryllium, carbon, chrome and cobalt. Contact materials are usually fabricated by adding specific metals (Cu, W, Ni, C) or ceramic materials (SnO_2, In_2O_3, ZnO, CdO) to the basic metal by tempering or sintering. For plating are used several techniques as electroplating, autokatalisys, mechanical plating, hot tub method. The plating itself can be performed in a different phases of the contact fabrication (before, during or after stamping). Selection of the plating material and technique and timing of plating in the fabrication sequence depends on the main demands that contact layer has to fulfil [30].

1.3.1 Mechanical aspects

Despite the detailed and careful design process, devices can fail due to numerous reasons. The most common source of the failures related to the design is due to the basic difference between the definitions of the elastic limit and 0.2% offset yield strength of a given material. The strength of the material is usually determined by tensile testing and represented by stress–strain curve. This curve is crucial for the selection of material from the mechanical aspect of the contact design. Basic stress–strain curve of metals is presented in Fig.1.6.

The stress is defined as tensile force per unit area of a specimen, while strain value corresponds to relative change of the specimen length caused by the stretching. To the point A, there is a linear relationship between stress S and strain ϵ, defined by the elastic

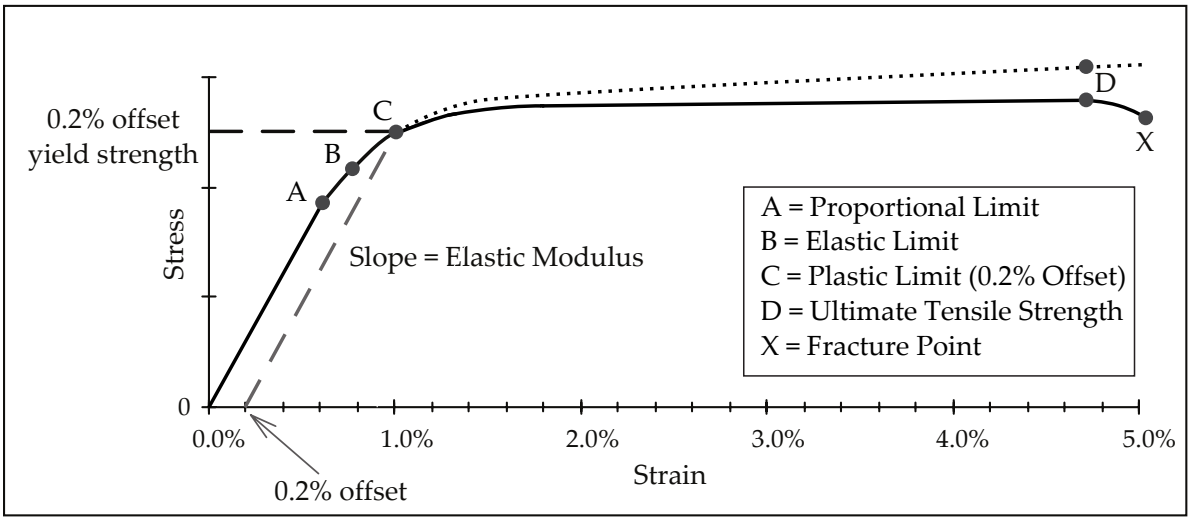

Figure 1.6: Stress–strain curve of metals for tensile testing.

modulus (Young's modulus) E_m in the form $S = E_m\epsilon$. Point B is the elastic limit and it divides stress–strain curve into the elastic region (left of the point B) and the plastic region (right of thw point B). Metals subjected to the tensile load below the elastic limit, after removal of the load, returns to the original state by the same stress–strain curve. Similarly, if the tensile load is above the elastic limit, when it is removed specimen will relax by the curve parallel to the original one, and permanent deformation (known as yielding) will occur in it. Further tensile load increase leads to the ultimate tensile strength (point D) when the specimen begins to neck and eventually it reaches the fracture point. During the exploitation electrical contacts should not exhibit permanent deformation. Therefore, in the design of contacts, stress limits of used materials have to be considered. Usually it is 0.2% offset yield strength (determined by point C at stress–strain curve). At this stress value, after removal of the load, in material resides deformation of 0.2% strain value. This limit is co–called *plastic limit* of the material. However, for stress values just below 0.2% offset yield strength, there is some permanent deformation and designs that theoretically fulfil all demands may fail in the practice.

During the stretching or compression of the specimen, its original cross–section area changes. As a result, the real stress value in the specimen has complex dependence on the tensile force value and cross–section area. Real stress–strain curve above the plastic limit is presented by doted line in Fig. 1.6. The overall real stress–strain curve can be represented by so-called bilinear approximation, i.e. by the two straight lines connected at the plastic limit point. The slope of the first line is equal to the *elastic modulus*, while the second line connects plastic limit point with ultimate tensile strength and its slope is determined by the *tangent modulus*. In numerical programs for structural linear analysis by the finite element method, mechanical properties of the material are described by elastic modulus and Poisson's coefficient (ratio of material deformation in tangential and longitudinal directions during the stressing). On the other hand, in nonlinear analysis the whole curve is used or its bilinear approximation [52].

To achieve appropriate contact force value it is desirable to select material that can sustain higher strain values but still exhibit elastic behaviour. This requires material with optimum combination of the elastic modulus and plastic limit. The real elastic limit of the material which separates elastic and plastic regions is presented in Fig. 1.6 (point B). However, if the contact is stressed in elastic region under higher temperature long

enough, the part of elastic deformation can transform into the plastic one. Moreover, value of the plastic deformation increases with time due to the gradual increase in plastic strain under constant stress (creep), and due to reduced ability of a material to return to its original state when unloaded (stress relaxation). Both effects are more pronounced at higher initial values of the stress and temperature. Therefore, well designed contacts must encounter thermal effects, as well as effects of stress relaxation over time [53], [54].

Material yielding under certain stress value increases with temperature due to the increased movement of dislocations within the grains in the material. Grain boundaries stop dislocation movement and materials with finer grain structure have higher plastic limit, yield strength and resistance to stress relaxation of the finished product. Also, fine grained materials exhibit better formability properties due to the isotropic nature of specific mechanical quantities [55–57].

Plastic limit of certain material is increased by preventing the movement of dislocations within the grains. In that manner, solid solutions i.e. alloys are widely used in the electronic devices technology. Namely, weather the alloy is substitutional or interstitial one, alloying element atoms prevent movement of dislocations and therefore increase plastic limit of the base material. The other methods for improvement of material strength are mechanical hardening and/or temper.

The strain hardening represents the permanent deformation of the material in order to increase its strength and it is achieved by so–called cold work or work hardening. Typically, it is cold rolling process used to increase the temper of strip materials by elongation of the grains in it. This permanent deformation inhibits movement and creation of new dislocations and increases the strength of the material. Cold work reduces ductility and formability of material and it has to be applied in conjunction with annealing and recrystallization in order to obtain desirable product form [58].

Thermal treatment can increase strength of the final product. Metals that can be thermally strengthened offer the best combination of strength and formability. *Thermal hardening* includes several methods such as: solid solution hardening, dispersion strengthening, quench hardening, precipitation age hardening, spinodall decomposition [59].

The hardening procedures change the stress–strain curve by increase of the plastic limit. The real stress–strain curve in the plastic region follows the power low of the form $S = K\epsilon^n$, where the strain hardening exponent n and the strength coefficient K describe material behaviour during the forming. The higher n values give better formability, while higher K values indicate higher strength temper. The values of these parameters, as well as the anisotropy coefficient are important for contact manufacturing. Bending and stretching of the material require high strain hardening exponent value, while drawing of the strip material requires high anisotropy coefficient [60], [61], [62]. However, it has to be noted that the number of fabrication steps in the material processing determines its yielding [63].

Information about material hardness and mechanical properties of the fabricated part are obtained by different hardness testing methods like: *Brinell*, *Rockwell*, *Vickers*, and *Knoop* [64], [65].

1.3.2 Electrical aspects

The values of electrical quantities (rated voltage, rated current, inrush current) that contacts have to sustain are basic parameters in the design of contacts and therefore are

crucial for contact material selection. High values of the rated and inrush currents are sources of different degradation effects in contacts as mentioned in Subsection 1.1.1. The resistance of certain material to degradation effects is crucial for its selection for contacts installed in high power relays and switches. Basic classification of silver based contact materials in a view of rated and inrush current values for use in home appliances (AC current) and automotive industry (DC current) is presented in Fig. 1.7.

1.3.3 Overview of the common contact materials

Taking into account material properties which are important for the functioning of the electrical contacts, advantages and disadvantages of commonly used contact materials are listed in Table 1.1 [28,30,59,66–75].

It is evident that variety of parameters affect contacts performance, as well as that there is a wide range of materials that can meet certain requirements. Basically, application of the contact determines selection of the contact material and plating method. Proper choice of the plating material (beside the costs) depends on the temperature and chemical reactivity of the contacting ambient, values of the rated and inrush currents, and desired number of reliable switching cycles. Furthermore, selection of the contact material determines the contact force value.

As part of the global trend of decreasing dimensions of electrical devices, reduction of contacts dimensions has as a consequence decrease of electrical current transfer capabilities. Due to the decreased areas that can dissipate heat, contact temperature rises and consequently resistance of the contact body increases. This implies usage of materials with high electrical conductivity despite their high price [76]. Small contact dimensions require materials with high formability to avoid cracks during manufacturing of the contacting surfaces with small radius [77]. Since high plastic limit and formability of the material are usually not compliant, compromise between values of these two parameters is necessary. Therefore, optimal selection of materials for small contacts should be the best combination between strength, electrical and thermal conductivity, fatigue, resistance to stress relaxation and formability [29].

1.4 Determination of the geometry and dimensions of electrical contacts

Electrical contacts are elements of versatile switching devices and they can occur in several forms and have very different dimensions. The most common contact shapes are: rivet, cross, rectangle, disk and button. Regarding the construction they can be solid or clad [70,72]. Solid contacts are entirely made of highly conductive material (usually precious metals or their alloys). Clad contacts are basically made of copper with one or both contacting surfaces plated by the selected contact material.

Design process of electrical contacts requires determination of the basic contact shape, construction type, and precise dimensions and tolerances. Contact shape is defined by the mounting procedure, place within the switching device and contacting method. Construction type mainly depends on the price and manufacturing techniques. Specification of dimensions and tolerances is determined by the rated current values and technological constrains [70,78].

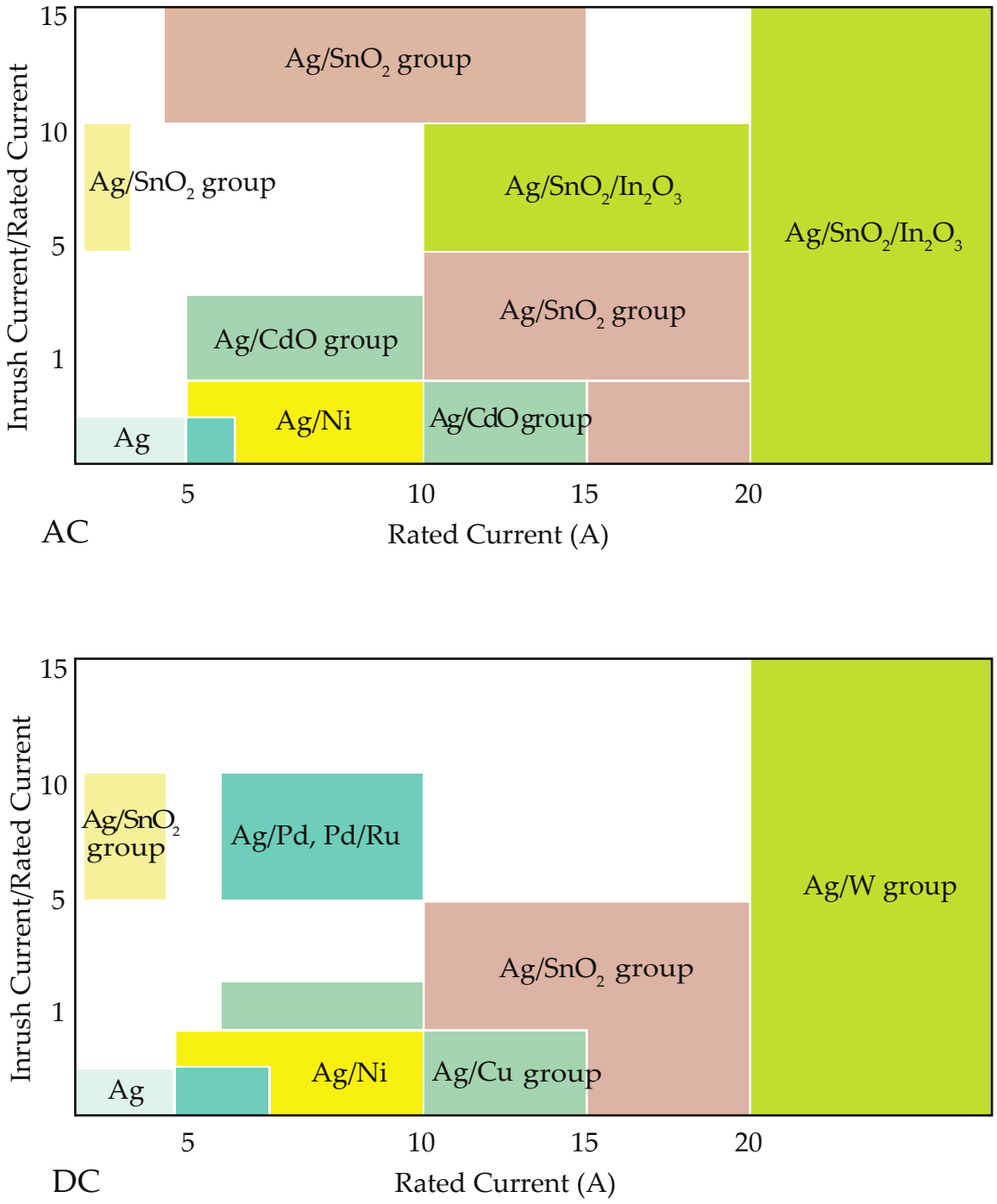

Figure 1.7: Classification of silver based contact materials in a view of rated and inrush current values [66].

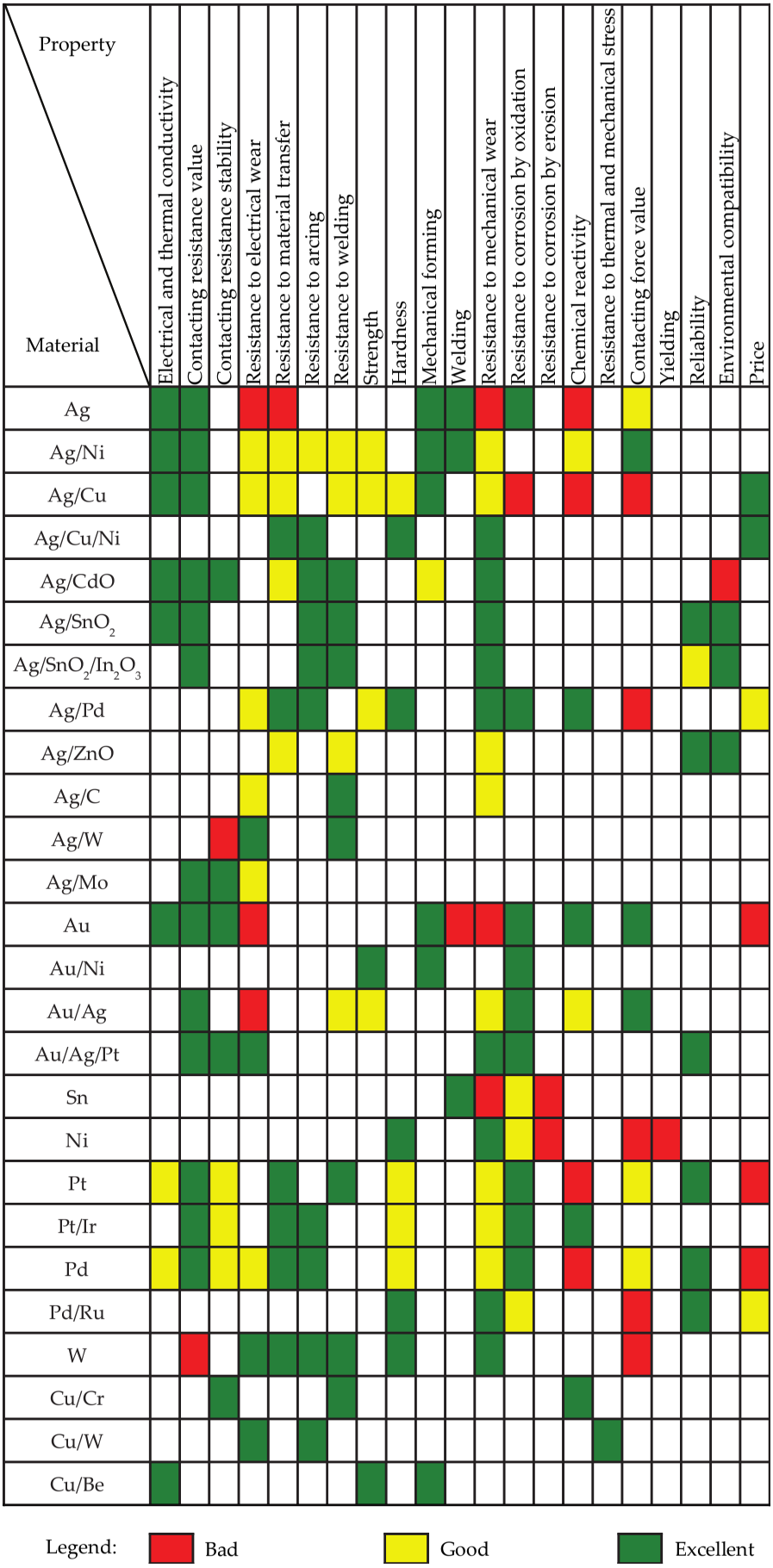

Table 1.1: Advantages and disadvantages of the common contact materials.

The most commonly used shape of contact is the rivet. These contacts are used in home switches and appliances, consumer devices, and nowadays in the automotive industry. The advantages of this contact shape are [66,72]:

- simple automated riveting,
- strong and stable joint with the supporting structure at low and medium rated currents,
- no loss of elastic features of the supporting structure since there is no temperature rise induced by the arc discharge,
- no oxidation and corrosion at joint with the supporting structure.

Depending on the construction, rivet contacts may be solid or clad (bimetallic or trimetallic). Solid rivet contacts are produced by plastic deformation of the base material in the form of a wire, thereby forming a contact head in specially designed molds. Due to the limitations imposed by dimensions, rivet contacts are recently made by the extrusion technique. Clad contacts are made by plating of the basic material by welding or mechanical sticking of the plating material in the form of a strip.

Rivet contacts have clearly separated head and shank. Depending on the head shape contacts are classified as the one with flat, rounded or conical head, while by the shank shape they can be of flat, tubular or chamfer type. Classification of rivet contacts by construction and shape is presented in Fig. 1.8. Standard rivet contact types are solid and bimetallic with flat or rounded head and flat shank. The flat head is used for fixed and rounded head for moving contacts. The conical head is used in contacts where contacting resistance has importance and it provides resistance to corrosion and good contacting in the presence of dust. The tubular shank shape enables joining with brittle supporting structures like bakelite and hard plastics, while the chamfer shank provides simple and fast automatic riveting. Usage of trimetallic contacts reduces costs of the contact production in cases where contacting is performed at both sides (usually moving contacts). Special trimetallic contacts, dedicated to the high temperature applications, have plated bottom side of the head and the shank which simultaneously provides mechanical and electrical connection with the supporting structure [70].

Dimensions of the selected contact type are determined by value of the rated current, geometry of the supporting structure, and technological limitations concerning the ratio of specific dimensions. Fig. 1.9 represents cross-sections of the solid and bimetallic rivet contacts with the rounded head and flat shank, with dimensions as specified in Table 1.2.

Specification of the contact dimensions during design process is based on the determination of the initial contact head diameter depending on the rated current value. Due to the technical constrains, this value should be a multiple of 0.5 mm and should to comply to appropriate standards. Generally accepted rules prescribe usage of solid contacts for head diameters bellow 2.5 mm, while for diameters above 6.5 mm it is recommended to use clad contacts. The tolerance value of this dimension is 0.1 mm. For solid contacts made from silver and its alloys, applicable diameter of the contact head at low values of the rated current is presented in Fig. 1.10. For high values of the rated current applicable head diameter of clad contacts is shown in Fig. 1.11.

The shank diameter of clad contacts should also be a multiple of 0.5 mm, while for solid contacts (usually for a head diameter of less than 2 mm) common values are 0.8 mm,

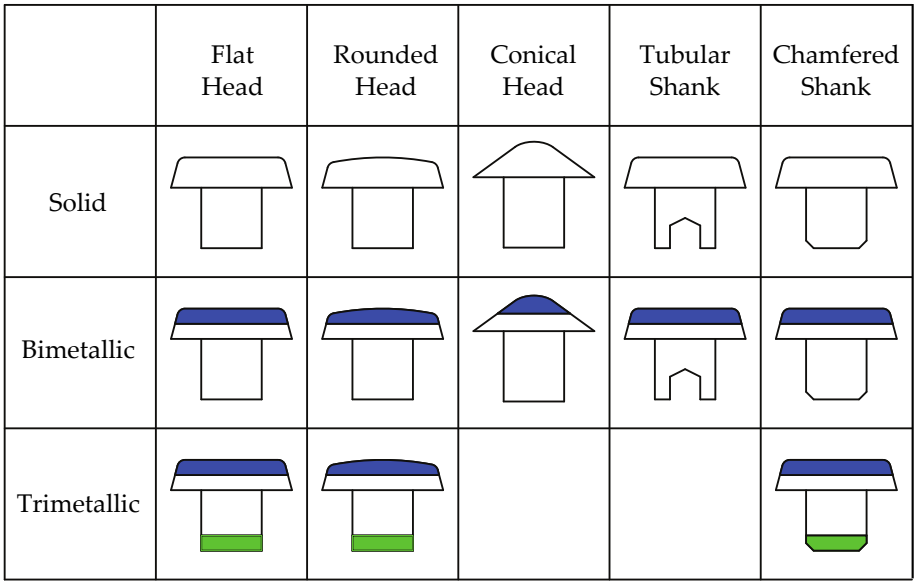

Figure 1.8: Classification of rivet contacts by the construction and shape.

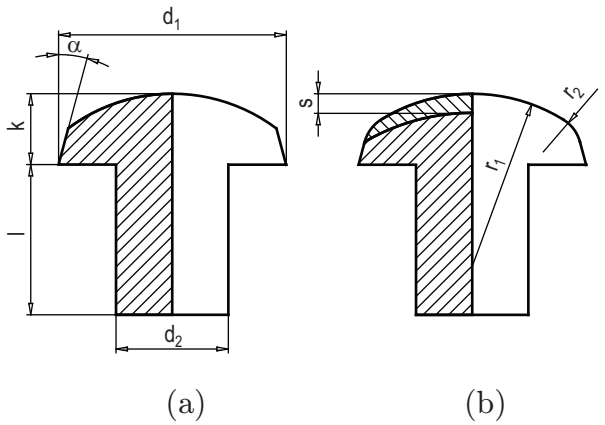

Figure 1.9: Cross–section of the solid (a) and bimetallic (b) rivet electrical contact.

Dimension	Notation
Head diameter	d_1
Shank diameter	d_2
Total head height	k
Contacting layer height	s
Shank length	l
Head rounding radii	r_1 i r_2
Head taper angle	α

Table 1.2: Notation of rivet electrical contacts dimensions.

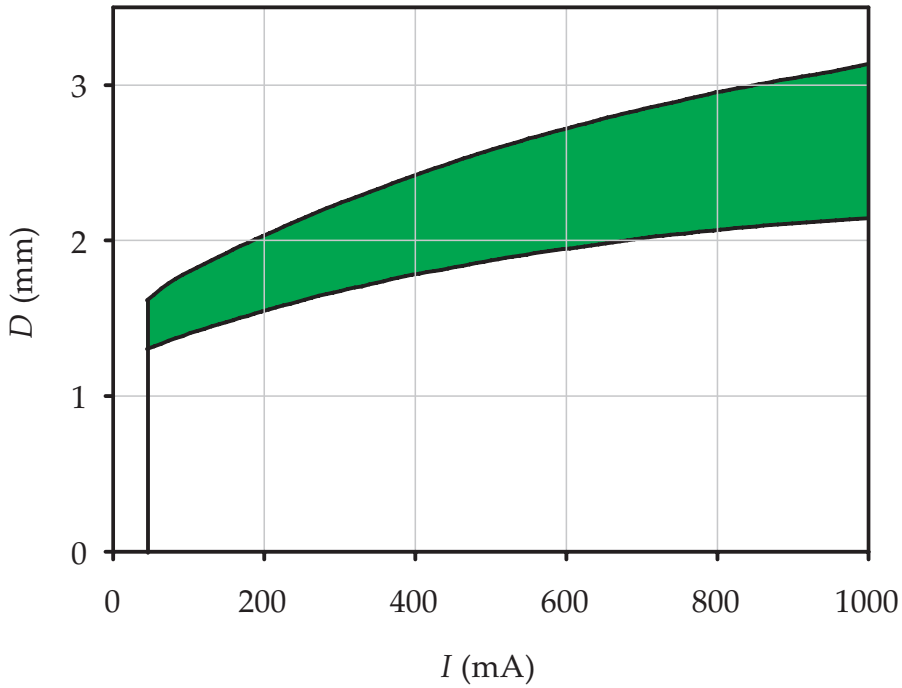

Figure 1.10: Applicable diameter of the contact head at low values of the rated current [79].

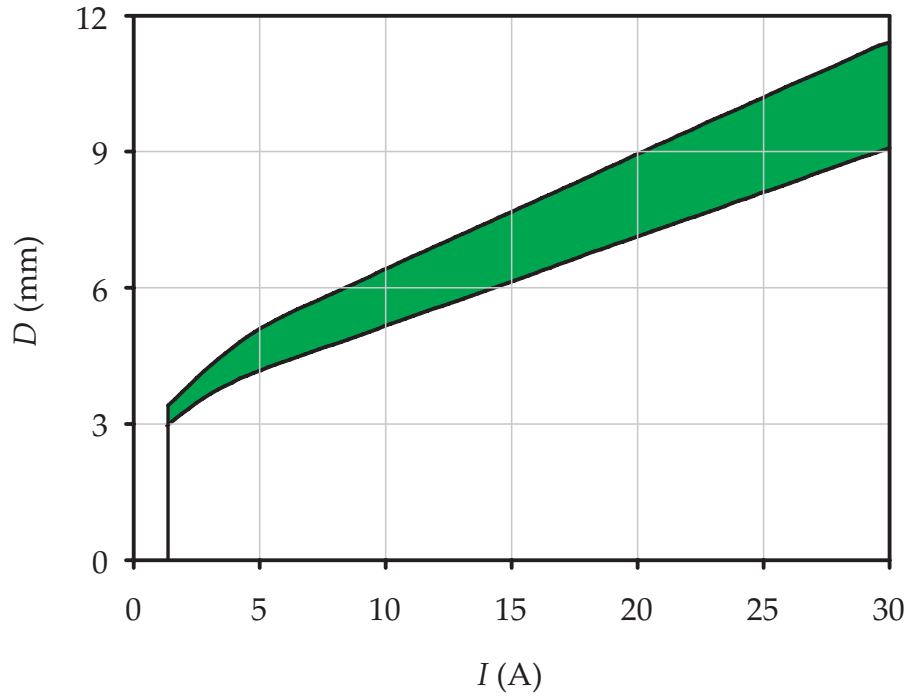

Figure 1.11: Applicable diameter of the contact head at high values of the rated current [79].

1 mm, and 1.2 mm. This diameter must be in correlation with diameter of the contact head, so as to enable its efficient production and provide the functionality. Basically, the required ratio should be $d_1/d_2 = 1.7 - 2.3$. This ratio provides a good fit of the contact head to the supporting structure and eliminates the occurrence of a parasitic transition resistance [80]. Recently, manufacturing of rivet contacts whose ratio d_1/d_2 is out of these ranges is enabled by introduction of extrusion techniques. In this way, it is possible to obtain specific types of contacts, while maintaining a given quality [72]. The allowed deviation of this dimension value is +0.0/-0.1 mm, thereby avoiding impossibility to insert the contact into corresponding opening in the supporting structure.

Well–designed contacts have the overall head height at least 0.5 mm for solid, and 0.7 mm for clad contacts. Recommended relation is $k/d_1 = 0.2 - 0.4$. Greater head height allows better removal of the heat and reduced operating temperature rise. However, it should be noted that too low and too high values can induce difficulties in technological processes for contacts manufacturing. The lower limit of the tolerance should be set to -0.0 mm, with respect to the fact that riveting of the contact into the supporting structure reduces overall height of the contact head. The upper limit of tolerance is generally +0.05 mm, with fact that for a head diameter greater than 6 mm, this value can be raised to +0.1 mm.

The contact plating is thickest at the middle of the contact head, whereas towards its perimeter decreases (except for the flat heads). Riveting of the contacts into the supporting structure leads to a partial levelling of the thicker part of the plating. The thickness of the plating on the central part is generally 25% – 65% of the total head height, and depends on the selected contact material. The optimum value is 50 %, while its tolerances are ± 0.05 mm.

The length of the shank is usually 0.8 – 1.5 mm greater than the thickness of the supporting structure and in the manufacturing process it is easily resizeable. To ensure efficient and reliable riveting process allowed deviation of this value is -0.0/+0.15 mm.

The radius of the head rounding r_1 ranges from $1.2 \cdot d_1$ in solid to $4 \cdot d_1$ in clad contacts. Its tolerance is ± 2 mm.

The taper angle of the contact head is standard from 9° to 15°, with a tolerance of ±2°.

The manufacturing process of designed contacts depends on their geometry and the mechanical properties of used materials. In addition, manufacturing process development requires determination of a suitable cross-section of the base material volume (strip or wire) [81], as well as knowledge of the dependence of the material properties on the orientation (longitudinal or transverse) [82].

1.5 Determination of the minimum contact force

Electrical contacts design procedure, after selection of the contact material, geometry and dimensions of the contacts, involves determination of the minimum contact force (minimum contact pressure). The value of contact force should ensure good contacting between the two surfaces, the minimum bouncing of contacts at switching and their reliable operation during the projected lifetime. Specification of this value is determined by the value of the rated current, geometry of the contact, required number of switching cycles, as well as by properties of the contact material and supporting structure [13].

Total contact resistance is composed of the bulk resistance and the contacting resistance. Bulk resistance depends on the electrical resistance of the contact material and

shape of the contact. Contacting resistance is composed of a *constriction resistance* and *film resistance* and it depends on the contact force between two surfaces. Since contacting surfaces are not ideally smooth (contain a number of picks and valleys), so that the actual transfer of electrical signals takes place in spots where these picks are touching. The constriction resistance exists due to the fact that the electric current lines squeeze to pass through these contacting spots. The film resistance is a consequence of the existence of thin oxide layers and dirt on the surfaces of contact. Increase in the contact force value leads to an increase of the contacting spots area and consequently to reduction of the constriction and film resistance values. At sufficiently high values of contact force, total contact resistance is reduced to the bulk resistance. Also, with a reduction in contact force, film resistance becomes the predominant component of the total resistance of the contact. The dependence of total contact resistance on contact force is shown in Fig. 1.12.

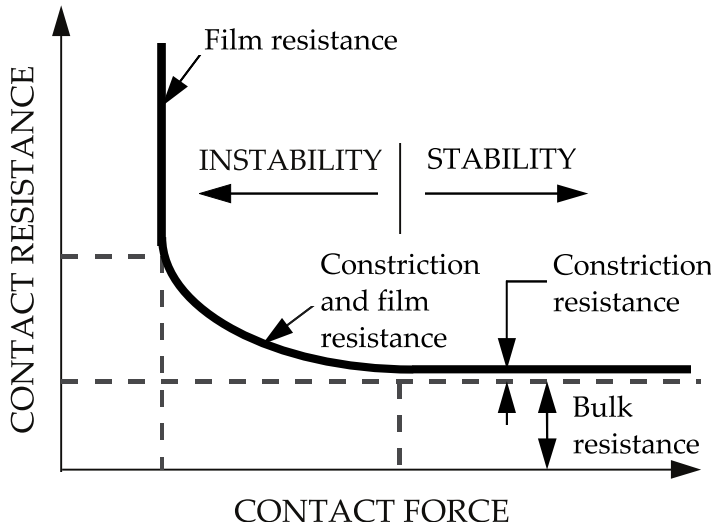

Figure 1.12: Dependence of the total contact resistance on the contact force value [83].

Often, the minimum contact pressure value is provided instead of the minimum contact force. The force and the pressure are connected by the contact area. Common dependence of the minimum contact pressure for low rated currents for solid contacts made of silver and its alloys is shown in Fig. 1.13. For high values of the rated current, this dependence is shown in Fig. 1.14.

The minimum contact pressure value, determined from Figs. 1.10, 1.11, 1.13, and 1.14, enables to specify the minimum contact force needed to achieve good contact. In practice, for the fast determination of the minimum contact force F_{min}, depending on the rated current I_{rat}, an approximation $F_{min} = p \cdot I_{rat}$ is used, where the coefficient of proportionality p has value of 0.15 N/A for $I_{rat} \leq 1$ A; 0.2 N/A for 1 A $< I_{rat} \leq 5$ A; 0.36 N/A for 5 A $< I_{rat} \leq 50$ A [80].

Mechanical properties of the material which affect the value of the contact force are primarily the value of elastic modulus, yield strength, the plastic limit and the stress relaxation over time [84]. Low constriction resistance value is achieved with materials with high ratio of yield strength to elastic modulus, while reduction of the film resistance is realized by using chemically non-aggressive materials that disables corrosion.

During the projected lifetime contacts should maintain appropriate contact force value. Since the properties of the contacts degrade over time, their design has to take into account information about the expected time of reliable operation, as well as the necessary number of switching cycles without failure. Reduction in contact force during

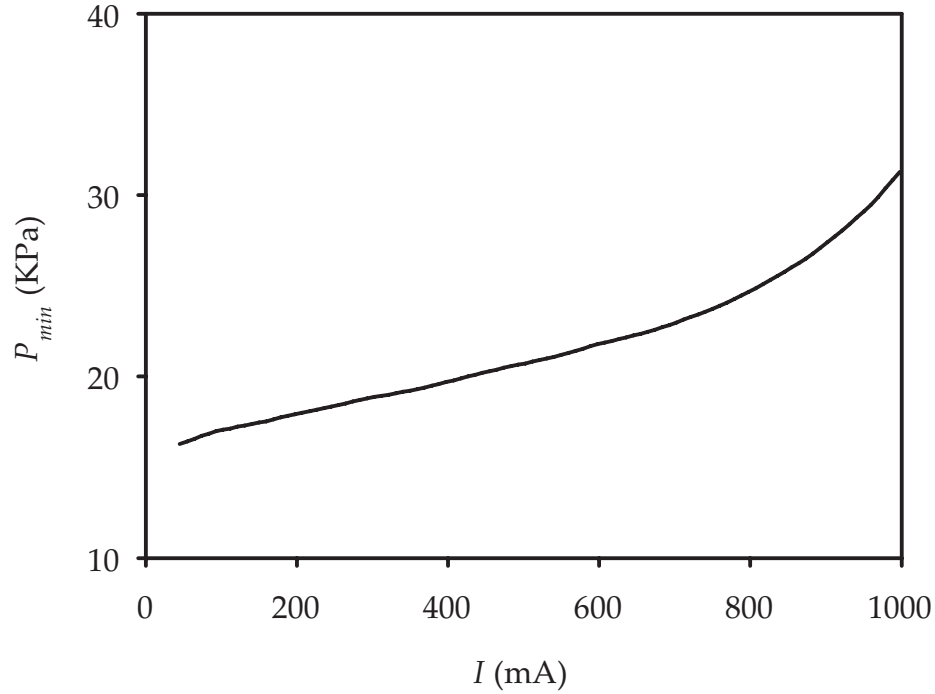

Figure 1.13: The minimum contact pressure value for low rated current values [79].

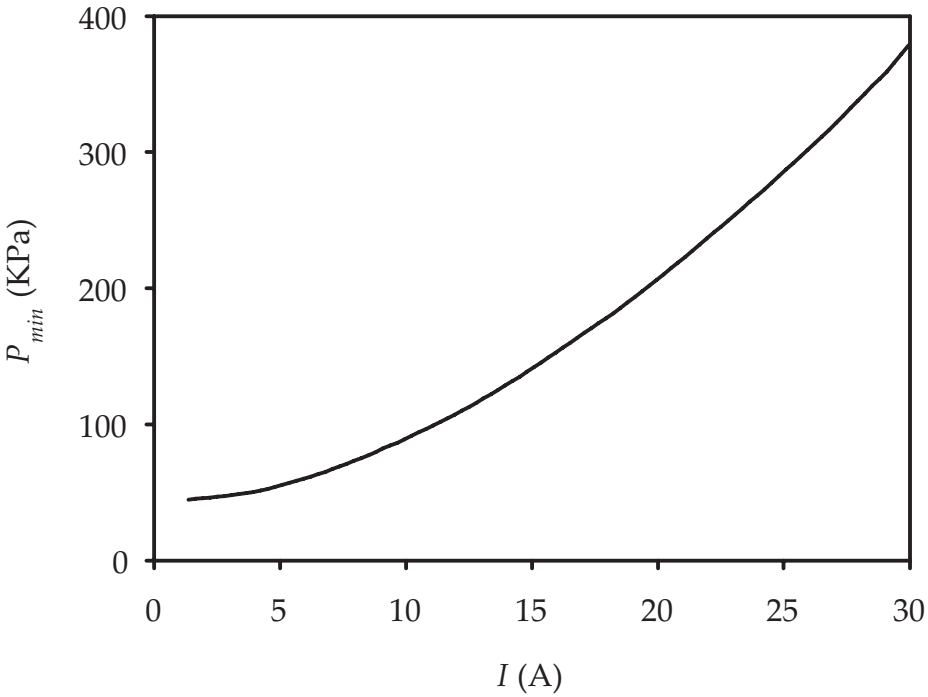

Figure 1.14: The minimum contact pressure value for high rated current values [79].

time occurs if there are deformation of contacts due to the manufacturing processes, if there is a stress relaxation over time or due to the fatigue.

Manufacturing processes of electrical contacts involve a variety of operations such are pressing, rolling, stamping, extrusion, rounding and they cause so–called residual stress in the final product. In combination with the stress that contacts are exposed during operation, the residual stress can lead to unexpected values of the equivalent stress, its relaxation over time, permanent deformation of the contact and gradual loss of the contact force. Stress relaxation over time in the contact depends on the temperature, the initial stress value and the material. In order to eliminate the residual stress in contacts, materials that are subjected to hardening by heat treatment or ageing process are used [85].

The value of the contact force at the end of contact lifetime depends on the material fatigue. Since the contact force produces stress in the contact material, in accordance with the consideration given in Section 1.1.1, its value has to be reduced if contact has to withstand a higher number of switching cycles.

Moreover, the calculation of contact force usually assumes that all dimensions of the contacts fall in the middle of the allowed range of values. In practice, there is a deviation of the real values within the given tolerances, so that the contact force varies with respect to the designed value. Bad selection of the contact material with predefined values of the designed and end–of–life contact force and dimension tolerances are presented in Fig. 1.15 [86].

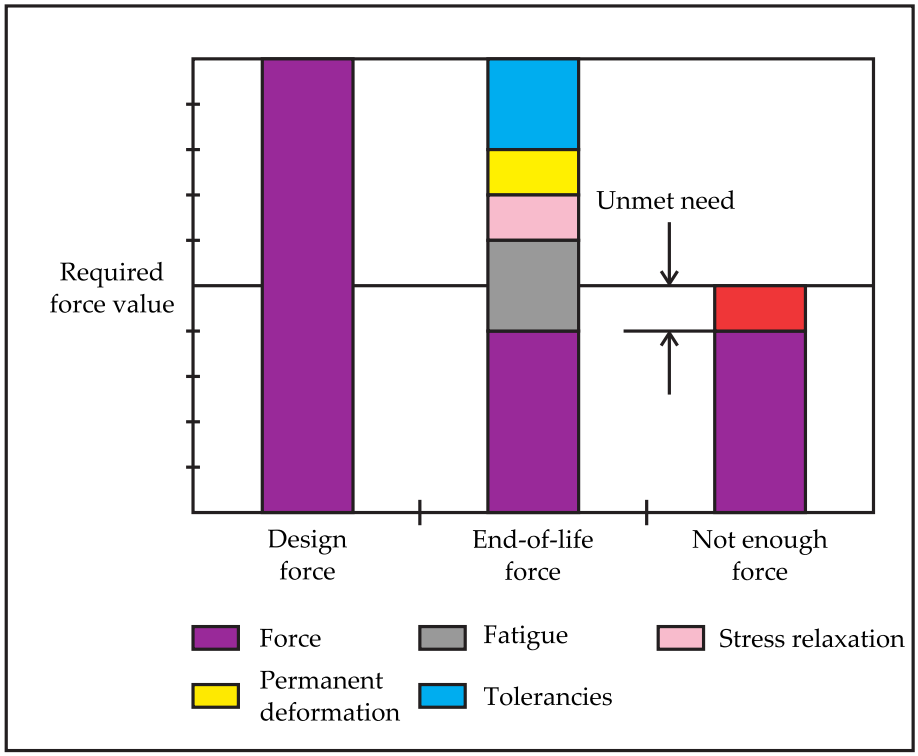

Figure 1.15: Bad selection of the contact material in respect to the contact force [86].

Materials with a higher plastic limit enable higher values of the contact force, whereas materials with smaller stress relaxation over time provide a constant value of the contact force over time. In addition, materials with less fatigue give higher contact force for a specific number of switching cycles or have longer lifetime at a constant value of force.

By appropriate selection of the contact material, it is ensured that contact force at the end–of–lifetime has value beyond the required. Figure 1.16 presents design of the contact from Fig. 1.15 when appropriate material is selected.

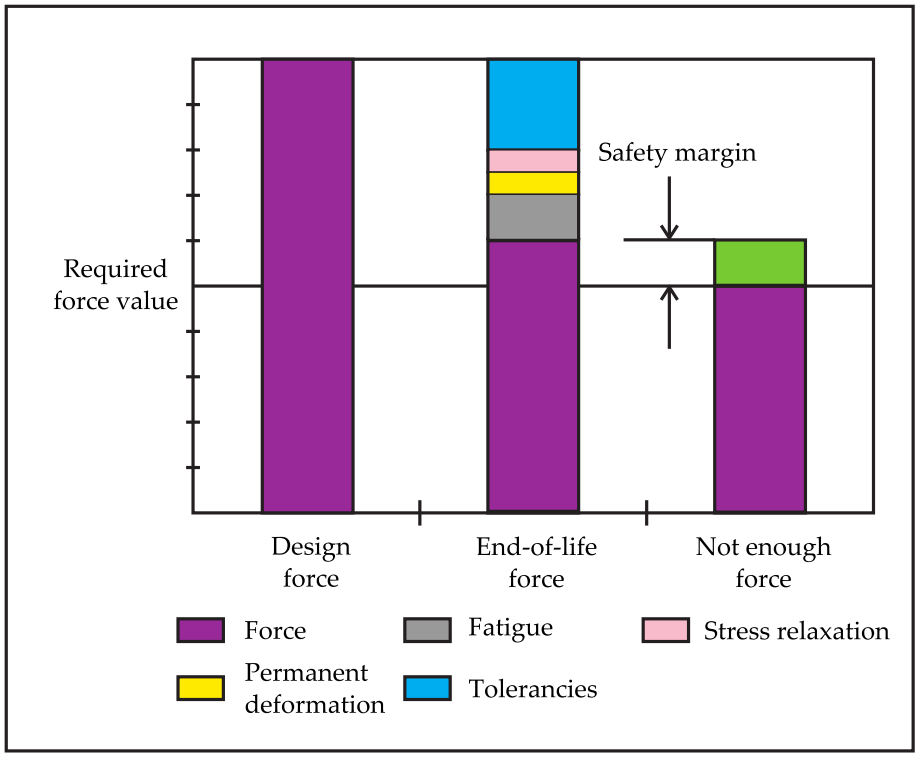

Figure 1.16: Good selection of the contact material in respect to the contact force [86].

Electrical contacts are mounted into the appropriate supporting structure. Characteristics of the supporting structure determine quality of the contact in the electrical sense, significantly affect the sliding and bouncing of the contacts during closing and therefore define the minimum contact force value. In many cases, the supporting structure has the form of a cantilever beam which is fixed at one end and exposed to the contact force at the other end. In the switching devices, surface of such beam is often used as one of the contacting surfaces. Cantilever material, its dimensions, and the method of fixation within the switching device determine the functionality of contacts in mechanical, electrical and thermal domains. Horizontal cantilever beam with specified dimensions and deformation due to applied contact force is shown in Fig. 1.17.

The maximum value of the stress in the cantilever beam is on its upper and lower surfaces at the fixed end. If deformation does not exceed the proportionality limit, the maximum stress value depends on the elastic modulus E_m, and is given by [84]:

$$S_{max} = \frac{3E_m t}{2L^2} \cdot d, \tag{1.2}$$

where t is thickness, L is length, and d is deflection of the beam.

Design of contacts should specify sufficient contact force value F for a given value of the beam deflection. This force is given by:

$$F = \frac{E_m w t^3}{4L^3} \cdot d, \tag{1.3}$$

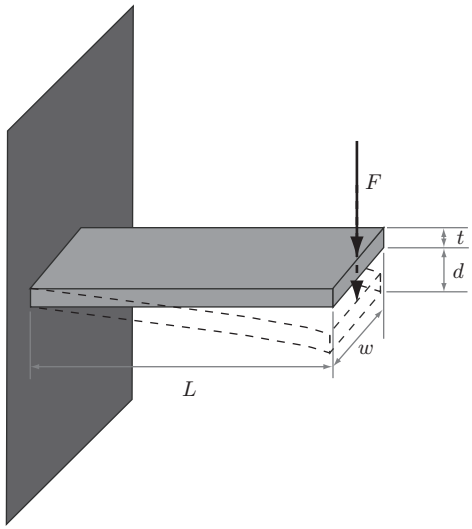

Figure 1.17: Cantilever beam subjected to the contact force [84].

where w is with of the beam.

During the operation, the cantilever beam must not be permanently deformed. Therefore, from the relation (1.2), for the value of the maximum stress which corresponds to the plastic limit of the cantilever material S_{plast}, the allowable deflection d_{plast} is:

$$d_{plast} = \frac{2L^2}{3E_m t} \cdot S_{plast}. \tag{1.4}$$

This deflection value corresponds to the contact force at the plastic limit F_{plast}:

$$F_{plast} = \frac{wt^2}{6L} \cdot S_{plast}. \tag{1.5}$$

Design rules for the supporting structure of contacts in the form of a cantilever beam demand the higher values of allowable deflection and contact force at the plastic limit. Based on the expression (1.4) and (1.5) it could be concluded that the increase in length, width and thickness of the beam can improve its characteristics. On the other hand, modern trends in the design of electrical and electronic devices seek for miniaturization. The value of the contact force is directly proportional to the stress and reduction of contact dimensions imposes increase of the designed stress value in order to maintain the desired value of the contact force. Thus, there is a need for implementation of materials whose mechanical properties overcome geometric constraints. The best solution are materials that have a large ratio of the plastic limit and elastic modulus i.e. a high elastic resilience. In practice, an indicator if the selected material is convenient for cantilever beams is modulus of elastic resilience. It represents the density of strain energy necessary to deform material to the plastic limit. The value of this modulus depends on the shape of the stress – strain curve of the selected material, and its higher value provides better contact force [87].

Chapter 2

3–D simulation of electrical contacts in electrical, thermal and mechanical domains

Prediction of electrical contacts characteristics at a given operating conditions is a complex task, since there is a lack of the precise information on the parameters of functionality and reliability of contacts. Exposed to high currents, multiple and frequent switching cycles, as well as chemically aggressive environment, contacts eventually lose some functionality, and often fail due to various degradation effects described in Section 1.1. To solve some of these problems, the simulation of contacts characteristics in 3–D domain is used as a powerful CAD - CAE (Computer Aided Design - Computer Aided Engineering) tool.

Therefore, the results of simulation of contacts characteristics in electrical, thermal and mechanical domains, with the consideration of all available information on the conditions of their operation, provide the information necessary for successful design and optimization of contacts. It is possible to evaluate the influence of the selected contact material and geometrical and construction details on reliable operation of the contacts and the switching device.

2.1 Considered structures

Design of electrical contacts requires the selection of a certain type, geometry and dimensions of the contact, specification of the contact material, and definition of the minimum contact force or pressure. For the consumer devices, home switches and appliances, where rated current does not exceed 15 A, according to the considerations listed in Section 1.4, solid rivet contacts with a rounded head are the best selection. This shape of contacts is suitable due to the simple riveting procedure with the supporting structure which makes good contact between them. At the same time, direct heating of the supporting structure in the high-temperature current switching processes, and thus the degradation of its elastic properties, is avoided. The rounded head minimizes contact bouncing during the switching. As contact material, based on the characteristics described in Section 1.3 and demands of the market, the silver of 99.99 % purity was selected. Adopted contact force value was 0.15 N/A for currents up to 1 A and 0.2 N/A for higher current values (according to Fig. 1.13 and Fig. 1.14).

Similar considerations apply to electrical contacts for use in power switching devices

with currents up to 40 A. Bimetallic rivet contacts with a rounded head are appropriate. As the basic material was selected copper, and for plating alloys: 90%Ag–10%Ni, 97%Ag–3%Cu (hard silver) and 90%Ag–10%CdO. Contact force in this case has a value of 0.36 N/A.

Dimensions of the considered contacts, indicated in Fig. 1.9, were determined according to fundamentals from Section 1.4 and they are specified in Table 2.1.

Dimension	Value (mm)	
	solid	bimetallic
Head diameter – d_1	3	5; 5.5; 6
Shank diameter – d_2	1.5	2.5
Total head height – k	0.7	1
Contacting layer height – s	-	0.5
Shank length – l	0.7	1
Head rounding radii – r_1; r_2	10; 0.5	10
Head taper angle – α	15°	0°;15°

Table 2.1: Dimensions of the considered rivet contacts.

Given values of the shank length are those existing after riveting of contacts into the supporting structure. Manufactured contacts usually have this value slightly higher. To optimize the size and geometry of bimetallic contacts, and determine the influence of specific effects on their reliability, three different diameters and two taper angles of the contact head were adopted.

Designed contacts are considered within the appropriate supporting structure since their functioning depends on the mounting position. Solid contacts as the supporting structure have a cantilever beam of dimensions (10 mm × 4 mm × 0.5 mm), while for the bimetallic contacts it is (15 mm × 6 mm × 0.5 mm). Copper is selected as a supporting structure material since it is the main conductive material in the switching devices and satisfies the postulates given in Section 1.5. The cross section of the system contact–supporting structure after riveting is presented in Fig. 2.1, with indicated areas where the appropriate mechanical and electrical loads are applied (contacting areas).

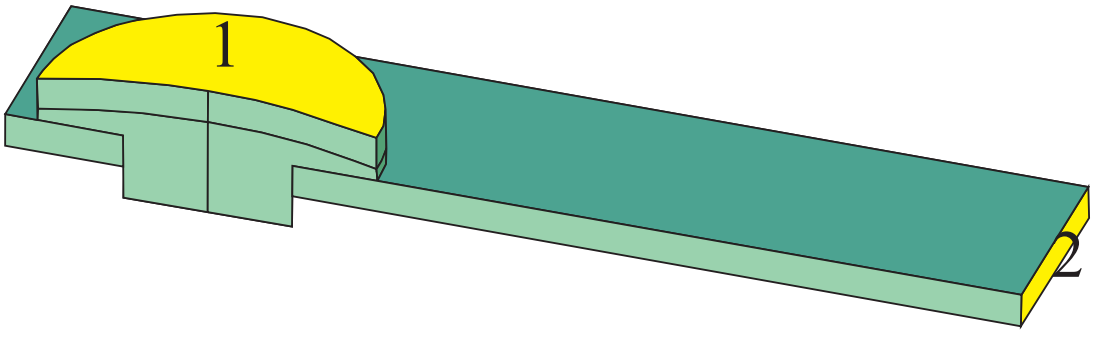

Figure 2.1: The cross section of the system contact–supporting structure with indicated contacting areas.

As mentioned, for manufacturing of solid contacts silver of 99.99 % purity was selected. This material is widely used in applications where low to moderate current values are applied. It has the highest electrical and thermal conductivity, provides low contacting resistance, it is easily worked and soldered, and it is resistant to oxidation

process. On the other hand, silver is easily wear out mechanically and electrically (material transfer, arc discharge, welding), and has a strong tendency towards the formation of sulphides.

The bimetallic contacts have bulk made of copper, whereas the contact head is plated with a layer of the alloy 90%Ag–10%Ni or 97% Ag–3%Cu, obtained by sintering. Since the bimetallic contacts have larger dimensions, due to the application at higher currents, replacing the solid structure by the clad one provides less consumption of silver for 60–70%, and thus the significant economic effects. Alloying of the silver by nickel and copper maintains high electrical and thermal conductivity, low contact resistance, and easy workability, but also preserves reactivity with H_2S and formation of the sulphide layer on the surface. On the other hand, alloying significantly increases the hardness, resistance to wear and welding. The selection of these alloys as plating material is justified by the similarity in characteristics with the alloy 90%Ag–10%CdO, which is common in electrical contacts, but is environmentally unsuitable and requires replacement [88].

2.2 Simulation procedure

3–D simulation of the contacts within the appropriate supporting structure is performed by a computer program that complex physical phenomena treats numerically – ANSYS [89]. This program is based on the Finite Element Analysis (FEA) and use adaptive iterative techniques in order to achieve the optimal solution. Problems that can be simulated include a wide range of analysis, from simple, linear and static to complex, nonlinear and dynamic. Since the operation of electrical contacts involves mutually dependent effects of mechanical, electrical and thermal character, coupled–field analysis by the direct method is used. This analysis is performed by implementing a special type of finite elements. Alternatively, the sequential method with series of successive analyses that belong to different domains can be employed. The coupling between the domains is achieved through the load vector and requires at least two iteration cycles. For this purpose, the ANSYS Multyphysics APDL module that solves the complete set of Maxwell's equations simultaneously with equations of the heat flow and elasticity of the material is used.

2.2.1 Theory of the coupled–field simulation

Electromagnetic phenomena are described by the set of Maxwell's equations:

$$rot\,\vec{H} = \vec{J} + \frac{\partial \vec{D}}{\partial t}, \tag{2.1}$$

$$rot\,\vec{E} = -\frac{\partial \vec{B}}{\partial t}, \tag{2.2}$$

$$div\,\vec{D} = \rho_s, \tag{2.3}$$

$$div\,\vec{B} = 0, \tag{2.4}$$

where $\vec{H}$ is magnetic field strength, $\vec{E}$ is electric field, $\vec{D}$ is electric displacement, $\vec{B}$ is magnetic field, $\vec{J}$ is current density, ρ_s is charge density and t is time. This set of

equations is accompanied by the relations that describe behaviour of the materials:

$$\vec{J} = \overleftrightarrow{\sigma}\,[\vec{E} + \vec{v} \times \vec{B}], \tag{2.5}$$

$$\vec{D} = \overleftrightarrow{\epsilon_e}\,\vec{E}, \tag{2.6}$$

$$\vec{B} = \overleftrightarrow{\mu}\,\vec{H}, \tag{2.7}$$

where $\overleftrightarrow{\sigma}$ is electric conductivity tensor, $\overleftrightarrow{\epsilon_e}$ is permittivity tensor, $\overleftrightarrow{\mu}$ is permeability tensor and $\vec{v}$ is velocity.

In the electrically conductive mediums, where magnetic domain is not considered, equations (2.1)–(2.4) are reduced to the continuity equation in the expanded form:

$$\frac{\partial J_x}{\partial x} + \frac{\partial J_y}{\partial y} + \frac{\partial J_z}{\partial z} = -\frac{\partial \rho_s}{\partial t}. \tag{2.8}$$

Electrical connections between the components of the current density J_x, J_y, J_z and the components of the electric field E_x, E_y, E_z are expressed by transport equations:

$$J_x = \sigma_{xx} E_x, \tag{2.9}$$

$$J_y = \sigma_{yy} E_y, \tag{2.10}$$

$$J_z = \sigma_{zz} E_z, \tag{2.11}$$

where $\sigma_{xx}, \sigma_{yy}, \sigma_{zz}$ are values of the electrical conductivity in x, y and z directions, respectively.

Heat flow equation in the expanded form incorporates the first law of thermodynamics and the Fourier's law as:

$$\rho c \left(\frac{\partial T}{\partial t} + v_{qx} \frac{\partial T}{\partial x} + v_{qy} \frac{\partial T}{\partial y} + v_{qz} \frac{\partial T}{\partial z} \right) = q_v + \frac{\partial}{\partial x} \left(k_x \frac{\partial T}{\partial x} + k_y \frac{\partial T}{\partial y} + k_z \frac{\partial T}{\partial z} \right), \tag{2.12}$$

where ρ is material density, c is material specific heat, q_v is heat generation rate per unit of volume, v_{qx}, v_{qy}, v_{qz} are components of a heat transfer rate, k_x, k_y, k_z are thermal conductivities in x, y and z directions, respectively, while $T = f(x, y, z, t)$ is temperature. Equation (2.12) is accompanied by the three possible boundary conditions:

1. specified temperature value at the considered surface;
2. specified heat flow from the considered surface;
3. specified convection conditions at the considered surface (Newton's law of cooling) by the relation:

$$\vec{q} \circ \hat{n} = h_f (T_S - T_B), \tag{2.13}$$

where $\vec{q}$ is heat flux, h_f is convection coefficient, T_S is temperature of the surface, T_B is ambient temperature, and $\hat{n}$ is unity vector of the considered surface.

Thermal and electrical domains are connected through the heat generation rate per unit of volume, which also includes the heat generation due to current flow (Joule's heating), and through the temperature dependence of the electrical conductivity $\sigma = f(T)$.

Structural domain of the analysis, for linear materials, is described by the elasticity equations which give the relation between stress and strain due to tension, compression, and shear. In their explicit form they represent a system of six equations:

$$\epsilon_x = \alpha_x \Delta T + \frac{S_x}{E_{m_x}} - \frac{\nu_{xy} S_y}{E_{m_x}} - \frac{\nu_{xz} S_z}{E_{m_x}}, \tag{2.14}$$

$$\epsilon_y = \alpha_y \Delta T - \frac{\nu_{xy} S_x}{E_{m_x}} + \frac{S_y}{E_{m_y}} - \frac{\nu_{yz} S_z}{E_{m_y}}, \tag{2.15}$$

$$\epsilon_z = \alpha_z \Delta T - \frac{\nu_{xz} S_x}{E_{m_x}} - \frac{\nu_{yz} S_y}{E_{m_y}} + \frac{S_z}{E_{m_z}}, \tag{2.16}$$

$$\epsilon_{xy} = \frac{S_{xy}}{G_{xy}}, \tag{2.17}$$

$$\epsilon_{yz} = \frac{S_{yz}}{G_{yz}}, \tag{2.18}$$

$$\epsilon_{xz} = \frac{S_{xz}}{G_{xz}}, \tag{2.19}$$

where ϵ_x, ϵ_y, ϵ_z are strain values, S_x, S_y, S_z are stress values, α_x, α_y, α_z are thermal expansion coefficients, E_{m_x}, E_{m_y}, E_{m_z} are elastic moduli in x, y and z directions, respectively, while ϵ_{xy}, ϵ_{yz}, ϵ_{xz} are shear strain values, S_{xy}, S_{yz}, S_{xz} are shear stress values, G_{xy}, G_{yz}, G_{xz} are components of the shear modulus, and ν_{xy}, ν_{yz}, ν_{xz} are Poisson's coefficients in xy, yz and xz planes, respectively. Relations (2.14)–(2.16) connect thermal and mechanical domains by thermal expansion coefficients and temperature difference $\Delta T = T - T_{ref}$, where T_{ref} is the reference temperature without stress effects. Shear moduli in isotropic materials are calculated based on the relation:

$$G_{xy} = G_{yz} = G_{xz} = \frac{E_{m_x}}{2(1 + \nu_{xy})}. \tag{2.20}$$

2.2.2 Simulation procedure steps

Simulation procedure in ANSYS Multiphysics APDL module incorporates three basics steps:

1. construction of the model and mesh generation;
2. specification of the boundary conditions and loads, and problem solving;
3. results overview.

These steps are implemented through an appropriate user interface, which includes setting of the global simulation parameters, preprocessing, problem solving and post-processing. Figure 2.2 shows detailed steps of the simulation procedure.

Naming simulation is a recommended, but not required step in the simulation. Defining the applied system of units is necessary, given that the program can work with arbitrary system of units if they are consistent for all of the input variables.

Preprocessing is done through a specific module and the main part is setting the type of finite elements for simulation and defining simulation real constants. Library of elements contains over 150 types of finite elements grouped into 25 categories. Element type is defined by its dimensionality (1–D, 2–D and 3–D) and by the set of freedom degrees that determine the simulation domain. Real constants of element are properties

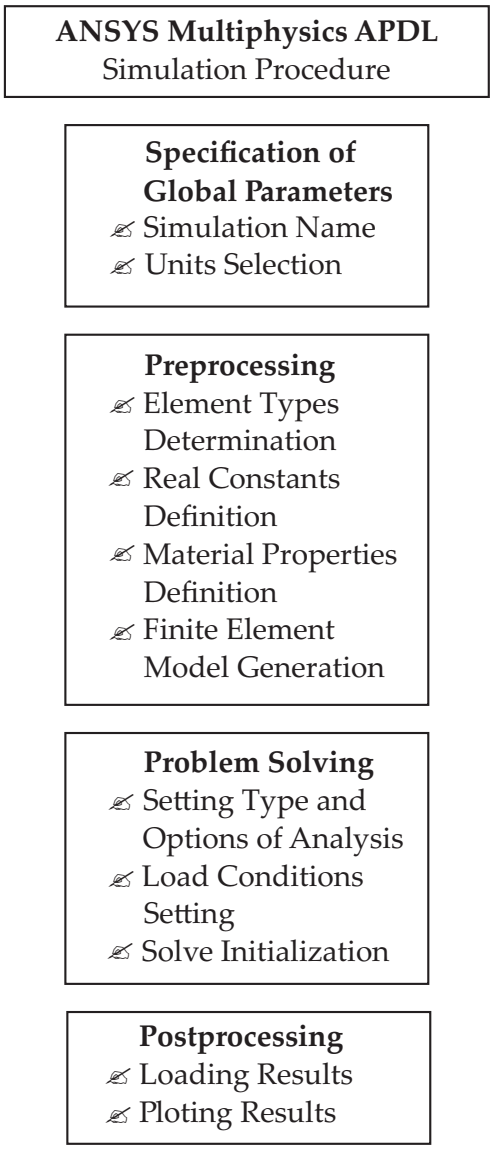

Figure 2.2: Simulation procedure steps in ANSYS Multiphysics APDL module.

that depend on its type, but are not necessary for all elements. The different elements of the same type may have different values of real constants.

The preprocessing procedure defines the properties of the materials that may be linear (constant or temperature-dependent, isotropic or orthotropic) and nonlinear (presented in tabular, matrix, or approximating format). Each set of material properties has a unique reference number, so that for the same material can be defined several specific sets of properties. The properties of materials are classified as physical, structural (mechanical), thermal, electrical and magnetic.

Generation of the finite element model of the simulated structure involves definition of the nodes and elements that adequately describe the considered structure. There are two ways to generate the finite element model: solid modeling and direct modeling. In solid modeling, the geometric shape of the structure is described, while the program performs automatic generation of the mesh within it, basing on the defined shape and size of elements. In direct modeling, location of the mesh nodes and links between them are given. Modeling procedure in the program ANSYS is supported by the possibility to import a mesh of structures generated in another CAD program.

Problem solving procedure initially requires definition of the analysis type basing on the load conditions and desired results of the simulation. The available types of analysis are: steady–state, transient, harmonic, modal, spectral, substructural and buckling analysis. Analysis options allow its customization to the considered problem and include a solving method, numerical integration method, taking of certain physical phenomena into consideration or not.

The load conditions in ANSYS include boundary conditions, as well as externally applied or internally generated loads. The basic division is into six categories: constrains of the freedom degrees, forces, surface load, volume load, inertial and coupled field load. Most of the loads can be applied on the solid model (the keypoints, lines and areas) or on the finite element model (the nodes and elements). Load conditions are related with terms *load step* (set of loads for which is solution), and *load substep* (load segment within a single step). Load step options define the number of substeps, time at the end of a step, and format of the output data. Depending on the type of analysis, load step options may not be required as input parameters. Type of analysis, its options, and load conditions can be also defined through the preprocessing module.

During the solution step, program takes information about the model and loads from the appropriate database and solves the problem. The results are stored in the specified file or database.

The overview of the simulation results is performed by two postprocessing modules. The module of general purpose enables overview of the results from specified load substep in the whole system or in its selected part. For the interpretation of the results are available contour plot, tabular, and deformed shape representation. The chronological postprocessing module provides an overview of the results in certain points of the model during all load substeps. Graphical representation includes diagram of the considered variable values over time, while numerical results are of the tabular type. The combination of both postprocessing modules provides animated view of the selected variable through the time within the entire simulated structure.

2.2.3 Simulation parameters

Simulation of electrical contacts within the appropriate supporting structure is performed for the steady–state regime and, due to coupled field analysis, it includes nonlinear iterative techniques such as Newton–Raphson's method. It was selected SOLID98 type of finite elements that allows 3–D electromagnetic, thermal, structural and piezoelectric coupled analysis. This type of elements is a tetrahedron defined by 10 nodes with up to 6 freedom degrees. The geometry of SOLID98 element type with denoted nodes is shown in Figure 2.3.

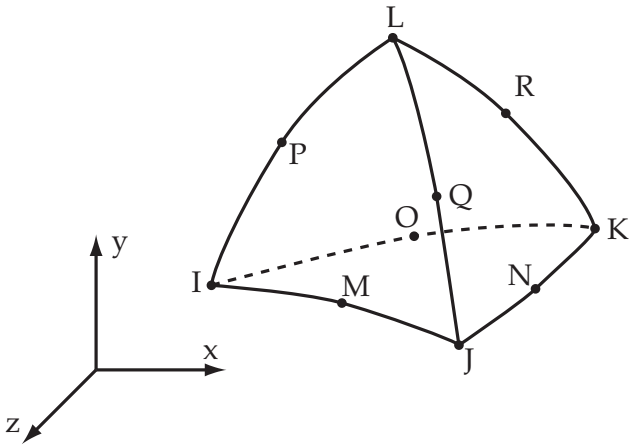

Figure 2.3: The geometry of SOLID98 element type [89].

The freedom degrees in the nodes are: displacements in x, y and z directions, temperature, electric potential and magnetic scalar potential. Load values in the nodes are determined by the freedom degrees and by the values of the applied force, heat flow, electrical current or charge, and magnetic flux. Element loads include values of the pressure, heat flux or convection, radiation and Maxwell's force. Output variables that this type of element provides are: values of the defined freedom degrees, reaction forces, heat flow, electrical current and magnetic flux in the nodes, and the values of the stress, strain, electric potential and Joule's heat within the solid model. In the considered analysis magnetic domain is not of the interest and magnetic quantities are not calculated. The SOLID98 type of finite elements does not require setting of the real constant values.

Input preprocessing parameters of the simulated structure are specified through the user interface in steps indicated in Fig.2.4.

The finite element model is generated by the solid modeling, while values of the physical, mechanical, electrical and thermal parameters of the contact materials used in the simulation are shown in Table 2.2.

The loads of the simulated structures have been set through the symmetry boundary conditions, mechanical constrains of the structure through freedom degrees, values of the surface electrical and mechanical loads, and the thermal parameters of cooling.

Due to the symmetry of the considered structures, simulations were performed for half of the system bimetallic contact–supporting structure which is shown in Fig. 2.1. The section plane is the boundary condition of symmetry. Mechanical constrain in solid Ag contacts is only on the contacting area No. 2. Bimetallic contacts are considered with two types of the mechanical constrain (fixing of the supporting structure): a) only on the contacting area No. 2; b) on the contacting area No. 2 and on the bottom of the cantilever which prevents its bending when the contact force is applied. Electrical load

Material	Cu	Ag	90%Ag–10%Ni	97%Ag–3%Cu	90%Ag–10%CdO
Density (kg/m^3)	8960	10500	10300	10400	10200
Joung's modulus (GPa)	130	83	95	84	80
Poisson's coefficient	0.34	0.37	0.36	0.37	0.36
Hardness by Vickers (MN/m^2)	40	26	65	45	70
Electrical resistivity (Ωm)	$1.69 \cdot 10^{-8}$	$1.62 \cdot 10^{-8}$	$1.89 \cdot 10^{-8}$	$1.75 \cdot 10^{-8}$	$2.08 \cdot 10^{-8}$
Thermal coefficient of electrical resistivity (1/K)	$4.29 \cdot 10^{-3}$	$4.10 \cdot 10^{-3}$			
Thermal expansion coefficient (1/K)	$16.5 \cdot 10^{-6}$	$18.9 \cdot 10^{-6}$	$18.9 \cdot 10^{-6}$	$18.9 \cdot 10^{-6}$	$18.9 \cdot 10^{-6}$
Thermal conductivity (W/mK)	401	419	310	350	330

Table 2.2: Physical, mechanical, electrical and thermal parameters of the considered contact materials [71, 72, 74].

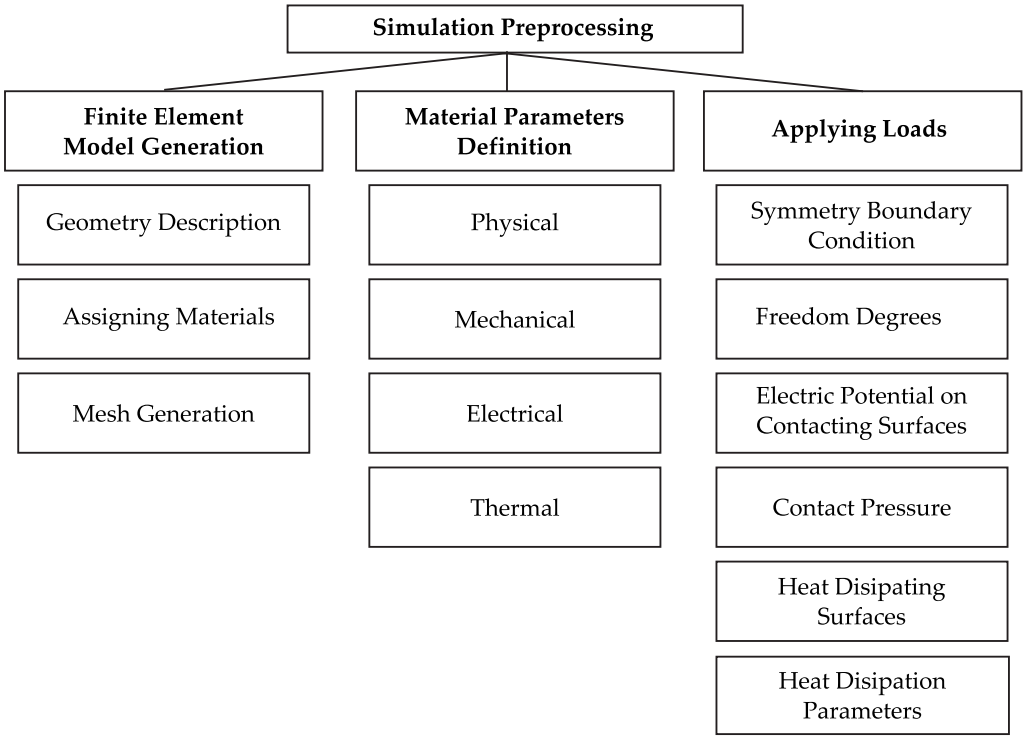

Figure 2.4: Steps of the preprocessing procedure.

is defined by the value of the electric potential at the contacting area No. 2, which is kept at zero value, while the value of the current flowing through the contacting area No. 1 is changed in the range from 0.15 A to 15 A with a solid, and 0.16 A to 45 A with bimetallic contacts. This corresponds to values of the potential difference at the contacting areas of $1{\cdot}10^{-5} - 1 \cdot 10^{-3}$ V in solid, and $1{\cdot}10^{-5} - 3 \cdot 10^{-3}$ V in bimetallic contacts. Mechanical load is defined by the contact pressure applied on the contacting area No. 1. Contact pressure values are equivalent to the contact force of 0.15 N/A for currents up to 1 A and 0.2 N/A for higher current values in solid contact, and 0.36 N/A for all current values in bimetallic contacts. Parameters of the thermal load are determined by the convection from free surfaces of the contacts and supporting structure. It is assumed that the system is in air with a temperature of 300 K, and that the value of the convection coefficient is 28.4 W/m^{2}K.

2.3 Distribution of electrical, thermal and mechanical quantities

As a result of 3–D simulations, distributions of various electrical, thermal and mechanical quantities in electrical contacts were obtained. Quantities that are important for the design and optimization of electrical contacts are the values of structural deformation, temperature, electric potential, electric current density (equivalent to the density of the generated Joule's heat) and equivalent stress. Depending on the nature, quantities are graphically presented in contour or vector form.

2.3.1 Solid Ag contacts

Solid Ag contacts are considered within supporting structure in the form of a conductive elastic cantilever beam described in Section 1.5, made of copper and fixed at the contacting area No. 2. Structural deformation of the system under applied contact force of 0.12 N (current of 0.8 A) is shown in Fig. 2.5.

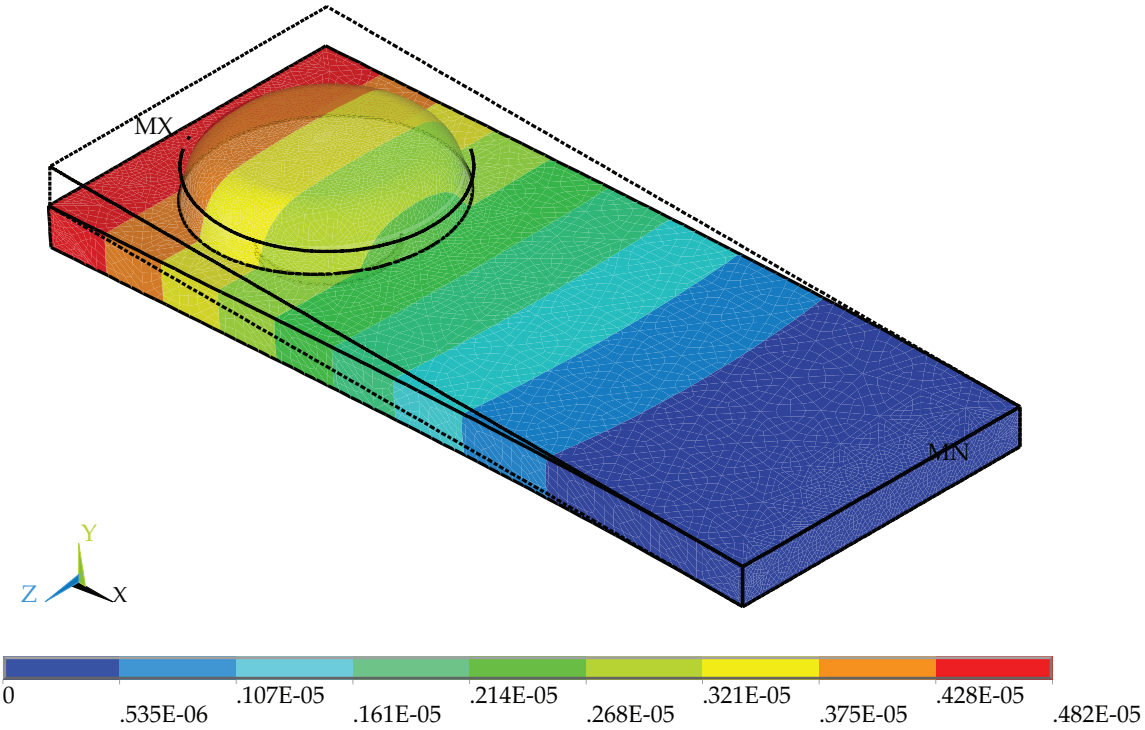

Figure 2.5: Structural deformation of the system at applied current of 0.8 A

Deformation of the system is determined by the fixed area of the supporting structure, and values are defined primarily by elastic properties of the used materials. Undeformed system is also shown in the figure, and maximum bending of the free end of the cantilever beam is 4.8 μm. Bending of the beam in the region where contact force acts over the contact body is calculated from the expression (1.3) as 3.8 μm. From the distribution in Fig. 2.5 bending value is 3.5 μm. The difference is result of actually lower value of the force acting on the beam due to its distribution, as well as the elastic properties of the contact material (in this case silver). Deformation of the system is qualitatively the same for moderate values of the applied current, with adequately increased quantitative values. Changes of dimensions due to the thermal expansion are manifested only at high applied currents. For low and moderate current values these changes are few orders of magnitude less than the deformation due to mechanical effects, and do not affect the considered distribution.

Temperature distribution in the structure depends on the load conditions, temperature coefficient of the electrical resistivity and thermal conductivity of material, free surfaces of the system, and mechanisms of the heat dissipation. Simulations have shown that, due to the high electrical and thermal conductivity of used materials and large areas of the system from which the heat is dissipated, the distribution of temperature in the contacts for the given loads can be considered as constant. As an example, in Fig. 2.6 is presented temperature distribution in the system with applied current of 10 A and

contact force of 2 N. The observed range of temperature is only 0.01 K (at low currents it is even smaller).

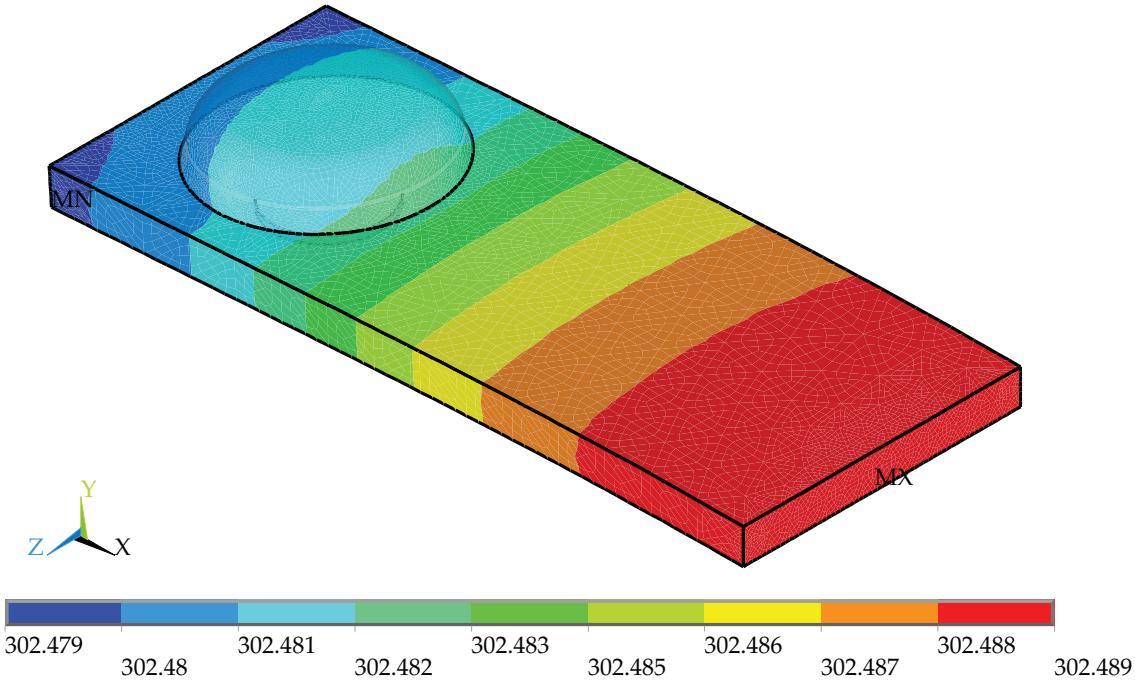

Figure 2.6: Temperature distribution in the system with solid Ag contact at applied current of 10 A.

Electric potential distribution in the system at current of 0.8 A is shown in Fig. 2.7. Potential difference between the contacting areas is 5.4 $\cdot 10^{-5}$ V. It is evident that equipotential surfaces are determined by specific geometry of the structure and high electrical and thermal conductivities of contact materials. Distributions of the electric potential at higher currents are qualitatively identical to one presented in Fig. 2.7, with adequately modified values at the contacting area No. 1.

Vector representation of the current density distribution in the system with solid Ag contact at applied current of 0.8 A is shown in Fig. 2.8. Distribution at the cross section is shown to distinguish areas of the greatest current density, which are also areas of maximal Joule's heating. These areas are "hot" spots in the structure where initialisation of various thermally activated degradation processes, such as welding and migration of the metal, can be expected. In the considered structure these areas are in the central part of the contact head and at the joint of the head and the shank with current density value of $6 \cdot 10^5$ A/m^2. Distributions are identical for higher current values with proportional increase of the current density vector magnitude.

Contact pressure applied on the contact head and thermal expansion of the material caused by Joule's heating generate equivalent stress in the system. Distribution of the equivalent stress at applied current of 0.8 A (contact force of 0.12 N) is shown in Fig. 2.9. Displacement of such a system is limited by the fixed contacting surface No. 2 and maximum stress is in the supporting structure. In accordance with the considerations from Section 1.5, maximum stress occurs on the top and bottom surfaces of the cantilever beam close to the fixed edge and has a value of 6 MPa. For the higher current values, equivalent stress distribution is identical, with higher maximum value (for the applied current of 10 A maximum value of the stress is 100 MPa).

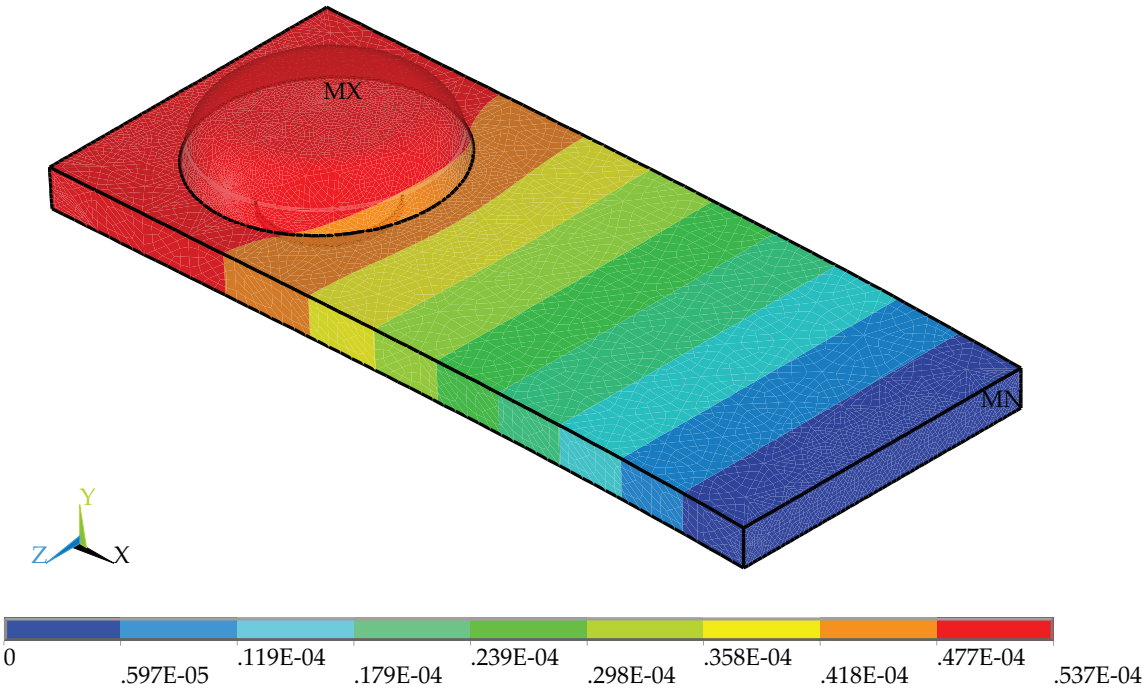

Figure 2.7: Electric potential distribution in the system with solid Ag contact at applied current of 0.8 A.

Distribution of equivalent stress in the contact is presented in Fig. 2.10 in details. The maximum of the equivalent stress is at the edge of contact close to the supporting structure in the direction of the maximum current density with a value of 1.4 MPa. Simulation showed that this area in contact has the highest equivalent stress value for the whole range of applied currents. At the operating conditions, equivalent stress in the contacts additionally contains residual stress as a result of the riveting process. The value of the residual stress can not be precisely determined, and it is included in tolerances of the manufacturing processes.

2.3.2 Bimetallic contacts

Bimetallic contacts were considered within the supporting structure in the form of a copper cantilever beam of dimensions (15 mm × 6 mm × 0,5 mm) with two possible mechanical constrains: a) only at the contacting surface No. 2, and b) at the contacting surface No. 2 and at the bottom surface of the beam. In the second case, thermal cooling of the system from the bottom surface of the beam is suppressed. Contacts with alloys 90%Ag–10%Ni, 97%Ag–3%Cu (solid silver), and 90%Ag–10%CdO as plating materials were considered.

Displacement of the system with bimetallic contact of 5 mm head diameter and Ag–Ni as the plating material is presented in Fig. 2.11. It is determined by the fixed contact area No. 2, while the contact area No. 1 is subjected to the contact force 10.8 N, which corresponds to the current of 30 A.

Maximum bending of the beam free end is approximately 1 mm. As in solid contacts, the supporting structure is an example of elastic cantilever beam. Its bending in the region where contact force acts over the contact body is calculated from the expression (1.3) as 764 μm. From the distribution presented in Fig. 2.11, value of the bending is

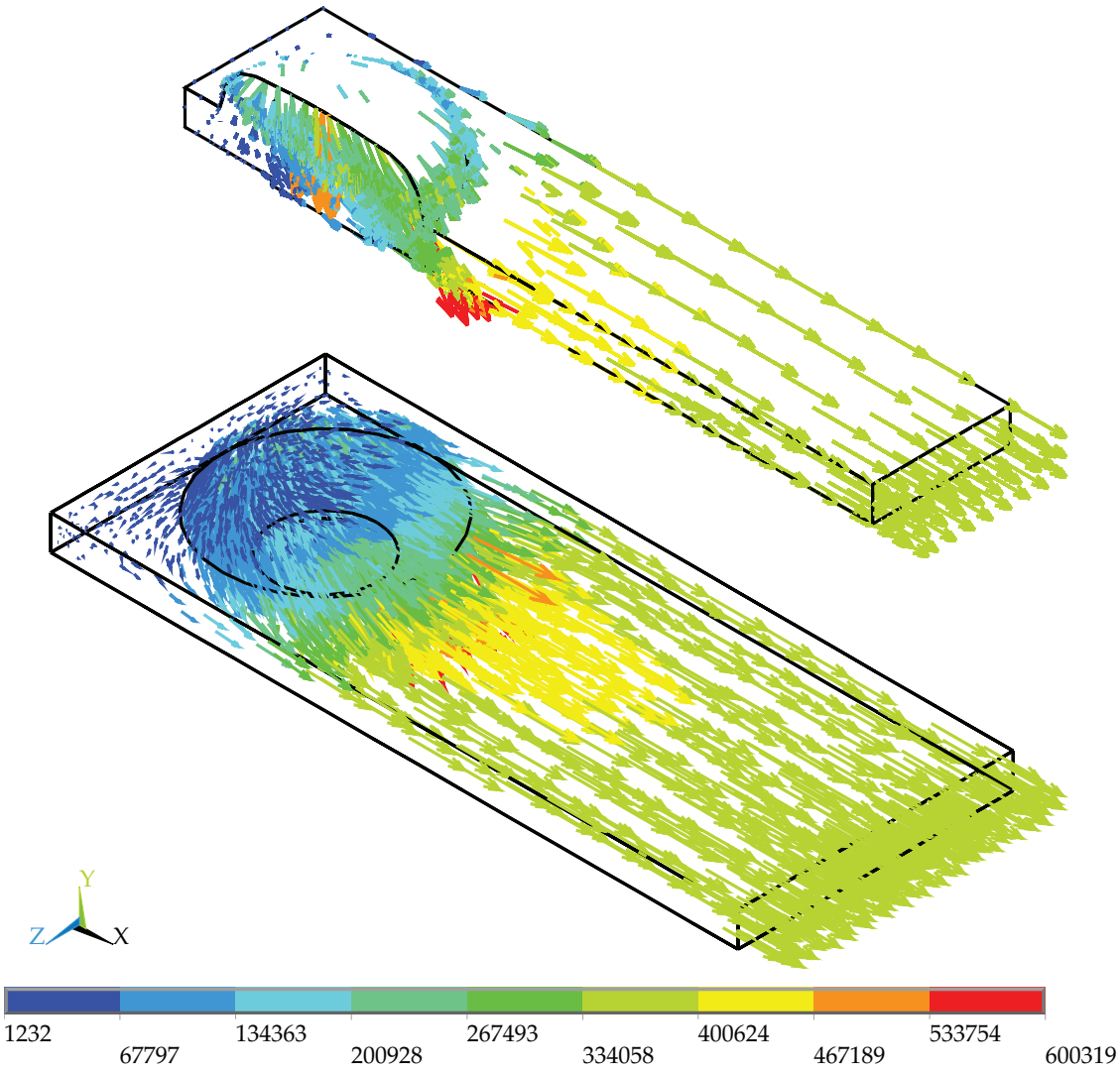

Figure 2.8: Vector representation of the current density distribution in the system with solid Ag contact at applied current of 0.8 A.

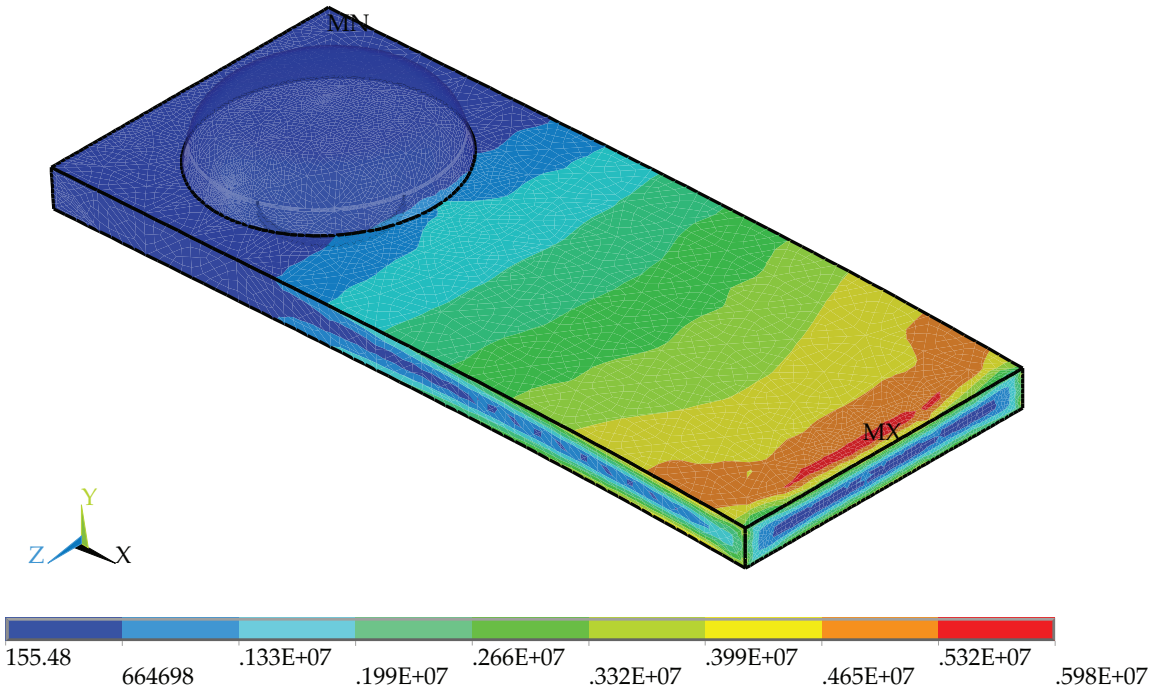

Figure 2.9: Equivalent stress distribution in the system with solid Ag contact at applied current of 0.8 A.

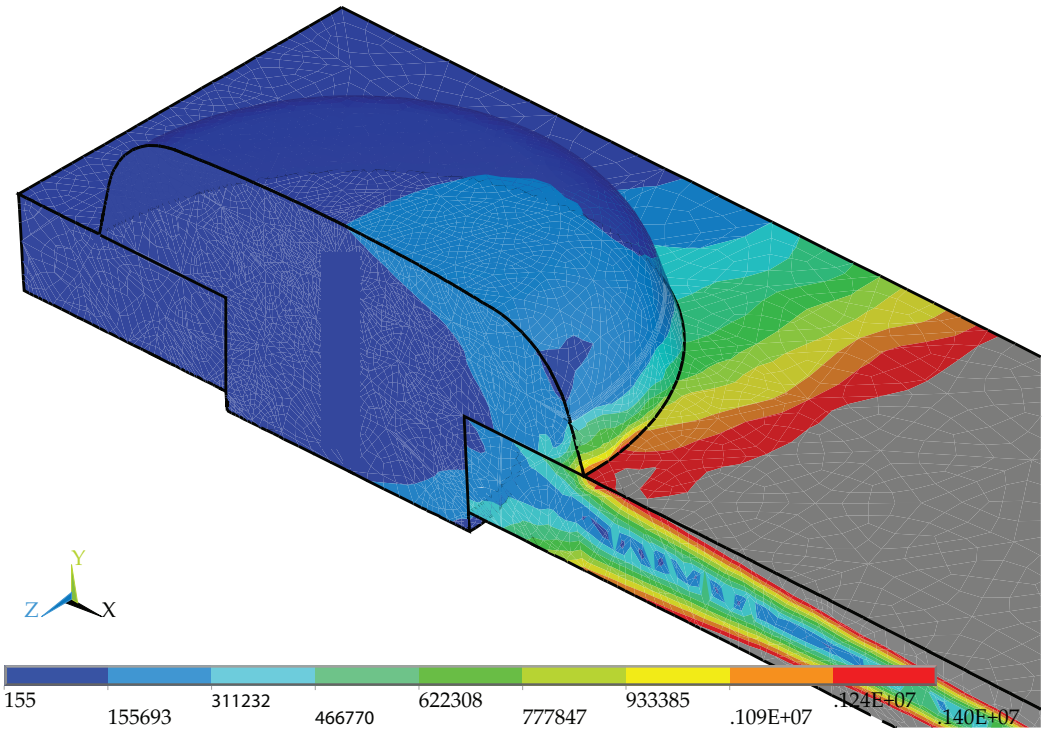

Figure 2.10: Equivalent stress distribution in the solid Ag contact at applied current of 0.8 A.

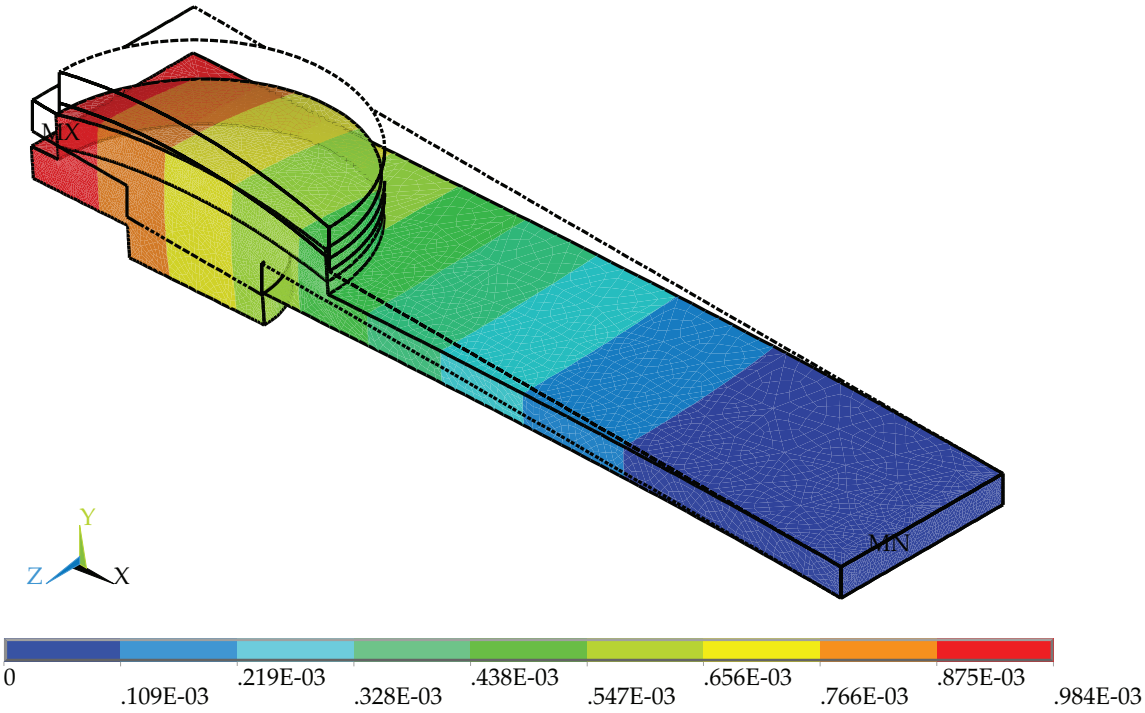

Figure 2.11: Displacement of the system with bimetallic Cu/Ag–Ni contact at applied current of 30 A.

710 μm. The difference between the theoretical and simulated values originates from actually lower force value acting on the beam due to its distribution, as well as from the elastic properties of the contact body and plating materials (copper and alloy Ag–Ni). Deformation is primarily induced by the mechanical stress, while the effects of thermal expansion are of the second order. On the other hand, in systems where the beam is additionally fixed at the bottom surface, there is a redistribution of the contact force from the contacting area No. 1 to the entire structure of the contact, and the effects of deformation due to the contact pressure and thermal expansion are equivalent. Displacement of the system with bimetallic Cu/Ag–Cu contact at the applied current of 30 A and with two fixed surfaces is presented in Fig. 2.12. This displacement is of the order of μm.

Systems with bimetallic contacts, as in the case with solid contacts, have uniform temperature distribution. Corresponding value of the temperature in contacts depends on the plating material, applied current, and fixing of the supporting structure.

Distribution of the electric potential in the system with bimetallic Cu/Ag–Ni contact with applied current of 30 A is shown in Fig. 2.13. This distribution is determined by the geometry of the system and potential difference between the contacting areas is 1.95 mV. In systems with two fixed surfaces there is identical distribution of potential with a slightly different values due to changed thermal cooling conditions.

Distribution of the current density, and by analogy distribution of the Joule's heat, in systems with bimetallic contacts for both fixing methods has an almost identical form for the whole range of considered currents. Distribution of the generated Joule's heat for the system with bimetallic Cu/Ag–Cu contact and two fixed surfaces at applied current of 30 A is shown in Fig. 2.14.

Area of the most generated heat (at the same time area with the maximum current density) is at the contact head near the junction with the supporting structure and has a value of $5.5 \cdot 10^6$ W/m^3. This is an area where thermally–generated degradation effects

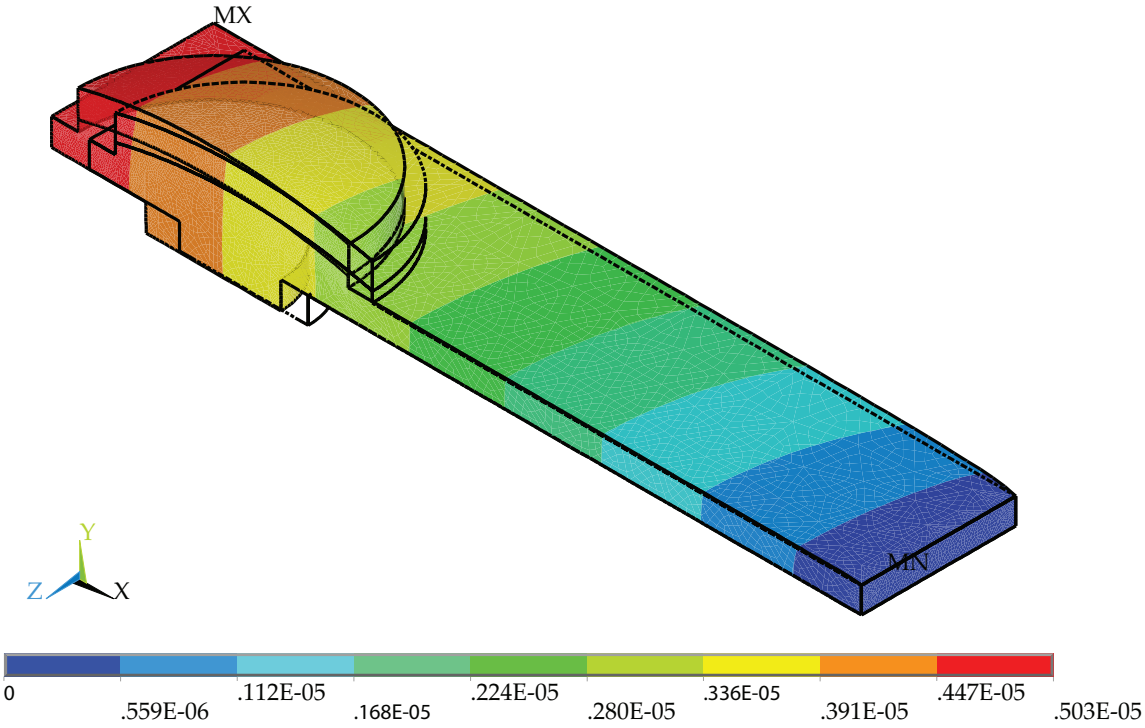

Figure 2.12: Displacement of the system with bimetallic Cu/Ag–Cu contact with two fixed surfaces at applied current of 30 A.

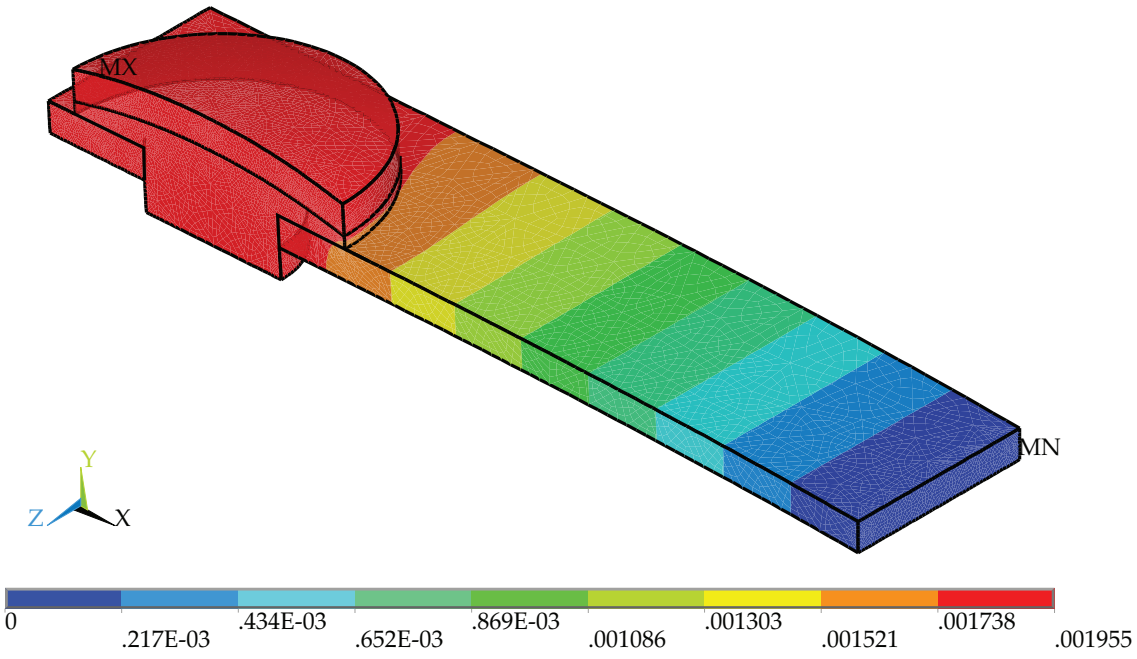

Figure 2.13: Electric potential distribution in the system with bimetallic Cu/Ag–Ni contact at applied current of 30 A.

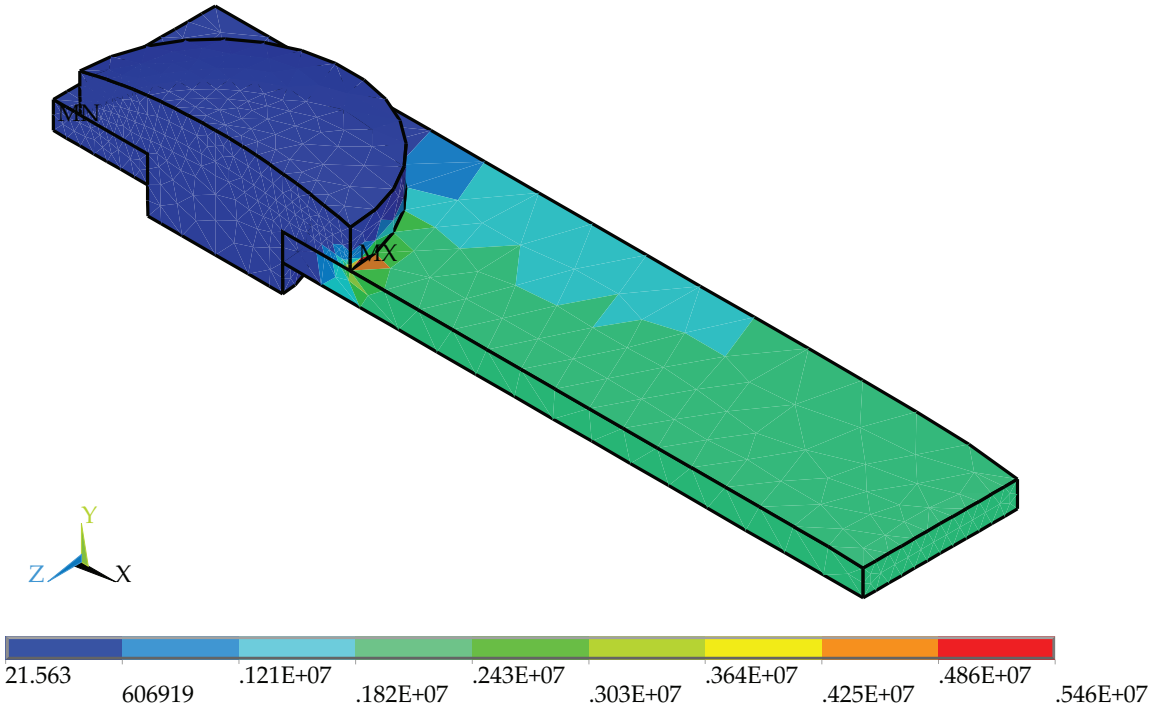

Figure 2.14: Generated Joule's heat distribution for the system with bimetallic Cu/Ag–Cu contact and two fixed surfaces at applied current of 30 A.

and distortion of the structure may occur.

Equivalent stress in the systems with fixed contacting surface No. 2 is primarily a consequence of the contact pressure and has the highest value in the supporting structure. This can be observed from Fig. 2.15 which represents distribution of the equivalent stress in the system with bimetallic Cu/Ag–Ni contact and applied current of 30 A. In this case, the maximum equivalent stress is about 650 MPa, which exceeds the plastic limit of copper, and in designing of the switching circuits this must be taken into account.

For the determination of the reliable operation time of electrical contacts, the areas and values of the maximum equivalent stress in contacts as presented in Fig. 2.16 are important. The maximum of the equivalent stress is on the edge of the contact head close to the supporting structure in the direction of the maximum current density and its value is 220 MPa. As in the case of solid contacts, simulations indicate that this is the area of maximum equivalent stress for the entire range of considered currents.

On the other hand, in systems with two fixed surfaces, the area of maximum equivalent stress depends on the value of the applied current, as shown in Figs. 2.17 and 2.18. For low current values maximum equivalent stress is in the contact shank. It is primarily result of the application of contact pressure on materials with different elastic properties, since electro–thermal expansion is neglectable. At higher values of the applied current (in Fig. 2.18 it is the value of 30 A), the effects of electro–thermal expansion produce that maximum stress is at the edge of the contact head with a value of 12 MPa.

In bimetallic contacts, higher values of the equivalent stress are in the part of the body made of copper near the plating. Such stress distribution is a consequence of joining materials with the different elastic parameters and strength, and in long–term exploitation of contacts it may result in a separation of the plating and loss of the functionality. This is especially important in contacts with the modified geometry (head taper angle of 15°), since the maximum equivalent stress for medium and higher current

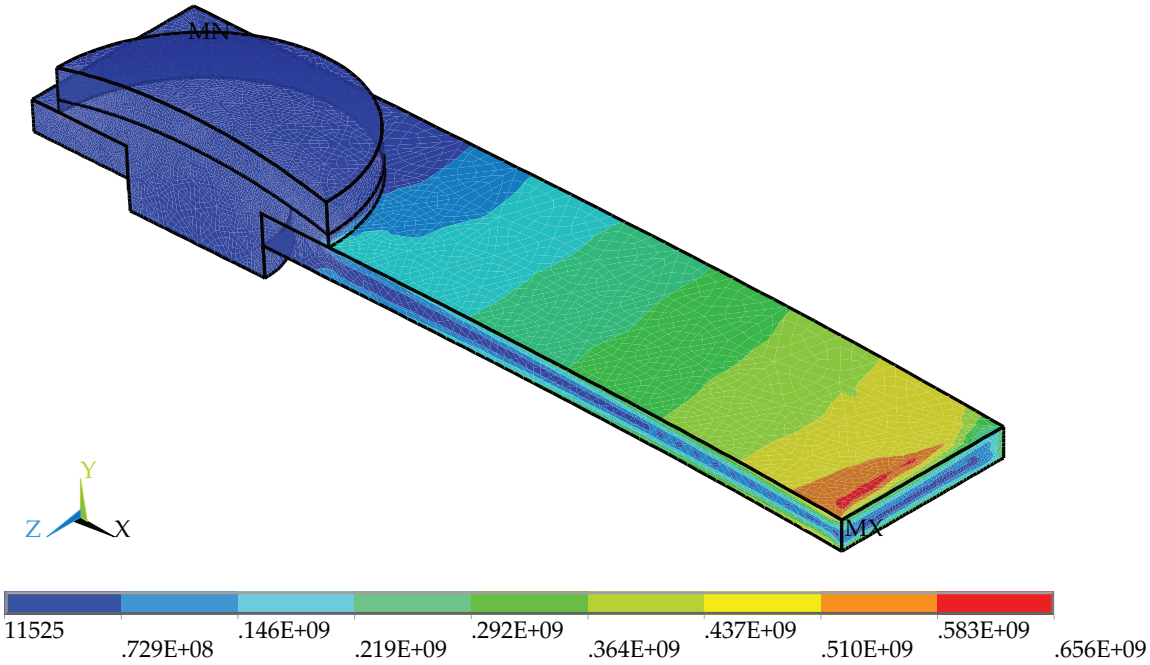

Figure 2.15: Equivalent stress distribution in the system with bimetallic Cu/Ag–Ni contact at applied current of 30 A.

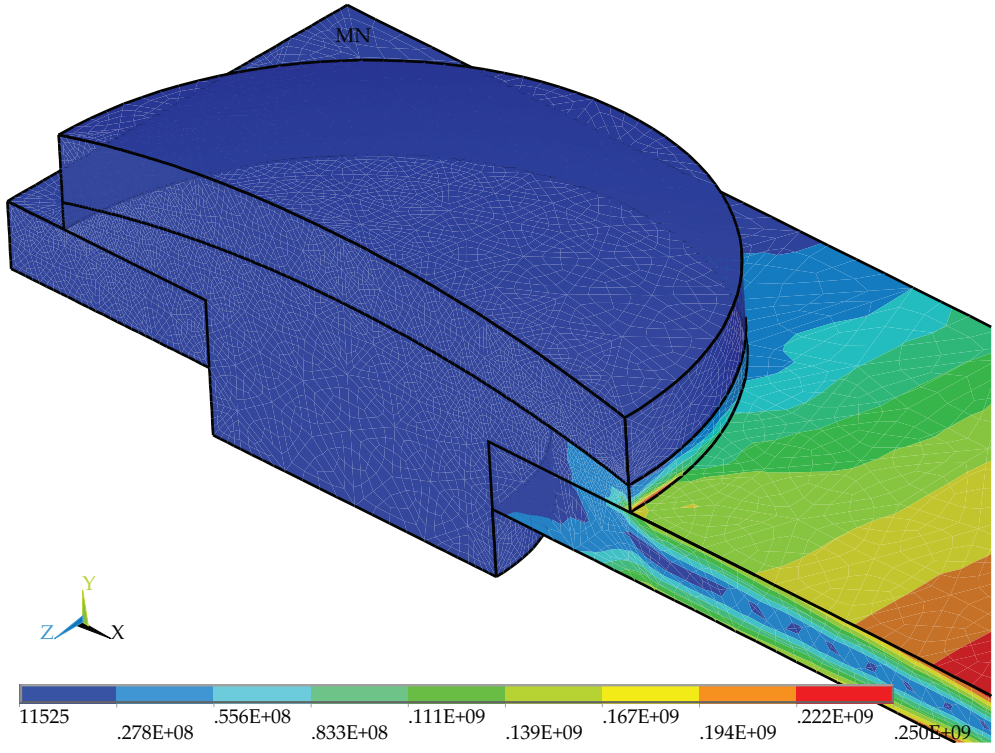

Figure 2.16: Equivalent stress distribution in the bimetallic Cu/Ag–Ni contact at applied current of 30 A.

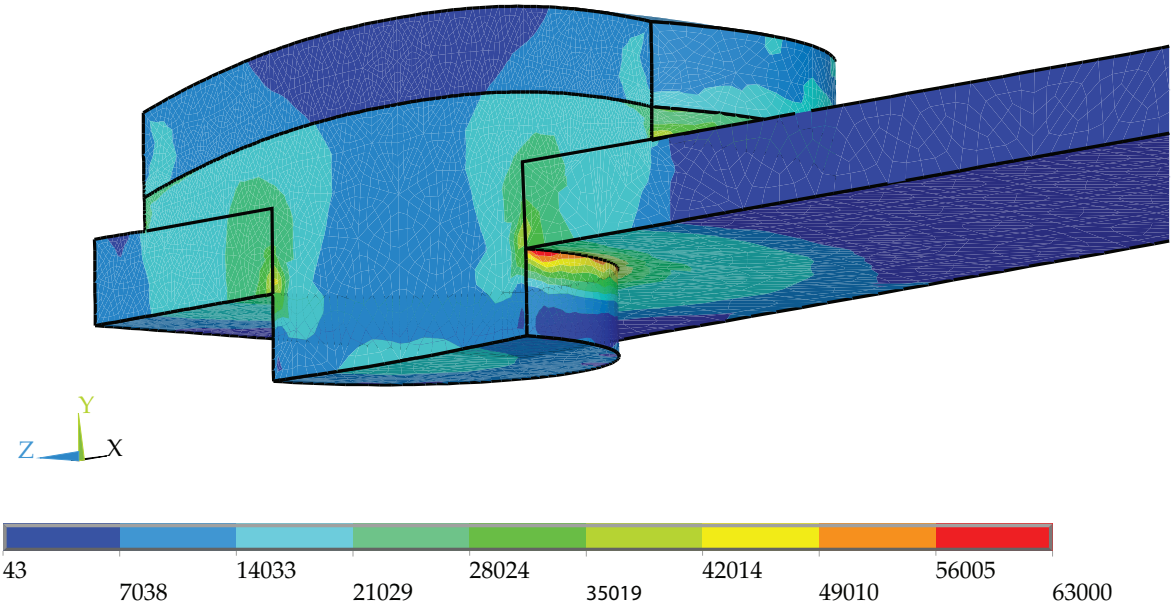

Figure 2.17: Equivalent stress distribution in the bimetallic Cu/Ag–Cu contact at applied current of 1 A.

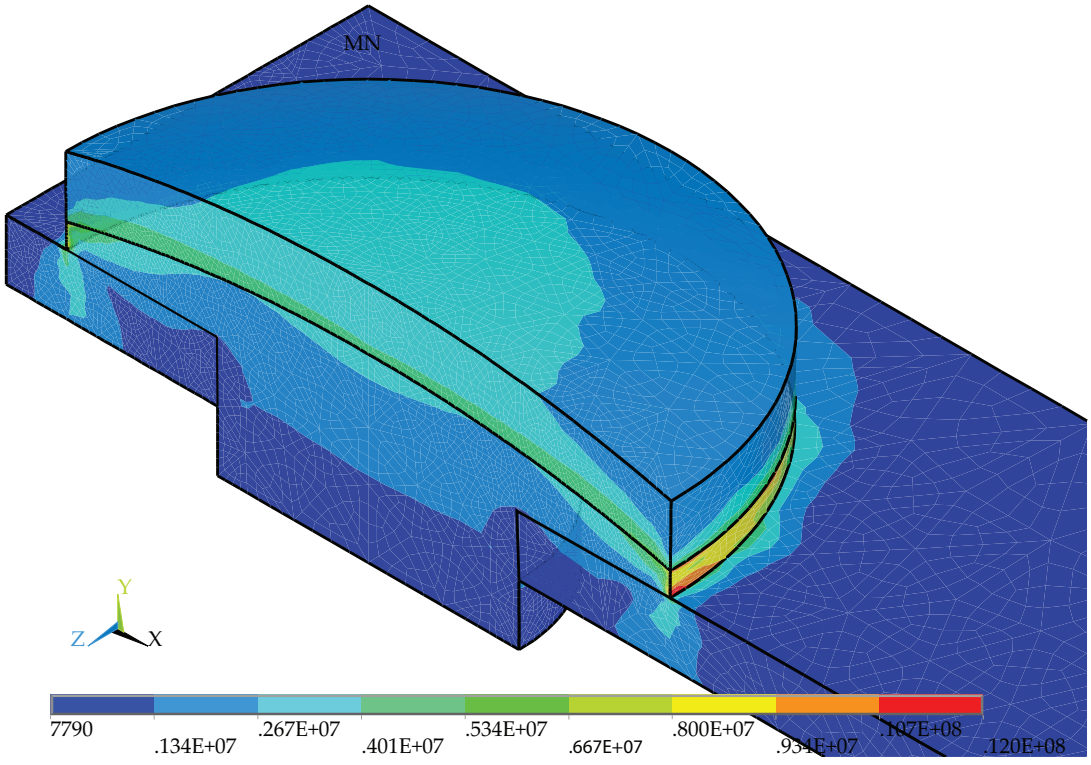

Figure 2.18: Equivalent stress distribution in the bimetallic Cu/Ag–Cu contact at applied current of 30 A.

values is localized at the edge of the junction of the body and plating. Figure 2.19 represents distribution of the equivalent stress in the system with bimetallic Cu/Ag–Cu contact which head taper angle is 15° at applied current of 10 A. From this figure is easy to observe the area of possible structural damage. For lower current values, area of maximum stress is in the contact shank which is not critical for its operation.

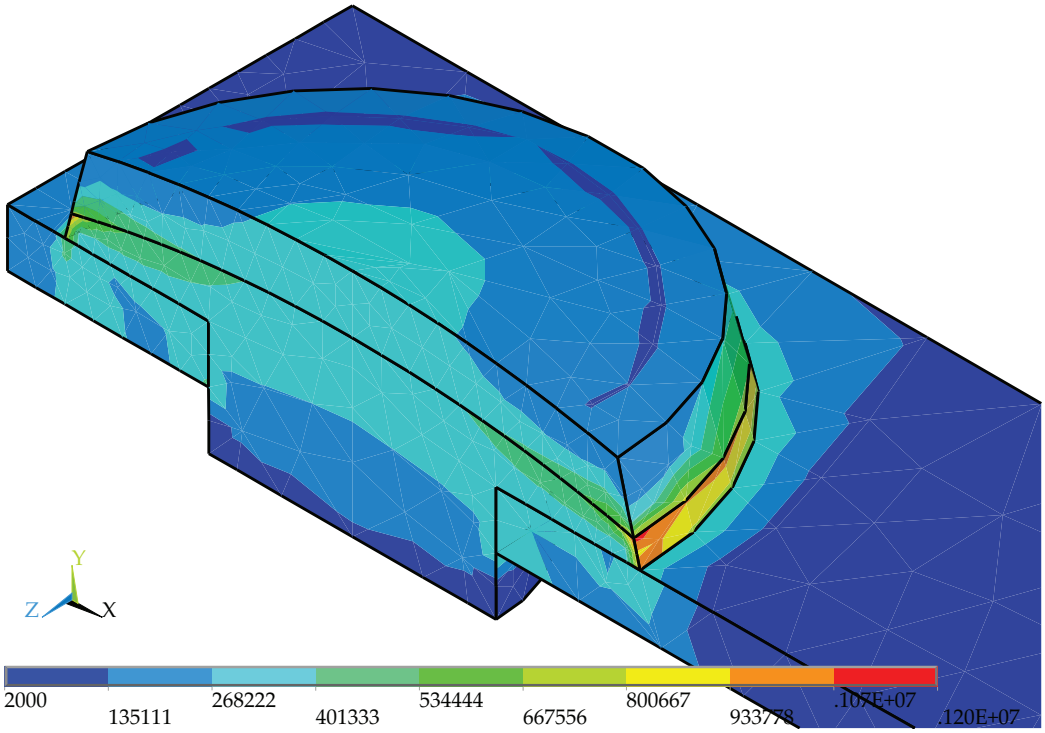

Figure 2.19: Equivalent stress distribution in the system with bimetallic Cu/Ag–Cu contact, head taper angle of 15°, two fixed surfaces, and applied current of 30 A.

Chapter 3

Optimization of the rivet electrical contacts

Design and optimization procedures of the rivet electrical contacts require knowledge of the temperature and maximum equivalent stress distributions in the contacts for different values of the applied current in order to meet the functional, economic, environmental and reliability demands. Therefore, these distributions were obtained by simulations of electrical contacts for different contact materials, specific set of dimensional and geometric parameters, and two ways of fixing the supporting structure.

3.1 Dependence of the temperature on the applied current

As stated in Section 2.3, value of temperature in systems with rivet contacts depends on the load conditions, electrical and thermal conductivity of the used materials, as well as on free surfaces of the system and mechanisms of the heat dissipation. Dependences of contact temperature value on the applied current for solid – Ag, bimetallic Cu/Ag–Ni and bimetallic Cu/Ag–Cu contacts are given in Fig. 3.1. Set of dimensions from Table 2.1 is considered, while for solid and bimetallic Cu/Ag–Ni contacts system was fixed at one surface and for bimetallic Cu/Ag–Cu at two surfaces. It can be observed that temperatures in bimetallic contacts made of Cu/Ag–Cu are much higher compared to Cu/Ag–Ni contacts with the same dimensions and applied currents. This is caused by additional fixing of the supporting structure on the bottom surface, thus reducing the area through which the heat is dissipated by convection.

Influence of the head diameter of bimetallic contacts on their temperature is considered for Ag–Cu as a plating material and the results are shown in Fig. 3.2 for a system with a single fixed surface and Fig. 3.3 for a system with two fixed surfaces. It is evident that head diameter of contacts does not influence the value of the temperature within a particular system. However, fixing of the supporting structure is of importance for a temperature value.

Head taper angle for defined head diameter of contacts does not effect the temperature dependence on the applied current. On the other hand, the method of fixing the supporting structure has a crucial role in defining the values of temperature, as observed from Fig. 3.4.

Contacts of identical geometries, made of materials with similar electrical and thermal conductivities, under the same load conditions have close temperatures, as can be seen in Fig. 3.5. This figure presents dependences of the temperature on the applied current

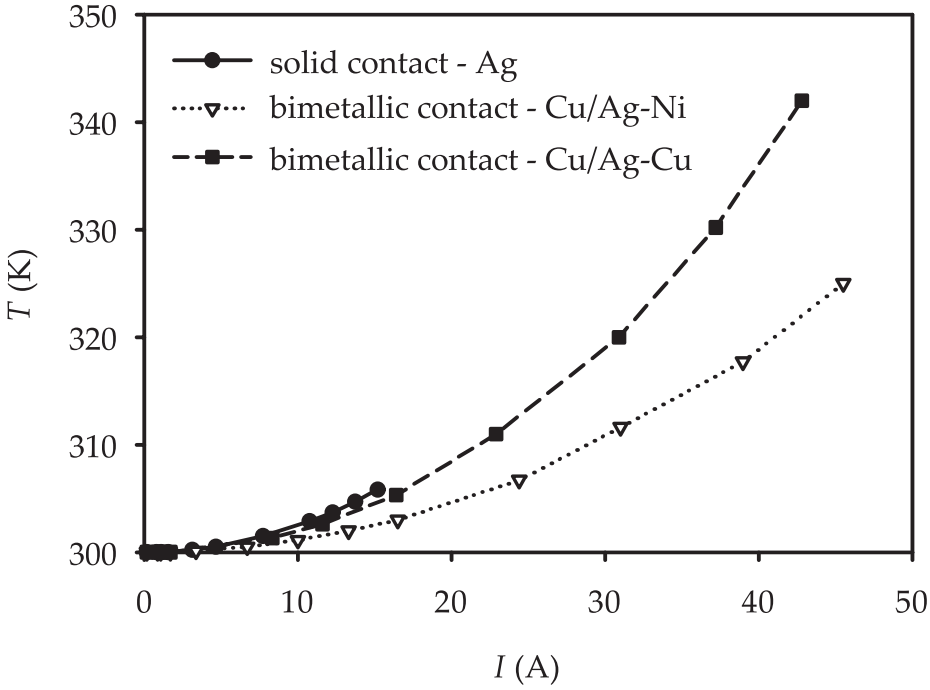

Figure 3.1: Dependences of the contact temperature on the applied current.

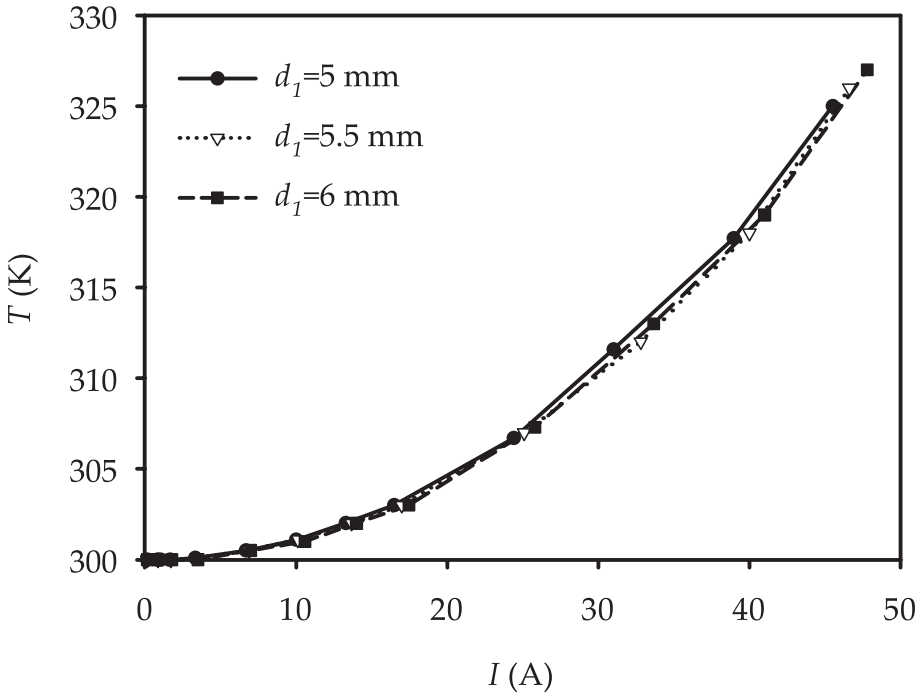

Figure 3.2: Dependences of the contact temperature on the applied current in bimetallic Cu/Ag–Cu contacts in a system with one fixed surface for three different diameters of the contact head.

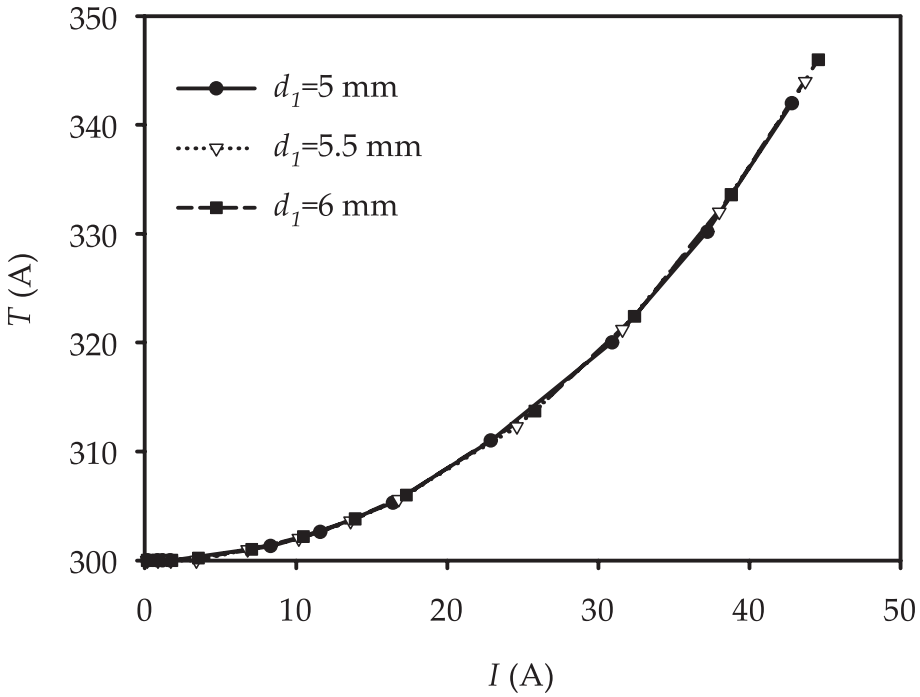

Figure 3.3: Dependences of the contact temperature on the applied current in bimetallic Cu/Ag–Cu contacts in a system with two fixed surfaces for three different diameters of the contact head.

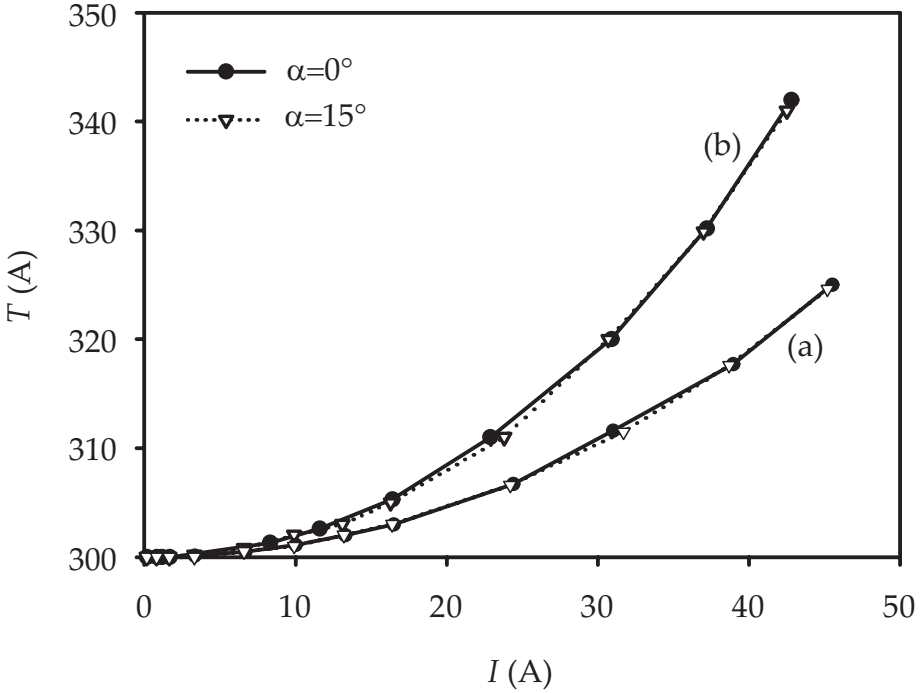

Figure 3.4: Dependences of the contact temperature on the applied current in bimetallic Cu/Ag–Cu contacts for two taper angles of the contact head in a system with (a) one and (b) two fixed surfaces.

for bimetallic contacts of the same size, made of three different plating materials, and incorporated into the same supporting structures (with two fixed surfaces).

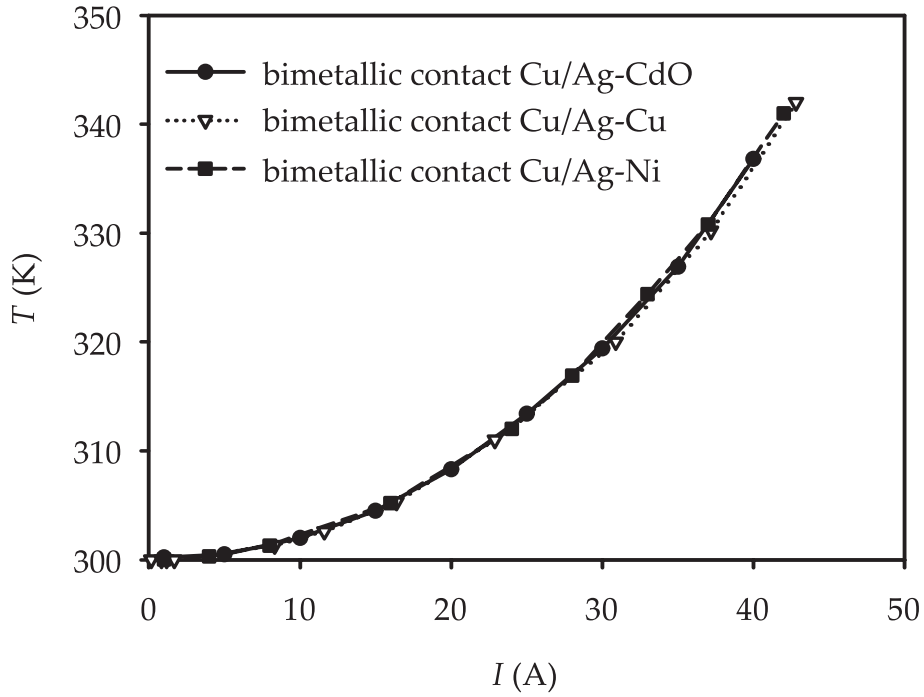

Figure 3.5: Dependences of the contact temperature on the applied current in bimetallic contacts within the system with two fixed surfaces for three plating materials.

From Figs. 3.1 – 3.5, knowing the allowed temperature rise in contacts with respect to defined ambient temperature, rated current values for contacts and therefore the possible application field can be determined. Allowed temperature rise in contacts is defined by the appropriate standards and for silver–plated copper contacts in the air, it is 50 K [34]. For proper analysis of possible application of certain contact type in thermal sense, it is necessary to know their mounting position in a switching device. Displayed dependences enable selection of the contact material from the ecological aspect since they provide data for alternative alloys as replacement for widespread but toxic alloy 90%Ag–10%CdO.

3.2 Dependence of the maximum equivalent stress on the applied current

Equivalent stress in contacts is result of the mechanical action of contact force on the contact head and thermal expansion of the material due to Joule's heating. The area of maximum stress in the structure and its value are determined by the selection of contact material, by values of the applied current and contact pressure, and by mechanical constrains. According to considerations given in Section 2.3, stress in the supporting structure for the solid contacts (contact force value below 3 N) and bimetallic contacts with two fixed surfaces is not a critical for the design of switching devices. In systems with a single fixed surface, maximum equivalent stress in the supporting structure for

high values of the applied current exceeds the plastic limit, so that this fact must be taken into account when selecting a switching device. The dependence of maximum equivalent stress on the applied current in contacts has great importance for definition of parameters of their reliable operation.

Dependences of the maximum equivalent stress on the applied current for solid – Ag, bimetallic Cu/Ag–Ni, and bimetallic Cu/Ag-Cu contacts are presented in Fig. 3.6. Dimensions of contacts are given in Table 2.1, while solid and bimetallic Cu/Ag–Ni contacts are fixed at one and bimetallic Cu/Ag–Cu contact at two surfaces.

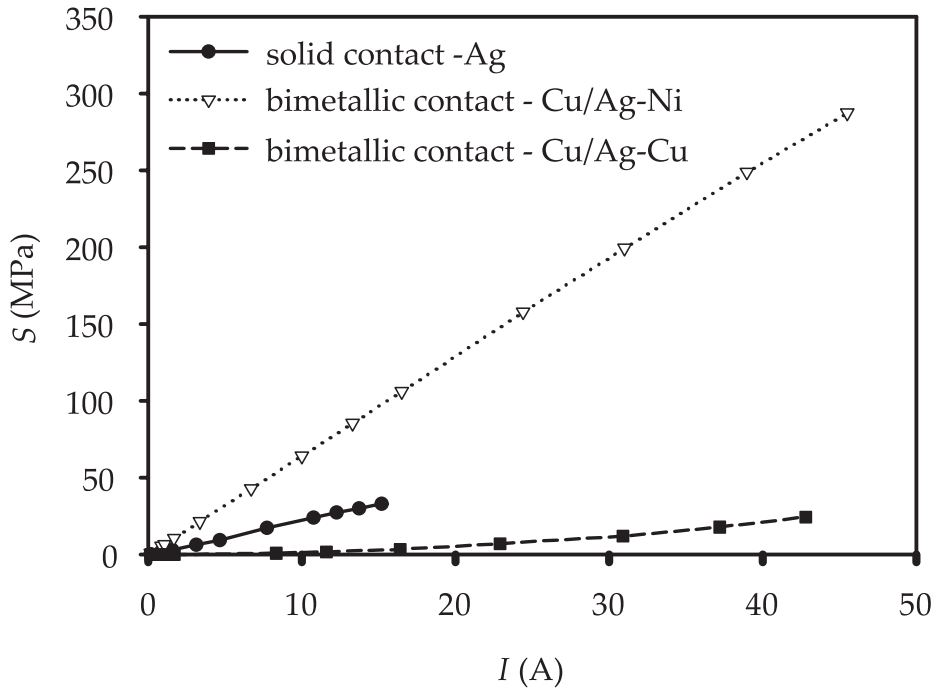

Figure 3.6: Dependence of the maximum equivalent stress in electrical contacts on the applied current.

An almost linear dependence of the maximum equivalent stress can be observed in the solid and bimetallic Cu/Ag–Ni contact, as a consequence of a direct relation between the value of the applied contact pressure and electric current. In these structures equivalent stress is largely determined by the mechanical load and electro–thermal stress is effect of the second order. In the systems with two fixed surfaces, dependence of the maximum equivalent stress value on the applied current is exponential with significantly lower values. In this case, despite the distribution of contact force, at higher applied currents electro–thermal stress has significant role. Therefore, an area of the maximum equivalent stress is shifted, as specified in Subsection 2.3.2.

Influence of head diameter of bimetallic contacts on maximum equivalent stress value for a range of applied currents is considered for Ag–Cu as a plating material and the results are shown in Fig. 3.7 for the system with one and Fig. 3.8 for the system with two fixed surfaces.

In the first system, there is nearly linear dependence of the maximum stress on the applied current (Fig. 3.7) for all considered diameters of the contact head. However, due to bimetallic structure, where two materials with different mechanical, electrical and thermal properties are joined, there is no apparent relationship between the diameter of

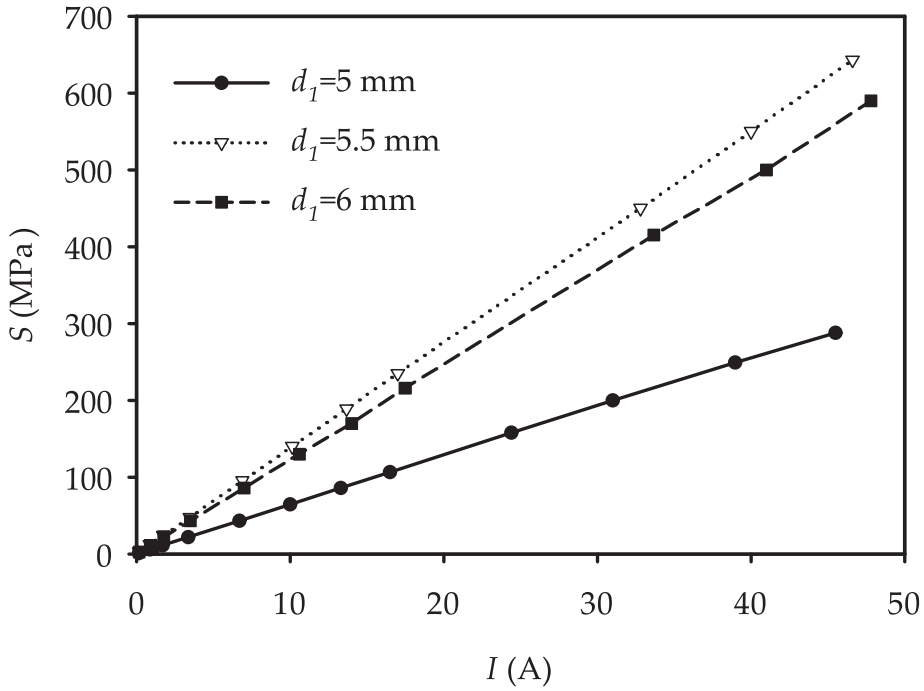

Figure 3.7: Dependences of the maximum equivalent stress on the applied current in bimetallic Cu/Ag–Cu contacts within the system with one fixed surface for three contact head diameters.

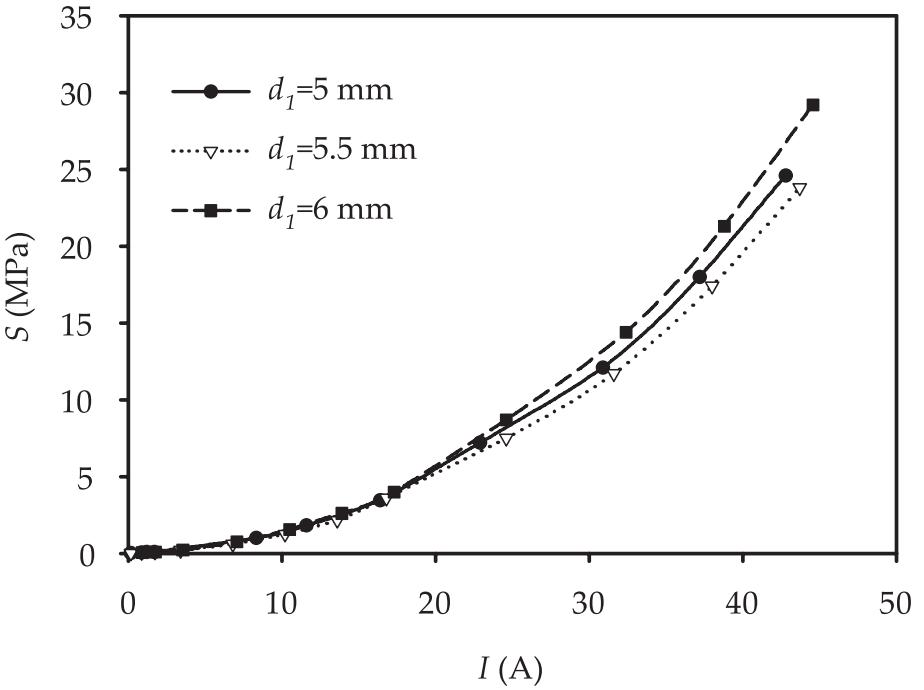

Figure 3.8: Dependence of the maximum equivalent stress on the applied current in bimetallic Cu/Ag–Cu contacts within the system with two fixed surfaces for three contact head diameters.

the contact head and the value of the maximum equivalent stress. In the second system (Fig. 3.8), values of the maximum equivalent stress for all three head diameters are close to each other with the exponential dependence on the applied current. As in the first system, their values can not be explicitly predicted.

The dependences of maximum equivalent stress on the applied current for Cu/Ag–Cu bimetallic contacts with head diameter of 5 mm and taper angles of 15° and 0° are given in Figs. 3.9 and 3.10. In the system with one fixed surface (Fig. 3.9), the dependence

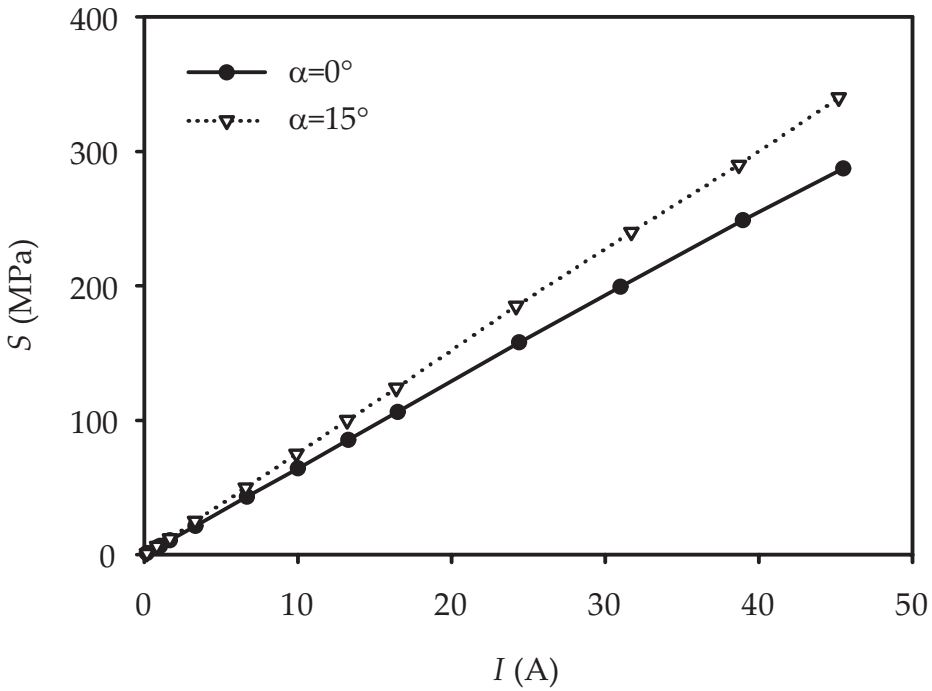

Figure 3.9: Dependence of the maximum equivalent stress on the applied current in bimetallic Cu/Ag–Cu contacts within the system with one fixed surface for two contact head taper angles.

is linear with a conclusion that changed taper angle, in respect to the basic realization of contact, significantly increases value of the maximum equivalent stress, which is an undesirable effect. In systems with two fixed surfaces (Fig. 3.10) values of the maximum equivalent stress for the head taper angle of 15° are slightly lower. To optimize contacts, there is a need to find a compromise between lower material consumption and slightly lower values of the maximum stress that provides a modified geometry, compared to the possibilities of a rapid detaching of the plating described in Subsection 2.3.2.

Dependence of the maximum equivalent stress on the applied current at bimetallic contacts in the system with two fixed surfaces with plating material as a parameter is shown in Fig. 3.11. It is confirmed that contacts made of materials with close electrical and mechanical characteristics have almost identical these dependencies, which allows selection of the most appropriate material in terms of environmental and economic parameters.

Dependencies of the maximum equivalent stress on the applied current for different realizations of contacts allow determination of their lifetime due to fatigue. Based on the so–called S–N curves described in Section 1.1, the maximum number of switching cycles which provides reliable operation of the switching device for a given value of

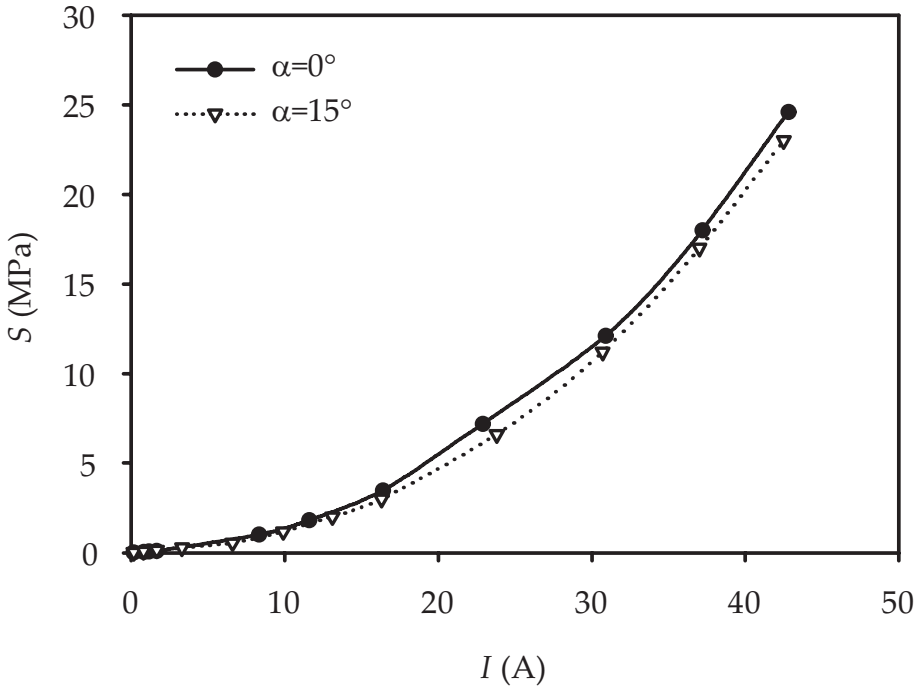

Figure 3.10: Dependence of the maximum equivalent stress on the applied current in bimetallic Cu/Ag–Cu contacts within the system with two fixed surfaces for two contact head taper angles.

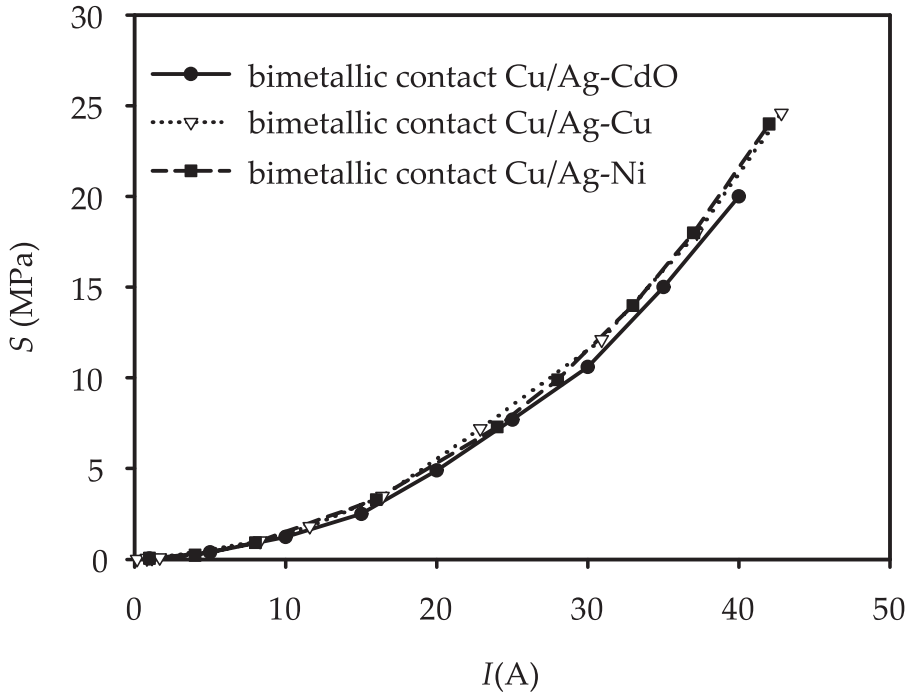

Figure 3.11: Dependence of the maximum equivalent stress on the applied current in bimetallic contacts within the system with two fixed surfaces for three contact materials.

stress can be defined. Also, based on these curves, the value of stress at which contacts may fail upon application of a specified number of switching cycles can be determined. This stress value defines operating conditions of contacts, including applied current and contact force, as well as the switching device design.

3.3 Optimization results

For basic geometry of the rivet electrical contacts adopted during the design process and for specified supporting structure optimization of the contacts is performed with respect to the selection of contact material, diameter and taper angle values of the contact head and definition of the rated current. Functional, economic, environmental and reliability aspects are considered [90–92]. Based on the results described in the previous two subsections there are three systems contact–supporting structure that need to be separately considered. Those are: system with solid Ag contact, system with bimetallic contact and one fixed surface, and system with bimetallic contact and two fixed surfaces.

3.3.1 Solid Ag contacts

Verification of the functionality of designed system with solid Ag contact at the specified operating conditions and estimation of its reliability parameters were performed. As contact material was selected silver of 99.99 % purity, which is the best material for contacts in the electrical and thermal terms. The geometry and dimensions were adopted based on the market demands, while the contact force was determined by the practical realization of a switching device. Contact temperature dependence on the applied current defines functionality for the rated current value. From Fig. 3.1 is evident that this functionality is satisfied in terms of temperature rise for the rated current value of 15 A. The temperature rise value is about 5 K, while the standards allow value of 50 K. The maximum equivalent stress at rated current from Fig. 3.6 is 33 MPa. This value of stress determines lifetime of contacts due to fatigue, and based on S–N curves for silver given in Fig. 1.5, it is above 10^6 switching cycles.

The supporting structure is made of copper which, depending on the applied processing and hardening methods, has a value of stress at the plastic limit of 55-330 MPa and does not exhibit the effect of residual stress due to the riveting process. Bearing in mind that, for the rated current, value of the maximum stress in the cantilever beam is about 150 MPa, and that its bending is 120 μm, realization of the supporting structure is not a critical parameter in the design and optimization of solid electrical contacts.

3.3.2 Bimetallic contacts in the system with one fixed surface

Design of bimetallic contacts was made for applications with rated currents up to 40 A. Based on the Fig. 3.1, it can be observed that for currents above the rated value of 40 A temperature rise does not exceed the prescribed 50 K. The same values of the temperature rise are in Cu/Ag–Cu contacts with different head diameters (Fig. 3.2), as well as for changed taper angle of the contact head (Fig. 3.4). This fact redirects the optimization procedure from thermal to electrical and mechanical parameters.

By increasing the diameter of the contact head, the decrease of contact resistance is achieved, but, as shown in Fig. 3.7, it increases value of the maximum equivalent stress

twice for the rated current value. Since the area of the maximum equivalent stress is in the bulk part of the contacts (see 2.3.2), based on S–N curves from Fig. 1.5, for the value of the maximum equivalent stress corresponding to the rated current (255 MPa) and head diameter of 5 mm, the number of switching cycles which ensures reliable operation is of the order of 10^4. By increasing the diameter of the contact head this number rapidly decreases and for the desired lifetime of the switching devices it is necessary to adopt a head diameter of 5 mm. In addition, for long–term functionality of contacts, the value of the rated current should be decreased. For 10^5 switching cycles it should be 15 A and for 10^6 cycles 11 A.

Analogous considerations apply to contacts with contact head taper angle of 15°. This reduces the consumption of plating material and increases value of the contact pressure, but also increases the maximum equivalent stress as indicated in Fig. 3.9. This increase in stress will shorten the reliability lifetime of contacts for the rated current value below acceptable limits. However, an adequate reduction of rated current value to 15 A, enables realization of switching devices with these contacts that ensure reliable operation for 80,000 switching cycles since localization of the maximum equivalent stress is not a critical parameter (see 2.3.2).

In systems with one fixed surface it is necessary to consider the equivalent stress in the supporting structure. Based on the expression (1.3), for the copper cantilever beam of considered dimensions (15 mm × 6 mm × 0.5 mm) and defined contact force of 0.36 N/A, the maximum allowed current is 15 A and the bending of the free end is 0.5 mm. This limits are consistent with the values of the rated current that provides long–term reliable operation of the contacts with head diameter of 5 mm and head taper angle of 15°. On the other hand, if it is necessary to realize switching device for rated 40 A, and up to 10^4 switching cycles, the basic geometry of the bimetallic contacts (d_1=5 mm, $\alpha = 0°$) and slightly altered supporting structure of dimensions (15 mm × 6 mm × 0.8 mm) must be used.

3.3.3 Bimetallic contacts in the system with two fixed surfaces

Switching devices with two fixed surfaces of the supporting structure show higher values of temperature then devices with one fixed surface at identical applied electrical and mechanical loads. The difference is caused by different thermal conditions of operation, and Fig. 3.1 shows that for the bimetallic Cu/Ag–Cu contact at maximum current of 40 A, this difference is 17 K. However, this increased value of temperature rise does not exceed the allowed 50 K. Changes of head diameter value and head taper angle do not introduce changes in the temperature dependence on the applied current, as illustrated in Figs. 3.3 and 3.4.

Different mechanical boundary conditions due to redistribution of the contact force reduce value of the maximum equivalent stress to 20 MPa (Fig. 3.6), which provides reliable operation of contacts for more than 10^6 switching cycles. In addition, for different values of the head diameter, the maximum equivalent stress values are close to each other with the maximum difference at rated current of 13 %, as shown in 3.8. Since there is no explicit relation between the contact head diameter and the value of the maximum equivalent stress, a compromise between the economic parameters (amount of used materials) and the value of contact resistance need to be achieved.

Contacts with taper angle of 15° have slightly lower values of the maximum equivalent stress for the specified load conditions (see Fig. 3.10). Realization of switching

devices with this type of contacts is optimal, since it provides reduced material costs, higher values of the contact pressure and lower values of the maximum equivalent stress. Its only drawback is localization of the maximum stress at higher currents along the junction of the contact body and plating, which under certain operating conditions can lead to a reduced lifetime due to desoldering of the plating.

The supporting structure for the systems with two fixed surfaces does not suffer significant stress, and its designed geometry is fully functional for currents up to the rated value.

From the environmental aspect of contacts optimization, implementation of Ag–Ni and Ag–Cu alloys as plating materials, instead of widespread but toxic alloy Ag–CdO, is completely justified. Namely, based on the Figs. 3.5 and 3.11, it can be concluded that the functionality of contacts at the given operating conditions, for all investigated materials, is the same and thus their mutual substitution is justified.

Part II

Thermal cutoffs

Chapter 4

Fundamentals of thermal cutoffs design and optimization

Thermal cutoffs (also known as thermal fuses or thermal links), should provide a rapid and permanent termination of the electrical current when in the circuit occurs a temperature above the certain prescribed value. They protect electrical appliances against overheating and possible burning. Thermal cutoffs change their state from closed to open regardless of the origin of the excessive heat (the elevated ambient temperature and/or generated Joule's heat due to the increased current flow through the circuit).

Thermal cutoffs are produced as reversible and irreversible. The first class is mainly used in household appliances, while the second one is exploited in industrial and office systems. Irreversible devices are used due to the fact that overheating often indicates some serious problem within or around the system, which requires human intervention [93]. Classification of the cutoffs is based on their construction and values of the temperature and electrical operating parameters [15, 17, 94]. Construction of the cutoffs is determined by the mechanism of the current termination, shape and dimensions of the leads and type and appearance of the housing. The temperature operating parameters include [15]:

- *Functioning temperature* T_F – the ambient temperature at which a thermal cutoff enters open state with detection current as the only load. Functioning temperature that comply appropriate safety standards is designated as *rated functioning temperature*;
- *Holding temperature* T_H – the maximum ambient temperature at which a thermal cutoff can be maintained while conducting rated current for 168 hours without opening;
- *Maximum temperature* T_M – the maximum temperature at which a thermal cutoff in the open state can be maintained for 10 min without degradation of its mechanical and electrical characteristics;
- *Cutoff temperature* T_C – the temperature at which connection between the conductive elements within the thermal cutoff breaks.

Basic electrical parameters are [16]:

- *Rated current* – the maximum current that thermal cutoff can conduct for certain time at the holding temperature without change of its functioning temperature;

- *Rated voltage* – the maximum voltage that can be applied at thermal cutoff leads;
- *Cutoff current* – the current that thermal cutoff can reliably terminate at rated voltage;
- *Transient overload current* – a direct current pulse train which thermal cutoff can conduct without degradation of its characteristics.

Design and optimization procedures should ensure mass production of thermal cutoffs with accurate and stable cutoff temperature, high sensitivity to changes in the ambient temperature, very low and stable internal resistance, and clearly defined irreversibility. These characteristics are achieved by proper shape and dimensions of the thermal cutoff constructive elements and by adequate selection of materials from which they are made.

4.1 Functionality, quality and reliability parameters of thermal cutoffs

Functionality, quality and reliability of thermal cutoffs are considered on the basis of values and stability of their functioning temperature, response time, electrical resistance of the conductive and insulating parts, and mechanical strength at various operating conditions. Criteria are maintaining the functionality of cutoffs and keeping values of these parameters within the specified tolerances. All parameters are generally considered from thermal, electrical and mechanical aspects.

4.1.1 Thermal parameters

The main parameter of thermal cutoffs is *functioning temperature*. It is defined for the condition where effects of Joule's heating are negligible and ambient temperature is increased by the specified rate (0.5–1 °C/min) so that thermal equilibrium is established. For the specification of cutoffs is used *rated functioning temperature*, which complies appropriate safety standards. For the functioning temperature allowed tolerances from the rated value are -10 °C to +0 °C.

The *response time* of thermal cutoffs is determined when they are suddenly exposed to an elevated temperature, while resting at the room temperature. It is used to determine the quality of the thermal cutoffs and should be of the order of 5–60 s, depending on their construction [95]. Measurement of the response time is done by immersing the cutoff in a silicon oil bath of a defined temperature and by registering the time before the cutoff. Since the heat transfer parameters of silicone oil and air (where cutoffs actually work) are significantly different, the response time of cutoffs in the real operating conditions is higher than a given laboratory value. Therefore, assessment of the real values of the response time for various operating conditions of the cutoff is a complex task considered in the design and optimization procedures.

The long–term exposure of thermal cutoffs to extreme operating conditions leads to degradation of materials they are made of. Therefore, as the reliability parameter of cutoffs, *stability of the functioning temperature during the accelerated ageing* is considered. The cutoff must maintain stable value of the functioning temperature within the given tolerances after exposure to temperatures of 20 °C below the rated functioning temperature value, and at the relative humidity of 45–85% in the period of 1000 hours [14]. Also,

the cutoffs have to maintain functionality when exposed to environments with 90-95 % humidity and temperature of 40 °C (for $T_F \leq 100$ °C) or 65 °C (for $T_F > 100$ °C) during 500 hours [16]. This parameter is determined by the thermal and hygroscopic characteristics of the housing, as well as the structure and quality of the thermosensitive part of the cutoff.

4.1.2 Electrical parameters

Quality of thermal cutoffs in the electrical sense is determined by the electrical resistance of conductive, as well as insulating elements, and dielectric strength of the insulation material.

Internal resistance of the thermal cutoff is an electric resistance of its conductive elements and should be of the order of a few mΩ.

Insulation resistance of the thermal cutoff should be of the order of 100 MΩ. Testing conditions include 500 V voltage applied between one lead and the housing of the opened cutoff for 1 min.

Resistance to overvoltage depends on the dielectric strength of the insulation material inside a thermal cutoff, which should prevent the creation of a conductive path between the cutoff leads at high applied voltages after its opening. This value should be of the order of 1000 – 2000 V.

Resistance to current overload is a parameter which examines the functionality of the cutoffs after applying between its leads 100 current pulses having an amplitude of 15 times larger than the rated current value with duration of 3 ms at 10s intervals.

Parameter that includes both, the thermal and electrical domain, is *rise of the operating temperature* due to the Joule's effect. This parameter defines the quality of the cutoff within the specified type and is usually given for currents twice of the rated value for device operating at room temperature.

4.1.3 Mechanical parameters

Mechanical stability of thermal cutoffs is described by the *housing strength*, *resistance to bending and twisting of the leads*, and *strength to compression and tension of the leads*. These characteristics are determined by the cutoff design and materials of its housing and leads.

Thermal cutoff housing must provide adequate protection of its functional part from damaging by mechanical forces of the specified intensity (100 N) or constant low amplitude vibrations. This parameter has a special significance in the applications where the housing represents a conductive part of the cutoff and in cases where mechanical damage can prevent cutoff from the opening.

The thermal cutoff has to remain intact after bending its leads up to 90° at a distance of 10 mm from the cutoff body and their subsequent twisting through 180°. Also, it should maintain full functionality when compression or tensile forces of the specified value are applied on its leads.

4.2 Determination of the geometry and dimensions of thermal cutoffs

Thermal cutoffs are used in a wide range of devices which are characterized by different values of the operating voltage, current, and dimensions. As a result, thermal cutoffs may have different shapes, while their basic classification is done according to the construction, rated functioning temperature and rated voltage and current. The basic parts of the cutoff are leads and the conductive strip which are hermetically sealed in the appropriate housing. Regarding the construction, thermal cutoffs are divided by realization of the conductive strip, method of its joining with the leads, shape and dimensions of the leads, as well as the housing type.

Based on the method of electrical current termination, thermal cutoffs can be with a fusible material or with a spring. In the first group, part of the conductive strip is made of thermally sensitive material covered with a layer of special compound based on rosin. When a defined temperature is reached, thermal material melts, conductive strip shrinks and, due to the surface tension of the compound, forms two spheres at lead ends, thus permanently terminating the current. In cutoffs with the spring, leads and conductive strip are made from a standard conductive materials and joined with thermally sensitive material by soldering. At a defined temperature, soldered joints melt and spring, which is located inside the housing, pushes the conductive strip and breaks the conductive path between the leads.

By the shape and dimensions of the leads thermal cutoffs are classified as axial, radial and strip [17], while the housing may be metal, plastic or ceramic. In all realizations, the leads are fixed to the housing by special epoxy resin which provides hermetically sealed cutoff. Inside the housing is usually air, but in cases that require a high dielectric strength of the insulation material, suitable insulating fluid can be used.

Thermal cutoff design and optimization procedures, in terms of geometry and dimensions, include selection of an appropriate construction type and sizing of the constitutive elements on the basis of the rated current value. In applications where dimensions of the cutoff are not a critical parameter, cutoffs with a spring are often applied. These cutoffs are characterized by short current path through the thermally sensitive material, extremely low internal resistance and stable value of the functioning temperature over a long period of time. Also, they allow high overload current value during numerous switching cycles of the device. Thermal cutoffs with a spring are produced in two types. One is with axial leads and metal housing, which can be a part of the conductive path, while the second type is with radial leads and plastic or ceramic housing. Plastic housing provides insulation of the thermosensitive part of the cutoff in an electrical sense and satisfies demands of thermal conductivity and mechanical strength. Therefore, thermal cutoffs of the radial type with a spring in a plastic housing (so–called S–type) are widely used. Their cross–sections before and after the opening are shown in Fig. 4.1, while the basic structural elements are indicated in Fig. 4.2.

The conductive bridge of cutoff consists of the leads formed from two conductive wires shaped at one end into the appropriate contacting heads, and the conductive strip soldered to the leads by thermally sensitive material. The leads are fixed to the housing by the epoxy resin in a position that ensures that the spring, which is beneath the conductive strip, is in a compressed state. Characteristic dimensions of the conductive bridge elements, housing and spring which are of the interest for design of thermal cutoffs are listed in Table 4.1. Diameter of the leads is determined by the rated current

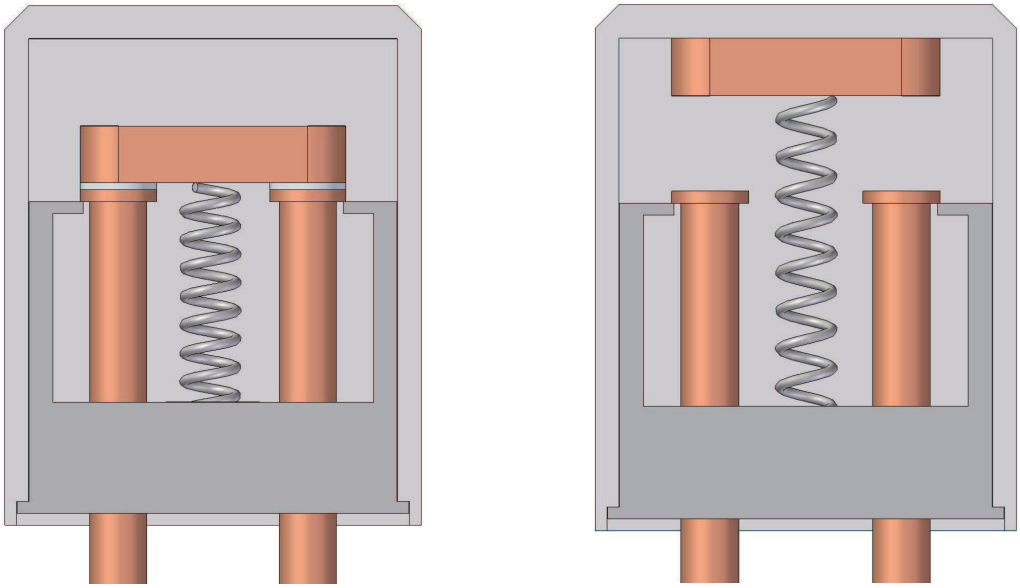

(a) (b)

Figure 4.1: Cross section of the S–type thermal cutoff before (a) and after (b) the opening.

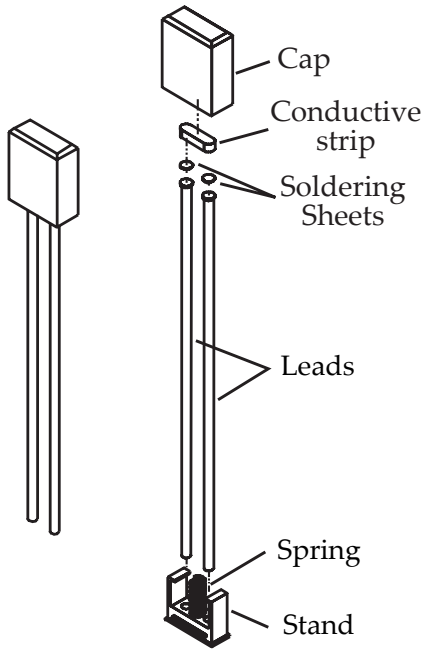

Figure 4.2: Basic construction elements of the S–type thermal cutoff.

Element	Material	Characteristic dimension
Leads	Conductive material	Length
		Diameter
		Contacting head diameter
		Contacting head thickness
		Length outside the housing
Conductive strip	Conductive material	Length
		Width
		Depth
Soldering sheets	Thermosensitive material	Diameter
		Depth
Housing	Flame retardant plastic	Height
		Width
		Thickness
		Stand Height
		Wall thickness
Spring	Steel	Diameter
		Length

Table 4.1: Characteristic dimensions of the S–type thermal cutoffs.

value. Adopted diameter should provide temperature rise in the cutoff due to Joule's heating within the limits of 10–20 K. Approximate values of the lead diameter used for the realization of thermal cutoffs for different rated currents and rated voltage of AC 250 V are shown in Table 4.2.

Rated current (A)	1	2	3	5	12	20
Lead diameter (mm)	0.53	0.55	0.6	0.7	1.2	2

Table 4.2: Lead diameters of S–type thermal cutoffs depending on the rated current value.

The contacting head of leads is in the form of a rivet. Rivet shape enables better fitting of the leads on the conductive strip, and thus a tighter connection between the elements of the conductive bridge in the closed state. At the same time, contacting heads provide lower value of the temperature at soldered joints at normal operating conditions as a result of the reduced Joule's heating. Diameter of the contacting head is 0.2–0.4 mm larger than the lead diameter while its thickness is 0.25 mm.

Adopted value of the lead length outside the housing depends on the desired application and it is easy changeable value. The standard defines short, medium and long leads with values of the length of 35 mm, 50 mm and 65 mm, respectively. Lead length within the housing is adapted to the dimensions and elastic properties of the spring that provides the functionality of the cutoff. The spring should be at a maximum compressed state under normal operating conditions to ensure rapid response of the cutoff when opening condition occurs. Accordingly, the designed length of the leads has the value 40–72 mm.

Dimensions of the conductive strip are adjusted to the dimensions of the leads. In the basic design strip width is matched to the diameter of the contacting head, strip

thickness to the lead diameter, while the length is determined by the distance between the leads and their diameter. On the other hand, distance between the leads is subjected to the dimensions of the applied spring, thermal properties of the housing material and desired resistance to the voltage overload. After the opening of the cutoff, with high values of the voltage applied between the leads, electrical breakdown of dielectric inside the cutoff must not occur (in the case of the air electric field must not exceed the value of 3×10^6 V/m [96]).

Soldering sheets have a diameter determined by the contacting heads of the leads and thickness of 150 μm.

The housing of S–type cutoffs has cuboid form which provides adequate heat exchange between the cutoff and environment by convection. It consists of a stand and a cap. The stand is also a support for the conductive bridge, while sealing of the leads with epoxy resin provides its mechanical strength. The spring is placed into the stand, while the cap provides sealing of the cutoff interior. Shape of the housing allows high sensitivity to changes in ambient temperature, and its dimensions should enable reliable operation of the thermal cutoff with minimum external dimensions. In this sense, sufficient space within the housing above and around a conductive bridge should be provided. The thickness of the housing walls depends on the material and it represents a compromise between two mutually opposite conditions. A greater thickness is needed for better mechanical properties, while a lower one is preferable for short response times. Standardized housing dimensions that meet the above requirements are 4–13.5 mm for the height, 5–13 mm for the width, and 2–4.3 mm for the thickness. In addition, characteristic dimensions are ruled by the dimensions of the conductive bridge, which basically depend on the value of the rated current.

The spring is selected from the range of standard steel springs whereby its size is adjusted to dimensions of the conductive bridge.

4.3 Selection of materials for thermal cutoff structural elements

Selection of materials for realization of thermal cutoff structural elements is governed by their electrical, thermal and mechanical properties. For the conductive bridge of primary importance are electrical and thermal, for the housing thermal and mechanical, and for the spring mechanical properties of the material.

Elements of the conductive bridge (the leads and the conductive strip) are commonly made of copper as electrically and thermally highly conductive material. Protection against the oxidation process of the copper is achieved by plating with a few μm thick layer of tin or nickel. Since copper is a relatively soft material easy forming and efficient mounting is enabled.

The elements are connected by soldering with thermosensitive material. The soldering material characteristics define cutoff temperature which is basic for the device functionality. Different low melting alloys of two–component or multi–component composition are used for this purpose. These alloys have a melting temperature below 250 °C and they are composed of tin, lead or silver with addition of a low melting element such are bismuth, indium, antimony or gallium. Solidus and liquidus temperatures of these alloys overlap (have eutectic character) or are within couple of °C close to each other. Selection of the low melting alloy is defined by the desired cutoff temperature, costs and

environmental suitability. Some of the commercially available low melting alloys are listed in Table 4.3 [18–20, 97–101].

Low melting alloy	SnPb	SnBi	SnIn	SnAg	SnSb	SnCu
	InBi	PbBi	InAg	InPb	InGa	BiCd
	SnPbBi	SnBiIn	SnPbIn	SnBiAg	SnPbAg	SnInGa
	PbBiIn	PbInAg	BiInCd	SnInCd	SnPbBiAg	SnPbBiIn

Table 4.3: Most often used low melting alloys.

Alloys of different compositions have different melting temperatures and characteristics. The desired cutoff temperature usually can be achieved by several alloys and economic aspect represents another criterion for selcetion of materials for thermal cutoffs. Elements such as indium, gallium and antimony have a high price, and alloys with a high percentage of these elements are used for specific purposes. On the other hand, the toxicity of lead and cadmium imposes the need of their removal from the manufacturing processes of electronic devices and the alternative alloys are more used.

Low melting alloys are comprised of a highly conductive chemical elements and therefore they have electrical conductivity which meets soldering needs. Their microstructural characteristics, depending of the manufacturing method, can contribute to a better wetting of the soldering surface. Mechanical properties of the soldering alloy are not critical parameter for the thermal cutoffs.

Thermal cutoffs with spring and radial leads are made with ceramic or plastic housing. Both housing types provide electrical insulation of the functional part of the cutoff. Ceramic materials have higher thermal conductivity, but the use of plastic allows smaller external dimensions for adopted dimensions of the conductive bridge. Applied plastic needs to have flame retardant property and good thermal conductivity in order to ensure a short response time of the cutoff. Thermal properties of plastic determine the maximum temperature of the cutoff. Mechanical properties of plastic should provide resistance of the housing to mechanical forces under elevated temperature conditions. Also, low–amplitude vibrations, which are often present in devices that thermal cutoffs protect, must not mechanically damage the housing or compromise the functionality of the cutoff. In electrical sense, plastic should have adequate electric resistance to ensure a satisfactory value of the insulation resistance defined in Subsection 4.1.2.

Spring material is steel whose mechanical properties enable production of the spring with specified dimensions. Since the spring is used as a pre–defined structural element, the process of thermal cutoff design involves selection of the appropriate spring from the standard list.

Chapter 5

Characterization of low melting alloys for thermal cutoff purposes

Functionality of thermal cutoffs is based on thermal response of the low melting alloy that make solder joints between the conductive elements. Low melting alloys have melting temperature below 250 °C and usually are multi–component. The basic element is tin, lead or silver, while addition of a low melting elements such are bismuth, indium, antimony or gallium enables achievement of the desired melting temperature or temperature range. These alloys are also used in SMD technology for devices whose exploitation does not include high temperatures. Thermal characteristics of low melting alloys (primarily dependence of the melting point on the composition) are necessary for thermal cutoffs application, while knowledge of microstructural characteristics of the alloys (structure and composition of the grains) provides the basis for their better processing.

5.1 Generation of 3–D phase diagrams of ternary systems

Development of multi–component alloys with predefined characteristics, specifying conditions of their fabrication and forecasting of their behaviour in operating conditions are based on phase diagrams i.e. visual presentation of the state of the material as a function of the composition, temperature and pressure. Determination of phase diagrams of multicomponent alloys by experiments involves different techniques such as differential thermal analysis [97], diffraction and fluorescence of X-rays [102], electron microprobe analysis [103], synchrotron radiation [104], diffusion coupling [105]. These techniques include time consuming, expensive and difficult processes. Thus, a numerical modeling based on a minimal set of experimental data has great importance in the design of phase diagrams.

Alloys normally do not melt at a single temperature, but in a temperature range. The liquidus temperature is the lowest temperature at which a particular alloy is completely in a liquid state, and the solidus temperature is the highest temperature at which the alloy is completely in a solid state. At temperatures in the range between the liquidus and solidus, the alloy is in the mixed liquid–solid state. Alloy of the particular composition, whose liquidus and solidus temperatures coincide represents an eutectic alloy. Collection of liquidus temperatures of alloys of different compositions at constant pressure defines liquidus line in binary systems, or liquidus surface in multicomponent systems. Analogously, a collection of solidus temperatures defines solidus line or surface. Liq-

uidus and solidus surfaces in the ternary system are three–dimensional, and the phase diagrams that they define require spatial representation. Depending on the nature of the binary subsystems, ternary liquidus and solidus surfaces may appear tessellated and consist of one or more stitched subsurfaces. For characterization of these alloys, phase diagrams are presented in the form of a two–dimensional projection through a series of characteristic lines within the so-called *Gibbs* triangle. It is an equilateral triangle on whose sides are chemical compositions of binary subsystems. The characteristic lines are isotherms (intersections of liquidus and solidus surfaces with a plane representing a constant temperature) and cotectic lines (intersection of liquidus and solidus subsurfaces). Intersection points of these lines are eutectic points (temperature of direct transition from the liquid to the solid phase) or peritectic points (the temperature at which a solid phase in the reaction with the liquid phase changes its form). Determination of the characteristic lines and points of multicomponent alloys and generation of their phase diagrams are interest of the so–called CALPHAD (Calculation of Phase Diagrams) group [21].

Standard methods for the determination of phase equilibrium in multicomponent systems are based on the minimization of the total free Gibbs energy of the system. *CALPHAD method* uses multiple mathematical models to describe dependence of the Gibbs energy on the temperature, pressure and concentration of individual phases. On the basis of thermodynamic data for the lower order systems and appropriate software, the parameters of the selected mathematical model are extracted and a phase diagram of higher order generated. However, the existing databases of thermodynamic data, specialized software for generation of spatial diagrams, as well as most of multicomponent phase diagrams obtained by CALPHAD method are commercial and not public available [106, 107]. Therefore, alternative methods that allow generation of phase diagrams of multicomponent systems based on public available data could be applied. One such method has been proposed in this Dissertation. It is named *the surface modeling method* and intended for determination of the liquidus surface of the ternary system based on the phase diagrams of its binary subsystems and a minimal set of experimental data.

5.1.1 CALPHAD method

The main objective of CALPHAD method is calculation (prediction) of the phase equilibrium in unfamiliar multicomponent system on the basis of information available for the constituent subsystems of lower order [108]. Experimental data for the subsystems are used to optimize thermodynamic parameters whose values are verified through the generation of known phase diagrams and later used to calculate the unknown phase diagrams by extrapolation method.

Calculation of the phase equilibrium in multicomponent systems involves minimization of the total Gibbs energy of the system G by solving the relation:

$$G = \sum_{i=1}^{p} n_i G_i^{\varphi} = min, \tag{5.1}$$

where n_i is the number of moles and G_i^{φ} Gibbs energy of the i–th phase from total of p phases that constitute the system. Dependence of the free Gibbs energy of each phase on composition, temperature and pressure is given by the appropriate thermodynamic function. For a description of this function different models which include a range of thermodynamic parameters are used.

Gibbs energy of the individual phases can be separated into three terms that depend on the concentrations of components:

$$G^{\varphi} = G^{0} + G^{en} + G^{ex}. \tag{5.2}$$

The term G^0 represents Gibbs energy of the mechanical mixture of phase constituents, G^{en} corresponds to the mixing entropy of an ideal solution, while G^{ex} is so–called excessive energy and includes all deviations from the ideal solution. In the ternary systems, the first two terms are defined from the basic laws of thermodynamics and the third is based on generally accepted Muggianu method for extrapolation of excess energy parameters in binary systems. For a system consisting of components A, B and C, with corresponding binary subsystems AB, AC and BC, members of the expression 5.2 can be represented in the following form [109]:

$$G^{0} = x_A G^{0}_A + x_B G^{0}_B + x_C G^{0}_C \tag{5.3}$$

$$G^{en} = RT(x_A \ln x_A + x_B \ln x_B + x_C \ln x_C) \tag{5.4}$$

$$\begin{aligned} G^{ex} = {} & x_A x_B \sum_{i=0}^{2} A^{i}_{AB}(x_A - x_B)^i + x_A x_C \sum_{i=0}^{2} A^{i}_{AC}(x_A - x_C)^i + x_B x_C \sum_{i=0}^{2} A^{i}_{BC}(x_B - x_C)^i \\ & + f(T,x) x_A x_B x_C. \end{aligned} \tag{5.5}$$

In these relations x_A, x_B and x_C represent the mole fractions of components A, B and C in the system, G^0_A, G^0_B i G^0_C are appropriate reference states of specified components, R is Rydberg constant, and T is absolute temperature. Parameters A^i_{AB}, A^i_{AC} and A^i_{BC} depend only on temperature and they are determined by fitting of the dependences of excessive Gibbs energies of binary subsystems on the composition by relations:

$$G^{ex}_{AB} = x^b_A x^b_B \sum_{i=0}^{2} A^{i}_{AB}(x^b_A - x^b_B)^i \tag{5.6}$$

$$G^{ex}_{AC} = x^b_A x^b_C \sum_{i=0}^{2} A^{i}_{AC}(x^b_A - x^b_C)^i \tag{5.7}$$

$$G^{ex}_{BC} = x^b_B x^b_C \sum_{i=0}^{2} A^{i}_{BC}(x^b_B - x^b_C)^i, \tag{5.8}$$

where x^b_A, x^b_B and x^b_C are the mole fractions of components in the corresponding binary subsystems. The coefficient $f(T,x)$ is the ternary interaction coefficient which depends on temperature and mole fractions in the ternary system.

Parameters in terms (5.6)–(5.8) are determined from experimental data for each subsystem. To obtain an optimal set of model parameters, it is desirable to take into consideration several types of experimental data (phase diagrams, chemical potential and enthalpy), while for numerical calculation is convenient the least squares method. Procedure for calculation of the optimal set of parameters is often referred to as the calculation or optimization of the system. The obtained values of parameters are used for thermodynamic description of the binary subsystems and comparison with experimental values. Extrapolation method is then applied in order to obtain thermodynamic functions of the ternary system (relations (5.3)–(5.5)). The obtained extrapolated values represent the basis for setup of required experimental tests for the considered system.

Results of experiments are compared with extrapolated data and value of the ternary interaction coefficient is determined. Optimized set of parameters is stored in the so–called thermodynamic database. Calculation of phase diagrams, determination of thermodynamic and physical properties, and simulation of diffusion process in ternary system are possible using this database. The usual procedure for prediction of thermodynamic properties of ternary systems by CALPHAD method is shown in Fig. 5.1.

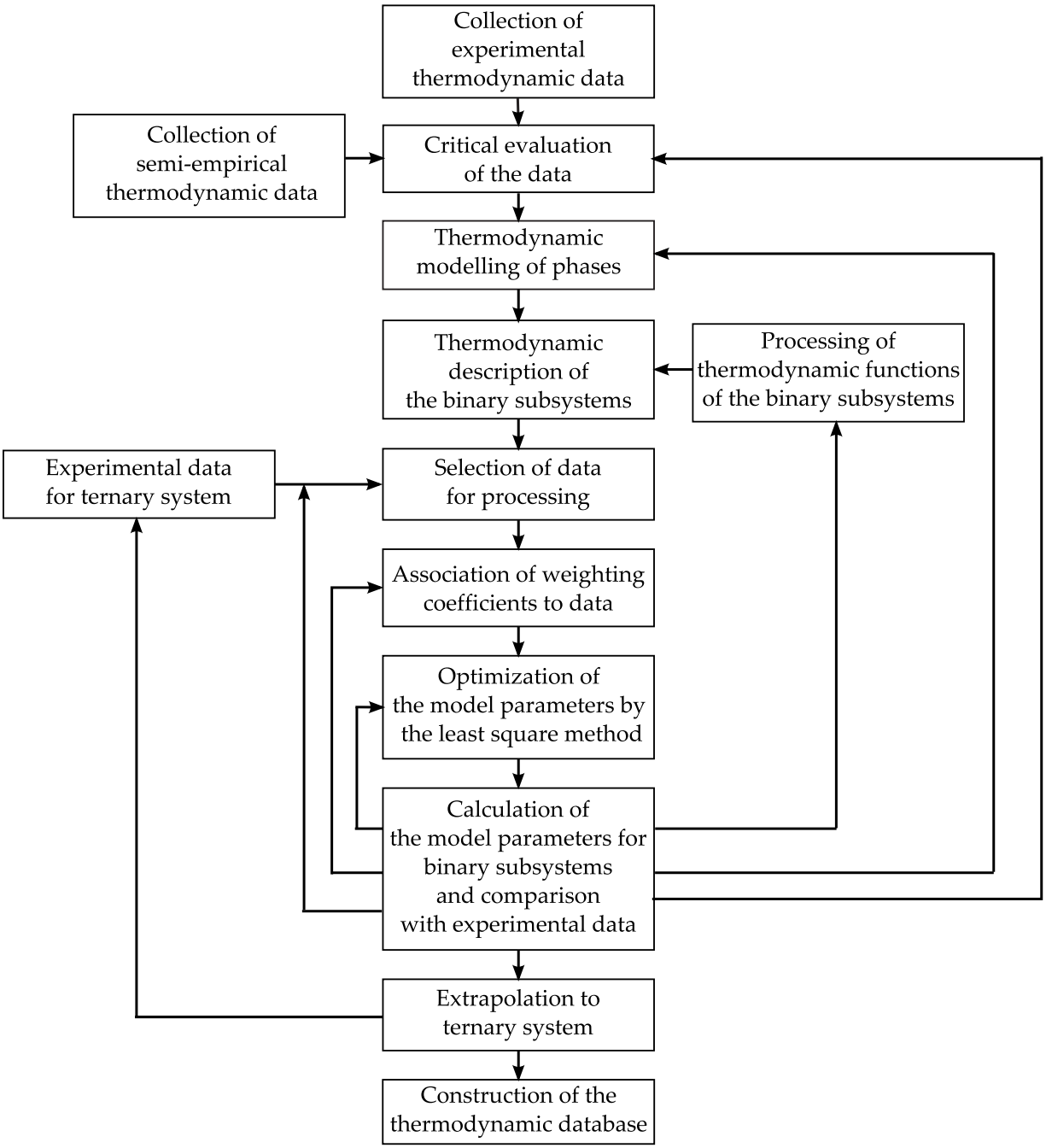

Figure 5.1: Flowchart of the CALPHAD method for prediction of thermodynamic properties of the ternary systems [110].

The successful implementation of CALPHAD method requires a reliable thermodynamic database which describes specific phases of the subsystems, and reliable computer programs that determine the optimal set of parameters. Well-known thermodynamic

databases are *SGTE* (Scientific Group Thermodata Europe), [111] and *FACT* (Facility for the Analysis of Chemical Thermodynamics) [112]. These databases, as public available, include data for a large number of binary, but only for a limited number of ternary systems. The most commonly used computer programs for the calculation of phase diagrams are *FactSage* (a compilation of older programs ChemSage and FACT–Win) [113], *Thermo-Calc* [114], *MTDATA* [115], so–called *Lucas* program [116], and *PANDAT* [117,118]. These programs are used to calculate the phase equilibrium and they are different in features and user interface. Also, each computer program specifies the format of thermodynamic database with which ensures compatibility.

Disadvantage of the CALPHAD method is that it requires an appropriate set of initial values for the optimization of model parameters in order to obtain accurate phase diagrams of stable systems. This, in turn, requires the prior knowledge of the tested phase diagram or special skills of the software user. Program PANDAT represents a new generation of software whose algorithm for calculation of the stable phases enables the automatic generation of phase diagrams without setting the initial values [117].

In this Dissertation, results of the calculation of phase diagrams of ternary systems by CALPHAD method using Thermo-Calc program and SGTE thermodynamic database are used as a reference [119–121].

5.1.2 A new method – a surface modeling method

From the geometric point of view, phase diagrams of ternary systems are limited to a regular triangular prism which is constructed by connecting the phase diagrams of binary subsystems. Height of the prism represents the temperature axis. The liquidus surface of such system consists of one or more smooth 3–D subsurfaces that are bounded by liquidus lines of the binary subsystems.

Standard software packages for 3–D surface modeling use NURBS – (Non–Uniform Rational B–Splines) as a mathematical tool for definition of guided (bounded) surfaces. Complex surfaces are modelled on the basis of given guide lines and a set of control points. Thus, the liquidus surface of a ternary system can be constructed using binary liquidus lines as guides and experimentally determined liquidus temperatures for the specified compositions as control points. Number of liquidus subsurfaces, their intersecting lines (cotectic lines), eutectic and peritectic points determine the nature of subsystem phase diagrams, i.e. whether they are isomorphic or eutectic. As a software tool can be used almost all standard programs for the surface modeling. Accordingly, this method for generation of 3–D phase diagrams of ternary systems is called *surface modeling method* [122].

A procedure for generation of ternary liquidus surfaces by the surface modeling method using program package SolidEdge is schematically shown in Fig. 5.2.

A set of initial thermodynamic parameters consists of the phase diagrams of binary subsystems and a selected set of experimentally determined liquidus temperatures. Since the binary systems are relatively well studied and their phase diagrams are available in the literature, this part of the initial parameters is not critical. On the other hand, available experimental values of the liquidus temperatures of ternary systems of different composition are scarce and sometimes unreliable. Therefore, a careful selection of initial values of the model parameters is needed. Planes which define base and faces of the equilateral prism are the framework for setting positions of the experimental points from the Gibbs triangle and import of the graphically presented binary phase diagrams. Liq-

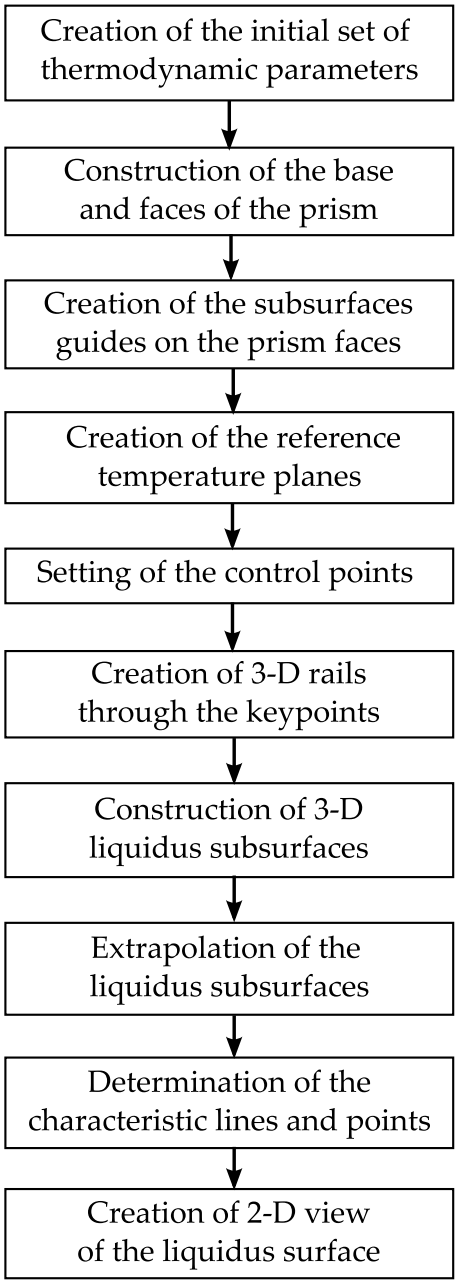

Figure 5.2: Procedure for generation of ternary liquidus surfaces by the surface modeling method.

uidus lines of these phase diagrams represent guides for creation of the liquidus surface. The shape of the liquidus line depends on the nature of the subsystem, and can consist of a single segment (isomorphic subsystem) or more segments (eutectic subsystem). Points corresponding to the ends of segments (equivalent to 100 % of individual system components and eutectic and peritectic points) are the keypoints. Reference temperature planes correspond to the adopted experimental liquidus temperatures and appropriate points from the Gibbs triangle are projected on it as the control points. Through these control and keypoints are set 3–D NURBS curves which, along with guides, allow formation of smooth, bounded 3–D liquidus subsurfaces. These subsurfaces are fully defined in the so–called angles of the phase triangle (near 100 % of the individual system components), and partly in the area of other key and control points. Depending on the number and positions of the control points, extrapolation of the created subsurfaces based on the smoothness criteria is necessary for a certain range of compositions. This yields a complete 3–D phase diagram of the ternary system. Characteristic lines are cotectic and isothermal lines, and the characteristic points are eutectic and peritectic points. Cotectic lines are determined by the intersection of adjacent subsurfaces, and isothermal lines by the intersection of the subsurface and corresponding temperature plane. Eutectic or peritectic points are defined by the intersection of cotectic lines. Projection of characteristic lines and points on the prism base (Gibbs triangle) give 2–D representation of the phase diagram of the considered ternary system.

Intersection of the generated 3–D liquidus surface with the selected isomorphic line enables to determine the lowest temperature at which the system of the given composition is completely in a liquid state. Also, it is possible to define compositions of the system which are characterized by desired melting temperature on the basis of the projection of the corresponding isothermal line onto the Gibbs triangle.

5.1.3 Liquidus surfaces of ternary systems for thermal cutoff purposes

The surface modeling method was applied to generate liquidus surfaces for ternary systems of Bi-Sn-Pb, Sn-Pb-In and Sn-In-Ga types. These systems form a series of low melting alloys, and knowledge of liquidus temperature for alloy of the predefined composition is important for the design and optimization of the solder joints in thermal cutoffs.

The system Bi-Sn-Pb

Liquidus surface of the system Bi-Sn-Pb is constructed using the phase diagrams of subsystems Sn-Pb, Sn-Bi and Pb-Bi which were taken from the literature [111, 121]. For control points were selected experimental values which gives one of the world most famous low melting alloys manufacturer [101] an they are listed in Table 5.1. 3–D liquidus surface of the system Bi-Sn-Pb generated using the surface modeling method is graphically presented in Fig. 5.3. Its 2–D representation in the form of isothermal and cotectic lines projections is shown in Fig. 5.4. Binary subsystems are eutectic, where Pb-Bi subsystem forms incongruently melting compound. Thus, from Fig. 5.3, four subsurfaces which are stitched along cotectic lines can be observed. Cotectic lines intersect in the eutectic (E) and peritectic (P) points.

For comparison, in Fig. 5.4 by black lines are shown projections of the liquidus surface of the system Bi-Sn-Pb calculated by the CALPHAD method [121] and experimentally obtained control points from Table 5.1. It can be seen that there is a good agreement

Control point No.	mass % Sn	mass % Pb	mass % Bi	liquidus T (°C)
1	60	14.5	25.5	180
2	46	46	8	173
3	27	51.5	21.5	170
4	37	42	21	152
5	30.8	38.4	30.8	139
6	22	22	56	104
7	22	28	50	100
8	15.5	32	52.5	95

Table 5.1: Experimental values of liquidus temperatures for alloys of Bi-Sn-Pb type [101].

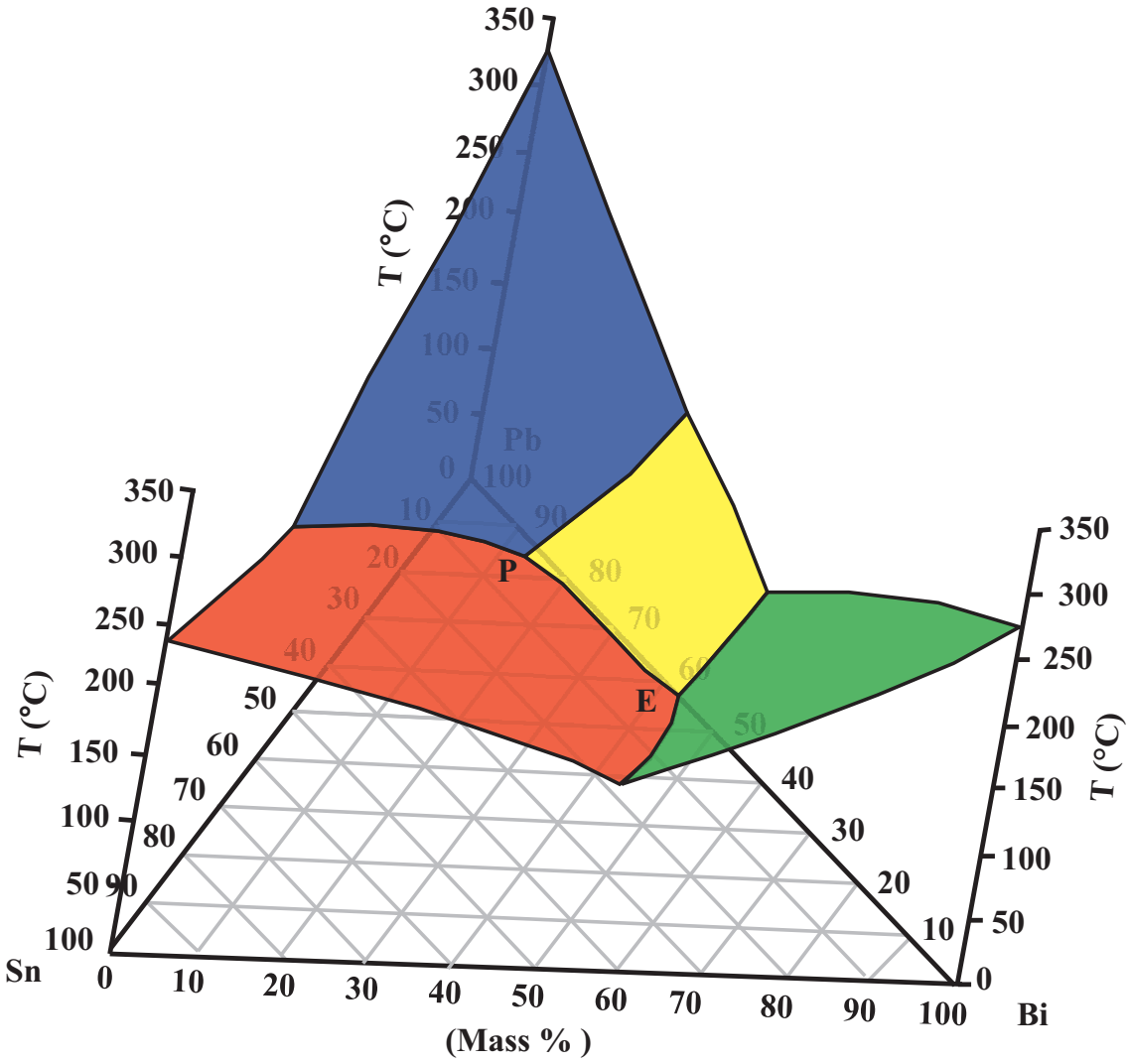

Figure 5.3: Liquidus surface of the system Bi-Sn-Pb generated by the surface modeling method.

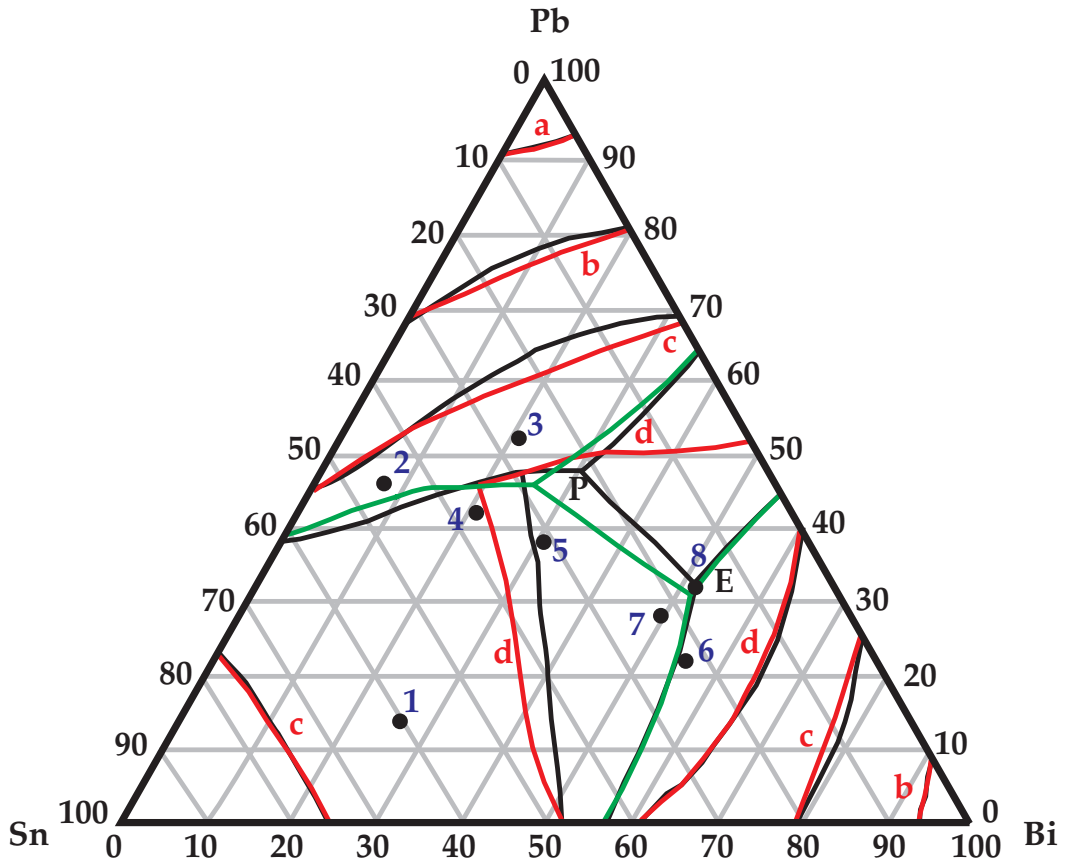

Figure 5.4: 2–D representation of Bi-Sn-Pb phase diagram generated by the surface modeling method (red and green lines) and CALPHAD method [121] (black lines); Isothermal lines are for: a) 300 °C, b) 250 °C, c) 200 °C, d) 150 °C; control points from Table 5.1 are presented by full circles.

between isothermal lines generated by both methods. Larger difference occurs only in the case defined by the isothermal line for 150 °C. Based on the fact that the isothermal line generated by the new method for 150 °C is very close to the control point 4 (152 °C), and that the isothermal line generated by the CALPHAD method for 150 °C is considerably closer to the control point 5 (139 °C), it can be concluded that the surface modeling method gives better agreement with the experimental values. As a consequence of the difference between the isothermal lines, mismatch of cotectic lines occurs. Namely, the intersection of cotectic lines (peritectic point) by the surface modeling method is at 139.6 °C (25%Bi-29%Sn-46%Pb) and by the CALPHAD method it is at 135.7 °C (30.5%Bi-21.9%Sn-47.6%Pb). On the other hand, eutectic points obtained by both methods are in good agreement and are very close to the control point 8 (95 °C).

The system Sn-Pb-In

Thermodynamic description of this system is rarely found in the literature [20, 120], despite the fact that its alloys are used in the surface mounting procedures for devices that do not work under high temperatures. Subsystems Sn-Pb, Sn-In and Pb-In are relatively well–known and their phase diagrams, used for design of liquidus surface, are taken from [112]. Experimental values of liquidus temperatures for this system (control points for the surface modeling method) are specified in Table 5.2, as taken from [101] (points 1–4) and [120] (points 5–7). Liquidus surface of the system Sn-Pb-In

Control point No.	mass % Sn	mass % Pb	mass % In	liquidus T (°C)
1	37.5	37.5	25	181
2	70	18	12	167
3	54	26	20	154
4	40	20	40	130
5	60.5	31.5	8	170
6	57	19	24	147
7	50.5	5.5	24	124

Table 5.2: Experimental values of liquidus temperatures for alloys of Sn-Pb-In type [101, 120].

generated by the surface modeling method in 3–D form is shown in Fig. 5.5. Since bynary subsystems Sn-Pb and Sn-In are eutectic, and subsystem Pb-In is peritectic, the liquidus surface consists of three subsurfaces that intersect along cotectic lines and form a peritectic point (P). Projections of cotectic and selected isothermal lines in the area of Gibbs triangle allow 2–D representation of the liquidus surface as shown in Fig. 5.6. The black line shows the projection of cotectic lines obtained by CALPHAD method [120] and black circles control points from Table 5.2. Differences between cotectic lines determined by two methods are due to the different choices of referent experimental points. For the same reason, the peritectic points determined by the surface modeling method at 123.2 °C (42.5%Sn-17.5%Pb-40%In) and CALPHAD method at 134.8 °C (47.5%Sn–7.6%Pb-24.9%In) diverge. Specifically, based on Table 5.2, an alloy of composition 70%Sn-18%Pb-12%In for temperatures above 167 °C should contain only a liquid phase. Results of the CALPHAD calculations at temperature of 172 °C for alloy of this composition attribute the liquid and solid phases [120]. Bearing in mind that the above control point is taken from the database specified by the world leading producer of indium alloys

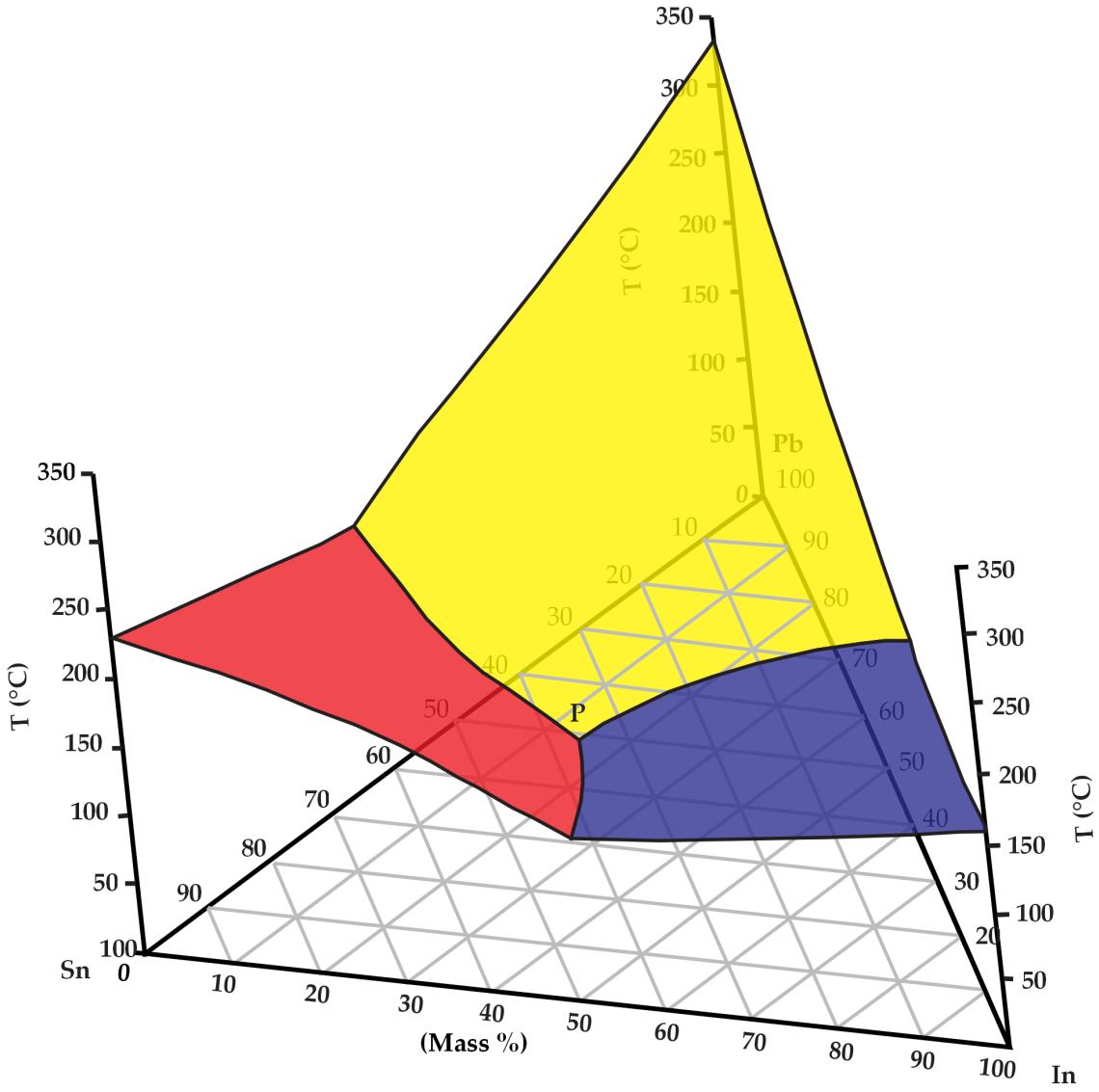

Figure 5.5: Liquidus surface of the system Sn-Pb-In generated by the surface modeling method.

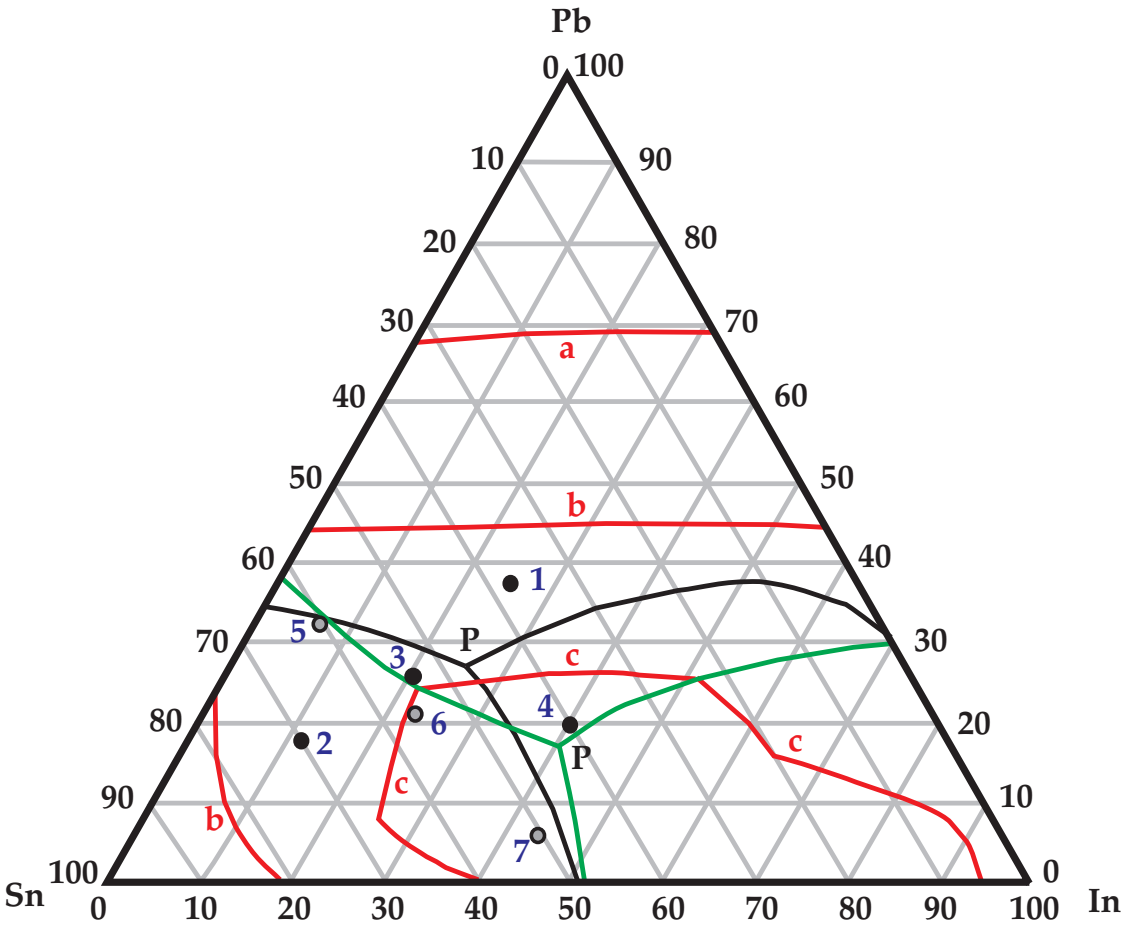

Figure 5.6: 2–D representation of Sn-Pb-In phase diagram generated by the surface modeling method (red and green lines) and CALPHAD method [120] (black lines); Isothermal lines are for: a) 250 °C, b) 200 °C, c) 150 °C; control points from Table 5.2 are presented by full circles.

[101], liquidus surface generated by the surface modeling method can be considered correct for the adopted set of experimental values. On the other hand, Fig. 5.6 shows that the isotherms for 250 °C and 200 °C are smooth curves, while the two curves for 150 °C are distorted as a result of the adjustment of liquidus surface to the control experimental values. It can be concluded that, regardless of the applied methodology, the lack of reliable experimental data for the ternary liquidus temperature brings a degree of uncertainty in the calculation of the liquidus surfaces.

The system Sn-In-Ga

The system of Sn-In-Ga type is interesting due to the striving for total elimination of lead from the soldering technology. It can also be used for thermal management applications and to replace mercury in applications such as motion switches and thermostats. Liquidus surface of this system is constructed based on the phase diagrams of subsystems Sn-In, Sn-Ga and In-Ga taken from [112] and the only literary available control point 10.7 °C (16%Sn–21.5%In–62.5%Ga) taken from [98]. All subsystems are eutectic, so that the generated 3–D liquidus surface consists of only three subsurfaces and one eutectic point (E), as can be seen in Fig. 5.7.

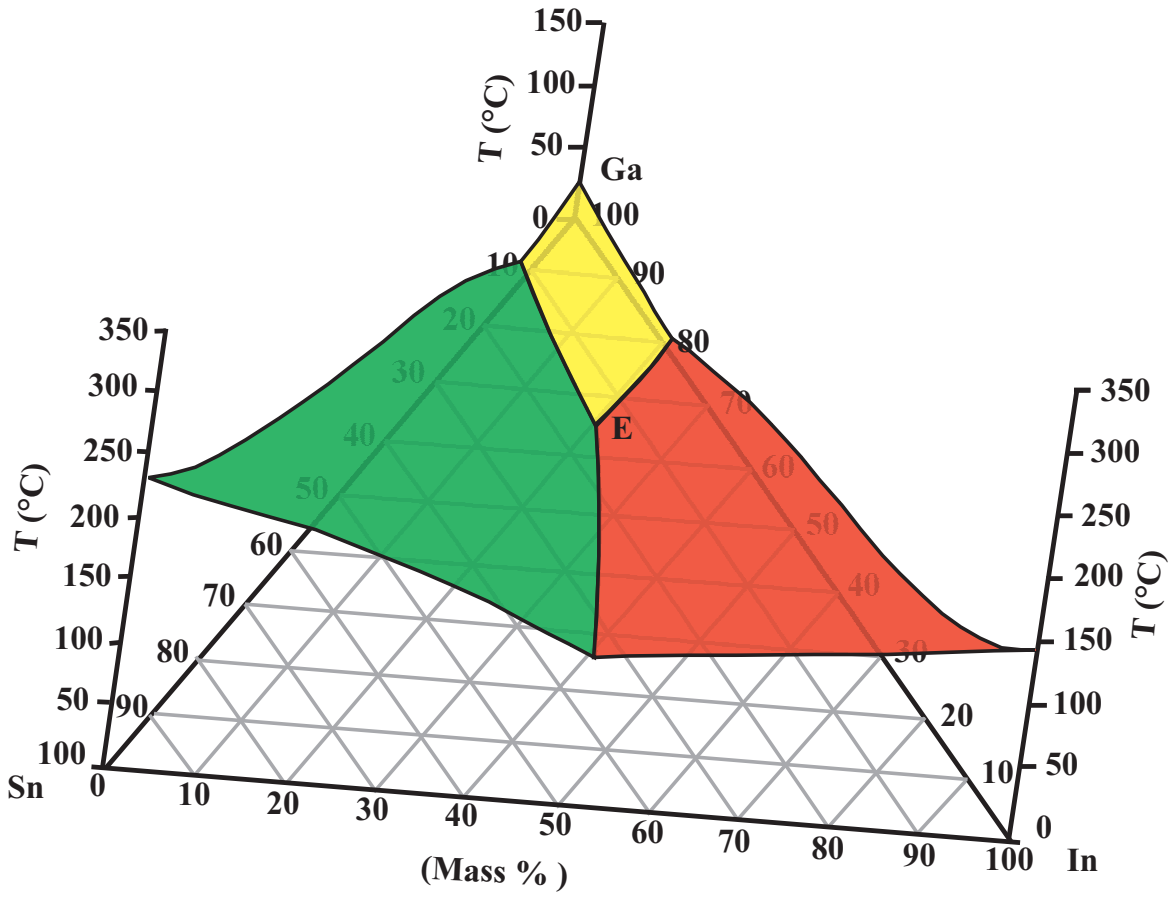

Figure 5.7: Liquidus surface of the system Sn-In-Ga generated by the surface modeling method.

Projections of isothermal and cotectic lines of Sn-In-Ga system generated by the surface modeling method are shown in Fig. 5.8. Since there are no data for the phase diagram of this system in the literature (except for the specified control point, which is

also the eutectic point), there is a lacks of comparison with the values modelled by some other method or obtained experimentally. The specificity of the system Sn-In-Ga is that it forms a series of alloys that are in liquid state at ambient temperature. Their chemical compositions can be read from the Fig. 5.8 within an area that is restricted by isotherms defined for 20 °C. These alloys are of interest for applications in nanocomposite systems and in devices that work in low–temperature environments. However, their drawback is relatively high price (due to the high content of Ga and In) and the necessity of providing special technological processing conditions (temperature lower than 10 °C).

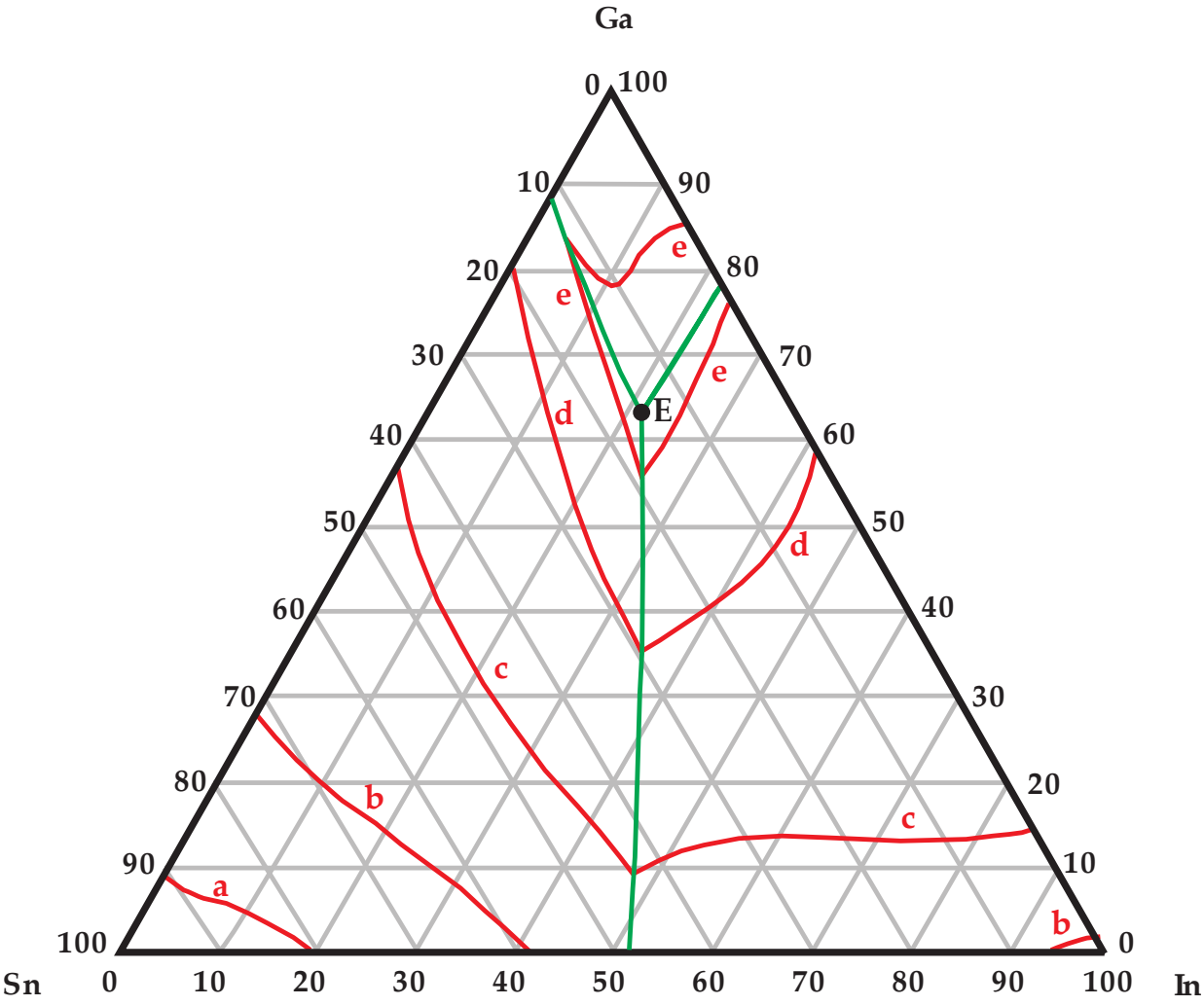

Figure 5.8: 2–D representation of Sn-In-Ga phase diagram generated by the surface modeling method. Isothermal lines are for: a) 200 °C, b) 150 °C, c) 100 °C, d) 50 °C, e) 20 °C.

5.2 Microstructural characterization of low melting alloys for thermal cutoff purposes

Investigation of microstructural characteristics of alloys that make soldering sheets in thermal cutoffs enables to specify conditions of their processing, as well as to predict

mechanical characteristics of solder joints [19,123]. The structure and grain size determine the strength of the alloy [19,57], while the composition of the grains directly affects wetting of the soldering surfaces [18,20].

Protection of boiling appliances requires the use of thermal cutoffs with rated functioning temperature below 100 °C. Based on generated liquidus surface for ternary Bi-Sn-Pb system described in the previous section, for making the cutoff for this purpose an alloy of composition 52.5%Bi-15.5%Sn-32%Pb can be used. This is an eutectic alloy whose melting point is 95 °C. On the other hand, the power electric motors require a rated functioning temperature of cutoff below 150 °C. For this purposes, soldering sheets are produced of 58%Bi-42%Sn alloy. It is also eutectic alloy with a melting point of 138 °C. With the aim of predicting the effectiveness of these alloys in appropriate thermal cutoffs, their microstructural characterization is performed. Since the binary Bi-Sn alloy is a subsystem of the ternary Bi-Sn-Pb system, the characterization of these two alloys is important for assessing the quality of solder joints made of 58%Bi-42%Sn alloy on the Pb substrate [18].

Microstructural analysis was carried out on refractive (internal) and physical (external) surface of samples taken from ingots of alloys. Examination by the SEM (Scanning Electron Microscopy) technique determined the form of grains, while the EDS (Energy Dispersive Spectroscopy) technique determined their composition.

SEM image and EDS spectra taken from the fracture surface of the 52.5%Bi-15.5%Sn-32% Pb alloy sample are shown in Fig. 5.9. It can be noticed the grained structure with non–uniform size and composition of the grains. Larger grains contain approximately 90% Bi (Fig. 5.9(b)), while in the smaller grains Bi and Pb dominate over Sn (Fig. 5.9(c)).

Results of the external surface analysis of the alloy sample, shown in Fig. 5.10, indicate the laminar structure where the content of Sn is over 80%.

From Fig. 5.11, which shows the SEM image and EDS spectrum of the fracture surface of the 58%Bi-42%Sn alloy sample, grained structure is noticeable. Compared to the ternary alloy, the grains are more uniform, have smaller size and approximate composition of 70%Bi and 30%Sn. The smaller grain size contributes to improved mechanical properties of the alloy, and thus a greater reliability of the solder joints made from it [20].

The microstructure of the external surface of the 58%Bi-42%Sn alloy sample has distinct laminar character, as observed in Fig. 5.12 which shows the corresponding SEM image and EDS spectrum. In the laminar sheets prevails Sn with 80%.

The fact that external surfaces of both alloys is dominated by tin is important for the processing of these materials during the production of thermal cutoffs. The ingots of alloys are shaped in the form of sheets by slicing and cold rolling methods. The sheets are connected with the conductive strip and copper leads by soldering. The copper leads are during the preparation for soldering coated with a layer of tin or nickel and great content of tin at the surface of the sheets enables better wetting of the soldering surface [20], and thus the quality of the solder joints. Bearing in mind that the temperature response of solder joints is the basis for the functioning of thermal cutoffs, their quality affects the quality of the cutoffs.

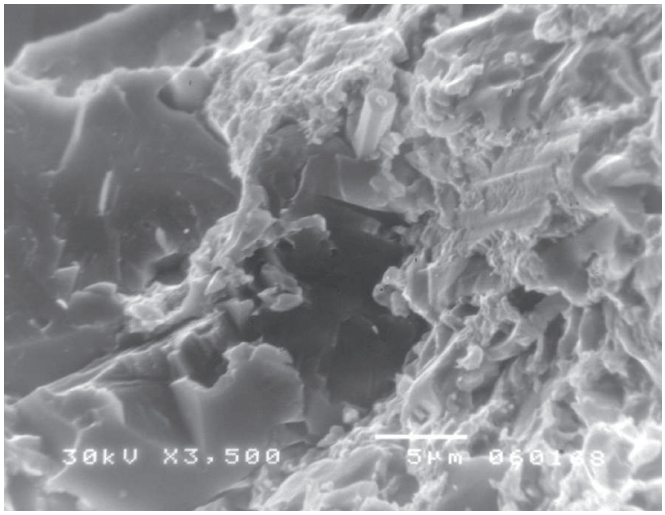

(a)

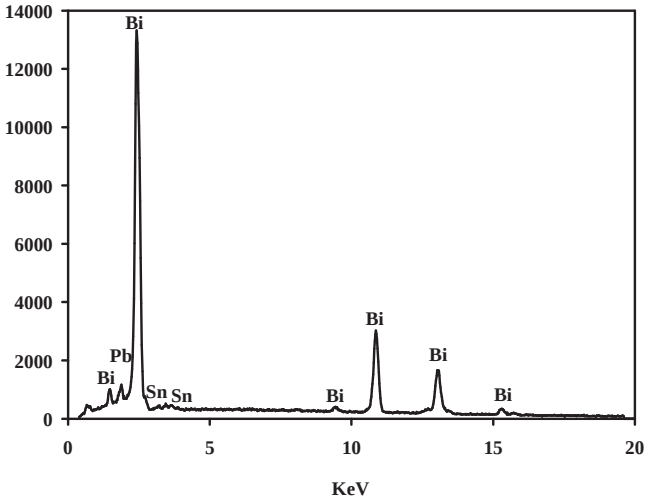

(b)

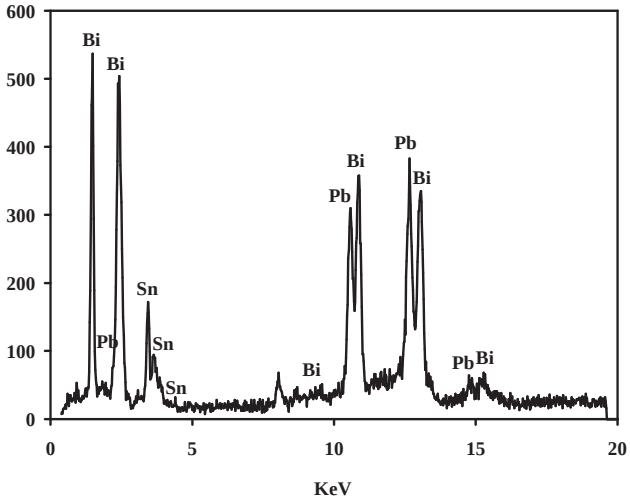

(c)

Figure 5.9: SEM image (a) and EDS spectra (b,c) taken from the fracture surface of the 52.5%Bi-15.5%Sn-32%Pb alloy sample. Spectrum (b) corresponds to the area on the left and spectrum (c) on the right side of the SEM image.

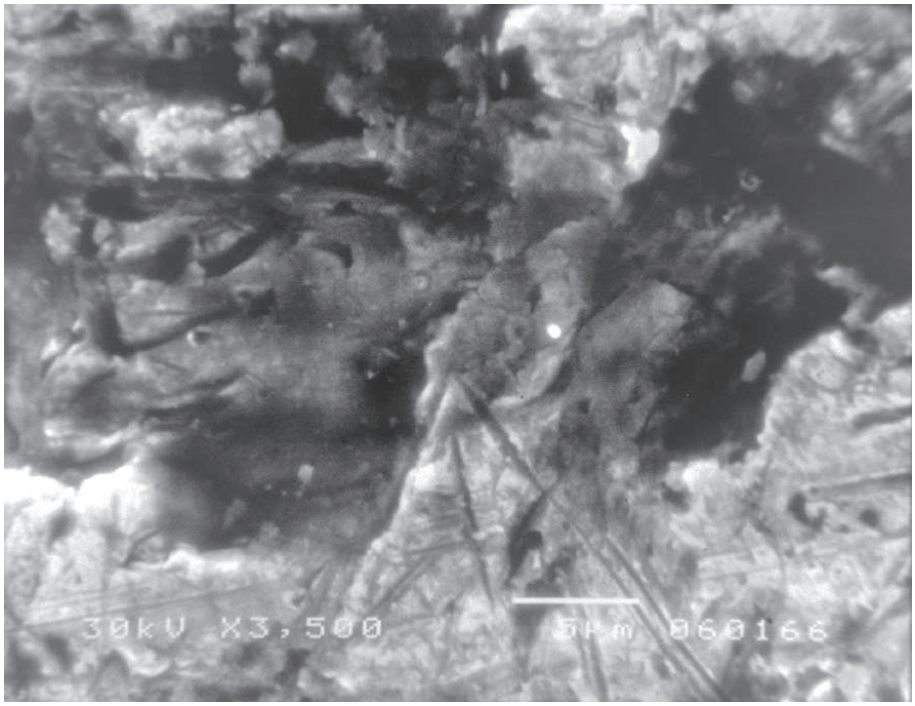

(a)

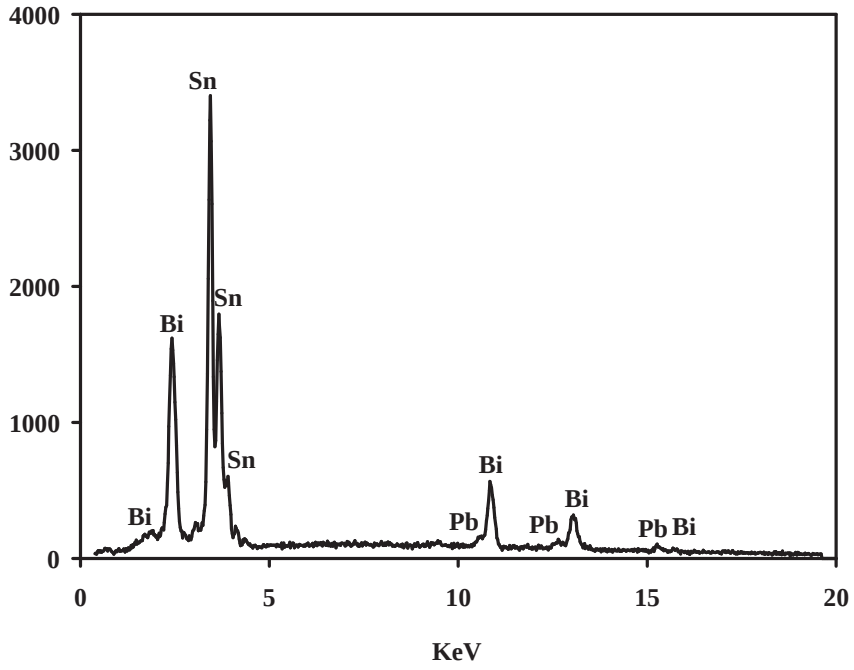

(b)

Figure 5.10: SEM image (a) and EDS spectrum (b) taken from the external surface of the 52.5%Bi-15.5%Sn-32%Pb alloy sample.

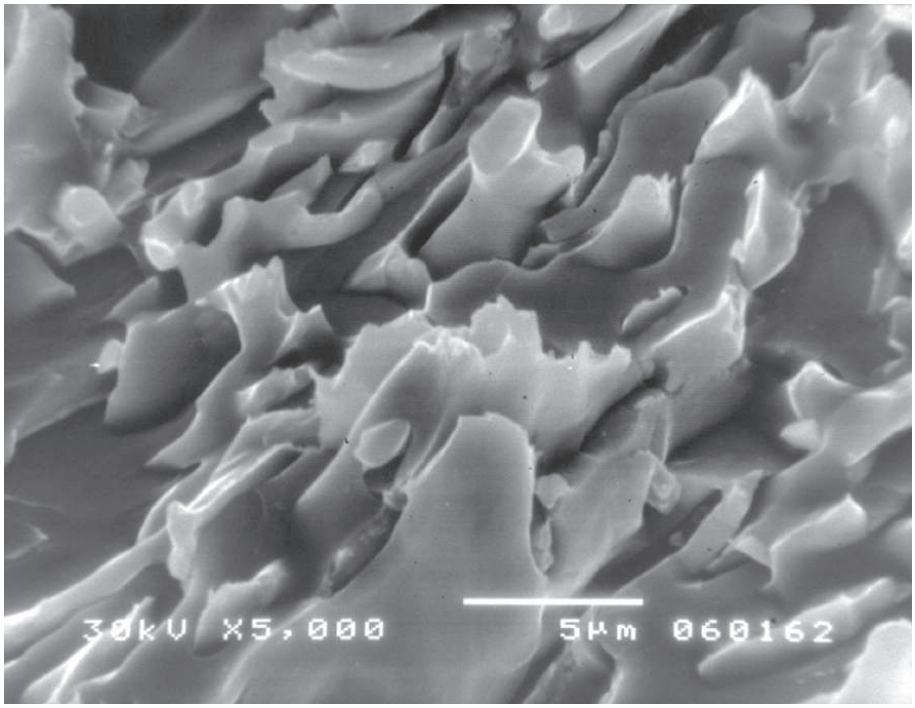

(a)

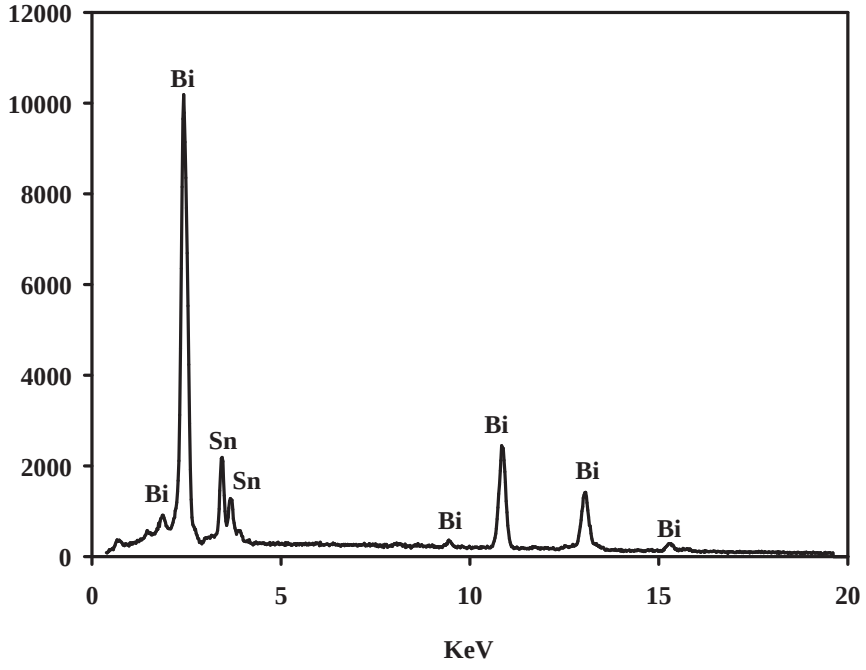

(b)

Figure 5.11: SEM image (a) and EDS spectrum (b) taken from the fracture surface of the 58%Bi-42%Sn alloy sample.

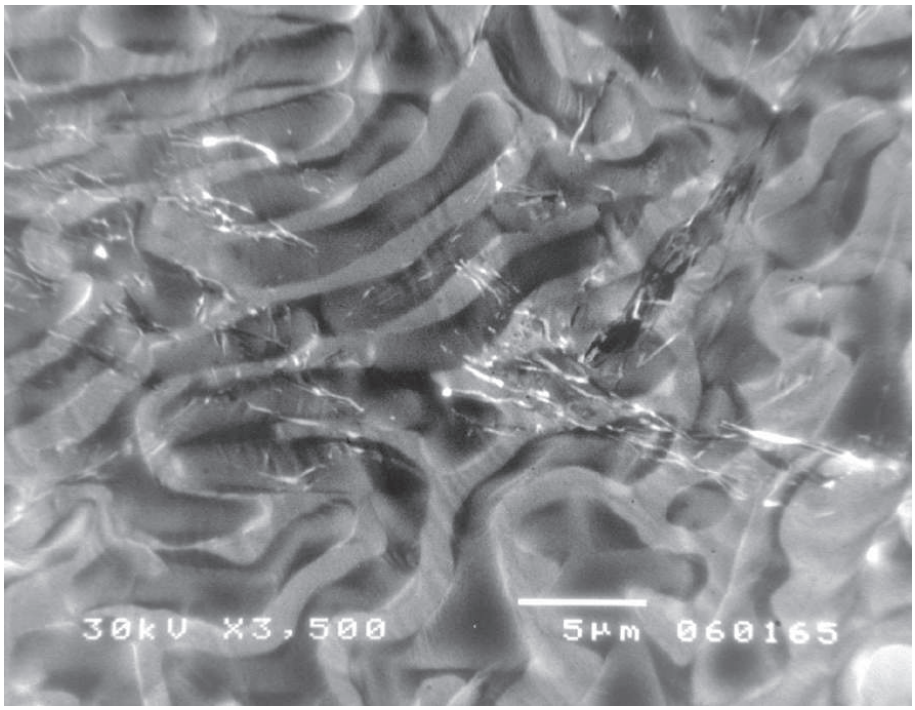

(a)

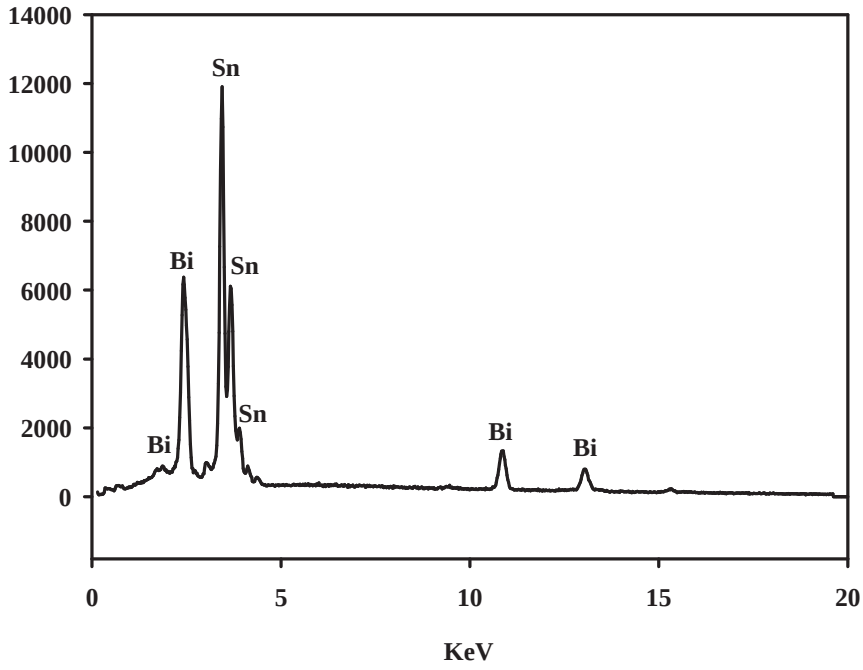

(b)

Figure 5.12: SEM image (a) and EDS spectrum (b) taken from the external surface of the 58%Bi-42%Sn alloy sample.

Chapter 6

3–D simulation of thermal cutoffs in electrical and thermal domains

The parameters of functionality, quality and reliability of thermal cutoffs are considered during their design and optimization procedures. Simulation of thermal cutoffs in electrical and thermal domains greatly simplifies and accelerates these processes. Simulation results allow to define optimal dimensions of thermal cutoff elements, as well as to predict the response time for the given operating conditions and reliability parameters.

6.1 Considered thermal cutoffs

For the protection of power electric motors and boiling appliances thermal cutoffs of the radial type with a spring and plastic housing are used. These cutoffs are described in Section 4.2 and their rated voltage is 250 V and rated current up to 12 A. Characteristic dimensions of cutoff elements designed on the basis of presented fundamentals and used in 3–D simulations are listed in Table 6.1.

The basic design of thermal cutoffs include leads without shaped contacting heads, the thickness of the conductive strip of 1.2 mm and a housing wall thickness of 1 mm. In the optimization process of cutoffs, implementation of specially formed contacting heads and consequently changed diameter of the soldering sheets, two thicknesses of the conductive strip, and reduced wall thickness of the housing are discussed. The spring is modelled as a cylinder whose base diameter corresponds to the diameter of the spring, and the height to the length of the spring.

Materials for realization of thermal cutoffs are selected in accordance with considerations given in Section 4.3. For leads and conductive strip in the simulation was taken copper without plating. As material for the soldering sheets are selected low melting alloys whose characterization for these purposes is described in Section 5.2. These are alloys of the composition 52.5%Bi-15.5%Sn-32%Pb and 58%Bi-42%Sn, whose melting temperatures are 95 °C and 138 °C, respectively. These temperatures determine the cutoff temperature of the devices, and accordingly two types of cutoffs: S–95 and S–138. The housing is made of the flame–resistant plastic, in this case polycarbonate – *Makrolon*. It is characterized by extreme resistance to mechanical stress, low coefficient of thermal expansion, high thermal resistance and strength at low temperatures [124]. Since the spring is taken as a standard element, its material is steel. As insulating fluid within the housing is used air.

Element	Material	Characteristic dimension	Value (mm)
Leads	Copper	Length	57
		Diameter	1.2
		Contacting head diameter	1.6
		Contacting head height	0.25
		Outside lead length	50
Conducting strip	Copper	Length	5.6
		Width	1.6
		Depth	0.6; 0.9; 1.2
Soldering sheets	Low melting alloy	Diameter	1.2; 1.6
		Depth	0.15
Housing	Makrolon	Height	11
		Width	8.8
		Depth	3.8
		Stand height	4
		Wall thickness	1; 0.5
Spring	Steel	Diameter	1
		Length	3

Table 6.1: Dimensions of the considered thermal cutoffs.

Physical, thermal and electrical parameters of materials that make constitutive elements of thermal cutoffs used in the simulation are given in Table 6.2.

6.2 Simulation procedure

3–D simulation of thermal cutoffs in thermal and electrical domains was performed by computer program ANSYS described in Section 2.2. Interdependence of thermal and electrical characteristics is achieved by *Multiphysics* module through coupled domain analysis and direct solving method. The simulation procedure follows the flow defined in Fig. 2.2, while the preprocessing steps are shown in Fig. 6.1.

Determination of thermal parameters of functionality, quality and reliability of thermal cutoffs within specific electrical constraints requires steady–state, as well as time dependent simulations. Therefore, the appropriate static and transient analyses were performed. A non–linear, iterative Newton–Raphson's method was employed with SOLID98 type of finite elements. In transient analysis an abrupt change of boundary conditions with adequate load substeps was defined.

The finite element model was generated by solid modeling and values of physical, electrical and thermal parameters of materials were assigned according to Table 6.2.

Mechanical load conditions of thermal cutoffs are defined by the symmetry boundary condition and freedom degrees. Section plane shown in Fig. 4.1 is a symmetry plane of the simulated structure, while mechanical movement is limited at free ends of the leads. Electrical load conditions are given by zero reference potential at one lead and value of the current flowing through the surface of the second lead in the range from 0.1 A to 15 A. Parameters of the thermal load are determined by convection from free surfaces of the housing and leads. Simulation assumed operation of the cutoff in a vertical position in the air whose reference temperature is 300 K. For determination of the response time

Material/ Parameter	Cu	52.5%Bi-15.5%Sn-32%Pb	58%Bi-42%Sn	Makrolon	Steel	Air
Melting point (K)/(°C)	1356/1083	368/95	411/138	563/290	1791/1518	
Density (kg/m^3)	8960	9600	8560	1200	7850	1.205
Thermal conductivity (W/mK)	401	13	18.4	0.2	50	0.026
Specific heat (J/kgK)	385	151	167	1172	460	1005
Coefficient of thermal expansion (1/K)	$16.5 \cdot 10^{-6}$	$2.5 \cdot 10^{-5}$	$1.5 \cdot 10^{-5}$	$6.5 \cdot 10^{-5}$	$1.2 \cdot 10^{-5}$	$3.4 \cdot 10^{-3}$
Electrical resistivity (Ωm)	$1.69 \cdot 10^{-8}$	$7.48 \cdot 10^{-7}$	$3.82 \cdot 10^{-7}$	$1 \cdot 10^{14}$	$1.69 \cdot 10^{-7}$	$1 \cdot 10^{14}$
Temp. coefficient of electrical resistivity (1/K)	$4,29 \cdot 10^{-3}$					

Table 6.2: Physical, thermal and electrical parameters of materials used for thermal cut-offs [96, 101, 121, 124, 125].

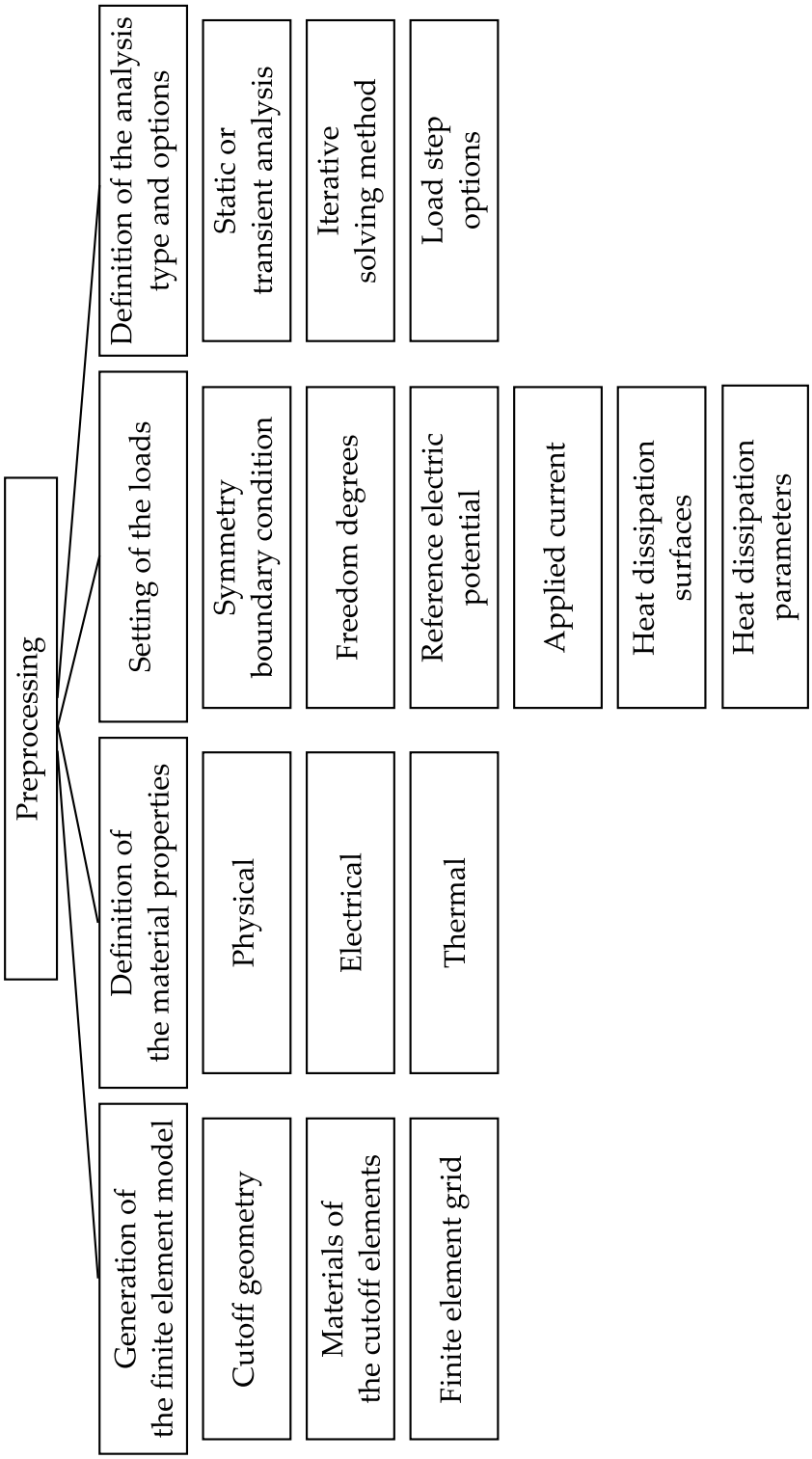

Figure 6.1: Preprocessing steps of the cutoffs simulation procedure.

of the cutoff, as stated in Section 4.1.1, for the surrounding fluid was taken a silicone oil. Convection coefficient is assumed to be constant throughout the whole considered area [126] and its dependence on the shape and dimensions of the surface, parameters of the surrounding fluid, and temperature difference between the surface and the ambient is included. The specific value of the convection coefficient h is calculated on the basis of the expression [127]:

$$h = \frac{Nuk}{H}, \tag{6.1}$$

where k is coefficient of thermal conductivity of the surrounding fluid and Nu is so–called Nusselt's number of the considered surface of height H, defined by the relation:

$$Nu = 0.59Ra^{0.25}. \tag{6.2}$$

For the cylindrical surfaces of leads with diameter D, correction due to the narrowness of the leads is included by multiplying the resulting value of Nu with correction factors for air f_a and silicone oil f_s:

$$f_a = 1 + 1.446\left[Gr^{-0.25}\left(\frac{H}{D}\right)\right]^{0.904}, \tag{6.3}$$

$$f_s = 1 + 0.141\left[Gr^{-0.25}\left(\frac{H}{D}\right)\right]. \tag{6.4}$$

In equation (6.2), Ra is the Rayleigh's number which depends on the coefficient of thermal expansion β, thermal diffusivity α and kinematic viscosity ν of the ambient fluid, and temperature difference between the examined surface and the fluid $\Delta T = T - T_O$, according to the expression:

$$Ra = \frac{g\beta\Delta TH^3}{\alpha\nu}. \tag{6.5}$$

A similar dependence has the Grashof's number:

$$Gr = \frac{g\beta\Delta TH^3}{\nu^2}, \tag{6.6}$$

where g is the gravity of Earth.

When considering air as the ambient fluid, dependence of its basic parameters on temperature was taken into account, and values implemented in the simulation are given in Table 6.3. Since convection coefficient depends on several factors, its theoretical value often requires adjustment based on the experiment. Simulation of designed thermal cutoffs was made with correction of the theoretical convection coefficient for air as the ambient fluid by a constant value of +10 W/m^2. This value is defined on the basis of the experimental data presented in detail in Chapter 7.

The other considered ambient fluid is a silicone oil DOW CORNING 210H [129] usually used in oil baths. Its parameters are considered as temperature–independent and have the values: $k = 0.11$ W/mK, $\alpha = 8{\cdot}10^{-8}$ m^2/s, $\beta = 9\cdot10^{-4}$ 1/K, $\nu = 10^{-4}$m ^{2}/s.

6.3 Distribution of electrical and thermal quantities

By simulation of thermal cutoffs in 3–D domain at various operating conditions distributions of different electrical and thermal parameters within them were obtained. The

T(°C)	k(W/mK)	α(m^2/s)	β(1/K)	ν(m^2/s)
0	0.0243	$1.8700 \cdot 10^{-5}$	$3.67 \cdot 10^{-3}$	$1.330 \cdot 10^{-5}$
20	0.0257	$2.1222 \cdot 10^{-5}$	$3.43 \cdot 10^{-3}$	$1.511 \cdot 10^{-5}$
40	0.0271	$2.3927 \cdot 10^{-5}$	$3.20 \cdot 10^{-3}$	$1.697 \cdot 10^{-5}$
60	0.0285	$2.6472 \cdot 10^{-5}$	$3.00 \cdot 10^{-3}$	$1.890 \cdot 10^{-5}$
80	0.0299	$2.9633 \cdot 10^{-5}$	$2.83 \cdot 10^{-3}$	$2.094 \cdot 10^{-5}$
100	0.0314	$3.2896 \cdot 10^{-5}$	$2.68 \cdot 10^{-3}$	$2.306 \cdot 10^{-5}$
120	0.0328	$3.6057 \cdot 10^{-5}$	$2.55 \cdot 10^{-3}$	$2.523 \cdot 10^{-5}$
140	0.0343	$3.9649 \cdot 10^{-5}$	$2.43 \cdot 10^{-3}$	$2.755 \cdot 10^{-5}$
160	0.0358	$4.3192 \cdot 10^{-5}$	$2.32 \cdot 10^{-3}$	$2.985 \cdot 10^{-5}$
180	0,0372	$4.6726 \cdot 10^{-5}$	$2.21 \cdot 10^{-3}$	$3.229 \cdot 10^{-5}$
200	0,0386	$5.0431 \cdot 10^{-5}$	$2.11 \cdot 10^{-3}$	$3.463 \cdot 10^{-5}$

Table 6.3: The main thermal parameters of air at different temperatures implemented in the simulation [128].

temperature distribution is of importance for cutoff functionality, while distributions of current density and electric potential enable better understanding of the influence of different geometry and dimensions of the cutoff elements during their optimization [130].

Electric potential distribution in S–95 thermal cutoff of the basic design at rated current of 12 A and at ambient temperature of 300 K is shown in Fig. 6.2. Uniform distribution of the electric potential is evident, with values up to 25 mV above the reference zero potential. On the basis of this dependence, electrical resistance of the conductive parts of the cutoff is determined as 2.1 mΩ. Identical distribution of electric potential exists for thermal cutoff of S–138 type, except that, due to the higher electrical conductivity of applied alloys, the maximum value of the electric potential is 24 mV, and it corresponds to the resistance of the conductive part of 2 mΩ.

Vector representation of the current density distribution in S–95 thermal cutoff of the basic design at rated current of 12 A and at ambient temperature of 300 K is shown in Fig. 6.3. Maximum current density exists at the interface of the soldering sheets and conductive strip and it has value of $1.4 \cdot 10^7$ A/m^2. Qualitatively and quantitatively the same distribution is obtained for cutoff of S–138 type.

Areas of the maximum current density are also areas of the maximum heating due to the Joule's effect. Significantly lower thermal conductivity of makrolon and air with respect to the conductive elements causes heat accumulation in the vicinity of the soldering sheets. On the other hand, due to the high thermal conductivity of the leads, conductive strip and soldering sheets, the heat is effectively distributed through these elements and released by convection from the free surfaces of the leads. Temperature distribution for S–95 cutoff is shown in Fig. 6.4 and for S–138 cutoff in Fig. 6.5.

As in the case of current density distribution, the maximum value of temperature exists at the interface of the soldering sheets and conductive strip, while the range of temperatures in the conductive parts of the cutoff is 1.5 K. The qualitative distributions of temperatures for both types of cutoffs are the same, while maximum temperatures differ a little due to the difference in conduction characteristics of the applied alloys.

Functional and thermal operating parameters of cutoffs are determined from temperature distributions in them. Therefore, it is important to consider temperature in cutoffs for the various designed configurations and dimensions of individual elements. In Figs. 6.6 and 6.7 are shown distributions of temperature in S–138 thermal cutoff type at rated

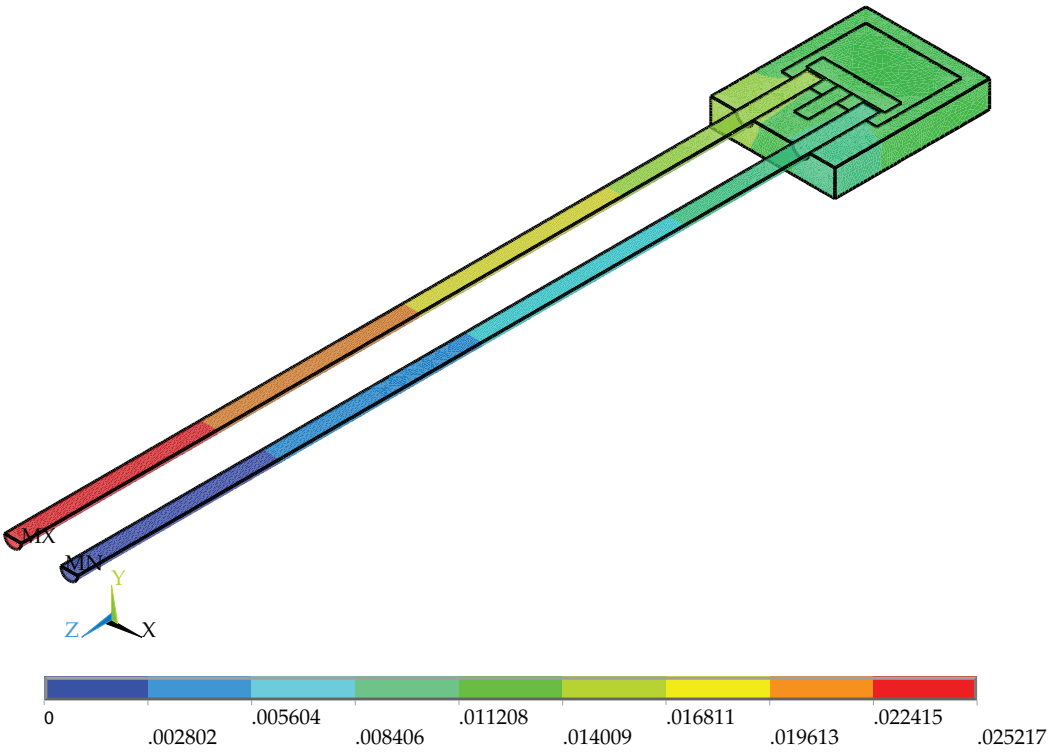

Figure 6.2: Electric potential distribution in S–95 thermal cutoff at rated current of 12 A and ambient temperature of 300 K.

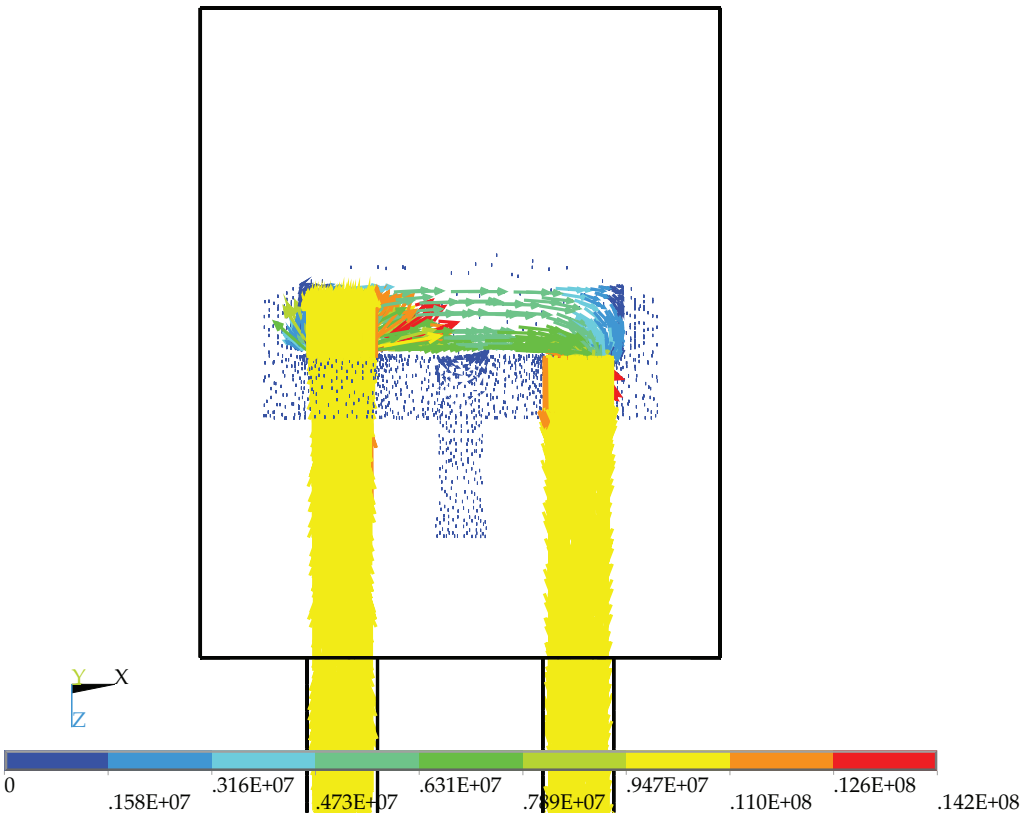

Figure 6.3: Vector representation of the current density distribution in S–95 thermal cutoff at rated current of 12 A and ambient temperature of 300K.

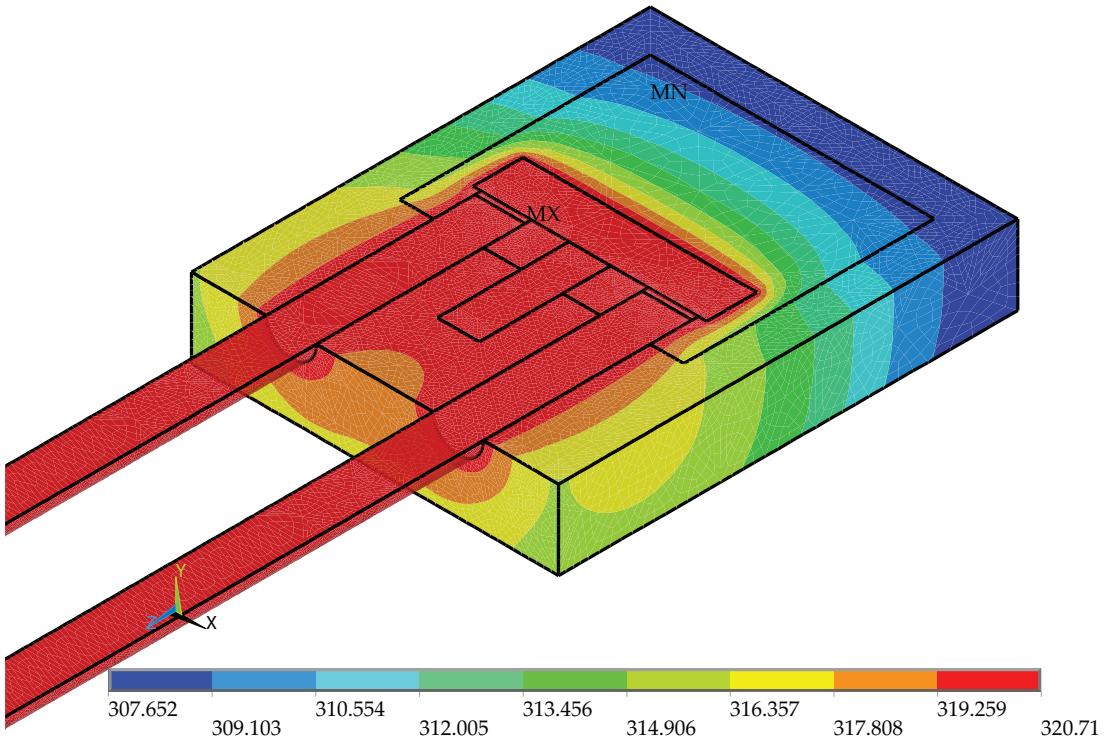

Figure 6.4: Temperature distribution in S–95 thermal cutoff at rated current of 12 A and ambient temperature of 300K.

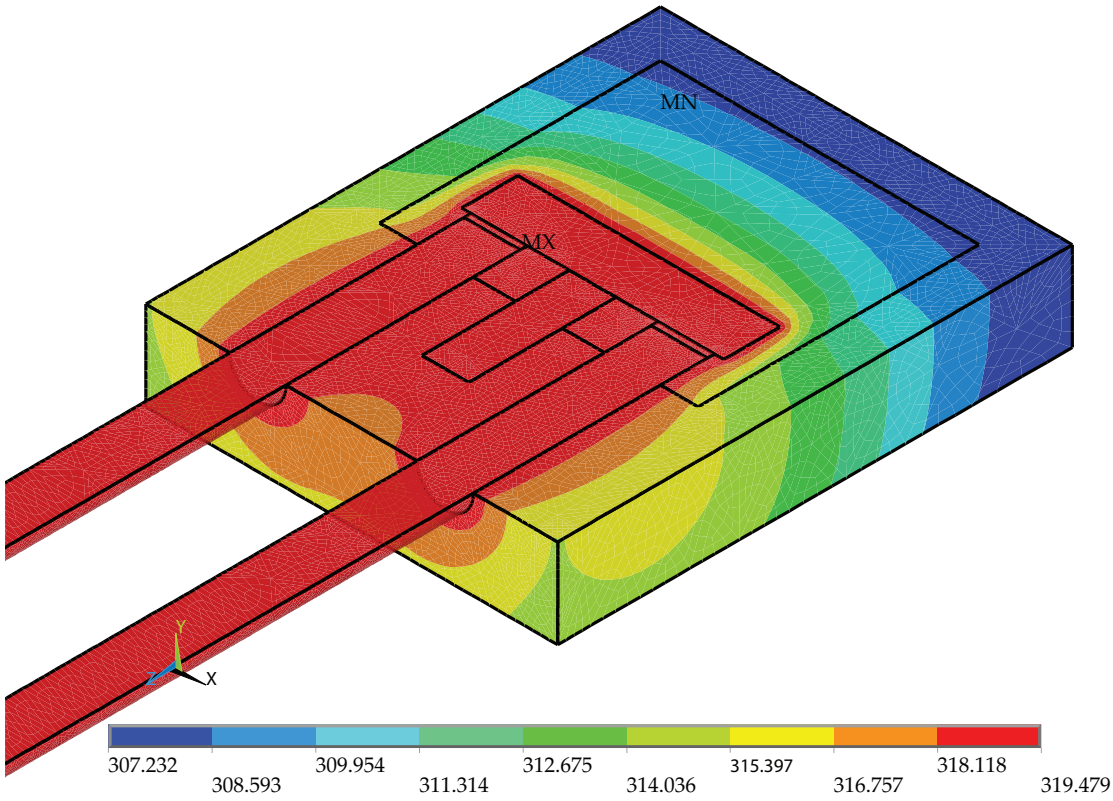

Figure 6.5: Temperature distribution in S–138 thermal cutoff at rated current of 12 A and ambient temperature of 300K.

current of 12 A, ambient temperature of 300 K, and reduced depth of the conductive strip to 0.9 mm and 0.6 mm.

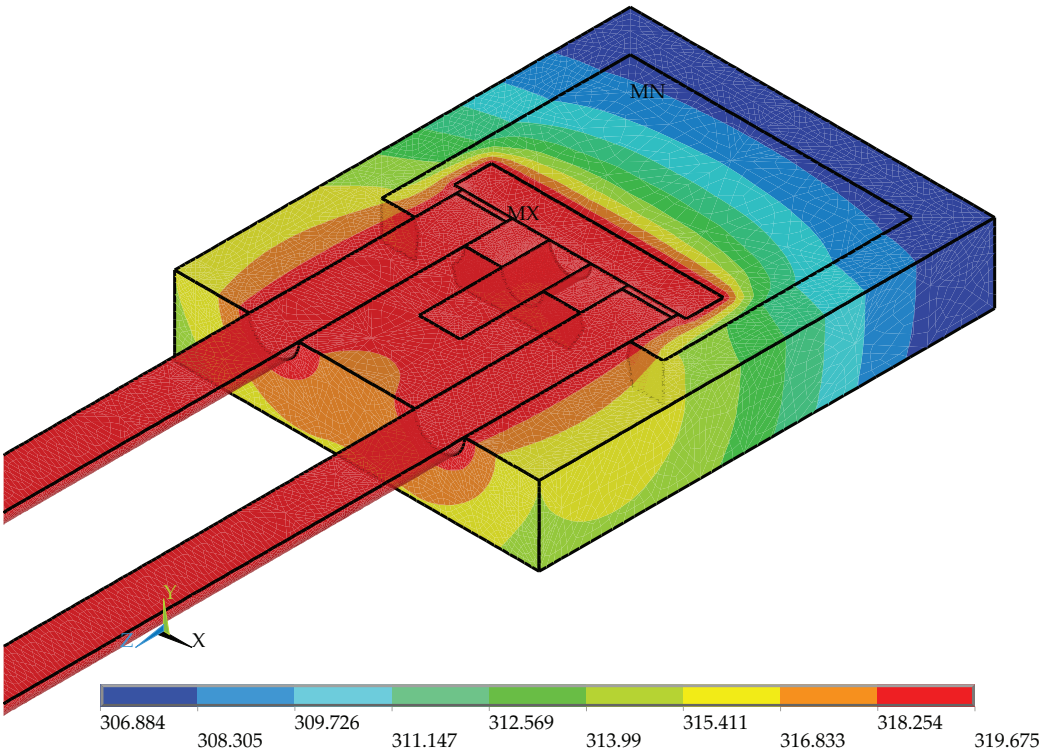

Figure 6.6: Temperature distribution in S–138 thermal cutoff at rated current of 12 A and ambient temperature of 300K for 0.9 mm conductive strip depth.

Comparing with Fig. 6.5, which is for 1.2 mm of the conductive strip thickness, qualitatively the same distributions are observed with a somewhat modified maximum values. Namely, a maximum of 319.5 K in the basic design, becomes 319.7 K for the thickness of the strip of 0.9 mm, and 320 K for the thickness of 0.6 mm.

Since the temperature of soldering sheet is determined by the current density value which flows from leads through the soldering sheets and the conductive strip, the influence of contacting head shape on the temperature distribution in the cutoffs was investigated. The flat shape of the contacting head is replaced with a riveted one. Formed contacting heads had dimensions listed in Table 4.1 and soldering sheets had properly adjusted diameter. Rivet contact head provides a better mechanical stability of the solder joint. The temperature distribution in the riveted thermal cutoff of S–95 type at rated current of 12 A and an ambient temperature of 300 K is shown in Fig. 6.8.

Comparing this distribution with the one in the thermal cutoff with the flat contacting head (Fig. 6.4) reduction in the maximum temperature of about 1 K can be observed. In the S–138 cutoff modification reduces the maximum temperature for approximately 0.5 K.

Thermal characteristics of the cutoff housing are primarily defined by the coefficient of thermal conductivity of material from which it is made, and by its geometry and dimensions. With the aim to investigate the influence of the thickness of the housing wall on the temperature characteristics of the cutoff, a temperature distribution for reduced thickness of the wall from 1 mm to 0.5 mm is obtained and shown in Fig. 6.9.

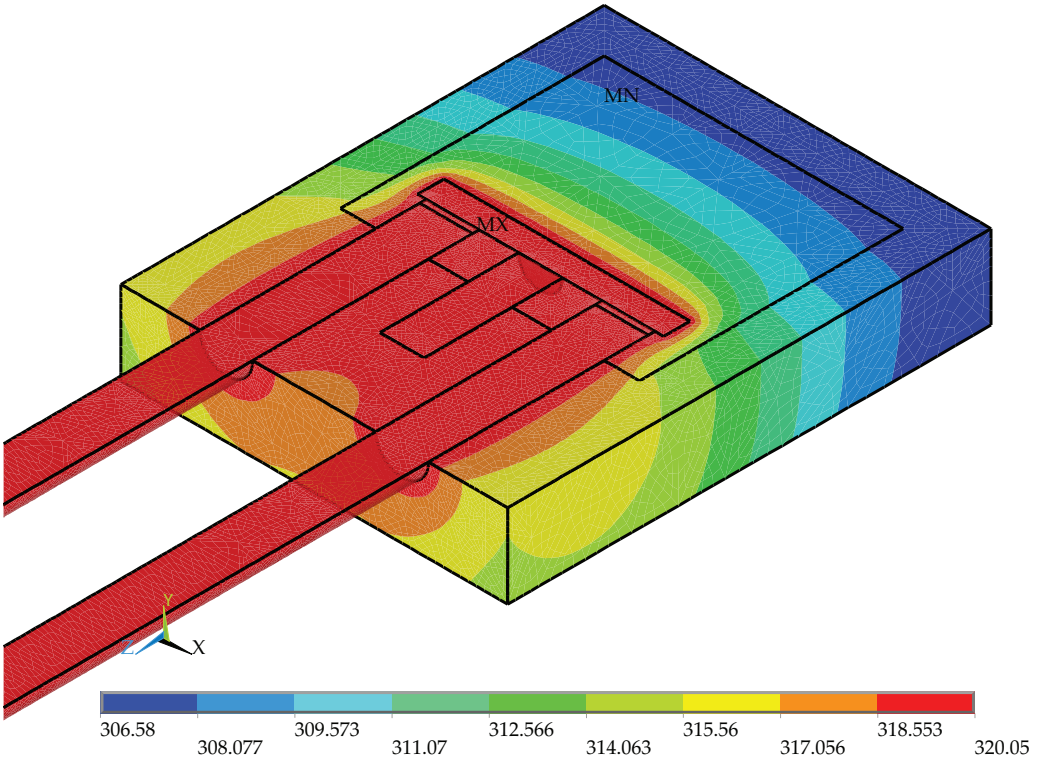

Figure 6.7: Temperature distribution in S–138 thermal cutoff at rated current of 12 A and ambient temperature of 300K for 0.6 mm conductive strip depth.

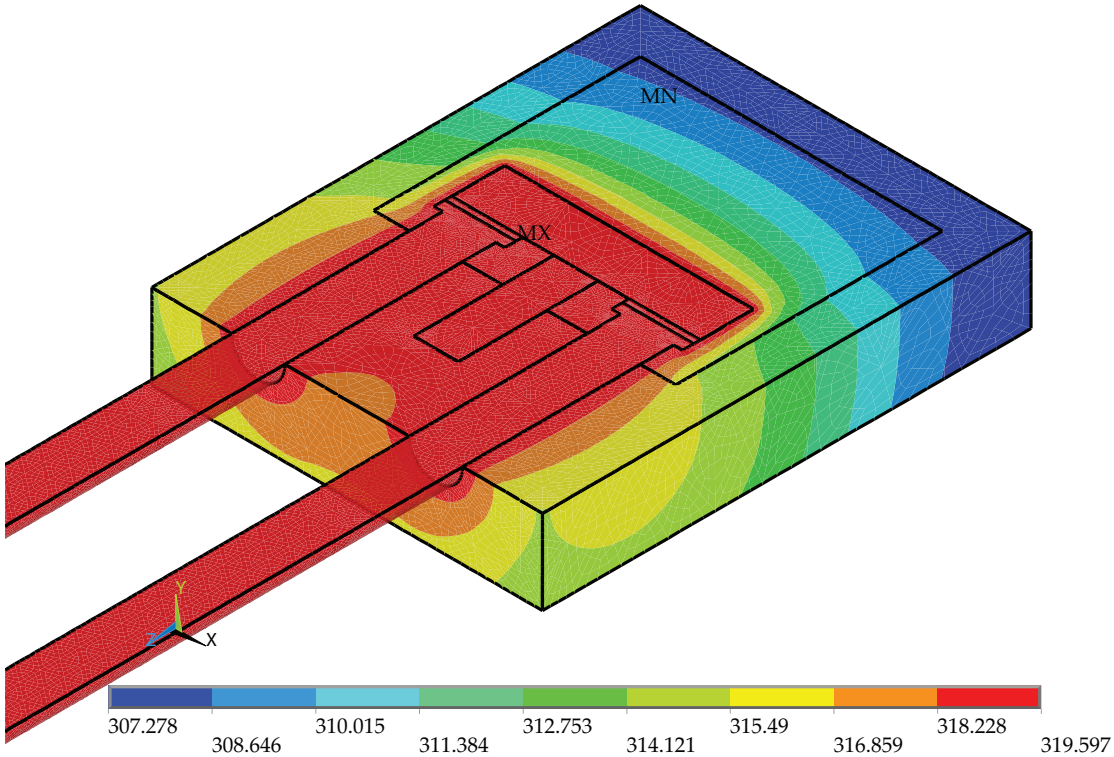

Figure 6.8: Temperature distribution in S–95 thermal cutoff with rivet contacting head at rated current of 12 A and ambient temperature of 300 K.

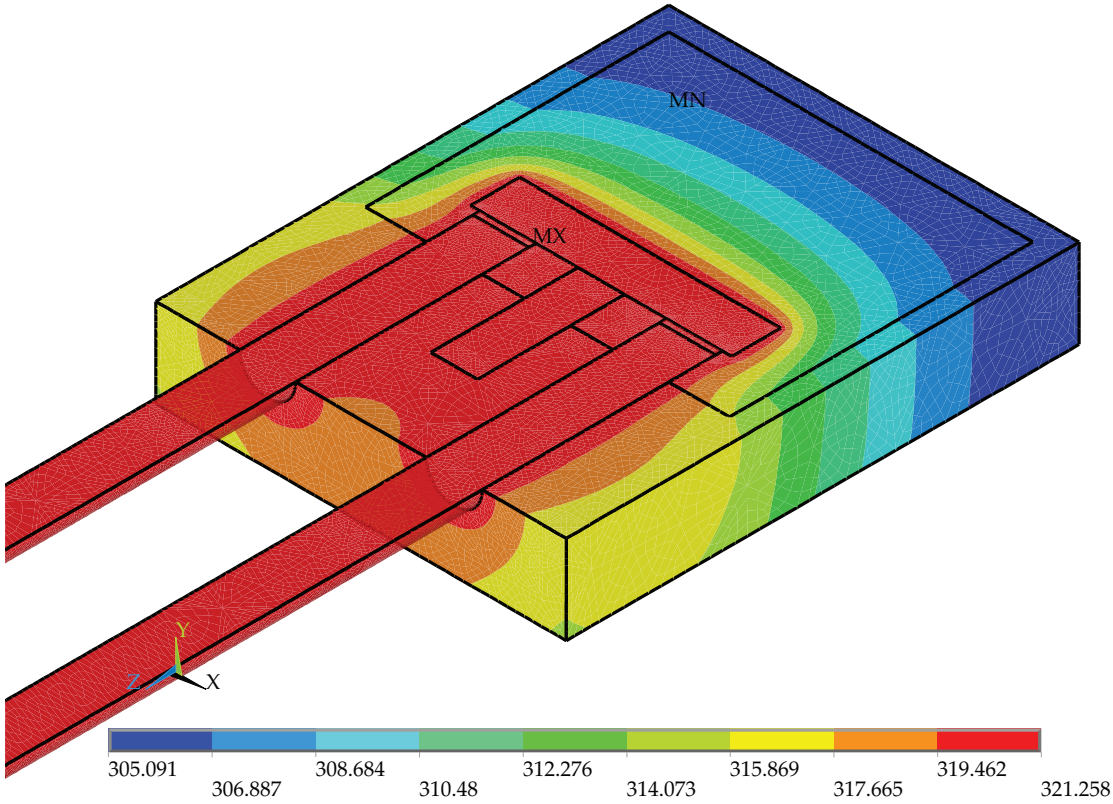

Figure 6.9: Temperature distribution in S–95 thermal cutoff with reduced thickness of the housing wall at rated current of 12 A and ambient temperature of 300K.

Temperature range in this case is wider compared to the standard design shown in Fig. 6.4. Value of the maximum temperature (on the soldering sheets) is increased by 0.5 K while value of the minimum temperature (at outer side of the housing) is 2.5 K lower. This distribution is explained by the increased role of air against makrolon in the process of heat removal from the conductive parts. Specifically, the thermal conductivity of air is 10 times lower than makrolon while the cooling conditions in both cases are the same.

6.4 Determination of thermal parameters

Successful implementation of thermal cutoffs is based on a detailed knowledge of their electrical and thermal operating conditions. Electrical operating conditions are determined by the values of the applied voltage and current, while cutoff temperature defines rated functioning temperature, holding temperature and response time.

With the aim to determine the holding temperature of cutoffs, dependencies of the soldering sheet temperature on the ambient temperature while conducting rated current were generated and they are shown in Fig. 6.10 for S–95 cutoff and Fig. 6.11 for S–138 cutoff of the basic design.

Value of the holding temperature is determined as the ambient temperature at which temperature on the soldering sheets reaches cutoff temperature, and for the S–95 cutoffs it is 347 K (74 °C), while for the S–138 type it is 388 K (115 °C).

Determination of the functioning temperature requires to bring the cutoff to a temperature 20 K below the cutoff temperature value and subsequently rise the ambient temperature by 1 K/min to achieve a complete thermal equilibrium between the cutoff

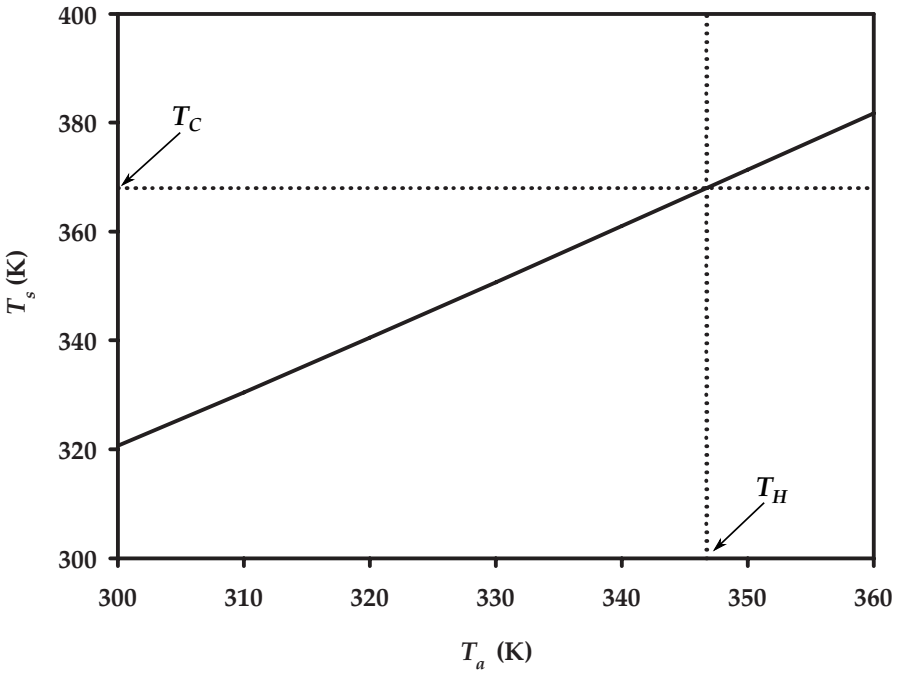

Figure 6.10: Temperature on the soldering sheets T_s versus ambient temperature T_a at rated current of 12 A for holding temperature determination of the S–95 thermal cutoff.

and the environment. The current flowing through the cutoff is only detection current (less than 10 mA). The ambient temperature at which the soldering sheet temperature reaches cutoff temperature is the functioning temperature. The closest value above this temperature that comply appropriate safety standards represents rated functioning temperature. In this case, simulation with time–dependent boundary conditions is required and results are shown in Fig. 6.12 for S–95 thermal cutoff and in Fig. 6.13 for S–138 thermal cutoff. Functioning temperatures specified on the basis of the presented dependencies are 1 K above the cutoff temperatures (T_F=369 K for S–95 type and T_F=412 K for S–138 type), due to the high thermal conductivity of the cutoff constitutive elements.

Comparison of thermal cutoffs of different structures from the quality aspect is often based on the values of the response time. This is the time required for the cutoff to open after its sudden exposure to the temperatures above the cutoff temperature value. Simulations were performed by setting the silicon oil as an ambient and then applying abrupt change of temperature boundary conditions. Simulated values of temperature on the soldering sheets after immersing thermal cutoff kept at a temperature of 300 K in a silicon oil bath whose temperature is ΔT above the cutoff temperature are shown in Figs. 6.14 and 6.15.

Response times determined on the basis of these curves are shown in Fig. 6.16 for both types of cutoff. It can be noticed that response time highly depends on the cutoff temperature and temperature of the silicone oil. Response time of S–95 thermal cutoff is in the interval 20 to 40 s, while for the S–138 type it is in the range 30 to 60 s. As described in Section 4.1.1, this value is used only for qualitative verification of the cutoff, but not to specify strict time necessary for cutoff to open, since it depends on the variety of other operating parameters.

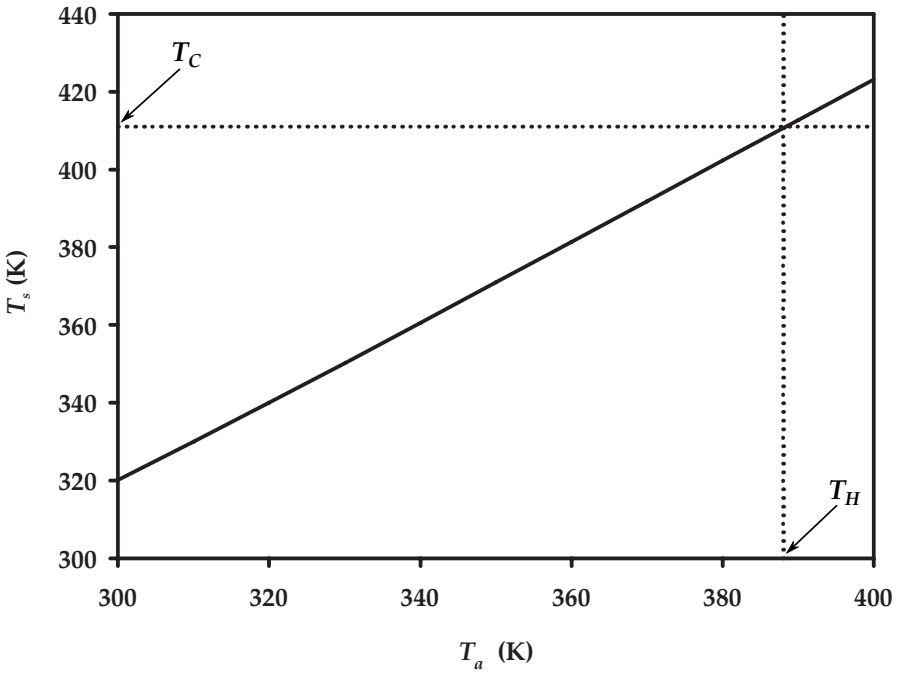

Figure 6.11: Temperature on the soldering sheets T_s versus ambient temperature T_a at rated current of 12 A for holding temperature determination of the S–138 thermal cutoff.

6.5 Optimization of the geometry and dimensions of thermal cutoffs

Optimization of the geometry and dimensions of thermal cutoffs is performed by considering the influence of the depth of the conductive strip, the shape of the contacting head, and the thickness of the housing wall to the basic cutoff thermal parameters of functionality and quality. The optimal structure was selected from the functional, economic and technological aspects.

The increase of the temperature on the soldering sheets due to Joule's effect reflects the influence of design parameters on the functionality of thermal cutoffs. The first analysis was performed for decreased depth of the conductive strip from initial 1.2 mm to 0.9 mm and 0.6 mm. Based on the distributions from Figs. 6.4 – 6.7 dependencies of the temperature on the soldering sheets on the applied current at different depths of the conductive strip and ambient temperature of 300 K are obtained. These dependencies are shown in Figs. 6.17 and 6.18 for S–95 and S–138 thermal cutoff, respectively.

Dependencies are identical for both types of cutoff with slightly lower values for S–138 type due to higher conductivity of the applied alloy. Also, decrease of the conductive strip thickness to 0.9 mm does not affect the increase in temperature, while for the thickness of 0.6 mm temperature is slightly increased.

Dependencies of the temperature on the soldering sheets on the ambient temperature for rated current value, shown in the Figs. 6.19 and 6.20, indicate that holding temperature does not change for 0.9 mm depth of the conductive strip, but for 0.6 mm it is lower by 1 K. Based on the above considerations, it can be concluded that decrease of the conductive strip depth to 0.9 mm is justified, since characteristics of the cutoffs remain unchanged while providing better manufacturing capabilities and minimum use of material.

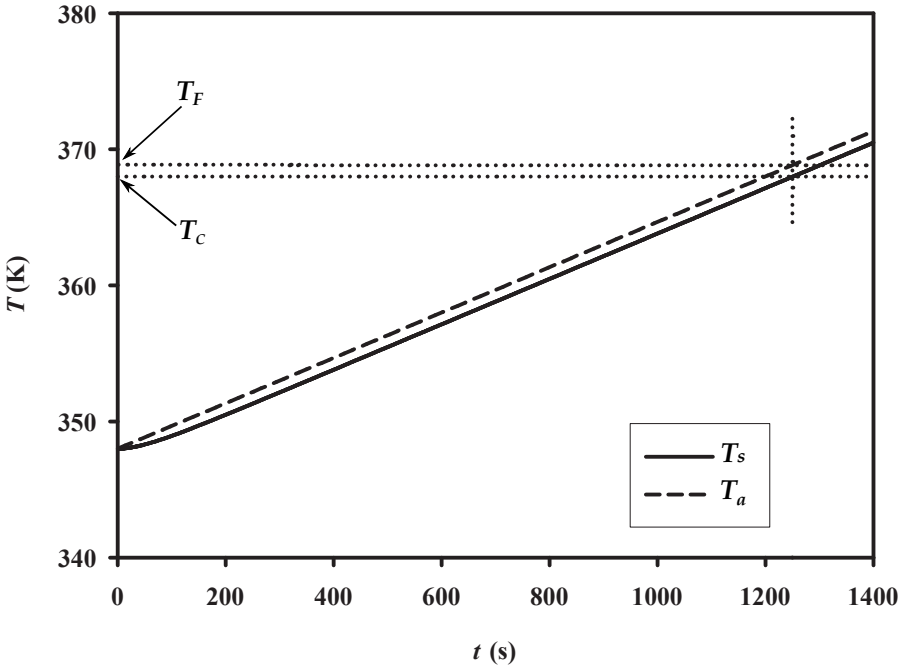

Figure 6.12: Temperature on the soldering sheets T_s and ambient temperature T_a versus time for the functioning temperature determination of the S–95 thermal cutoff.

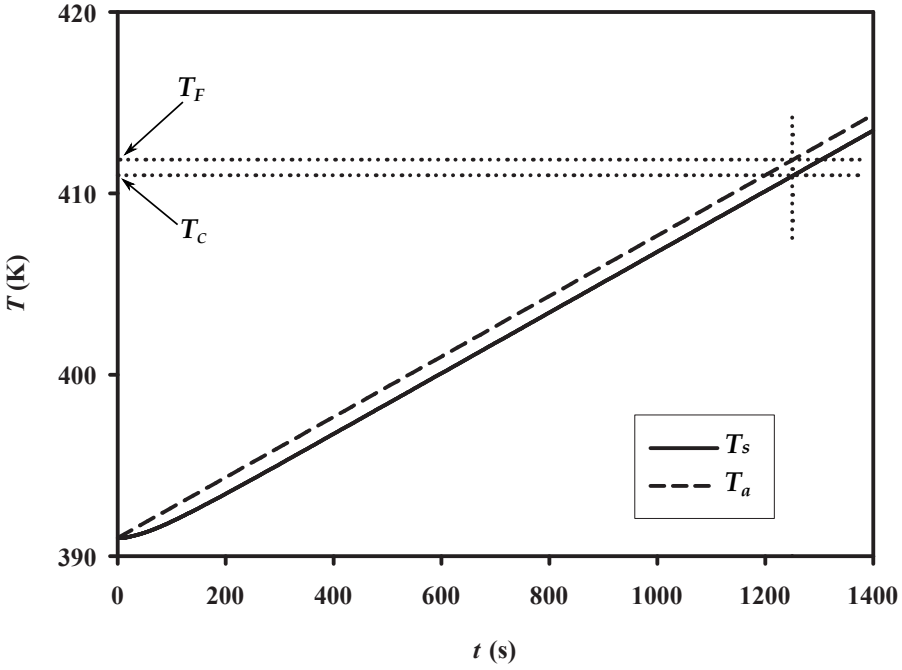

Figure 6.13: Temperature on the soldering sheets T_s and ambient temperature T_a versus time for the functioning temperature determination of the S–138 thermal cutoff.

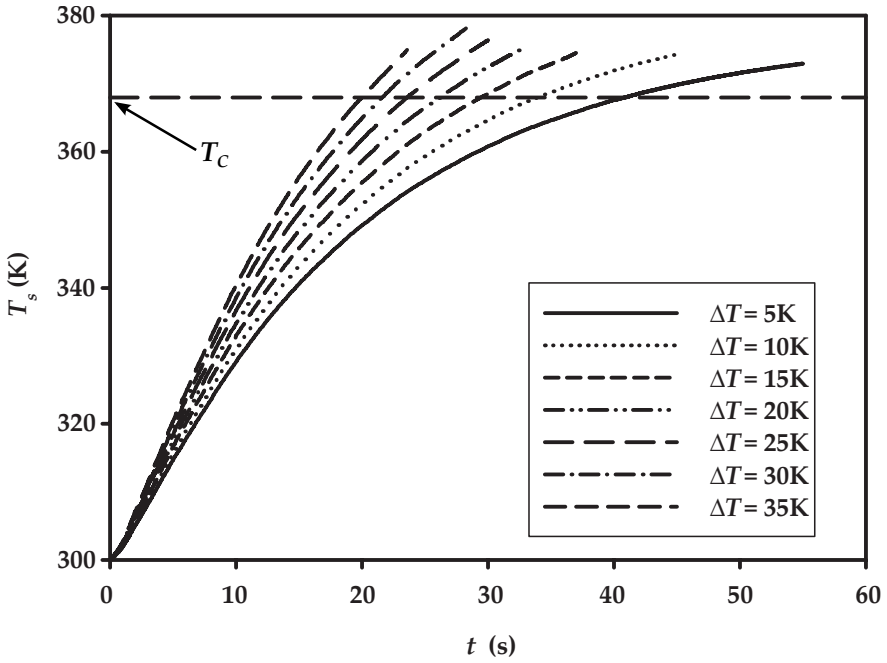

Figure 6.14: Temperature on the soldering sheets T_s versus time at different temperatures of the silicone oil for response time determination of the S–95 thermal cutoff.

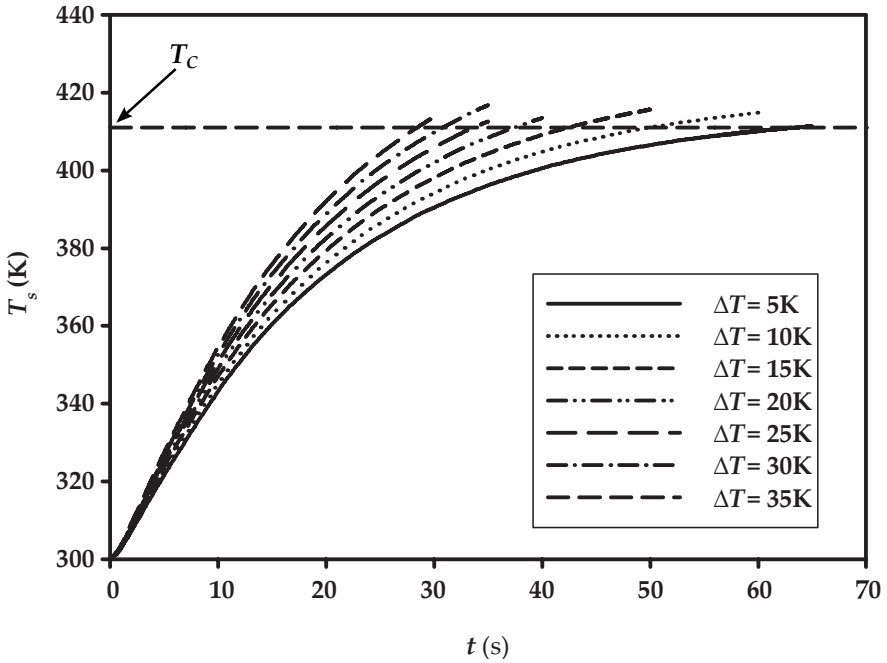

Figure 6.15: Temperature on the soldering sheets T_s versus time at different temperatures of the silicone oil for response time determination of the S–138 thermal cutoff.

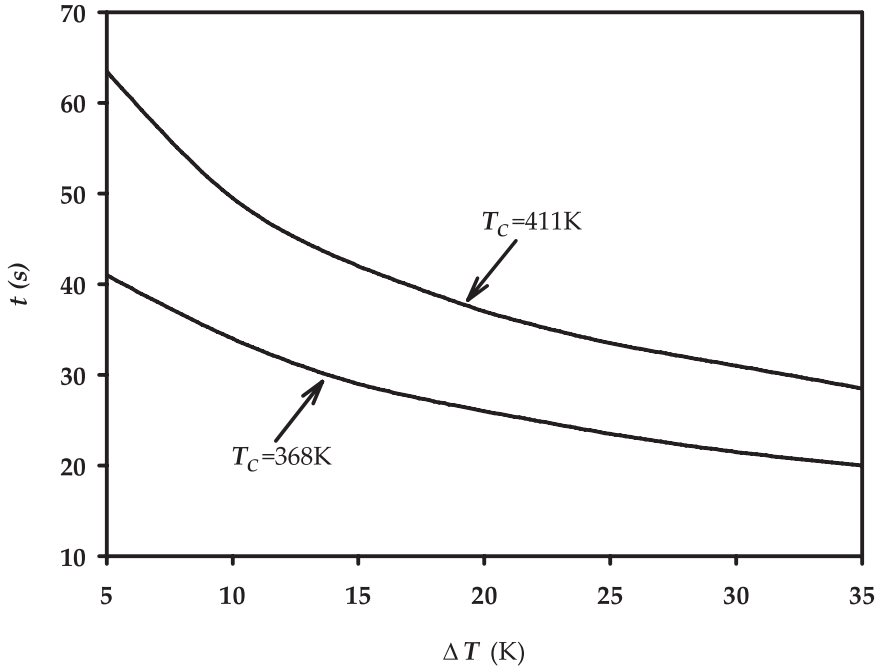

Figure 6.16: Response time of thermal cutoffs for different temperatures of the silicon oil.

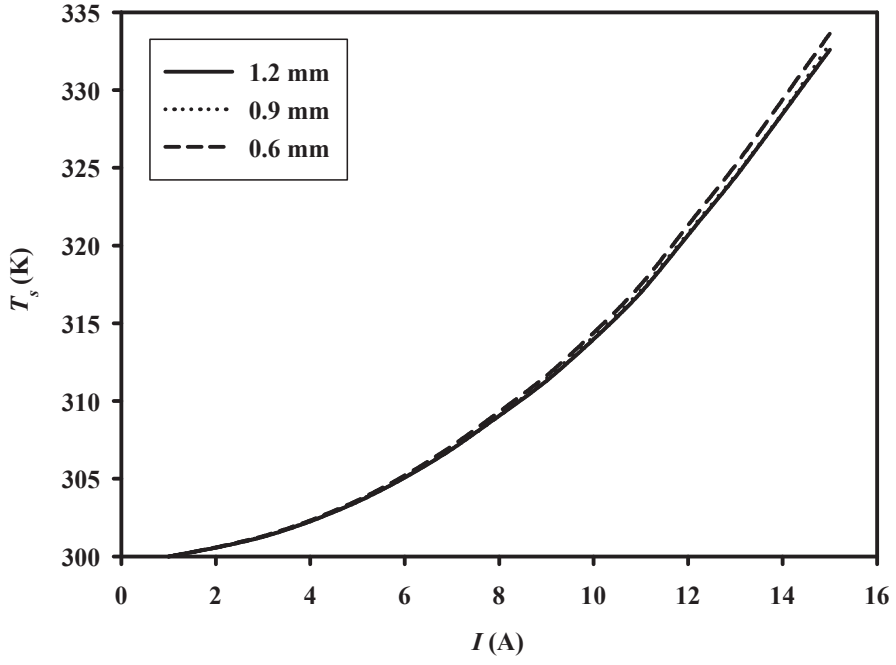

Figure 6.17: Temperature on the soldering sheets versus applied current for different depths of the conductive strip at ambient temperature of 300 K for S–95 thermal cutoff.

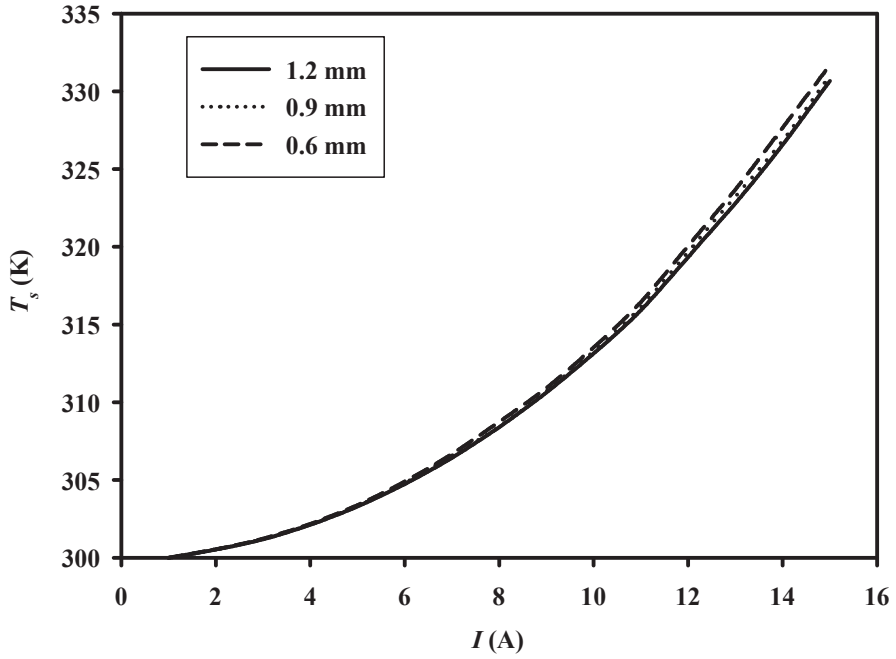

Figure 6.18: Temperature on the soldering sheets versus applied current for different depths of the conductive strip at ambient temperature of 300 K for S–138 thermal cutoff.

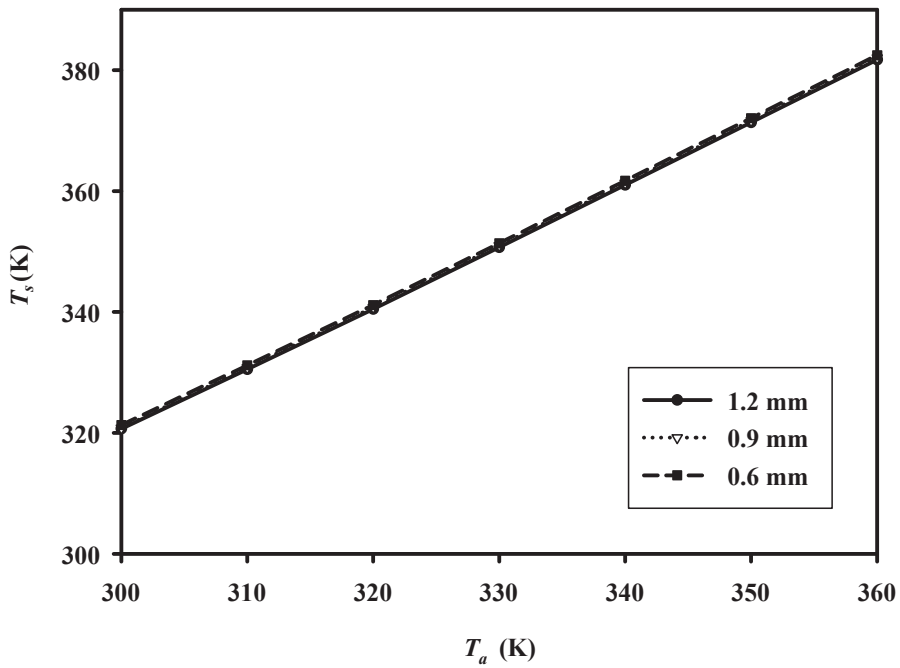

Figure 6.19: Temperature on the soldering sheets versus ambient temperature for different depths of the conductive strip at rated current for S–95 thermal cutoff.

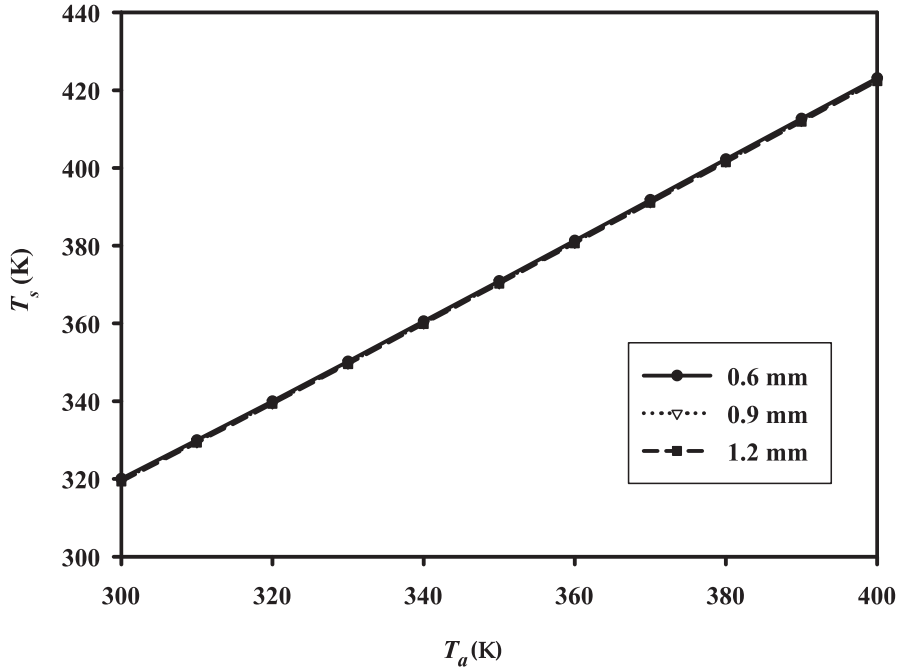

Figure 6.20: Temperature on the soldering sheets versus ambient temperature for different depths of the conductive strip at rated current for S–138 thermal cutoff.

The second analysis was oriented to rivet contacting heads of the leads. The increase in temperature due to electro–thermal effects for flat and rivet shape of the contacting head is shown in Figs. 6.21 and 6.22. Presented dependencies indicate lower temperature rise in rivet contacting heads by 1 K in S–95 (Fig. 6.8) and 0.5 K in S–138 cutoff at rated current value. However, these improvements are minimal, and modification of the initial design is not justified since it requires additional manufacturing steps.

In Section 6.3, the effect of reduced thickness of the housing wall on the temperature distribution in thermal cutoffs is presented. The minimum increase in the soldering sheet temperature at rated current and ambient temperature of 300 K does not affect the value of the functioning temperature of the considered cutoffs. Also, simulation results showed that the reduction in wall thickness of the housing does not affect the response time of the cutoffs if outside dimensions of the housing are kept constant. The conclusion is that higher value of the wall thickness of the housing is desirable, since it provides better mechanical properties of the cutoffs.

Based on these results, thermal cutoffs of the optimal geometry and dimensions for both types involve leads with the flat contacting heads, conductive strip depth of 0.9 mm and the housing wall thickness of 1 mm.

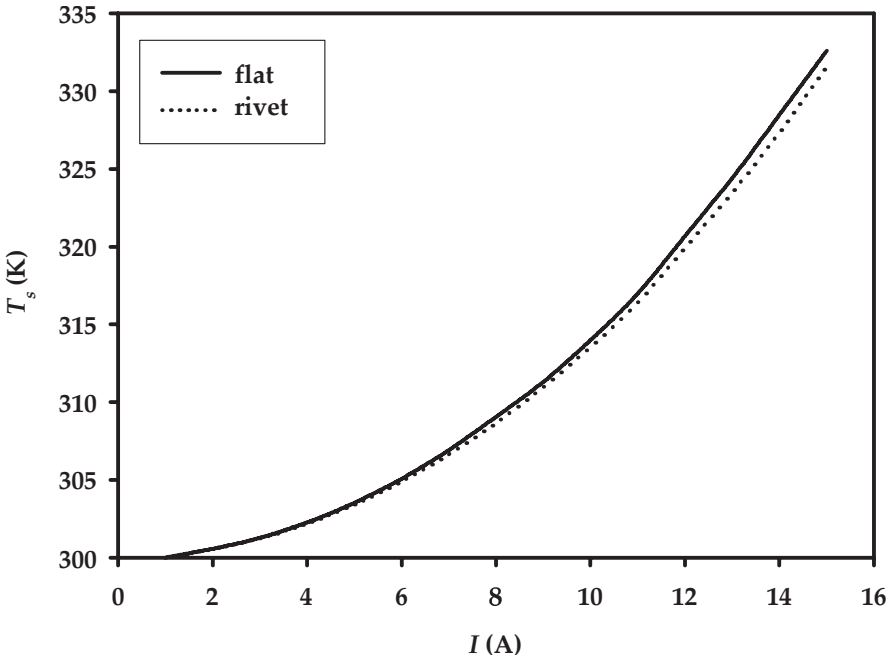

Figure 6.21: Temperature on the soldering sheets versus ambient temperature for different contacting heads and rated current for S–95 cutoff.

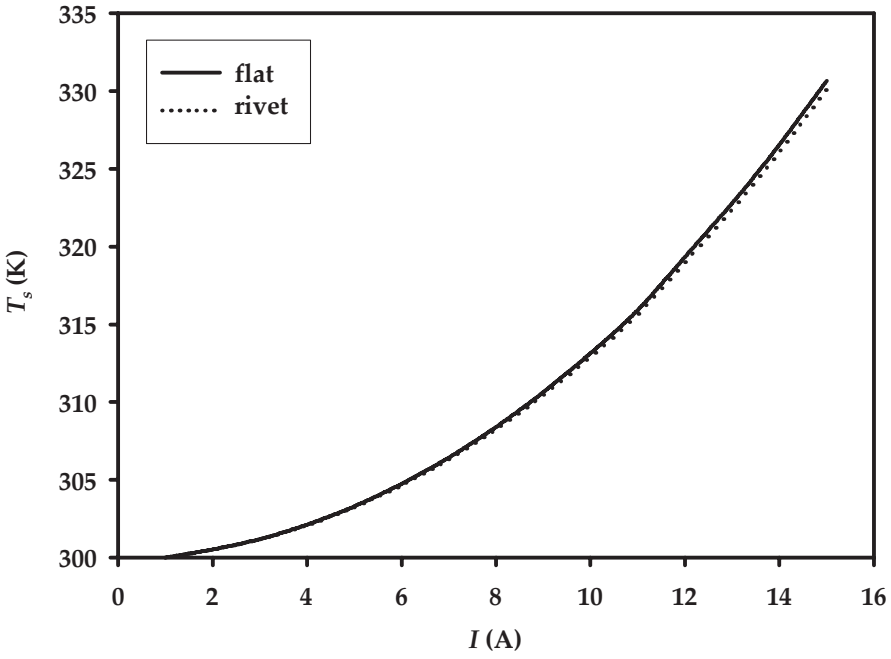

Figure 6.22: Temperature on the soldering sheets versus ambient temperature for different contacting heads and rated current for S–138 cutoff.

Chapter 7

Thermal parameters of functionality and quality of S–138 thermal cutoffs

The basic thermal parameters of functionality and quality of thermal cutoffs are value of the rated functioning temperature (its equivalent is cutoff temperature), value of the temperature rise due to electro–thermal effects, and response time, as indicated in Section 4.1.1. The response time of thermal cutoffs, as a quality parameter, is defined for specified laboratory operating conditions. The real application of thermal cutoffs includes a variety of implementations and values of the externally generated heat. Therefore, along with specific values of the response time of cutoffs, their operating conditions should be specified. Knowledge of the temperature distribution in the cutoff elements at defined currents and specific heating conditions enables to determine cutoff thermal parameters and characteristics of its individual elements.

Based on the optimization procedure described in Chapter 6, specific prototype of the S–138 thermal cutoff was produced and its functional and qualitative analysis are performed. The cutoff temperature of this thermal cutoff is 138 °C (411 K), the nominal voltage is 250 V, and the rated current is 12 A. Structure of the examined cutoff is the basic one, with dimensions listed in Table 6.1. The front side of the housing was mechanically removed and the thermovision measurement technique was applied in two measurement setups to observe thermal behaviour of the device under test.

7.1 Thermovision measurement technique

The applied measurement method is based on the use of thermal imaging (thermovision) camera, a regulated heat source and variable current source. Benefits of the thermal imaging in contactless temperature measurement are its compact size, mobility, easy operation and low energy consumption. Clearly and precisely defined thermogram, high quality images and a linear temperature scale with integrated control software allows easy interpretation of the results through the appropriate reports. Also, use of the thermal imaging camera eliminates the need for expensive and highly specialized chambers for temperature control. Thermovision camera Varioscan 3021ST is a scanning infrared thermovision measurement system designed for high–resolution detection of infrared radiation in the wavelength range from 8 μm to 12 μm. The signal from the infrared spectrum is amplified, digitized by 16–bits, and mapped to the visible spectrum with a resolution of 256 colors. Each color of the thermal image represents a certain range of temperatures [131]. The resolution of the system Varioscan is 0.03 °C in the

temperature range from -40 °C to +1200 °C. Also, there is a possibility for recording of temperature distribution during a given time interval, with a defined time step. This camera mode allows generation of video records of temperature changes in the considered structures. Differential mode of the camera allows extraction of details such is the change of temperature in two successive records [132]. Thermal images were processed by IRBIS V2.2 software with 240 × 360 pixels of geometrical resolution and 1 °C of temperature resolution. Prescribed global emissivity was set to 1.0 for the ambient temperature of 29 °C. It was determined that changes of the object emissivity values in the image correcture scheme have no effect on the obtained temperature distributions.

In the first measurement setup, presented in Fig. 7.1, thermal cutoff was subjected to the load currents from 5 A up to the cutoff current value, at the constant ambient temperature (297 K) and thermovision images of the cutoff interior were captured. Discrete values of the current were controlled by a variable source and thermovision imaging was performed after the establishment of the steady state regime. By applying current above the rated value, the cutoff was brought into the open state due to the self–heating effect. It was in a vertical position to allow cooling by convection from free surfaces of the housing and conductive bridge.

Figure 7.1: Thermovision measurement method with controlled current.

When defining functionality and quality parameters of thermal cutoffs their uniform exposure to the elevated temperature is assumed. In real operating conditions thermal cutoff is usually exposed to significant heating from one side comparing to the other parts. Heat dissipation from its free surfaces is also limited. Such operating conditions are commonly present in protection of the power motor windings or transformers from the overheating, where cutoff rests on windings. For these reasons, the second measurement setup included exposure of the samples to the controlled heat source from the back side in the absence of the electrical load. Hot air from a fan was applied to one side of the 3-mm thick pertinax plate, while on its other side was mounted cutoff in a vertical position. Such a simple and inexpensive system enables to achieve a regulated temperature of the plate up to a maximum of 600 K. The applied thermal fluxes were controlled by adjusting the distance between the plate and the fan. Their values were determined with the accuracy of 50 W/m^2 by monitoring the temperature of the plate. The ambient temperature was 292 K. Thermal fluxes of 3200 W/m^2 and 1050 W/m^2, corresponding to 0.6 K/s and 0.2 K/s of temperature rise on the cutoff backside, were applied. Temperature distribution inside the device was captured by the thermovision camera every 3 s, till its opening. This measurement setup is presented in Fig. 7.2.

In both setups investigated samples were prepared by removing the part of the

Figure 7.2: Thermovision measurement method with controlled heat source.

housing (Fig. 7.3 (a)), to make the interior of the thermal cutoff accessible for thermal imaging.

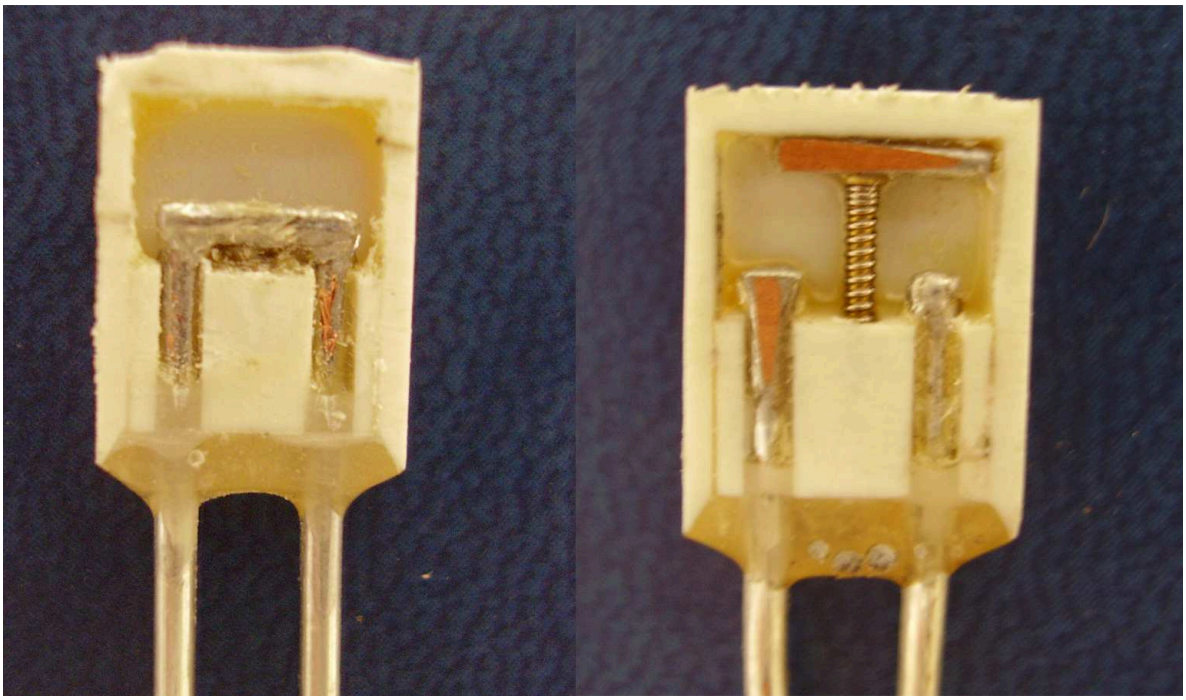

(a) (b)

Figure 7.3: Thermal cutoff samples before (a) and after (b) the opening.

7.2 Temperature rise due to the electro–thermal effects

As a result of the first measurement, change in the operating temperature of the cutoff active part due to electro–thermal effects at constant ambient temperature of 297 K was considered. The thermovision image of temperature distribution in the thermal cutoff at 10 A load current and 297 K ambient temperature is shown in Fig. 7.4. Obtained dependence of temperature on the soldering sheets for load currents up to the cutoff value (in this case 33.6 A) is shown in Fig. 7.5.

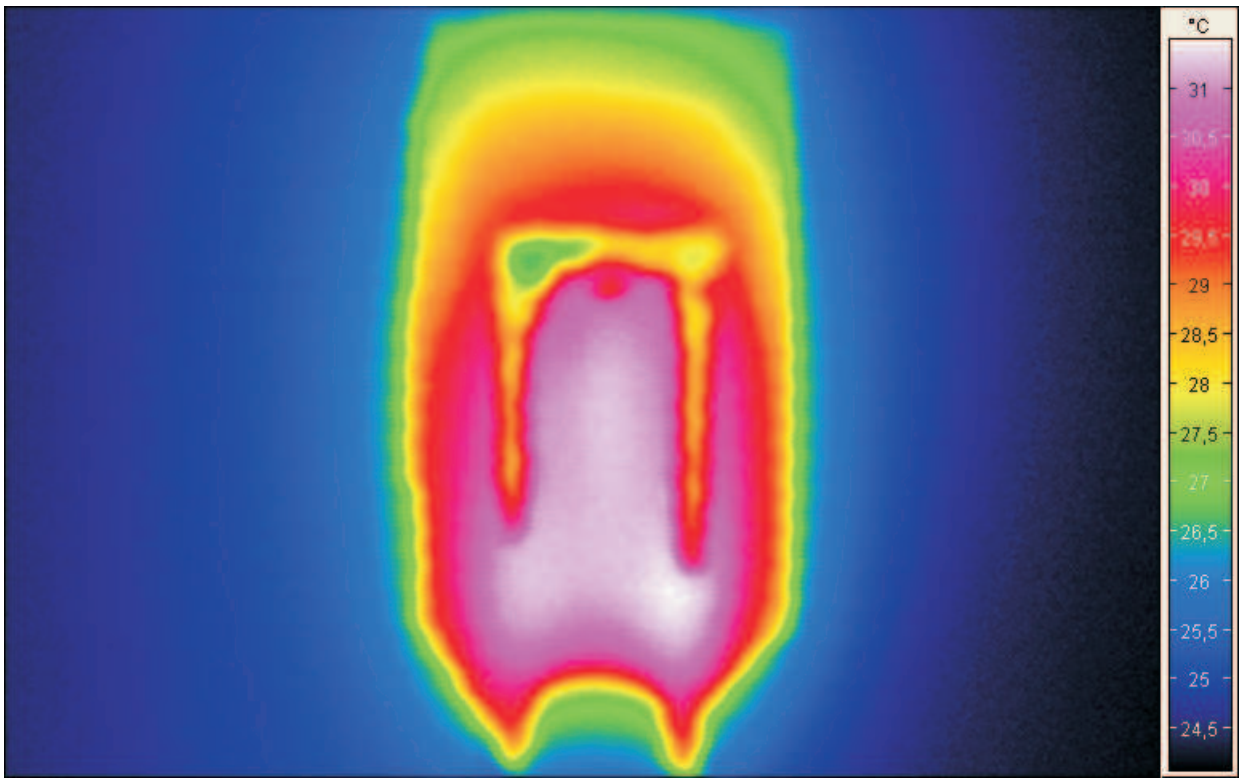

Figure 7.4: The thermovision image of temperature distribution in the thermal cutoff at 10 A load current and 297 K ambient temperature.

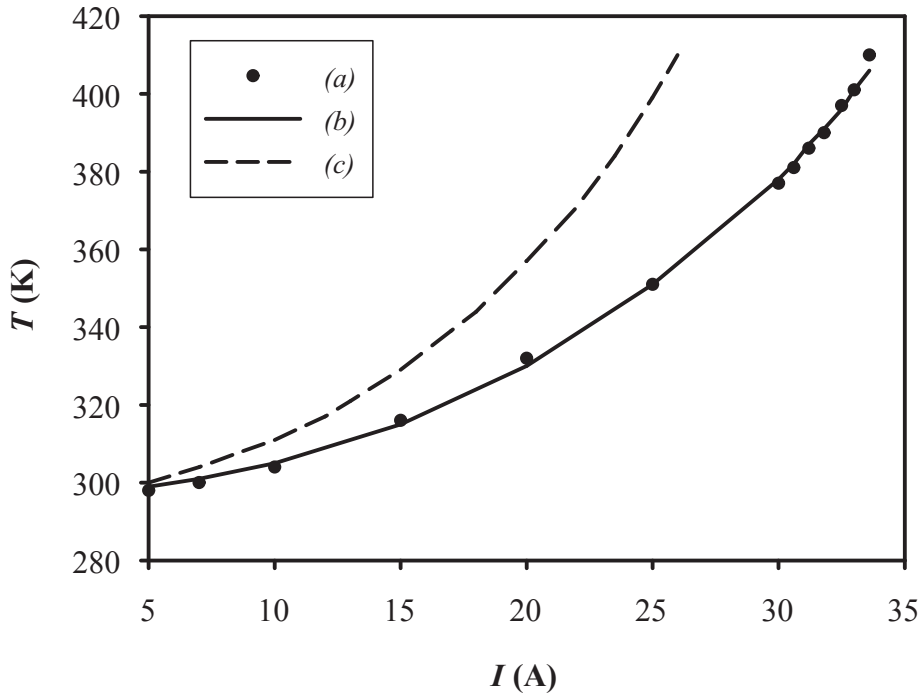

Figure 7.5: Temperature on the soldering sheets versus load current: (a) Thermovision data, (b) Simulation with one side of the housing removed. (c) Simulation with complete housing.

Standard exponential relationship can be observed with temperature rise of 12 K above the ambient temperature for 12 A of the load current. For the load current of 33.6 A, the cutoff opens and this defines value of the cutoff current. Temperature distributions in thermal cutoff for these operating conditions immediately before and after the opening are shown in Fig. 7.6. Based on these images, value of the cutoff temperature is determined as 410 K.

Dependence of the temperature on the soldering sheets on the applied current from Fig. 7.5 is used to specify boundary conditions for the simulation of thermal cutoffs. As discussed in Chapter 6, design and optimization of thermal cutoffs require simulation of these devices at different operating conditions. Properly selected values of the convection coefficient for the free surfaces of the cutoff are crucial to obtain the correct simulation results. Since the value of this coefficient depends on the shape and orientation of the surface, as well as on the physical and thermal properties of the surrounding fluid and its temperature, theoretically determined values often require corrections based on the experimental data. For considered thermal cutoffs, theoretical values of the convection coefficient for air as the surrounding fluid are adjusted for a constant value of 10 W/m^2K.

For implementation of the thermovision imaging it was necessary to allow visual access to the interior of the cutoff by removing part of the housing and, thereby, changing the real conditions of its thermal cooling. Convection coefficient is determined by taking into account these boundary conditions and temperature distribution in the cutoff at load current of 12 A for the case of the removed part of the housing obtained by simulation is shown in Fig. 7.7(a). It was subsequently performed a simulation of thermal cutoffs in real operating conditions (complete housing) and the resulting temperature distribution is shown in Fig. 7.7(b).

Dependence of the temperature on soldering sheets on the load current was simulated and agreement with the experimental data was within 4% of the relative error (Fig. 7.5 curve (b)). Therefore, it was assumed that the simulation results for the real device, i.e. the one with complete housing (Fig. 7.5 curve (c)), are founded to a reasonable degree. It was also confirmed by the cutoff current value of 23.8 A (at 297 K ambient temperature) experimentally determined in the real device, which is in a close agreement with the simulated value of 24 A depicted in Fig. 7.5. For the load current of 12 A, simulation results indicate that temperature rise in the complete device should be 20 K, in contrast to 12 K observed when one side of the housing was removed.

7.3 Response time

Time dependence of the temperature distribution within thermal cutoff obtained by the second measurement setup allows determination of the cutoff response time after its sudden exposure to an elevated temperature. Standards for specification of the thermal cutoff quality prescribe value of the elevated temperature as 35 K above the cutoff temperature [15]. As previously mentioned, the response time significantly depends on the heating rate of thermal cutoffs and place of their installation, and specific value of this parameter is related to the operating conditions. The response time is used approximately to compare the quality of different types of cutoffs. During the measurement, heating of the cutoffs was done continuously at two different rates. Zero time was defined at the moment when temperature on the back of the device had reached 35 K above the cutoff temperature (446 K). The cutoff moment was captured 33 s after zero time when exposed

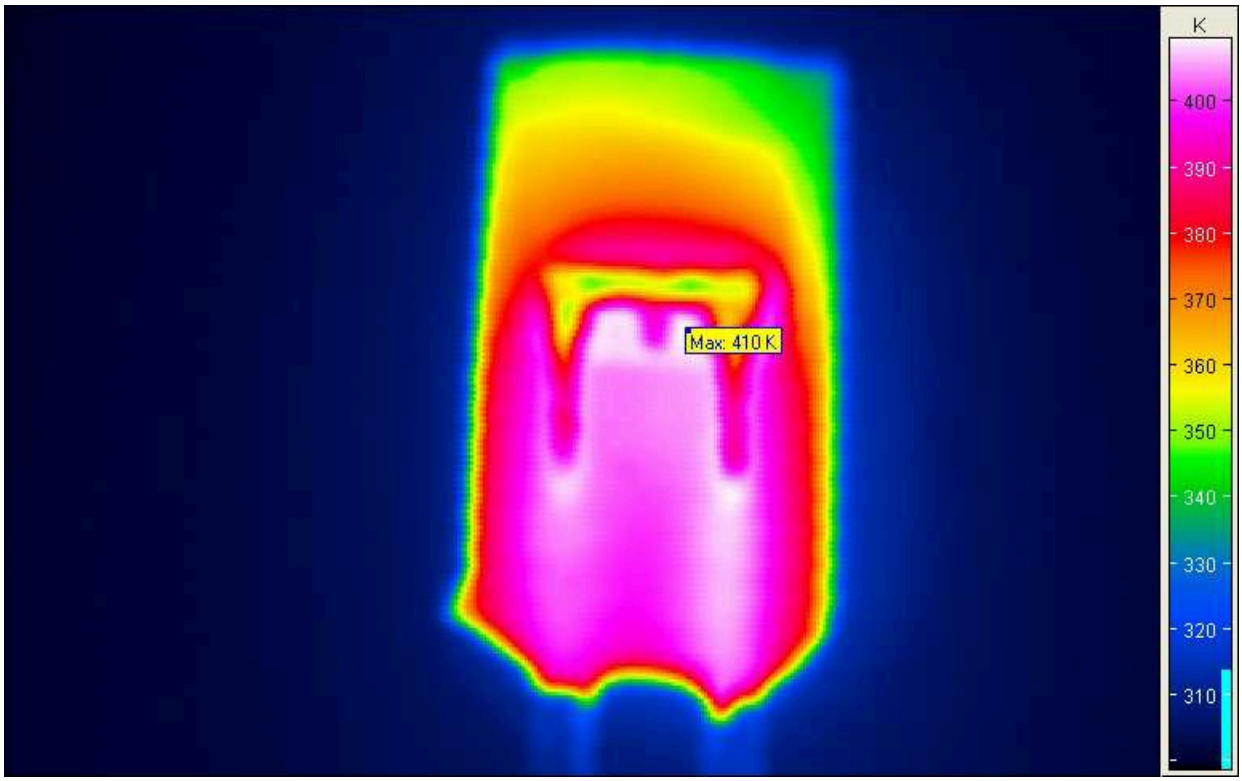

(a)

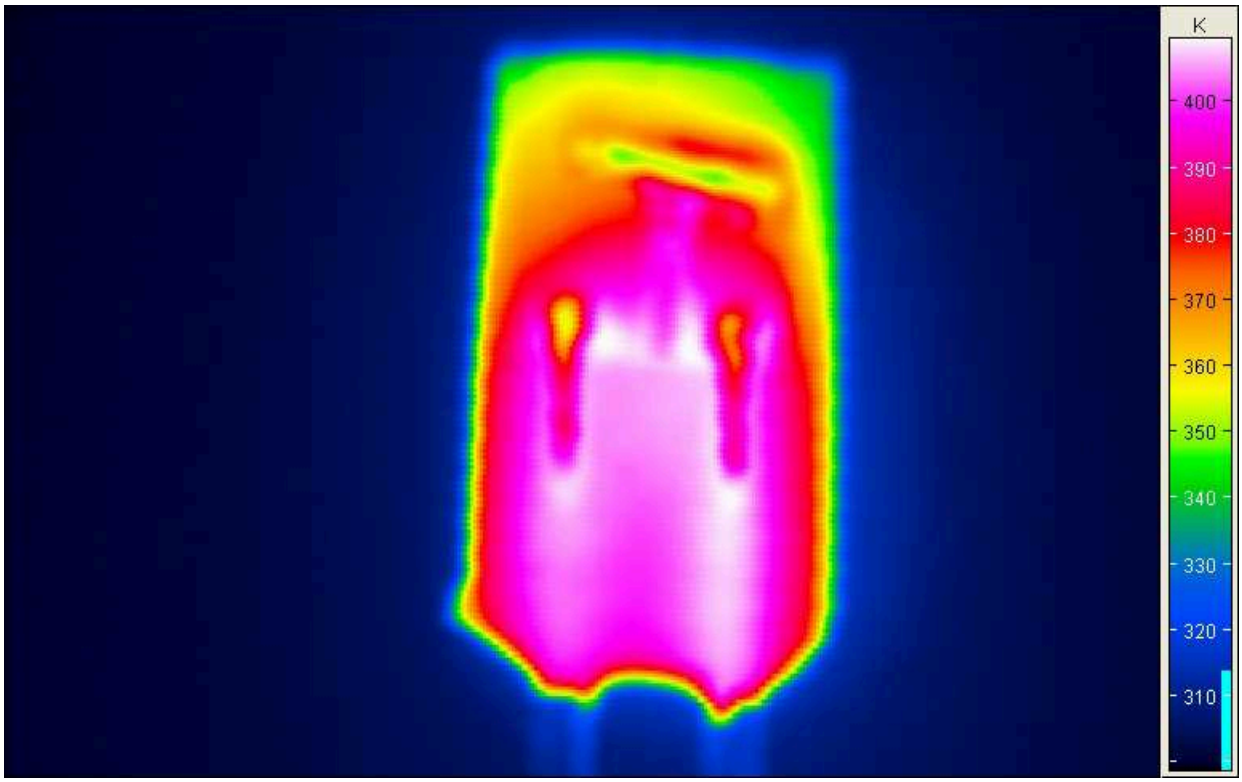

(b)

Figure 7.6: Thermovision images of temperature distribution in the thermal cutoff at 33.6 A of load current immediately before (a) and after (b) the opening.

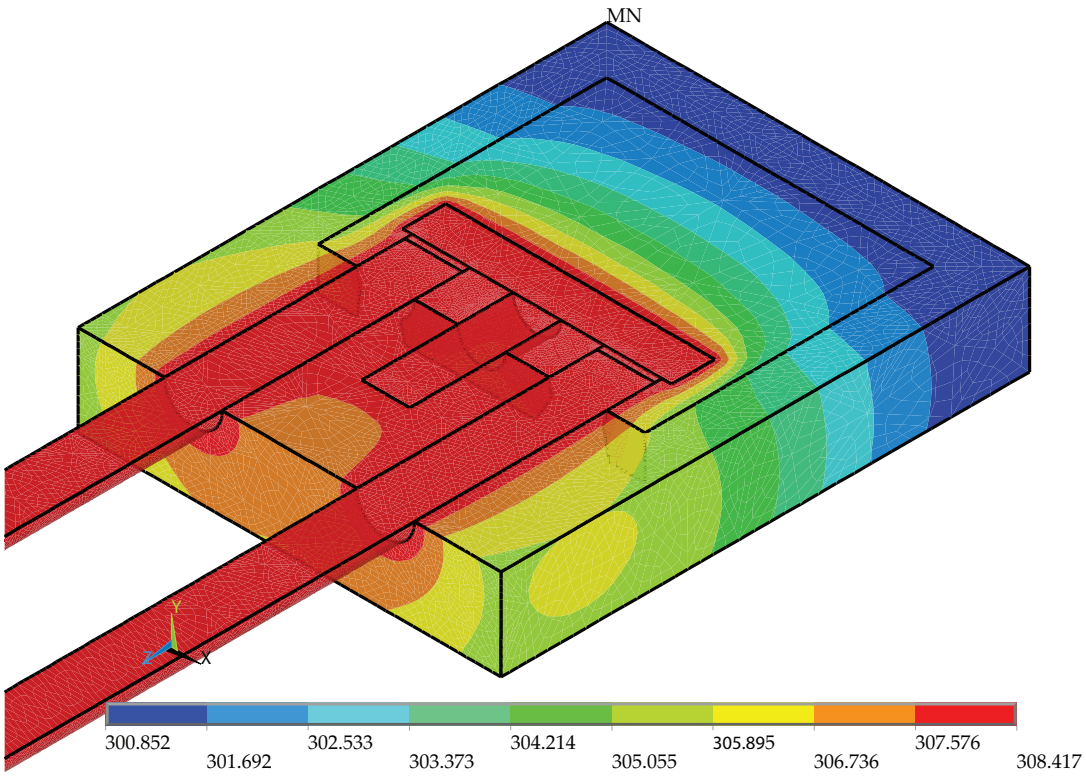

(a)

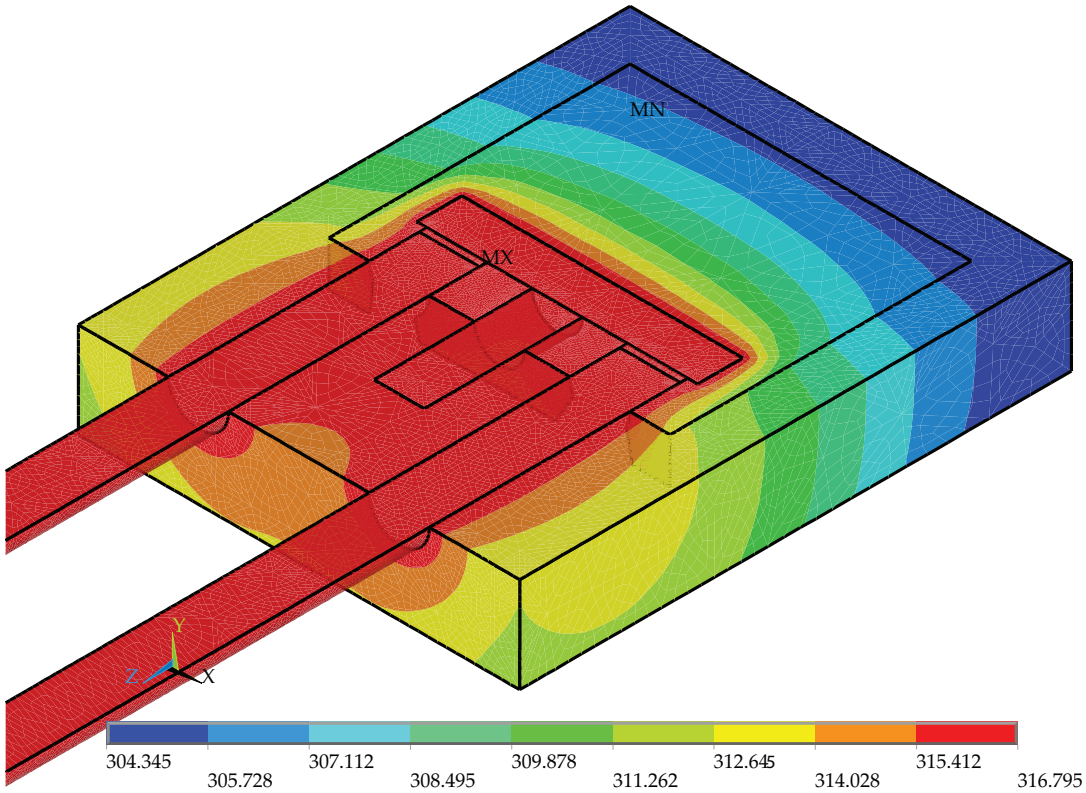

(b)

Figure 7.7: Simulated temperature distributions in thermal cutoff at load current of 12 A with one side of the housing removed (a) and with complete housing (b).

to a heat flux of 3200 W/m^2. Temperature distributions in thermal cutoff at the zero time and at the cutoff moment under the given conditions are shown in Fig. 7.8. Based on these distributions the cutoff temperature is determined, and for this cutoff it is 411 K.

When thermal cutoff was exposed to the heat flux of 1050 W/m^2, distributions of temperature at zero time and after cutoff are obtained and shown in Fig. 7.9. In this case response time was 100 s and cutoff temperature 411 K.

In the scope of the response time definition using silicon oil as an ambient, as discussed in Section 6.4, it can be concluded that these thermovision results could be used for better insight in the real response time values. Presented experimental conditions are close to the real working environment of the devices, with the distinction in the absence of the front side of the housing, which affects both convection and conduction, as illustrated in Fig. 7.10 [133]. In order to estimate real response time values, the device with complete housing was simulated. The discrepancy between the simulated and experimental data in the lower part of the curves is observed for the case when one side of the housing was removed. This is due to the difficulties in obtaining the exact experimental values at lower temperatures because the thermovision image is dithered in this region. At higher temperatures, which were of the major interest, experimental values were clearly distinguished and good agreement with simulation is observed. The complete housing implies greater volume of Makrolon and air inside, which effectively act as a heat sink, thus increasing the response time. Note that usage of the silicon oil as an ambient results in a much shorter response times (Fig. 6.16, [15], [95]), due to the fact that the rate of the heat exchange between the oil and the housing is much higher [127].

7.4 Thermal characteristics of the housing

For devices whose operation is based on the temperature response, it is important to study thermal behaviour of the housing. Therefore, a thermal resistance of the housing was investigated based on the temperature distribution along the device [cross section L01 in Fig. 7.8(a)] shown in Fig. 7.11. It can be seen that the backside of the housing with wall thickness of 1 mm lowers the temperature from the heat source for approximately 30 K. Local minima are observed on the housing boundaries. Asymmetry in the values occurs due to the imperfections caused by mechanical removal of the front side of the housing (in this case 1 mm in the length difference of the sidewalls causes 10 K temperature difference in the thermal image). Nonuniformity of the temperature distribution at two sides of the conductive bridge is not critical since functioning of the cutoff is accomplished as soon as one of the solder joints is broken. From this distribution, it could be expected that better response time of the device can be achieved by thinning the wall of the housing. The thermal resistance of the housing with respect to the heat source can be simply calculated as [134]:

$$R_\Theta = \frac{\Delta T}{F \cdot S}, \tag{7.1}$$

where ΔT is the temperature difference between outer and inner wall surfaces on the backside of the housing, F is thermal flux, while S is the wall area. Using $\Delta T = 30K$ value of $R_\Theta = 97K/W$ is obtained. The relatively high value is governed by the low thermal conductivity value of Makrolon polycarbonate. It was assumed that the wall thickness of 0.5 mm should lead to the value of $R_\Theta \approx 50K/W$, which may appear preferable. However, as pointed out in Section 6.3, simulation results showed that heat exchange

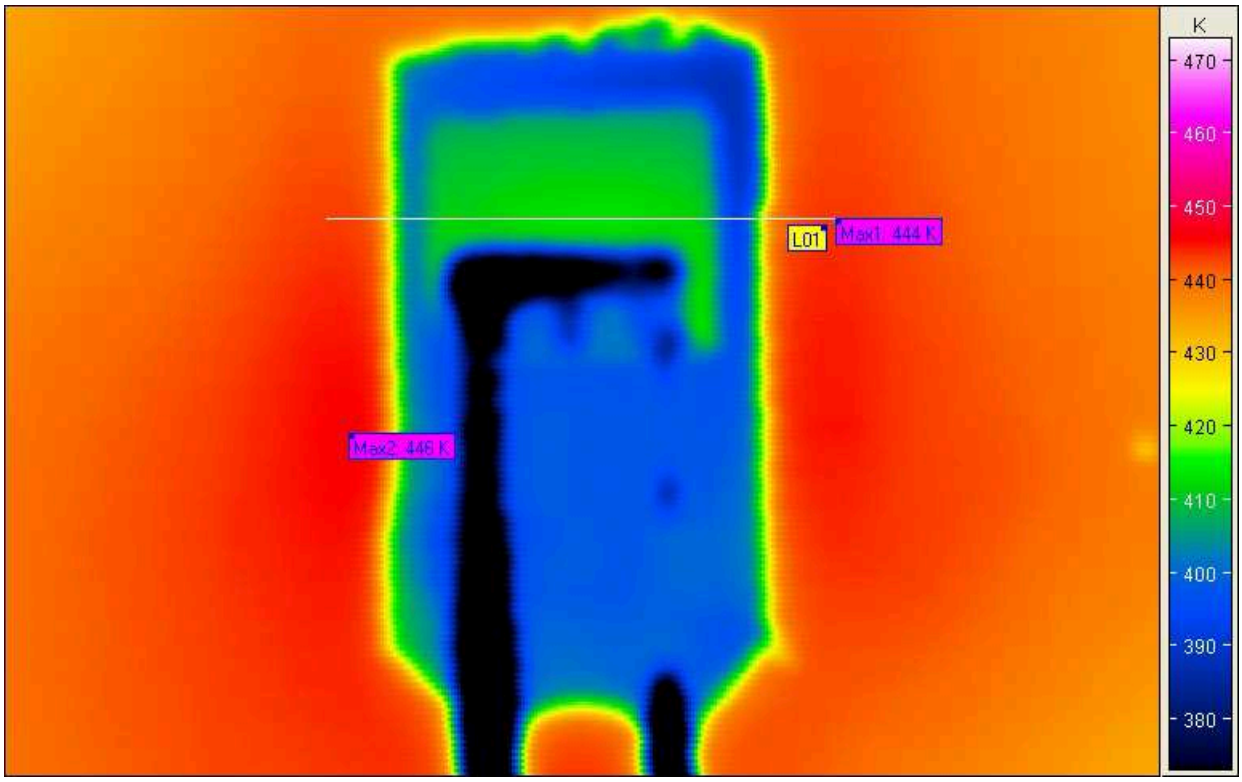

(a)

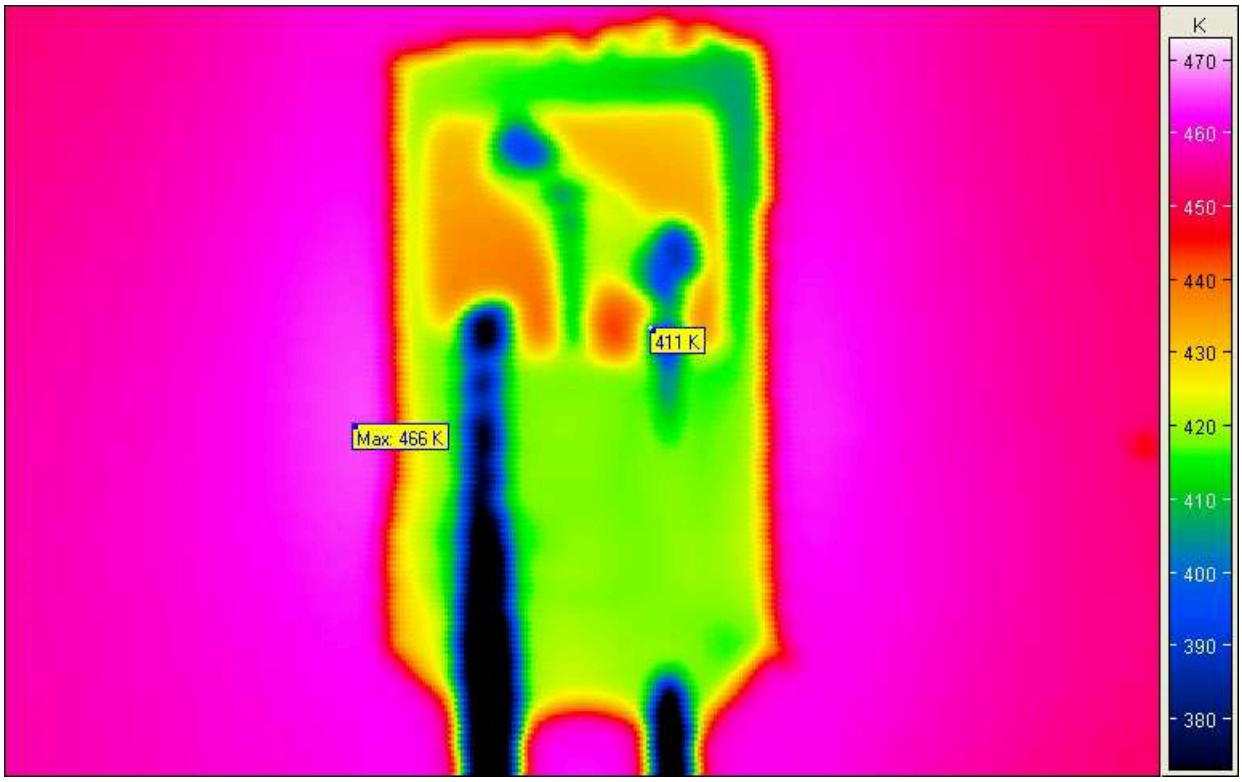

(b)

Figure 7.8: Thermovision images of temperature distribution in the thermal cutoff exposed to thermal flux of 3200 W/m^2. (a) Zero time (temperature on the back of the device is 35 K above the cutoff temperature). (b) After 33 s (the cutoff moment).

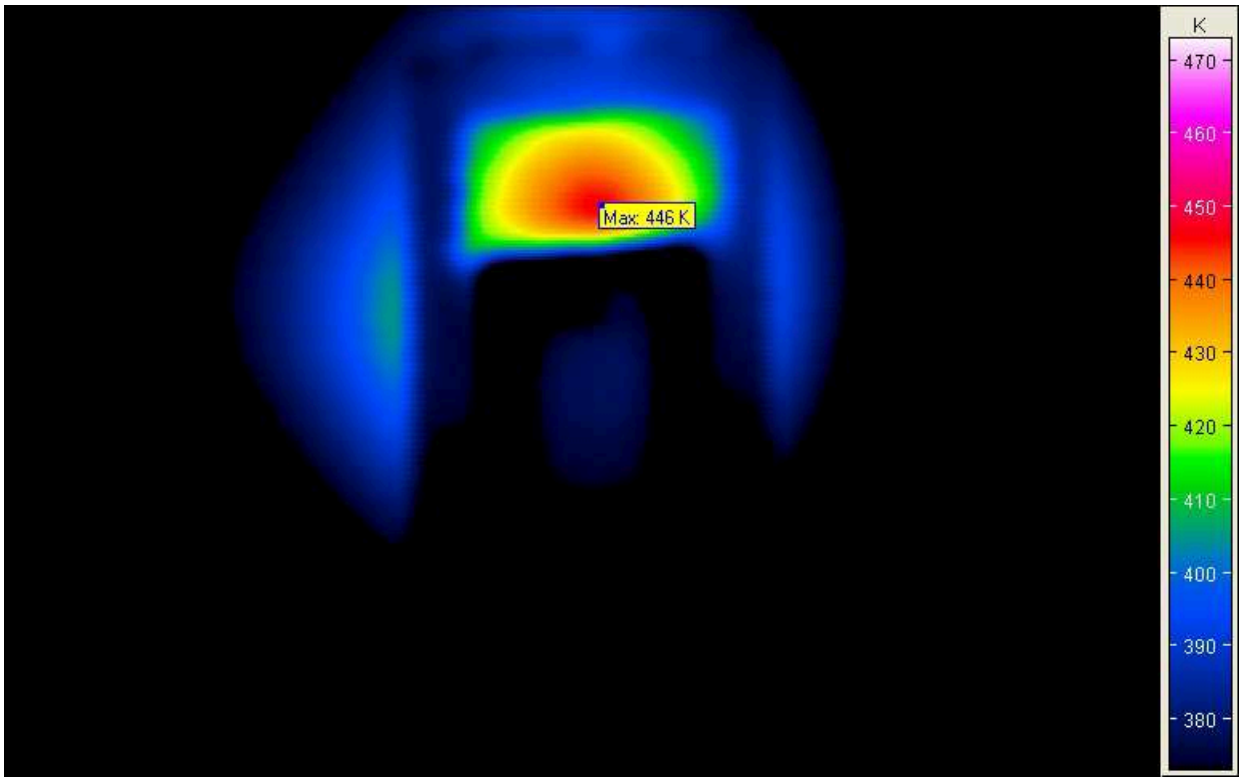

(a)

(b)

Figure 7.9: Thermovision images of temperature distribution in the thermal cutoff exposed to thermal flux of 1050 W/m^2. (a) Zero time (temperature on the back of the device is 35 K above the cutoff temperature). (b) After 100 s (the cutoff moment).

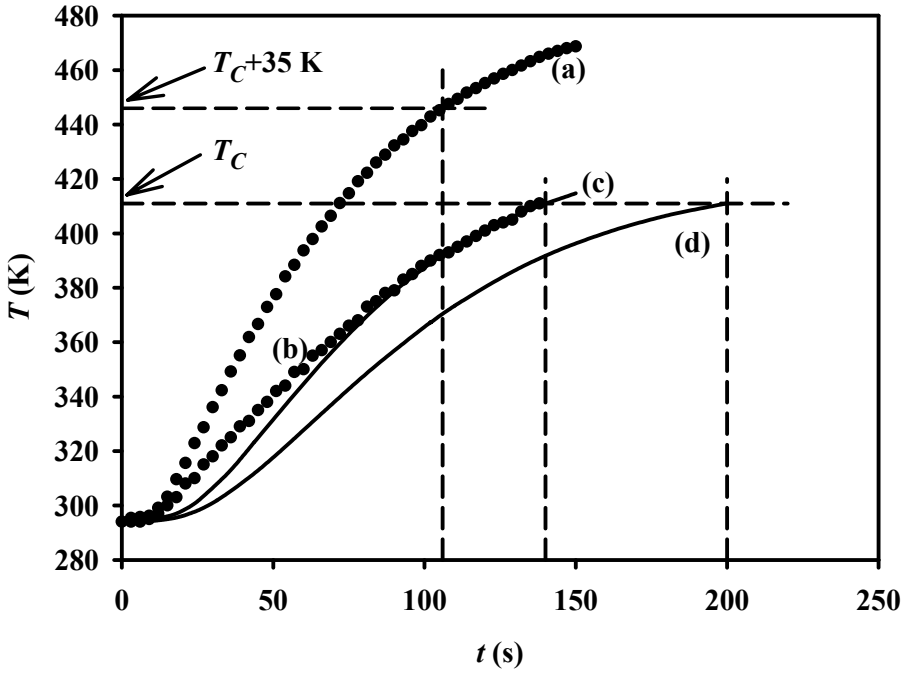

Figure 7.10: Temperature rise versus time for thermal cutoff exposed to thermal flux of 3200 W/m^2. (a) Thermovision data taken from the back of the device. (b) Thermovision data taken from the soldering sheets. (c) Simulation data for the soldering sheets with one side of the housing removed. (d) Simulation data for the soldering sheets with the complete housing. T_C is the cutoff temperature.

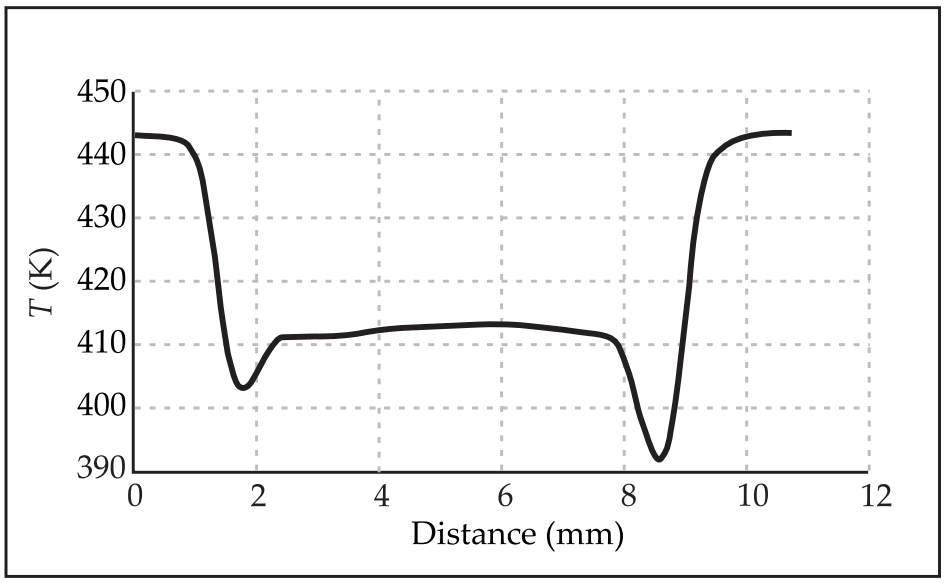

Figure 7.11: Temperature distribution along cross section L01 from Fig. 7.8(a).

within the cutoff and the temperature on the soldering sheets are mostly affected by the thermal conductivity of the air inside the device and not by the thermal resistance of the housing. Therefore, a performance improvement may not be achieved by reducing the wall thickness and 1 mm value is suggested as the optimal one.

Conclusion

Characteristics of electrical contacts in electrical, thermal and mechanical sense define the efficiency, quality and reliability of switching circuits within which they operate. Design and optimization of these devices should enable their implementation that meets the highest standards in terms of functionality, reliability, costs and environmental suitability. Determining the optimal design is a complex task since, in real applications, contacts are exposed to a variety of operating conditions. This Dissertation presents the design and optimization of rivet electrical contacts realized by 3–D numerical simulation of their electrical, thermal and mechanical properties in the steady–state regime. Simulations are performed for the solid contacts made of silver and bimetallic contacts made of copper and plated with a layer of three different silver based alloys. Contacts are considered within the appropriate supporting structure in the form of a cantilever beam made of copper. Two ways of its movement limitation are considered. Special emphasis is placed on obtaining dependencies of temperature and maximum equivalent stress in the contacts for different values of the applied current. It enabled good insight into simulation results for various applied materials and sets of dimensional and geometrical parameters. On the basis of implemented optimization procedures, appropriate contact materials are selected, values of the head diameter and head inclination angle are defined and maximum rated currents are specified. The results are presented for three systems which differ by the type of contacts and supporting structure movement limitation. These are systems with solid Ag and bimetallic contact and a single movement limitation and the system with bimetallic contact and twofold movement limitation.

For the system with solid Ag contact, functional verification of the design that includes a rounded head with a diameter of 3 mm, contact forces of 0.15 N/A and 0.2 N/A and rated current of 15 A was made. The estimated lifetime of the contact due to the fatigue is more than 10^6 contacting cycles. The supporting structure in the form of elastic beam made of copper, with the single movement limitation fully meets the required switching characteristics of the studied system.

In the systems with bimetallic contacts and single movement limitation, it was found that mechanical characteristics of the structure limit their application, while the temperature issue is not critical. To achieve the lifetime of the switching device of 10^4 contacting cycles, at rated current of 40 A and contacting force of 0.36 N/A, it is necessary to adopt a head diameter of 5 mm. Extended contact functionality requires a decrease in the value of the rated current to 15 A for 10^5 contacting cycles and to 11 A for 10^6 cycles. Adequate reduction of the rated current to 15 A also enables realization of the switching devices with contacts whose head inclination angle is 15 ° and reliable operation for 80 000 contacting cycles. In this way, consumption of the coating material is reduced, contacting pressure value is increased and contact resistance is decreased. Mechanical characteristics of the supporting structure also limit rated current to 15 A, while for the higher current values it is necessary to change contact dimensions.

It was shown that, in switching devices with twofold movement limitation, there is a redistribution of the contacting force, which provides reliable operation of contacts for more than 10^6 contacting cycles, at rated current of 40 A for all considered diameters of the contacting head. In thermal sense, such system has a higher temperature than the system with single movement limitation, but still within the prescribed limits. The optimal realization of switching devices with contacts whose head inclination angle is 15 ° is proposed. It provides 10^6 contacting cycles with less material consumption, higher values of the contact pressure and lower values of the maximum equivalent stress. It was found that the supporting structure in systems with twofold limitation is fully functional for currents up to the rated value.

Ecological aspect of the optimization of bimetallic contacts confirmed that implementation of Ag–Ni and Ag–Cu alloys as a plating material instead of widespread but toxic alloy Ag–CdO is fully justified .

Functionality, quality and reliability of thermal cutoffs are determined by the value and stability of their parameters at various operating conditions. These parameters are: functioning temperature, response time, electrical resistance of conductive and insulating parts and mechanical strength. A vital part of the thermal cutoff consists of soldering sheets made of low melting alloys and for design and optimisation it is necessary to know their thermal properties (primarily the dependence of the melting point on the composition) and microstructural characteristics (structure and composition of the grains). This Dissertation proposes a new method for generation of the liquidus surface of ternary systems which are many low melting alloys. It is named the surface modeling method and it exploits any software for modeling of arbitrary smooth 3–D surfaces, known phase diagrams of the binary subsystems and the minimum set of public available experimental data for obtaining the unknown phase diagram of the ternary system. By the new method one can extract the liquidus temperature for a given composition of the ternary system, but also can determine the composition of the system that meets the maximum melting temperature criterion. Application of the surface modeling method is verified by comparison of the generated 2–D representation of liquidus surface with the one obtained by CALPHAD method for three ternary low melting alloys.

This Dissertation presents the results of microstructural analysis by SEM and EDS techniques of two eutectic alloys important for use in thermal cutoffs. Determining the grain structure of alloys enabled the prediction of mechanical properties of solder joints made of them. On the other hand, knowledge of the grains composition enabled specification of their processing conditions.

In design and optimization of thermal cutoffs were used results of 3–D simulations in the electrical and thermal domains. The characteristics are analysed in steady-state and transient regimes with particular emphasis on the thermal parameters and response time. Thermal cutoffs whose construction includes radial leads, spring and plastic housing are considered. Its rated voltage is 250 V and rated current 12 A. Based on the temperature specifications, cutoffs are labelled as S–95 and S–138 types (with cutoff temperatures 95 °C and 138 °C). Simulation results enabled to determine optimal dimensions of the cutoff elements considering functional, economic and technological aspects. The prediction of the response time for given operating conditions and quality parameters of the cutoff are also performed. These are unique results of the application of simulation techniques in the design and optimization processes of thermal cutoffs since in the available literature this problem is not treated.

As part of the investigation, functional and qualitative analysis of S–138 cutoff type is carried out by recording the temperature distribution inside the cutoff at various operating conditions employing the thermovision measurement method. This method avoids the use of specialized chamber for temperature control and allows functioning of the cutoff in operating conditions close to the real one. Experimentally was investigated the increase of temperature due to the self–heating effect, verified the cutoff temperature value and estimated the response time. This allowed precise setting of the thermal boundary conditions necessary for the successful optimization of the cutoffs through the simulation of their electrical and thermal characteristics. Also, the obtained data were used for determining thermal properties of the housing and conductive elements of the cutoff.

As an overall result of the design and optimization of thermal cutoffs presented in this Dissertation, a flowchart of technological processes for production of thermal cutoffs is developed and a complete technical documentation is made. Defined flowchart of technological processes for the production of S-type thermal cutoffs with the specified steps of preparation, assembling and testing of the constitutive elements is illustrated in Fig. 8.1.

Technological line is defined by a total of 19 procedures related to the unique manufacturing process. All procedures are performed within a single production facility, with the exception of nickel plating and plastic injection molding which are performed as a service. Semi–finished products come out of the production facility to the external finishing just at one place (plating), which makes the flow of the manufacturing processes almost completely sequential.

Designed production line includes equipment for manufacturing and quality control of thermal cutoffs. Product documentation for each technological step includes definition of the required input parameters, the number of employees, security and safety measures. Technological line enables optimal flow of the raw materials and semi–finished products between working places and automation of the line at a level of approximately 50 %.

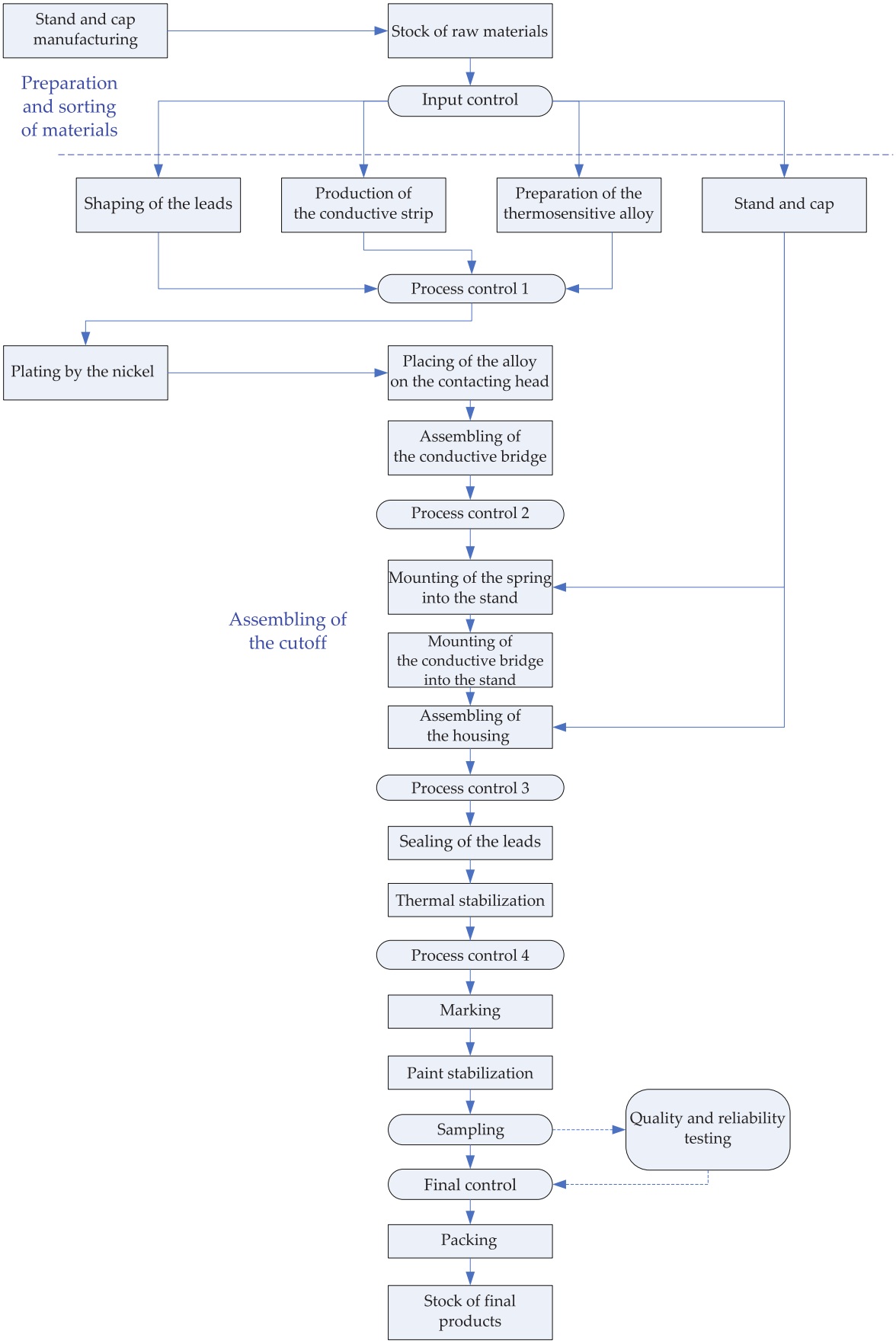

Figure 8.1: The flowchart of technological processes for the production of S-type thermal cutoffs.

Bibliography

[1] P. Goodman, "Electrical Contacts and Connectors - a comprehensive design and user guide," ERA Technology Ltd, Tech. Rep., 2002.

[2] M. Braunović, N. Myshkin, and V. Konchits, *Electrical Contacts: Fundamentals, Applications and Technology*. CRC Press, 2006.

[3] M. Braunovic, V. Izmailov, and M. Novoselova, "A Model for Life Time Evaluation of Closed Electrical Contacts," in *Proceedings of the Fifty-First IEEE Holm Conference on Electrical Contacts*, Chicago, Illinois, USA, September 2005, pp. 217–223.

[4] C. Aronis, C. Psomopoulos, C. Naragiannopouls, and P. Bourkas, "A Model of Electrical Contacts with Advanced Degradation," *International Journal of Modelling & Simulation*, vol. 26, no. 2, pp. 169–174, 2006.

[5] Y. Kawakami, M. Hasegawa, Y. Watanabe, and K. Sawa, "An Investigation for the Method of Lifetime Prediction of Ag-Ni Contacts for Electromagnetic Contactor," in *Proceedings of the Fifty-First IEEE Holm Conference on Electrical Contacts*, Chicago, Illinois, USA, September 2005, pp. 151–155.

[6] W. Xixiu, L. Zhenbiao, D. Meihua, W. Zhongchao, and S. Xiaoliang, "Simulation of Particle Flow in Molten Pool of Electric Contact of Power Switch," in *Proc. of 39th International Universities Power Engineering Conference*, Bristol, UK, September 2004.

[7] A. Monnier, B. Froidurot, C. Jarrige, R. Meyer, and P. Teste, "A Mechanical, Electrical, Thermal Coupled-Field Simulation of a Sphere-Plane Electrical Contact," in *Proceedings of the Fifty-First IEEE Holm Conference on Electrical Contacts*, Chicago, Illinois, USA, September 2005, pp. 224–231.

[8] ——, "A Coupled-Field Simulation of an Electrical Contact during Resistance Welding," in *Proceedings of the Fifty-Second IEEE Holm Conference on Electrical Contacts*, Montreal, Canada, September 2006, pp. 95–102.

[9] C. Weißenfels and P. Wriggers, "Numerical Modeling of Electrical Contacts," *Computational Mechanics*, vol. 46, no. 2, pp. 301–314, July 2010.

[10] G. Hrovat and A. Hamler, "The Heat Circumstances in Switch by Permanent Load," in *Computer Engineering in Applied Electromagnetism*. Springer, Netherlands, 2005, pp. 293–296.

[11] T. Imaizumi, N. Yamamoto, K. Sawa, M. Tomita, Murakami, and I. Hirabayashi, "Simulation of Current and Temperature Distribution in YBCO Bulk's Electrical Contact," *Physica C: Superconductivity*, vol. 412, no. 10, pp. 668–672., 2004.

[12] S. Bhashyam, G. Ambrosio, D. Chichili, L. Imbasciati, S. Yadav, R. Yamada, and A. Zlobin, "Predicting Temperature Rise Due to Resistive Heating in Splice Region of Cosθ Dipole Magnets using 2D ANSYS^{TM} Analysis," FermiLab, Batavia, Illinois, USA, Tech. Rep., 2002.

[13] V. Brizmer, Y. Zait, Y. Kligerman, and I. Etsion, "The Effect of Contat Conditions and Material Properties on Elastic–Plastic Sferical Contact," *Journal of Mechanics of Materials and Structures*, vol. 1, no. 5, pp. 865–879, 2006.

[14] [Online]. Available: http://www.powertech.co.nz

[15] *WTC–Thermal Cutoffs – catalog*.

[16] [Online]. Available: http://www.us-electronics.com/datasheets/thermalcutoffs.pdf

[17] *Panasonic–Thermal Cutoffs Data Sheet*.

[18] F. Hua, Z. Mei, and J. Glazer, "Eutectic Sn-Bi as an Alternative to Pb-Free Solders," in *Proc. of Electronic Component and Technology Conference*, Seattle, Washington, USA, 1998, pp. 277–283.

[19] M. McCormack, Y. Degani, H. Chen, and W. Gesick, "A Lower–Melting–Point Solder Alloy for Surface Mounts," *Journal of Materials*, vol. 48, no. 5, pp. 54–56, 1996.

[20] Z. Mei, H. Holder, and H. VanderPlas, "Low–Temperature Solders," *Hewlett-Packard Journal*, no. 8, p. art. 10, 1996.

[21] P. J. Spencer, "A brief history of CALPHAD," *Computer Coupling of Phase Diagrams and Thermochemistry*, vol. 32, pp. 1–8, 2008.

[22] X. Maldague and P. Moore, Eds., *Nondestructive Testing Handbook, Third Edition: Volume 3, Infrared and Thermal Testing*. American Society for Nondestructive Testing, 2001.

[23] A. Nowakowski, "Role of IR-Thermal Imaging and Electroimpedance Measurements in Medical Diagnostics," in *27th Annual International Conference of the Engineering in Medicine and Biology Society*, Shangai, China, September 2005, pp. 706–709.

[24] C. Meola, G. Carlomagno, and L. Giorleo, "The Use of Infrared Thermography for Materials Characterization," *Journal of Processing Materials Technology*, vol. 155-156, pp. 1132–1137, 2004.

[25] S. Dhokkar, B. Serio, J. Hunsinger, P. Lagonotte, C. Gorecki, A. Asundi, and W. Osten, "Thermal Characterization of Power Transistors by Close Infrared Thermography Method," *Proceedings of Society of Photo-optical Instrumentation Engineers*, vol. 6188, pp. 1E.1–1E.10, 2006.

[26] [Online]. Available: http://www.microscan.eu.com/projects/pr_16.jsp

[27] A. Herchang, J. JiinYuh, and Y. Jer-Nan, "Local Heat Transfer Measurements of Plate Finned-tube Heat Exchangers by Infrared Thermography," *International Journal of Heat and Mass Transfer*, vol. 45, no. 9, pp. 4069–4078, September 2002.

[28] *Engineers Relay Handbook – 6th edition*. Relay and Switch Industry Association, 2006.

[29] M. Gedeon, "Size Reduction," Brush Wellman Alloy Products, Technical Tidbit 3, April 2009. [Online]. Available: http://materion.com/~/media/Files/PDFs/Alloy/Newsletters/Technical Tidbits/Issue No 03 - Size Reduction.pdf

[30] P. Slade, Ed., *Electrical Contacts: Principles and Applications*. Marcel Dekker Inc., 1999.

[31] R. E. Colin, "Material Properties Affecting Electrical Switch Design," Ph.D. dissertation, Case Western Reserve University, Cleveland, Ohio, 1977.

[32] M. Gedeon, "Connector Temperature Rise," Brush Wellman Alloy Materials, Technical Tidbit 23, November 2010. [Online]. Available: http://materion.com/~/media/Files/PDFs/Alloy/Newsletters/Technical Tidbits/Issue No 23 - Connector Temperature Rise.pdf

[33] ——, "Current Carrying Capacity," Brush Wellman Alloy Products, Technical Tidbit 24, December 2010. [Online]. Available: http://materion.com/~/media/Files/PDFs/Alloy/Newsletters/Technical Tidbits/Issue No 24 - Current Carrying Capacity.pdf

[34] B. Belin, *Uvod u teoriju električnih sklopnih aparata*. Školska knjiga, Zagreb, 1987.

[35] L. Morin, N. B. Jemaa, and D. Jeannot, "Make Arc Erosion and Welding Study," *IEEE Trans. on Component, Packaging and Technology*, vol. 23, no. 2, pp. 240–245, 2000.

[36] J. McBride and S. Sharkh, "The Influence of Contact Opening Velocity on Arc Characteristics," in *Proc. of 16th International Conference on Electrical Contacts*, England, September 1992, pp. 395–400.

[37] N. B. Jemaa, "Contacts Conduction and Switching in DC Levels," in *Proceedings of the Forty-Eight IEEE Holm Conference on Electrical Contacts*, Orlando, USA, 2002, pp. 1–15.

[38] M. Gedeon, "Fretting Corrosion," Brush Performance Alloys, Technical Tidbit 33, September 2011. [Online]. Available: http://materion.com/~/media/Files/PDFs/Alloy/Newsletters/Technical Tidbits/Issue No 33 - Fretting Corrosion.pdf

[39] ——, "Creep Corrosion and Pore Corrosion," Brush Performance Alloys, Technical Tidbit 35, November 2011. [Online]. Available: http://materion.com/~/media/Files/PDFs/Alloy/Newsletters/Technical Tidbits/Issue No 35 - Creep Corrosion and Pore Corrosion.pdf

[40] R. S. Mroczkowski, *Electric Connector Handbook: Technology and Applications*. McGraw-Hill, 1998.

[41] A. Sun, H. Moffat, D. Enos, and C. Glauner, "Pore Corrosion Model for Gold-Plated Copper Contacts," in *Proceedings of the Fifty-First IEEE Holm Conference on Electrical Contacts*, Chicago, Illinois, USA, September 2005, pp. 232–237.

[42] T. Ito, M. Matsushima, K. Takata, and Y. Hattori, "Factors Influencing the Fretting Corrosion of Tin Plated Contacts," in *Proceedings of the Fifty-Second IEEE Holm Conference on Electrical Contacts*, Montreal, Canada, September 2006, pp. 267–272.

[43] N. Aukland and H. Hardee, "Improving Fretting Performance of Tin-Lead Contacts," *Connector Specifier*, vol. 3, pp. 10–12, 1999.

[44] J. McBride, "Developments in Fretting Studies applied to Electrical Contacts," in *Proceedings of the Fifty-Second IEEE Holm Conference on Electrical Contacts*, Montreal, Canada, September 2006, pp. 170–180.

[45] M. Gedeon, "S–n diagrams," Materion Brush Performance Alloys, Technical Tidbit 55, July 2013. [Online]. Available: http://materion.com/~/media/Files/PDFs/Alloy/Newsletters/Technical Tidbits/Issue No 55 - S-N Diagrams.pdf

[46] D. Smith and F. Ficket, "Low Temperature Properties of Silver," *Journal of Research of the National Institute of Standards and Technology*, vol. 100, p. 169, 1995.

[47] W. Weibull, "A Statistical Representation of Fatigue Failures in Solids," *Trans. of Royal Institute of Technology, Sweden*, no. 27, 1949.

[48] S. Heikkinen, "Fatigue of metals; Copper alloys," in *Proc. of CLICK Meeting*. Switzerland: CERN, 2003.

[49] M. Gedeon, "Cumulative Effects of Tolerances on Connector Performance - Part 1," Brush Wellman Alloy Products, Technical Tidbit 7, August 2009. [Online]. Available: http://materion.com/~/media/Files/PDFs/Alloy/Newsletters/Technical Tidbits/Issue No 07 - Cumulative Effects of Tolerances on Conector Performance - Part 1.pdf

[50] ——, "Cumulative Effects of Tolerances on Connector Performance - Part 2," Brush Wellman Alloy Products, Technical Tidbit 8, August 2009. [Online]. Available: http://materion.com/~/media/Files/PDFs/Alloy/Newsletters/Technical Tidbits/Issue No 08 - Cumulative Effects of Tolerances on Conector Performance - Part 2.pdf

[51] C. Turner, "Modern Trends in Contact Material Development," *IEE Colloquium on Electrical Contacts*, vol. 4, pp. 6/1–6/2, 1989.

[52] M. Gedeon, "Elastic Modulus," Materion Brush Performance Alloys, Technical Tidbit 48, December 2012. [Online]. Available: http://materion.com/~/media/Files/PDFs/Alloy/Newsletters/Technical Tidbits/Issue No 48 - Elastic Modulus.pdf

[53] ——, "Stress Relaxation and Creep," Brush Wellman Alloy Products, Technical Tidbit 12, December 2009. [Online]. Available: http://materion.com/~/media/Files/PDFs/Alloy/Newsletters/Technical Tidbits/Issue No 12 - Stress Relaxation and Creep.pdf

[54] ——, "Factors Affecting Stress Relaxation and Creep," Brush Wellman Alloy products, Technical Tidbit 13, January 2010. [Online]. Available: http://materion.com/~/media/Files/PDFs/Alloy/Newsletters/Technical Tidbits/Issue No 13 - Factors Affecting Stress Relaxation and Creep

[55] C. Weaver and G. Newey, Eds., *Materials: Principles and Practice*. The Open University, London, 1990.

[56] M. Gedeon, "What Happens During Yielding?" Brush Wellman Alloy Products, Technical Tidbit 14, February 2010. [Online]. Available: http://materion.com/~/media/Files/PDFs/Alloy/Newsletters/Technical Tidbits/Issue No 14 - Material Yielding.pdf

[57] ——, "Grain Size and Material Strength," Brush Wellman Alloy Products, Technical Tidbit 15, March 2010. [Online]. Available: http://materion.com/~/media/Files/PDFs/Alloy/Newsletters/Technical Tidbits/Issue No 15 - Grain Size and Material Strength

[58] ——, "Strain Hardening and Strength," Brush Wellman Alloy Products, Technical Tidbit 17, May 2010. [Online]. Available: http://materion.com/~/media/Files/PDFs/Alloy/Newsletters/Technical Tidbits/Issue No 17 Strain Hardening Strength

[59] J. Davis and et al., Eds., *ASM Handbook: Volume 2, Properties and Selection: Nonferrous Alloys and Special-Purpose Material*. ASM International, Materials Park, 1990.

[60] W. Hosford and R. Caddell, *Metal Forming: Mechanics and Metallurgy*. Prentice–Hall Inc., 1983.

[61] M. Gedeon, "Strain Hardening," Materion Brush Performance Alloys, Technical Tidbit 50, February 2013. [Online]. Available: http://materion.com/~/media/Files/PDFs/Alloy/Newsletters/Technical Tidbits/Issue No 50 - Strain Hardening.pdf

[62] ——, "Strain Hardening and Formability," Materion Brush Performance Alloys, Technical Tidbit 51, March 2013. [Online]. Available: http://materion.com/~/media/Files/PDFs/Alloy/Newsletters/Technical Tidbits/Issue No 51 - Strain Hardening and Formability.pdf

[63] ——, "Bend Testing vs. Forming Reality," Brush Wellman Alloy Products, Technical Tidbit 10, October 2009. [Online]. Available: http://materion.com/~/media/Files/PDFs/Alloy/Newsletters/Technical Tidbits/Issue No 10 - Bend Testing Versus Forming Reality.pdf

[64] J. Gubicza, A. Juhasz, P. Tasnadi, P. Arato, and G.Voros, "Determination of the Hardness and Elastic Modulus from Continous Vickers Indentation Testing," *Journal of Material Science*, vol. 31, pp. 3109–3114, 1996.

[65] S. Fee and Tobolski, *ASM Handbook: Volume 8*. ASM International, 1985, ch. Hardness Testing, pp. 69–113.

[66] [Online]. Available: http://www.hsmetal.co.kr

[67] J. Whitley, "The Tin Commandments," *Plating and Surface Finishing*, vol. 68, no. 10, pp. 38–39, 1981.

[68] F. Reidenbach, Ed., *ASM Handbook: Volume 5: Surface Engineering*. ASM International, Materials Park, 1994.

[69] J. Edwards, *Coating and Surface Treatment Systems for Metals: A Comprehensive Guide to Selection*. Finishing Publications Ltd. and ASM International, 1997.

[70] [Online]. Available: http://www.doduco.net/media/84012/produktinformation_niete_en_2013-08-30.pdf

[71] [Online]. Available: http://www.taling.com.tw

[72] [Online]. Available: https://www.tanaka-europe.eu

[73] [Online]. Available: http://www.mallory.com

[74] [Online]. Available: http://www.brainin.com/contactmaterials.cfm

[75] [Online]. Available: http://www.choksiheraeus.com

[76] W. Johler, "The Design Challenges Involved in Miniaturization of Electromechanical Relays," in *Proceedings of the Fifty-Second IEEE Holm Conference on Electrical Contacts*, Montreal, Canada, September 2006, pp. 151–152.

[77] J.Song, C. Helmig, J. Feye-Hohmann, and A. Schulz, "Bending Test of Contact Materials," in *Proceedings of the Fifty-Second IEEE Holm Conference on Electrical Contacts*, Montreal, Canada, September 2006, pp. 207–210.

[78] [Online]. Available: http://www.norstaninc.com/pdf/wsb300.pdf

[79] [Online]. Available: http://www.tecc.com.tw/index.htm

[80] "Proizvodnja elektroenergetskih kontakata," Ei Holding Co., DO "Ei Komponente", Tech. Rep., 2000.

[81] M. Gedeon, "Round vs. Rectangular Cross Sections," Brush Performance Alloys, Technical Tidbit 30, June 2011. [Online]. Available: http://materion.com/~/media/Files/PDFs/Alloy/Newsletters/Technical Tidbits/Issue No 30 - Round Versus Rectangular Cross Sections.pdf

[82] ——, "Material Property Directionality," Brush Performance Alloys, Technical Tidbit 28, April 2011. [Online]. Available: http://materion.com/~/media/Files/PDFs/Alloy/Newsletters/Technical Tidbits/Issue No 28 - Material Property Directionality.pdf

[83] ——, "The Importance of Contact Force," Brush Wellman Alloy Products, Technical Tidbit 6, July 2009. [Online]. Available: http://materion.com/~/media/Files/PDFs/Alloy/Newsletters/Technical Tidbits/Issue No 06 - The Importance of Contact Force.pdf

[84] ——, "Cantilever Beams – Part 2 – Analysis," Brush Wellman Alloy Products, Technical Tidbit 21, September 2010. [Online]. Available: http://materion.com/~/media/Files/PDFs/Alloy/Newsletters/Technical Tidbits/Issue No 21- Cantilever Beams - Part 2 Analysis.pdf

[85] ——, "Cumulative Stress and Bauschinger Effect," Brush Wellman Alloy Products, Technical Tidbit 4, May 2009. [Online]. Available: http://materion.com/~/media/Files/PDFs/Alloy/Newsletters/Technical Tidbits/Issue No 04 Cumulative Stress the Bauschinger Effect.pdf

[86] ——, "Reliability and End-of Life Contact Force," Brush Wellman Alloy Products, Technical Tidbit 5, June 2009. [Online]. Available: http://materion.com/~/media/Files/PDFs/Alloy/Newsletters/Technical Tidbits/Issue No 05 - Reliability and End-of-Life Contact Force.pdf

[87] ——, "Elastic Resilience," Brush Wellman Alloy Products, Technical Tidbit 22, October 2010. [Online]. Available: http://materion.com/~/media/Files/PDFs/Alloy/Newsletters/Technical Tidbits/Issue No 22- Elastic Resilience.pdf

[88] C. Bernauer, T. K. an V. Behrens, and T. Honig, "Substitution of Silver/Cadmium oxide in High Voltage Disconnectors," in *Proceedings of the Fifty-First IEEE Holm Conference on Electrical Contacts*, Chicago, Illinois, USA, September 2005, pp. 42–47.

[89] *Ansys, Inc. – Theory Reference*.

[90] A. Prijić, B. Pešić, Z. Prijić, D. Pantić, and Z. Pavlović, "3d Simulation of Electrical and Thermal Characteristics of Electric Contacts," *ELECTRONICS*, vol. 6, no. 2, pp. 3–5, 2002.

[91] ——, "3d Simulation of Electric Contacts – Temperatures and Yield Stress Distributions," in *Proc. 7th International Symposium on Microelectronics Technologies and Microsystem - MTM'03*. Sofia-Sozopol, Bulgaria: Technical University of Sofia, Bulgaria, September 2003, pp. 57–62.

[92] ——, "Temperature and Yield Stress Characterization of Electric Contacts by 3D Numerical Simulation," *Serbian Journal of Electrical Engineering*, vol. 1, no. 2, pp. 77–91, 2005.

[93] N. Vichare and M. Pecht, "Prognostics and Health Management of Electronics," *IEEE Trans. on Component and Packaging Technologies*, vol. 29, no. 1, pp. 222–229, March 2006.

[94] [Online]. Available: http//:www.thermtrol.com

[95] *NEC–Thermal Cutoff SEFUSE Data Sheeet*.

[96] J. Rigdeon, *Macmillan Encyclopedia of Physics*. Simon & Schuster, 1996.

[97] S. W. Yoon, B.-S. Rho, H. M. Lee, C.-U. Kim, and B.-J. Lee, "Investigation of the Phase Equilibria in the Sn-Bi-In Alloy System," *Metallurgical & Materials Transactions A*, vol. 30, no. 6, pp. 1503–1516, 1999.

[98] [Online]. Available: http://www.asi-tech.co.il/_Uploads/dbsAttachedFiles/AlloysSpecialty.pdf

[99] [Online]. Available: http://www.alchemycastings.com/lead-products/fusible.htm

[100] [Online]. Available: http://www.gselectronic.de/AIM-Specialty_Materials.htm

[101] [Online]. Available: http://www.indium.com/products/tableofalloys.xls

[102] O. Degtyareva, V. Degtyareva, F. Porsch, and W. Holzapfel, "Phase Transitions Under High Pressure in Binary Sn Alloys (with In, Hg and Ga)," *Journal of Physics: Condensed Matter*, vol. 14, pp. 389–406, 2002.

[103] T. Hatchard, J. Dahn, S. Trusslera, M. Fleischauer, A. Bonakdarpour, J. Mueller-Neuhaus, and K. Hewitt, "The Amorphous Range in Sputtered Si–Al–Sn Films," *Thin Solid Films*, vol. 443, pp. 144–150, 2003.

[104] E. Specht, A. Rar, G. Pharr, E. George, P. Yschack, H. Hong, and J. Ilavsky, "Rapid Structural and Chemical Characterization of Ternary Phase Diagrams using Synchrotron Radiation," *Journal of Material Research*, vol. 18, no. 10, pp. 2522–2127, 2003.

[105] G. Vassilev, "Application of Diffusion Couple Technique for the Determination of the Ti–Bi–Sn Phase Diagram," *Crystal Research and Technology*, vol. 40, no. 7, pp. 713–718, 2005.

[106] *Phase Equilibria Diagrams*, CD ed., ACerS-NIST. [Online]. Available: http://www.ceramics.org/phasecd

[107] P. Villars, A. Prince, and H. Okamoto, Eds., *Handbook of Ternary Alloy Phase Diagrams*. ASM International, 1995.

[108] D. Živković, D. Manasijević, D. Marković, B. Marjanović, M. Gorgievski, and I. Borisov, "Predviđanje termodinamičkih karakteristika i karakterizacija nekih legura u ternarnom sistemu Pb-Bi-In," *TEHNIKA*, vol. 14, no. 4, pp. R6–R10, 2005.

[109] U. Kattner, "The Thermodynamic Modeling of Multicomponent Phase Equilibria," *Journal of Materials*, vol. 49, no. 12, pp. 14–19, 1997.

[110] K. C. H. Kumar and P. Wollants, "Some guidelines for thermodynamic optimisation of phase diagrams," *Journal of Alloys and Compounds*, vol. 320, no. 2, p. 189/198, 2001. [Online]. Available: http://users.encs.concordia.ca/~kharma/PersonalWeb/exchange/guidelines for optimization by Kumar.pdf

[111] [Online]. Available: http://www.sgte.org

[112] [Online]. Available: http://www.crct.polymtl.ca/fact/documentation

[113] [Online]. Available: http://www.esm-software.com/factsage

[114] [Online]. Available: http://www.thermocalc.com

[115] [Online]. Available: http://www.npl.co.uk/mtdata

[116] H. Lukas, J. Weiss, and E. Henig, "Strategies for the Calculation of Phase Diagrams," *CALPHAD*, vol. 6, pp. 229–251, 1982.

[117] W. Cao, S. L. Chen, F. Zhang, K. Wu, Y. Yang, Y. A. Chang, R. Schmid-Fetzer, and W. A. Oates, "Pandat software with Panengine, Pnanoptimizer and Panprecipitation for multi-component phase diagram calculation and materials property simulation," *Calphad*, vol. 33, no. 2, pp. 328–342, 2009.

[118] [Online]. Available: http://www.computherm.com

[119] S. W. Yoon and H. M. Lee, "A Thermodynamic Study of Phase Equilibria in the Sn-Bi-Pb Solder System," *CALPHAD*, vol. 22, no. 2, p. 167–178, 1998.

[120] N. David, K. E. Aissaoui, J. Fiorani, J. Hertz, and M. Vilasi, "Thermodynamic Optimization of the In-Pb-Sn System Based on New Evaluations of the Binary Borders In-Pb and In-Sn," *Thermochimica Acta*, vol. 413, no. 413, pp. 127–137, 2004.

[121] [Online]. Available: http://www.metallurgy.nist.gov/phase/solder/bipbsn.html

[122] A. Prijić, Z. Prijić, and B. Pešić, "A New Method of Evaluation of Liquidus Temperatures of Ternary Alloys," in *Proc. 25th International Conference on Microelectronics (MIEL2006)*. Belgrade, Serbia: IEEE, May 2006, pp. 395–399.

[123] M. Kamal, S. Mazen, A. El-Bedivi, and E. Kashita, "Characterization of Bismuth–tin–lead and Bismuth–tin–lead–cadmium Fusible Alloys," *Radiation Effects and Defects in Solids*, vol. 160, pp. 369–375, 2005.

[124] [Online]. Available: http://www.bayermaterialsciencenafta.com/products

[125] [Online]. Available: http://zierick.com/pdf/materials.pdf

[126] C. Lasance, "The Influence of Various Common Assumptions on the Boundary–Condition–Independence of Compact Thermal Models," *IEEE Trans. on Component and Packaging Technologies*, vol. 27, no. 3, pp. 523–529, 2004.

[127] C. Popiel and J. Wojtkowiak, "Experiments on Free Convective Heat Transfer from Side Walls of a Vertical Square Cylinder in Air," *Experimental Thermal and Fluid Science*, vol. 29, no. 12, pp. 1–8, 2004.

[128] [Online]. Available: http://www.engineeringtoolbox.com/air-properties-d_156.html

[129] [Online]. Available: http://www.dowcorning.com

[130] A. Prijić, Z. Prijić, B. Pešić, D. Pantić, and S. Ristić, "Analysis of Electrical and Thermal Characteristics of Thermal Cutoffs," in *Proc. of XLII International Scientific Conference on Information, Communication and Energy Systems and Technologies – ICEST 2007*. Ohrid, Macedonia: Faculty of Technical Sciences, Bitola, Macedonia, June 2007, pp. 827–830.

[131] S. Schlesinger, *Infrared Technology Fundamentals*. Dekker–Verlag, New York und Basel, 1989.

[132] *Theoretical and Practical Aspects of Infrared Thermography*, Jenoptic L.O.S., GmbH, 2001.

[133] A. Prijić, Z. Prijić, B. Pešić, D. Pantić, S. Ristić, D. Mančić, and Z. Petrušić, "Design and optimization of s-type thermal cutoffs," *IEEE Trans. Components and Packaging Technologies*, vol. 31, no. 4, pp. 904–912, December 2008.

[134] H. Young and R. Freedman, *University Physics with Modern Physics*, 10th ed. Addison Wesley, 1999.